University of Bath

PHD

Quantitative methods in electron microscopy.

Love, G.

Award date:
1978

Awarding institution:
University of Bath

Link to publication

Alternative formats
If you require this document in an alternative format, please contact:
openaccess@bath.ac.uk

Copyright of this thesis rests with the author. Access is subject to the above licence, if given. If no licence is specified above, original content in this thesis is licensed under the terms of the Creative Commons Attribution-NonCommercial 4.0 International (CC BY-NC-ND 4.0) Licence (https://creativecommons.org/licenses/by-nc-nd/4.0/). Any third-party copyright material present remains the property of its respective owner(s) and is licensed under its existing terms.

Take down policy
If you consider content within Bath's Research Portal to be in breach of UK law, please contact: openaccess@bath.ac.uk with the details. Your claim will be investigated and, where appropriate, the item will be removed from public view as soon as possible.

Download date: 04. May. 2023

QUANTITATIVE METHODS IN ELECTRON MICROSCOPY

Submitted by G. Love for the degree of Ph.D. of the University of Bath 1978.

60 7802862 6 TELEPEN

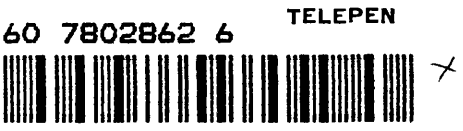

COPYRIGHT

"Attention is drawn to the fact that the copyright of this thesis rests with its author. This copy of the thesis has been supplied on condition that anyone who consults it is understood to recognise that its copyright rests with its author and that no quotation from this thesis and no information derived from it may be published without the prior written consent of the author".

"This thesis may be made available for consultation within the University Library and may be photocopied or lent to other libraries for the purpose of consultation".

G. Love

ProQuest Number: U435791

All rights reserved

INFORMATION TO ALL USERS
The quality of this reproduction is dependent upon the quality of the copy submitted.

In the unlikely event that the author did not send a complete manuscript
and there are missing pages, these will be noted. Also, if material had to be removed,
a note will indicate the deletion.

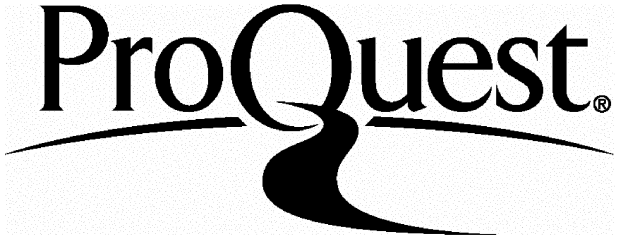

ProQuest U435791

Published by ProQuest LLC(2015). Copyright of the Dissertation is held by the Author.

All rights reserved.
This work is protected against unauthorized copying under Title 17, United States Code.
Microform Edition © ProQuest LLC.

ProQuest LLC
789 East Eisenhower Parkway
P.O. Box 1346
Ann Arbor, MI 48106-1346

Preface

This thesis comprises a series of published papers by the author and is submitted under the terms of the regulation Staff Candidature Method B. The research work which forms the basis for this submission has been published and these papers form § 7 of the thesis. The main findings in the research are highlighted in preceeding sections (§ 2 and § 3) and illustrate how the individual papers fit into the context of the overall research programme. An introduction, § 1, is included in order to provide a background for the new work; it shows how the research originated and its importance in the fields of quantitative microanalysis and microscopy. The results of the study are summarised under 'Conclusions', § 4, and some recommendations for further work are outlined in § 5.

Two of the papers (§ 7.3 and § 7.4) describe work relating to a successful submission for the degree of M.Sc. of the University of Bath in 1975, but these are included here because they help to establish the background to the investigation. None of the other publications have been used by the author before in a submission for a higher degree.

All of the papers incorporated in this thesis have been written in co-authorship with others and in the research described in § 2 of this thesis Dr Scott has acted as academic supervisor. Some of the remaining studies discussed in § 3 have been carried out in collaboration with members of staff from other Schools within the University. This fact is acknowledged in the text and the authors own contribution is described.

G. Love

Acknowledgements

Dr's A.W. Flegmann, R. G. Board, S.G. Tullett, B. McEnaney and Mr H.R. Perrott for their collaboration with some of the work described in this thesis.

Dr V.D. Scott, my supervisor, for instigating the research programme and for his encouragement and guidance throughout.

Dr M.G.C. Cox of Wilkinson Match Ltd for very many informative discussions on aspects of quantitative electron probe microanalysis and for his collaboration with much of the work described here.

Professor B Harris for his advice on presentation of the research.

Mr P.A. Wakeford for assistance with specimen preparation.

Members of staff of the University of Bath's Computer Unit for their assistance with programming.

Dr P Duncumb of Tube Investments Research Laboratories for many helpful comments on the research.

JEOL (U.K.) Ltd for providing analytical transmission electron microscope facilities at their laboratories in Colindale, London and in particular Mr K. Ibe for his assistance with the operation of this equipment.

Messrs W. Watt and W. Johnson of the Materials Department, Royal Aircraft Establishment Farnborough for provision of Orlon fibre specimens and for discussions on carbon fibre precursors.

Miss Angela Harrington for preparing the typescript of this thesis and for her patience in dealing with the numerous modifications which were involved when writing the papers.

CONTENTS

Summary

Existing absorption correction programmes used in quantitative electron probe microanalysis are assessed and their limitations discussed. It is shown that the Philibert absorption correction models (Philibert 1963) may be significantly improved by the adoption of new expressions for the σ and h terms. A new absorption correction proposed by Bishop (1974) is also investigated and its range of applicability is found to be greater than either of the two Philibert models. Accuracy of the Bishop approach has been improved by introducing a new expression for the mean depth of X-ray emission which is derived from a detailed study of electron-solid interactions using a Monte Carlo simulation of electron trajectories. Data from the Monte Carlo programme are also used in the development of a new atomic number correction. This new correction procedure overcomes some of the limitations in the Duncumb and Reed approach (Duncumb and Reed 1968) and provides an important advance in the field since it permits the computation of correction factors for specimens inclined to the incident electron beam.

Applications of quantitative electron probe microanalysis to research in both materials science and biology are described, the new data providing information which has advanced our understanding in diverse fields of study such as growth processes of avian eggshells and oxidation mechanisms in polymeric materials.

Complementary research using other electron optical techniques such as scanning and transmission microscopy is also described. These instruments have been employed to study the microstructure of materials and, more particularly, to provide quantitative data on defect populations in thin foils. In addition new techniques of foil thickness measurement are assessed and the prospects for improvement in this area are discussed.

1. An Introduction to the Research Programme

The theme of the research concerns the development and application of electron optical techniques to study the composition and structure of materials. A major part of the work has involved an investigation of limitations imposed upon quantitative electron probe microanalysis by the correction procedures and input data employed. As a result of this research some existing correction methods have been improved and new, more versatile models proposed. Particular attention has been focused upon quantitative electron probe microanalysisusing soft X-rays and, as well as discussing experimental aspects involved in this technique, some applications to the study of materials are described. Finally, quantitative factors associated with microstructural analysis using other electron optical techniques, such as scanning and transmission electron microscopy are dealt with.

The research programme began with an examination of the problems involved in quantitative electron-probe microanalysis of light elements ($Z < 11$). This study concerned the analysis of oxygen in oxides (Love, Cox and Scott, 1974a, 1974b; § 7.3 and § 7.4) and is of interest for two reasons. Firstly, it deals in detail with experimental factors involved in soft X-ray measurement. For example the performance of crystal analysers is assessed, electron trapping arrangements are described together with the stringent specimen requirements necessary for accurate analysis. Secondly, the work highlighted serious deficiencies in the methods adopted for obtaining quantitative data.

The accepted method of converting actual X-ray intensities into true chemical composition, involves comparing the characteristic X-ray intensity from the element of interest in the specimen with that of a reference standard (usually the pure element) and then applying separately the following correction factors:

(a) an atomic number correction to take account of the different electron scattering and energy loss effects in specimen and standard,

(b) an absorption factor to correct for the differing amounts of X-ray attenuation occurring in specimen and standard,

(c) a fluorescence correction to account for secondary X-ray excitation effects.

In soft X-ray work fluorescence may be ignored (Reed 1975) and the largest of the correction factors is almost without exception the absorption correction. It is therefore essential to use an accurate absorption model together with reliable input data when attempting quantitative studies using soft X-rays.

Unfortunately there is a lack of data on mass absorption coefficients and the first part of this research programme was devoted to obtaining a much needed set of oxygen mass absorption coefficients (Love et al 1974a; § 7.3). These new values were obtained by applying the thin film model of Duncumb and Melford (1966) and then carrying out a regression analysis on the experimental data. Having obtained a suitable set of mass absorption coefficients the next stage of the work was to incorporate these values in existing absorption correction procedures.

Three established correction models, the Andersen-Wittry (1968) simplified Philibert (1963) and full Philibert (1963), were considered and the predicted X-ray intensity ratios obtained were compared with experimental determinations (Love et al 1974b; § 7.4). From this evaluation it was concluded that none of the three models were entirely satisfactory but the full Philibert approach gave best agreement. The work revealed also, that many of the correction methods were likely to be inaccurate when analysing for heavy elements ($Z > 11$) under certain experimental conditions.

As a result of these findings the scope of the research programme was enlarged and it was decided to investigate the effectivenss of existing atomic number and absorption corrections when applied to heavy element analysis, to attempt to improve existing methods and to develop new ones. A major objective was the development of a new and more versatile correction procedure which could be applied to both light and heavy element analysis and to specimens inclined to the incident electron beam. The latter featurewas regarded as being particularly important since many scanning electron microscopes possessing inclined specimen geometry are fitted with microanalysis attachments.

In order to facilitate the presentation of this work it is useful at this stage to examine the physical bases of the individual correction factors and these are described in the following section.

2. Physical Basis of the ZAF Correction Procedure for Electron Probe Microanalysis

In quantitative electron probe microanalysis it is usual to compare the X-ray emission from an element (A) in the specimen (AB) with that from a reference standard which, for convenience, is generally the pure element A. To a first approximation we may then write $k_A = C_A$, where k_A is the measured X-ray intensity ratio and C_A is the weight concentration of A in AB. This simple procedure is frequently subject to large errors, however, particularly if the specimen and standard differ markedly in chemical composition, and in some cases discrepancies may amount to several hundred percent. Thus, in order to convert measured intensity ratios into true weight concentrations the previously mentioned correction factors must be used.

The underlying principles involved in applying appropriate correction factors may be understood by considering the X-ray generation and absorption processes which occur in the target material. This may be best explained by examining how the number of X-rays generated varies as a function of depth, z, in the specimen. Typical X-ray distribution profiles from a light and a heavy element are shown in figure 1. The initial rise in the curve is due to two factors:

(a) the efficiency of inner shell ionisation production increases as the incident electron energy drops to a value $\sim$ twice the critical ionsiation potential, E_C (i.e. at an overvoltage U given by $E/E_c \approx 2$). This is illustrated in figure 2 where Q, the ionisation cross section, is plotted as a function of overvoltage.

(b) the electron path length through each elemental layer, Δz, in the sample increases with depth due to elastic scattering of the incident electrons by the atomic nuclei of the target material; hence the probability of X-ray excitation increases

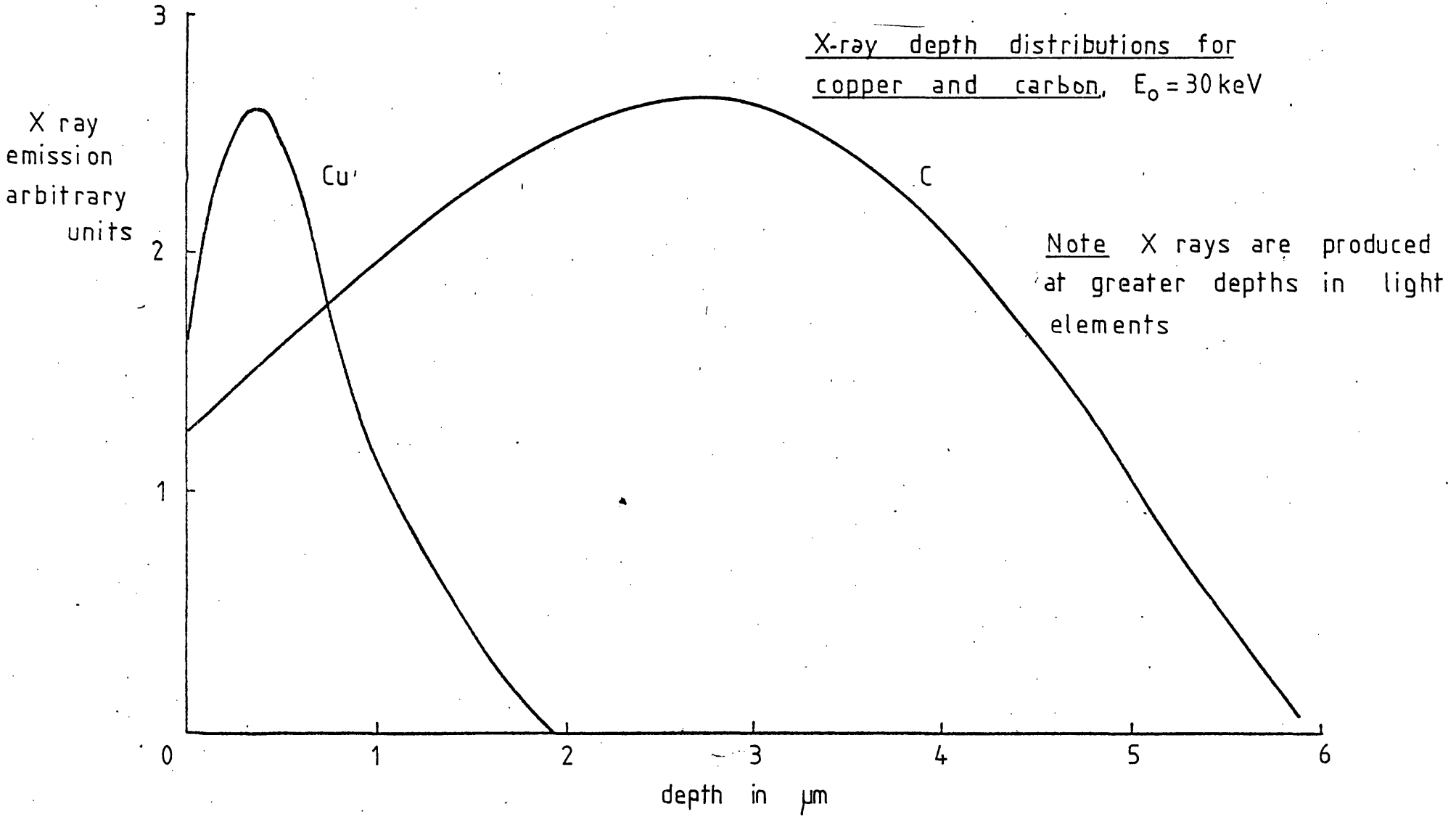
X-ray depth distributions for copper and carbon, $E_o = 30$ keV
X ray emission arbitrary units
Cu
C
Note X rays are produced at greater depths in light elements
3
2
1
0
1
2
3
4
5
6
depth in μm

figure 1

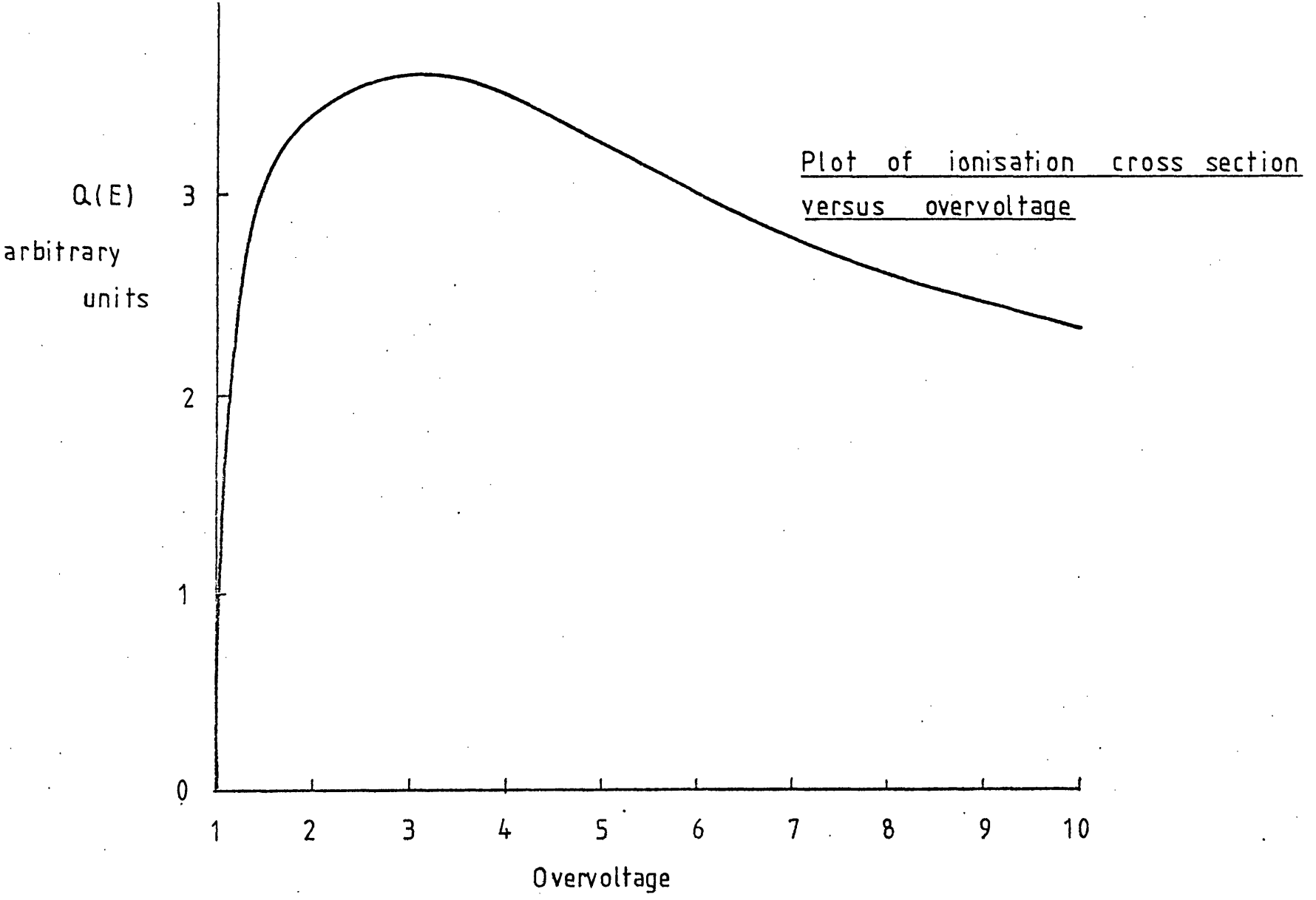

Plot of ionisation cross section versus overvoltage

figure 2

accordingly. The effective path length continues to get larger until the depth of complete diffusion is reached, i.e. the depth at which the electron trajectories may be considered as entirely random and therefore independent of the incident electron beam direction.

At greater depths the X-ray production begins to fall, firstly because there are fewer electrons reaching these levels and, secondly, because many electrons will have energies $< 2E_c$ and will therefore be either less effective or incapable of producing ionisations of the atom core level. The peak in the X-ray depth distribution occurs at smaller depths in heavy elements because, owing to the greater probability of elastic scattering, the diffusion depth is reached more quickly.

X-ray depth profiles are usually known as $\Phi(\rho z)$ curves and the distributions are expressed as a function of mass depth, ρz, in the specimen. One reason for this is that the X-ray emission is a function of the number of atoms of a particular type in the specimen and consequently ρz is a more fundamental parameter than z. In such distributions the X-ray intensity axis is normalised by comparing the X-ray emission from a layer $\Delta\rho z$ at thickness ρz in the bulk specimen with that from an isolated thin film of the same mass thickness. The procedure enables theoretical distributions to be readily compared with those obtained from direct experimental measurement. From the typical $\Phi(\rho z)$ curves shown in figure 3 it can be seen that the value at the surface $\Phi(0)$, is greater than unity. This is because in the bulk specimen backscattering of the electrons from deeper layers contributes to X-ray emission from the surface regions.

The number of X-rays emitted, I_e, may be determined directly from the $\Phi(\rho z)$ curve and is given by

$$I_e = \Phi(\Delta\rho z)\int_0^\infty \Phi(\rho z)\, \exp(-\chi\rho z)\, d\rho z \qquad - (1)$$

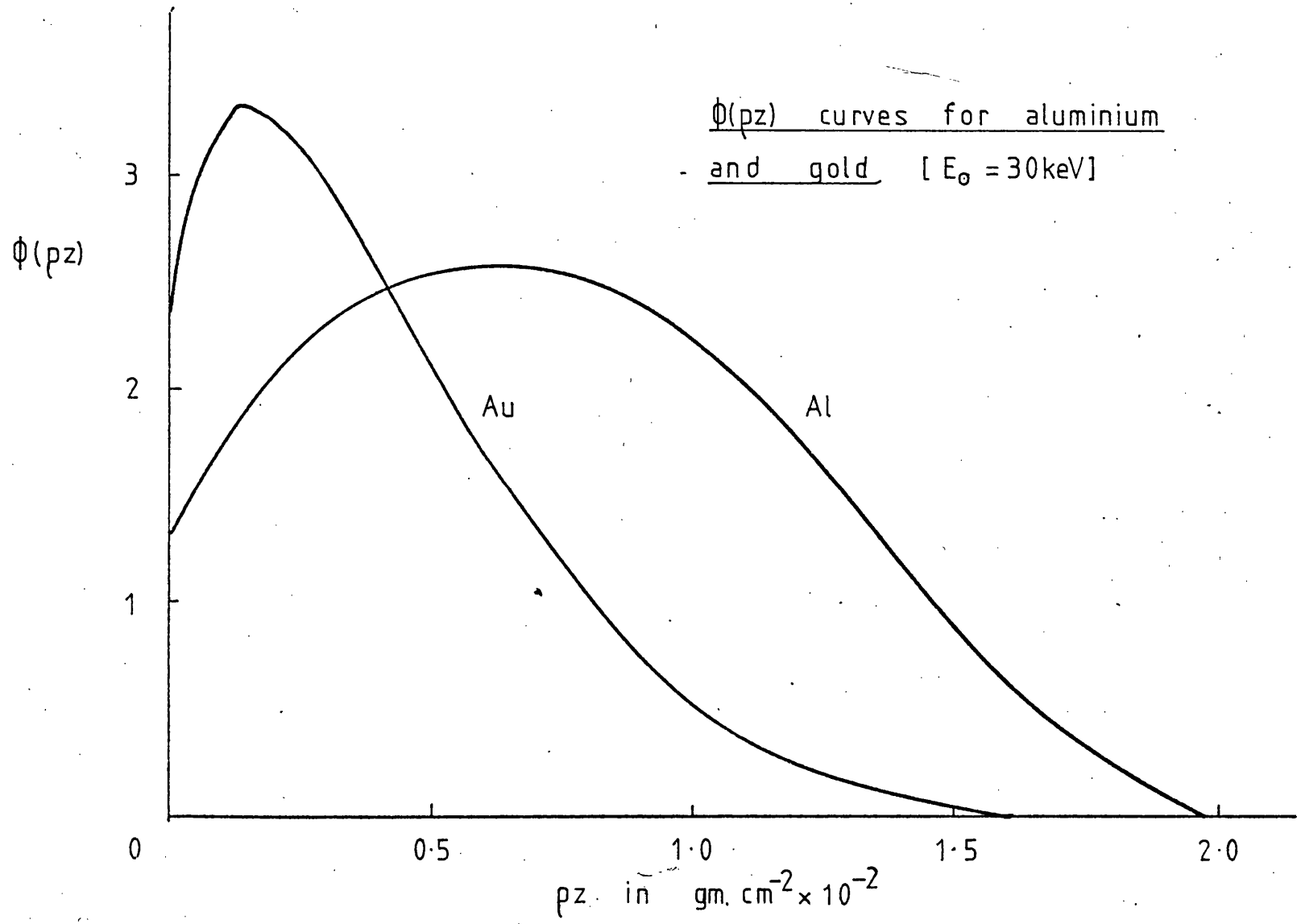
Φ(pz) curves for aluminium and gold [E_o = 30keV]
Φ(pz)
3
2
1
0
Au
Al
0·5
1·0
1·5
2·0
pz in gm. cm^{-2} × 10^{-2}

figure 3

$\Phi(\Delta\rho z)$ corresponds to the emission from the isolated thin film of mass thickness $\Delta\rho z$ and $\exp(-\chi\rho z)$ is the term introduced to take into account the absorption of X-rays in the specimen; $\chi = (^{\mu}/\rho)$ cosec θ, $^{\mu}/\rho$ is the mass absorption coefficient for the X-ray line of interest and θ is the X-ray take off angle. Equation (1) may be rewritten in the following form

$$I_e = \Phi(\Delta\rho z)\int_o^\infty \Phi(\rho z)\, d\rho z \left[\frac{\int_o^\infty \Phi(\rho z)\exp(-\chi\rho z)\, d\rho z}{\int_o^\infty \Phi(\rho z)\, d\rho z}\right] \quad -(2)$$

The expression $\Phi(\Delta\rho z)\int_o^\infty \Phi(\rho z)\, d\rho z$ corresponds the number of X-rays generated in the specimen and is related to its atomic number. The remaining terms correspond to the fraction of generated X-rays travelling at an angle θ to the specimen surface which are emitted; this is therefore the absorption factor and it is denoted by $f(\chi)$ $\left[f(\chi)=\frac{\int_o^\infty \Phi(\rho z)\exp(-\chi\rho z)d\rho z}{\int_o^\infty \Phi(\rho z)\, d\rho z}\right]$

If the X-ray emission from the specimen AB is compared to that from a pure element standard, A, we obtain

$$\frac{(I_e)_{AB}}{(I_e)_A} = k_A = \frac{\Phi(\Delta\rho z)^A_{AB}}{\Phi(\Delta\rho z)^A_A} \cdot \frac{\int_o^\infty \Phi(\rho z)_{AB}\, d(\rho z)_{AB}}{\int_o^\infty \Phi(\rho z)_A\, d(\rho z)_A} \cdot \frac{f(\chi)^A_{AB}}{f(\chi)^A_A}$$

$$= \frac{\Phi(\Delta\rho z)^A_{AB}}{\Phi(\Delta\rho z)^A_A} \cdot Z \cdot A$$

where Z is the atomic number correction and A the absorption correction. It may be shown that $\frac{\Phi(\Delta\rho z)^A_{AB}}{\Phi(\Delta\rho z)^A_A} = C_A$, where C_A is the true weight concentration of A in the specimen. Now, in the preceeding discussion we have only considered direct emission of X-rays by electrons but there

may be an additional contribution due to secondary emission caused by X-rays (fluorescence). Thus we may write

$$k_A = C_A \, Z.A.F.$$

where F is the factor introduced to account for the effects of fluorescence. Hence atomic number, absorption and fluorescence effects may be calculated separately and then combined in the manner shown to provide a complete correction procedure for quantitative electron probe microanalysis.

The fluorescence term will not be considered further since it is almost always the smallest of the correction factors and in light element analysis may be ignored altogether. Moreover existing methods of Reed (1965) for characteristic fluorescence and Springer (1967) for continuous fluorescence appear to be quite adequate in cases where such corrections are necessary.

However, in the following sections the more significant atomic number and absorption corrections will be discussed in some detail. It is usual to deal with the atomic number correction first because it concerns the X-ray generation process but from the point of view of the way in which the research programme developed it is convenient to begin with a discussion of absorption.

2.1 The Absorption Correction

As mentioned earlier, in order to calculate the absorption term the X-ray depth distribution must be known. Experimental data were first obtained by Castaing (1960) using a tracer technique. This permitted $\Phi(\rho z)$ curves to be constructed for a very restricted range of elements and incident electron energies. Using these data $f(\chi)$ curves (see figure 4) were plotted for the limited range of data available and the earliest absorption corrections were obtained by reading the $f(\chi)$ values directly from the appropriate curve. However the procedure was

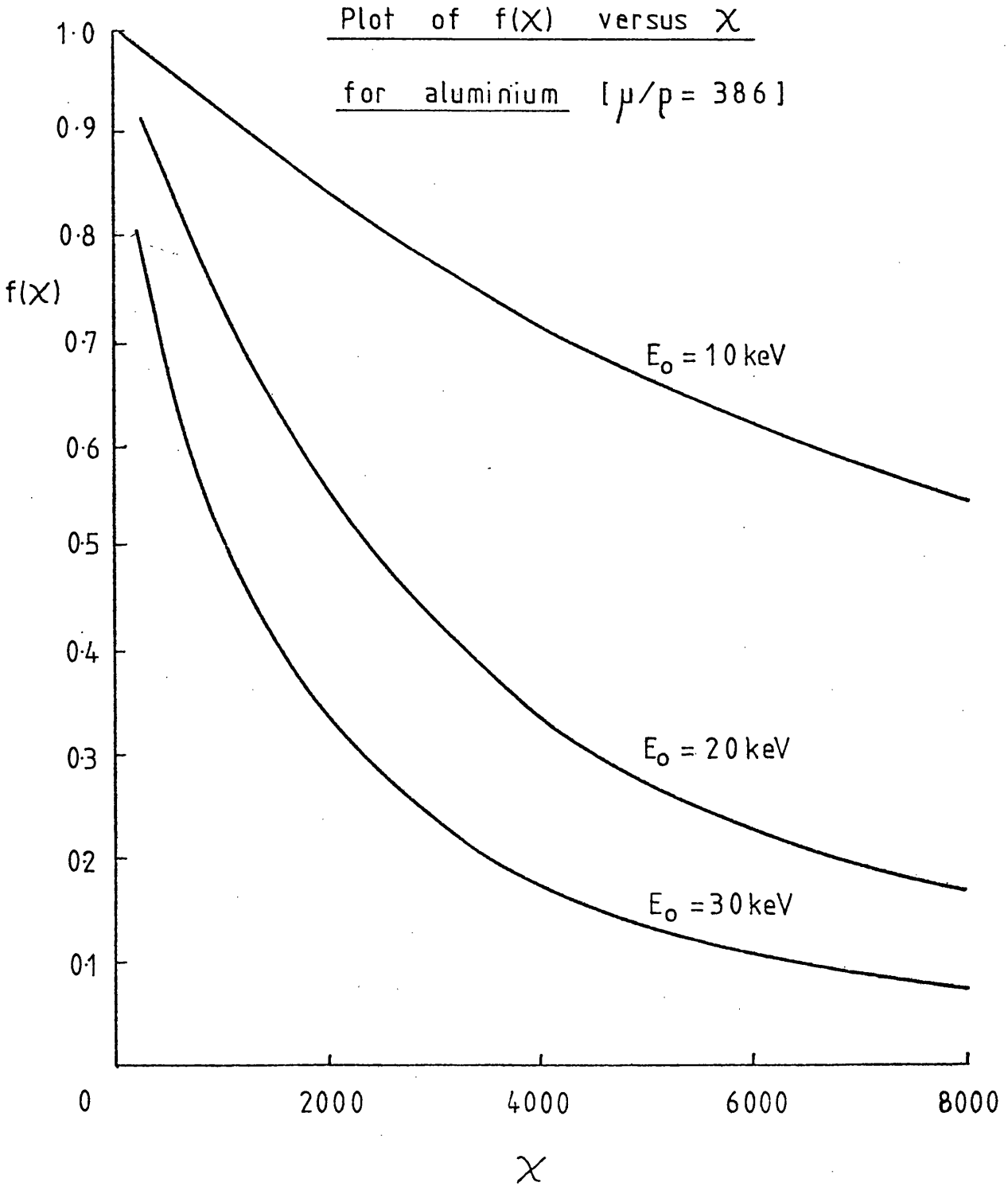
Plot of f(X) versus X
for aluminium [μ/ρ = 386]
1·0
0·9
0·8
f(X)
0·7
0·6
0·5
0·4
0·3
0·2
0·1
0
2000
4000
6000
8000
X
E_o = 10 keV
E_o = 20 keV
E_o = 30 keV

figure 4

not satisfactory because of the inaccuracies introduced by interpolation and extrapolation of the available data.

It is clearly desirable to obtain $\Phi(\rho z)$ curves by considering the physical processes involved in electron excited X-ray emission and one of the first of these approaches was that developed by Philibert (Philibert 1963) which, with certain modifications, is still widely used today. Philibert's original intention was to obtain an all-embracing correction method which could account for both atomic number and absorption effects. He assumed that the number, $n_{\rho z}$, of electrons reaching mass depth ρz in the sample could be described by the electron attenuation law of Lenard.

$$n_{\rho z} = n_o \exp(-\sigma \rho z), \text{ where } n_o$$

is the number of incident electrons and σ is a constant (Lenard's coefficient) for a particular incident electron energy.

The effective path length of the average incident electron in a layer $\Delta\rho z$ is assumed to increase from a value $R(o).\Delta\rho z$ at the surface to a maximum of $R_\infty.\Delta\rho z$ at the diffusion depth and thereafter remain constant. The value of R_∞ is taken as 4 since under diffusion conditions α, the angle made by average electron to the layer normal, is 60^o and the number of electrons travelling in the forward direction through the layer is the same as the number backscattered through it. The diffusion depth is determined by Bothe's Law (Bothe 1929) and the effective path length is assumed to increase in an exponential manner until the limiting value is reached. An expression for $\Phi(\rho z)$ may now be constructed incorporating these factors.

$$\Phi(\rho z) = C_A n_o \exp(-\sigma \rho z).\left[R_\infty - (R_\infty - R_o)\exp(-\rho z/h')\right]Q \quad -(3)$$

Q is the ionisation cross section and is a function of electron energy (see figure 2) which, in turn, is dependent upon the distance travelled by the electron. In Philibert's derivation the energy of the electrons

as a function of depth in the specimen has not been considered and this necessitates making the major approximation that the ionisation cross section is independent of electron energy. With this simplification an expression for $F(\chi)$ may be derived from equation 3, where $F(\chi)$ is defined as

$$F(\chi) = \int_0^\infty \Phi(\rho z) \exp(-\chi\rho z)\, d\rho z$$

Because of the approximations in the Philibert treatment however, adoption of this formula resulted in poor agreement with experimental determinations of areas under $\Phi(\rho z)$ curves, i.e. the expression for $F(\chi)$ was not dealing adequately with atomic number effects. Nevertheless, the general shape of the calculated $\Phi(\rho z)$ curves resembled those obtained experimentally and Philibert reasoned that the theory might still be adequate for the formulation of an absorption correction. Hence he derived the following expression for $f(\chi)$

$$f(\chi) = \frac{1 + \left[\Phi(o)h/(4 + \Phi(o)h)\right] \cdot \chi/\sigma}{(1 + \chi/\sigma)\left(1 + h/(1+h) \cdot \chi/\sigma\right)} \qquad - (4)$$

In equation (4) $R(o)$ has been replaced by $\Phi(o)$, the surface ionisation function, since the two are equivalent; h is related to variations in electron scattering with atomic number. The above expression for $f(\chi)$ will throughout this discussion be referred to as the full Philibert absorption correction.

2.1.1. Evaluation of Current Models

Duncumb and Melford (1966) carried out a preliminary investigation of the full Philibert model and adjusted values of the constants h and σ to give the best fit to experimentally determined $f(\chi)$ curves of Castaing (1960) and Green (1963).

The expressions proposed were

$$h = \frac{4.5A}{Z^2} \quad \text{and}$$

$$\sigma = \frac{2.54 \times 10^5}{E_o^{1.5} - E_c^{1.5}}$$

These formulae were employed in research carried out on oxide systems (Love et al 1974b; § 7.4) and it was shown that the full Philibert model was unsatisfactory for use over a wide kilovoltage range (figure 6, Love et al 1974b). This breakdown is due to the fact that the model predicts, firstly, a peak in the $\Phi(\rho z)$ distribution which is too close to the specimen surface and secondly a long exponential tail (figure 6a Love et al 1975b; § 7.6). To improve the effectiveness of the model it was decided to perform a more rigorous evaluation of the σ and h terms than that undertaken by Duncumb and Melford (1966). The difficulty with the method adopted by these authors is that the $f(\chi)$ data of Green are limited both in terms of atomic number and also range of excitation energy. A more effective approach is to examine a wide range of existing microanalysis data and then adjust accordingly the constants in the expressions for σ and h to give the best fit to experimental results.

Subsequently new values for h and σ were proposed (Love et al 1975b; § 7.6)

$$h = \frac{1.5\ A}{Z^2} \quad \text{and} \quad \sigma = \frac{9.5 \times 10^5}{(E_o^2 - E_c^2)} .$$

Adoption of these formulae was found to markedly improve the accuracy of microanalysis data, reducing the standard deviation from $\sim$ 9% to $\sim$ 6%. The reason for this can be seen by reference to figure 5 in Love et al 1975b (§ 7.6) where predicted $f(\chi)$ values are compared with experimentally determined values for aluminium at 20kV. The new values of σ and h more accurately represent $f(\chi)$ over the whole χ range likely to be experienced in microanalysis.

From a theoretical treatment it was shown that the correct method of averaging h for a multi-element specimen was by atomic averaging and not by weight averaging, the approach most frequently adopted. However, it was found that the accuracy of the corrected data was not sensitive to the way in which h was averaged.

When Philibert derived his expression for $f(\chi)$, data on surface ionisation, $\Phi(o)$, was sadly lacking. He was, however, able to demonstrate that if $\Phi(o)$ was set to zero the expression for $f(\chi)$ could still be used for much microanalysis work providing the values for h and σ were suitably adjusted. The new expression for $f(\chi)$ became

$$f(\chi) = \frac{1}{\left(1+\chi/\sigma\right)\left(1+h/(1+h)\chi/\sigma\right)}$$

and the set of constants in most common usage are those of Heinrich (1967)

$$h = \frac{1.2A}{Z^2} \quad \text{and} \quad \sigma = \frac{4.5 \times 10^5}{E_o^{1.65} - E_c^{1.65}}$$

An evaluation of this model on the oxide system (Love et al 1974b; § 7.4) showed quite clearly that it was totally unsuitable for light element analysis particularly at high kilovoltages where absorption is large. This is because under these experimental conditions most of the X-ray emission arises in the immediate surface regions of the specimen and, consequently, setting the surface ionisation function to zero is no longer valid. A similar regression analysis to that described for the full Philibert model was undertaken (Love et al 1975b; § 7.6) on the heavy element systems and it was shown that the use of the following h and σ values reduced the standard deviation from $\sim 7\frac{1}{2}\%$ to $\sim 6\%$

$$h = \frac{0.85A}{Z^2} \quad \text{and} \quad \sigma = \frac{6.8 \times 10^5}{E_o^{1.86} - E_c^{1.86}} .$$

2.1.2 Development of a New Model

It is worthwhile at this point to consider what properties a good absorption model should possess and this may be accomplished by examining the cases of high and low absorbing systems. If χ is small the exponential term in the expression for $f(\chi)$ may be expanded to give

$$f(\chi) = \frac{\int_o^\infty \Phi(\rho z)\ (1 - \chi.\rho z)\ d\rho z}{\int_o^\infty \Phi(\rho z)\ d\rho z}$$

$$= 1 - \chi \cdot \frac{\int_o^\infty \Phi(\rho z)\ \rho z\ d\rho z}{\int_o^\infty \Phi(\rho z)\ d\rho z} .$$

This may be written

$f(\chi) = 1 - \chi.\overline{\rho z}$, where $\overline{\rho z}$ is the first moment of the $\Phi(\rho z)$ distribution and is the mean depth of X-ray emission (i.e. the average depth at which X-rays are produced). For the case of a high absorber it has been shown (Love et al 1974a; § 7.3) that $f(\chi)_{\chi \to \infty} \propto \frac{1}{\chi}$. Any valid absorption model should predict the above limiting behaviour.

Recently Bishop (1974) has proposed a very much simplified profile for the $\Phi(\rho z)$ distribution which satisifes both these criteria. The form that this takes is shown in figure 1, Love et al 1976a (§ 7.7). The X-ray distribution is assumed to be constant with depth until twice the mean depth of X-ray generation, $\overline{\rho z}$, is reached; thereafter the generation is assumed to be zero. This results in a simple formula for $f(\chi)$ given by

$$f(\chi) = \frac{1}{2\chi\ \overline{\rho z}}\left[1 - \exp\ (-\ 2\chi\ \overline{\rho z})\right]$$

In order to test the model some expression for $\overline{\rho z}$ is required. It is possible to derive this from the simplified Philibert equation and one obtains

$$\overline{\rho z} = \frac{(1+2h)}{(1+h)\sigma}$$

At first sight it may appear unreasonable to use an expression derived from the simplified Philibert model in view of the reservations expressed earlier

However, no other formula for the mean depth existed at this time and so the Philibert expression was adopted purely as an interim measure. This course of action was also justified on the basis that the Philibert's model works fairly well for the low absorbing systems, where the mean depth is the dominant factor, and only breaks down for moderate and heavy absorbers where the shape function and the surface ionisation term become important.

Because, as mentioned previously, the h and σ factors have lost much of their physical significance it is necessary to carry out an optimisation process to determine the most appropriate values for use in the Bishop model, and the results of this are described in Love et al (1975a and 1976b; §7.7 and §7.8). It was shown that for hard X-rays the Bishop model is comparable to the simple Philibert method, but it is much better for soft X-ray analysis. The model is also superior to the full Philibert method for hard X-rays and only slightly inferior for soft x-rays. Bishop's approach therefore combines the best features of both Philibert models and might be further improved if a more rigorous expression for the mean depth can be established.

One way in which this can be achieved is by use of Monte Carlo techniques, because such an approach is not limited by experimental difficulties.

In Monte Carlo models individual electron trajectories are simulated in order to obtain a picture of the electrons in the target in terms of their energy, position and direction. From a knowledge of the ionisation cross section the X-ray distribution may then be evaluated.

A computer programme was written (Love et al 1977a; § 7.10) which was based upon a Monte Carlo model of Curgenven and Duncumb (1971) but which incorporated new developments to facilitate its use over a wide range of conditions. Before new data can be extracted from such a model however it is essential to make comparisons with experiment to ensure that the various electron scattering and energy loss laws incorporated within the model are sufficiently realistic. Results were therefore compared with experimental data on both backscattered electron energy and $\Phi(\rho z)$ distributions and agreement was shown to be very good (Love et al 1977a; § 7.10).

Having established the validity of the Monte Carlo method it was employed to derive a new expression for the mean depth of X-ray generation, which shows how this parameter depends upon atomic number, overvoltage and excitation energy

$$\overline{\rho z} = \frac{\rho s_m \, (0.49269 - 1.09870\eta + 0.78557\eta^2) \, \ln U_o}{0.70256 - 1.09865\eta + 1.00460\eta^2 + \ln U_o} \qquad -(5)$$

U_o is the overvoltage given by E_o/E_c, η is the backscatter coefficient and ρs_m is the total path length of the electron. Both these latter parameters are dealt with more fully later in the discussion of atomic number effects (§ 2.2). The above formula may now be incorporated into the absorption correction model of Bishop (1974) and the results of so doing are described in § 2.3 and Love and Scott 1978 (§ 7.14)

2.2 The Atomic Number Correction

As mentioned earlier this correction arises because the ratio of the number of X-rays *generated* in the specimen (AB) to those *generated* in the reference standard (A) will not equal the weight concentration, C_A, if the specimen and standard differ appreciably in atomic number. The amount of characteristic X-radiation generated in a specimen will be dependent upon the following factors.

a. the number of electrons incident upon the specimen per second, n_o,

b. the incident electron energy, E_o,

c. the number of atoms per unit volume of the element being analysed, $\frac{N\rho}{A_A}$; where N is Avogadro's number, ρ is the density and A_A is the atomic weight of element A.

d. the ionisation cross section, Q, for the particular X-ray shell under consideration

e. the fluorescent yield, ω, for the appropriate X-ray shell, i.e. the probability that ionisation of the shell will result in X-ray emission.

f. the transition probability, ρ, which is the fraction of the characteristic X-radiation resulting from transitions to the ionised inner electron shell corresponding to the X-ray line being measured.

For the purposes of argument we shall consider K_α X-ray emission. Then the intensity of K_α X-ray generation, I_{K_α}, is given by

$$I_{K_\alpha} = \rho_{K_\alpha} \left(\rho \frac{N}{A_A}\right) C_A \, n_o R_{AB} \int_o^{s_c} Q(E) \, ds$$

R_{AB} is a factor introduced to account for losses in X-ray generation due to electron backscattering, s is the path length of the electron and

s_c the distance over which the electron is capable of producing characteristic X-radiation.

The above equation may be rewritten to give

$$I_{K_\alpha} = \rho K_\alpha \omega_K \left(\frac{N}{A_A} C_A n_o \right) R_{AB} \int_{E_o}^{E_c} \frac{Q(E)}{dE/d\rho s} dE \quad -(6)$$

or $$I_{K_\alpha} = C_A \rho_{K_\alpha} \omega_K \left(\frac{N}{A_A} \right) n_o \frac{R_{AB}}{S_{AB}}$$

where $$\frac{1}{S_{AB}} = \int_{E_o}^{E_c} \frac{Q(E)}{\left(dE/d\rho s\right)_{AB}} dE \quad -(7)$$

It is usual practice to consider the backscatter factor, R, and the penetration factor, S, separately.

2.2.1. The Penetration Factor

The most commonly used expression for Q(E) is the Bethe(1930) formula modified by Green and Cosslett (1961),

$$Q(E) = \frac{\text{const}}{E_c^2} \frac{\ln U}{U} \quad -(8)$$

and the general shape of this function is shown in figure2.The term $dE/d\rho s$ in equation (6) corresponds to the rate at which the electron loses energy. In all practical microanalysis procedures the electron energy loss is assumed to be a continuous process but this is not true in practice because the electron loses energy in discrete amounts as it interacts with the orbital electrons of the target atoms. However large energy transfer involving K shell ionisations are comparatively rare events (Reed 1975) and hence the approximation may be considered reasonable. An expression for $dE/d\rho s$ has been given by Bethe (1930).

$$\frac{dE}{d\rho s} = -\text{const}\ \frac{Z}{A}\ .\ \ln\left(1{\cdot}166\ \frac{E}{J}\right) \qquad - (9)$$

where J is the mean ionisation potential. Many formulae for J exist and it is not clear which, if any, are correct. Probably the one most frequently employed is an empirical expression proposed by Duncumb and Da Casa (1967),

$$J = \left[14Z.(1 - \exp(-0.1Z)) + 75.5Z/Z^{Z/7{\cdot}5} - Z^2/(100 + Z)\right]$$

which was intended for use in the Duncumband Reed atomic number correction (Duncumb and Reed 1968).

It may be seen that the insertion of equations (8) and (9) into (7) result in a very complex expression which can only be evaluated using logarithmic integrals (Philibert and Tixier 1968)

A rigorous examination of the Philibert and Tixier method has been carried out (Love et al 1975b; §7.6) but it was found to give little, if any, improvement when compared with the simplified approach of Duncumb and Reed (1968). In their method these authors assume that the ratio of $^{dE}/_{d\rho s}$ for specimen to standard is approximately constant over the electron range. This is a reasonable assumption since the only variation is due to the slowly changing logarithmic term in equation (9). Thus when taking ratios for specimen to standard the approximationleads to

$$\frac{\int_{E_o}^{E_c} \frac{Q(E).dE}{(dE/d\rho s)_{AB}}}{\int_{E_o}^{E_c} \frac{Q(E).dE}{(dE/d\rho s)_{A}}} = \text{const}\frac{(dE/d\rho s)_A}{(dE/d\rho s)_{AB}}$$

and the exact form of the ionisation cross section is not required.

Previous work (Love et al 1975b; §7.6) showed however that the atomic number correction of Duncumb and Reed is not entirely satisfactory

when used at low overvoltages ($U_o < 2$) and these are usually associated with low electron energies. One of the principal reasons for this is that the Bethe energy loss equation gives unrealistic results at low electron energies. The equation predicts that $dE/d\rho s$ becomes zero when $E = J/1.166$, whereas $dE/d\rho s$ should increase more or less continuously as the electron energy decreases, becoming infinite as $E \to 0$.

A new energy loss equation was therefore developed in order to overcome this limitation (Love et al 1978a; § 7.12). It was shown that if the variable in the Bethe formula was changed from E to E/J, $d\rho s/dE$ could be expressed as a polynominal in $(E/J)^{\frac{1}{2}}$. The expression was adjusted so that a graph of $d\rho s/dE$ versus E/J passes through the origin in accordance with reality, figure 5. The following energy loss low was derived

$$dE/d\rho s = -\frac{1}{J}\ \frac{Z}{A}\ \frac{1}{1.18 \times 10^{-5}(E/J)^{\frac{1}{2}} + 1.47 \times 10^{-6}(E/J)} \qquad -(10)$$

which is in excellent agreement with the Bethe formula for values of $E/J > 9$ and possesses the correct limiting behaviour as discussed above. An additional advantage of the new approach is that $\int_{E_o}^{E_c} \frac{Q}{dE/d\rho s} \cdot dE$ may readily evaluated without making any approximations, to give

$$\frac{1}{S} = \left[1 + 16.05 \left(\frac{J}{E_c}\right)^{\frac{1}{2}} \left(\frac{U_o^{\frac{1}{2}} - 1}{U_o - 1}\right)^{1.07}\right] \Bigg/ \sum \frac{C_i Z_i}{A_i}$$

(terms which cancel when calculating the ratio S_{AB}/S_A have been omitted from the above equation). Furthermore, an analytical expression for the total electron range, ρs_m, can be obtained by direct integration of equation (10)

$$\rho s_m = \frac{A}{Z}\ (0.773 \times 10^{-5}\ J^{\frac{1}{2}}\ E_o^{3/2} + 0.735 \times 10^{-6} E_o^{2})$$

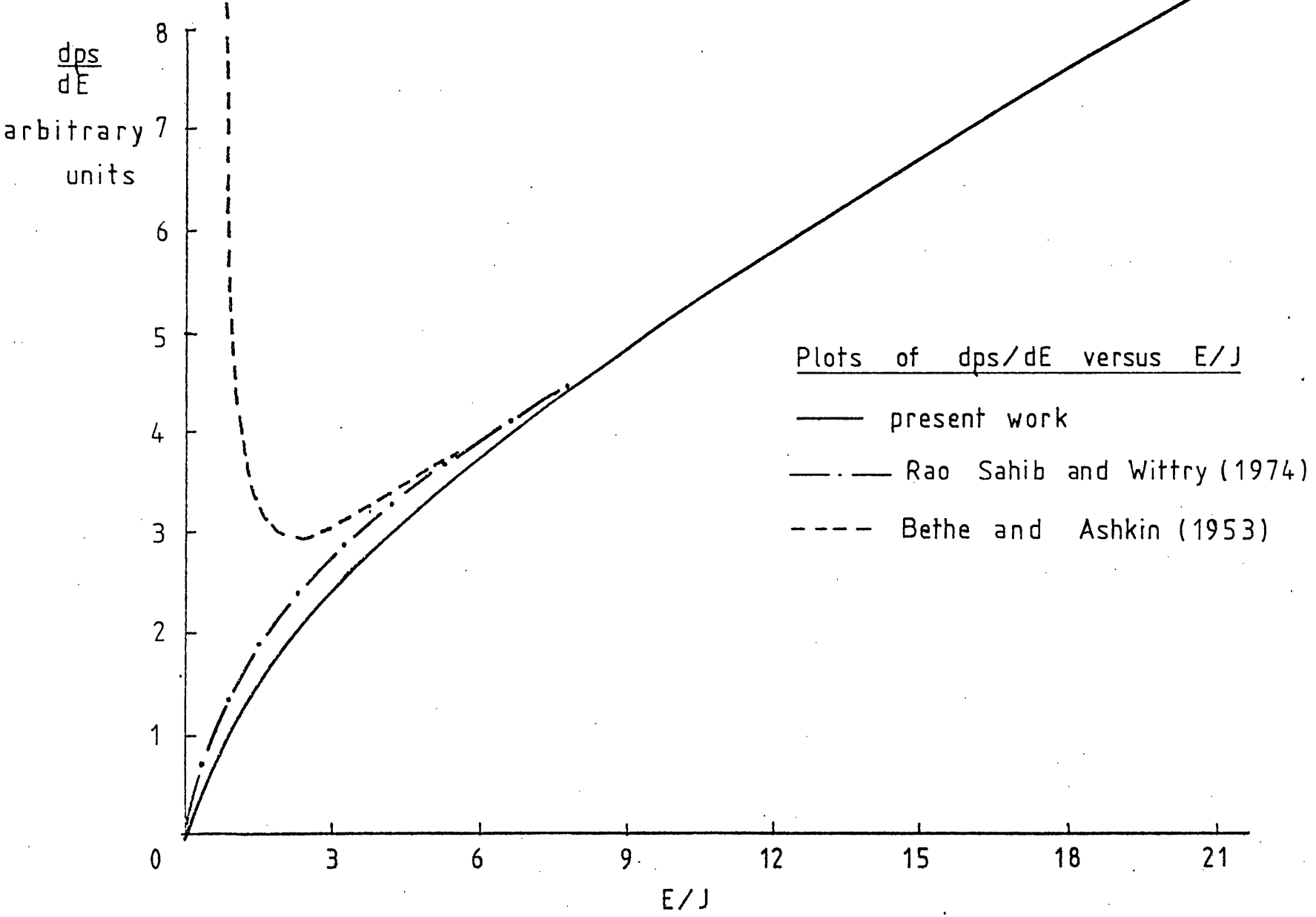
dps/dE
arbitrary units
8
7
6
5
4
3
2
1
0
3
6
9
12
15
18
21
E/J
Plots of dps/dE versus E/J
present work
Rao Sahib and Wittry (1974)
Bethe and Ashkin (1953)

figure 5

Such an expression is necessary in order to determine the mean depth of X-ray emission using equation (5) (see previous discussion, §2.1.2).

2.2.2. The Backscatter Factor

When a specimen is irradiated by a beam of high energy electrons a certain fraction, η, is backscattered from the sample. The fraction increases with atomic number because the probability of large angle elastic scattering is greater for heavy elements. To a first approximation η is independent of the incident electron energy although variations become marked for electron energies < 5 keV (Bishop 1966, Darlington and Cosslett 1972). In addition, the shape of the backscattered electron energy distribution is largely electron energy independent. Typical energy distributions are shown in figure 6. The horizontal axis is normalised to the incident electron energy E_o and the vertical axis represents the fraction of the backscattered electrons which have energies between E and E + ΔE. Some of the electrons which are backscattered would have produced characteristic X-rays had they remained in the specimen (i.e. they have an energy $E > E_c$) and consequently backscattering results in a loss of characteristic X-ray generation. The magnitude of the effect may be calculated as follows. If the group of electrons backscattered with energies between E and E + ΔE are considered (by definition $^{d\eta}/_{dW} \cdot dW$ where $W = {}^{E}/_{E_o}$) it may be seen by comparison with equation (6) that the loss in generated X-ray intensity is I_B where

$$dI_B = \text{const} \frac{d\eta}{dW} \cdot dW \int_{E_c}^{E} \frac{Q}{{}^{dE}/_{d\rho s}} dE$$

Thus integration over the whole backscattered electron energy distribution for $E > E_c$ gives the total loss in X-ray emission due to backscattering

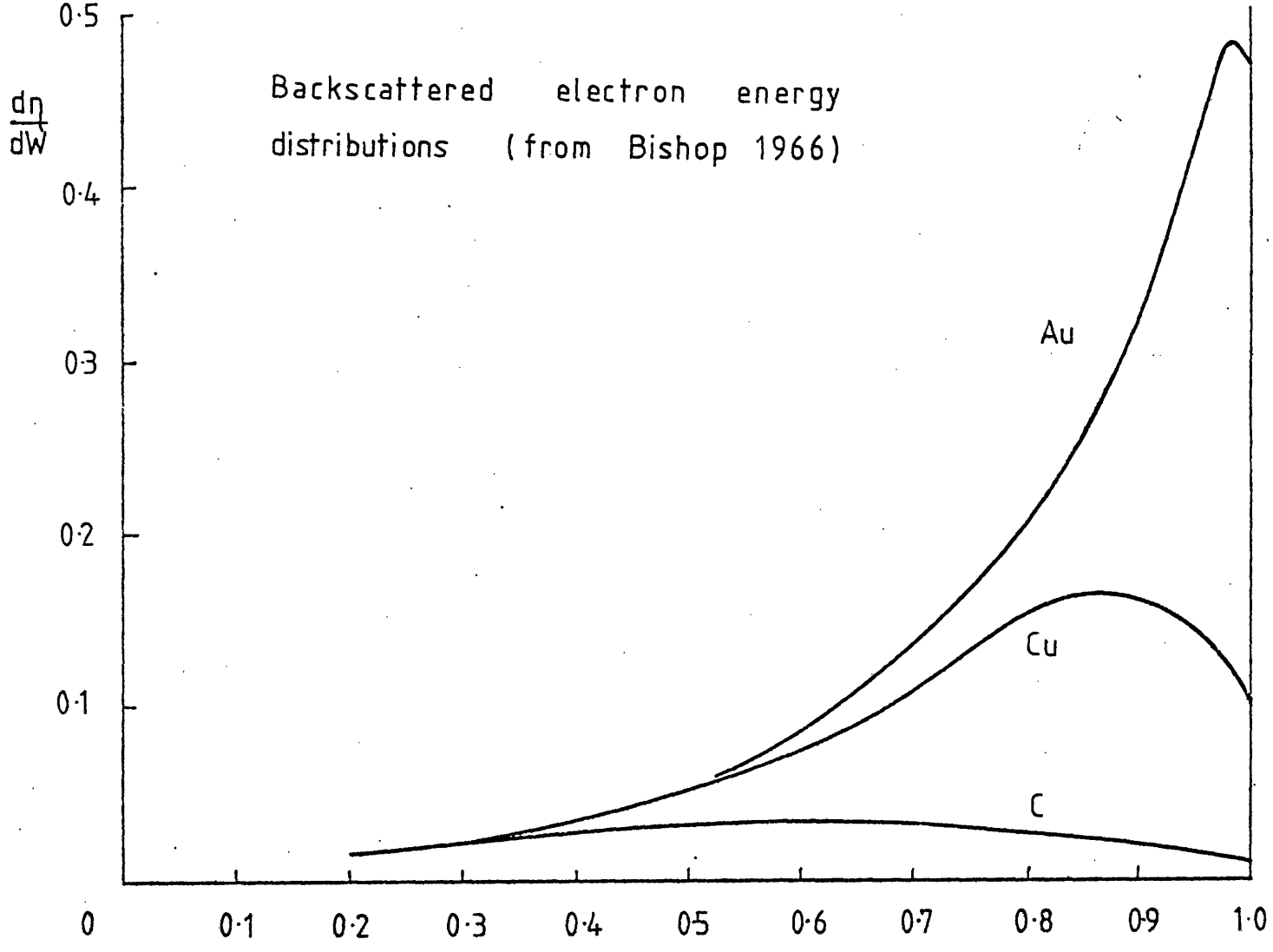
Backscattered electron energy distributions (from Bishop 1966)
dη/dW
0·5
0·4
0·3
0·2
0·1
0
0·1
0·2
0·3
0·4
0·5
0·6
0·7
0·8
0·9
1·0
W = E / E₀
Au
Cu
C

figure 6

$$I_B = \text{const} \int_{W_c}^{1} \frac{d\eta}{dW} \int_{E_c}^{E} \frac{Q}{dE/d\rho s} \, dE.dW$$

where $W_c = E_c/E_o$.

Now the fractional energy loss due to backscattering is equal to the X-ray intensity lost(I_B) divided by the X-ray intensity which would have been produced in the absence of backscattering (I_o)

$$\frac{I_B}{I_o} = \frac{\int_{W_c}^{1} \left(\frac{d\eta}{dW}\right) \int_{E_c}^{E} \left(\frac{Q}{dE/d\rho s}\right) dE.dW}{\int_{E_o}^{E_c} \frac{Q}{dE/d\rho s} . dE} \qquad -(11)$$

The fraction of X-rays generated in the specimen is given by $1 - I_B/I_o = R$ -(12) where R is the backscatter factor.

Salter (1970) has tabulated R data as a function of Z and W_c; since R is almost linearly dependent upon W_c for a given Z, values not given in the table may be obtained by linear interpolation. These tabulations were calculated from equations (11) and (12) using Bishop's data (1966) for both η and the electron energy distributions. They appear to give reasonable results for most microanalysis work but errors may become unacceptably large at low kilovoltages because the η values for Bishop are only applicable for 20 keV electrons and, as discussed previously the backscatter coefficient is energy dependent. Hence difficulties arise in light element analysis where it is necessary to use low electron energies in order to minimise X-ray absorption and increase detection efficiency.

As a result of this limitation work was undertaken to derive an analytical expression for R (Love et al 1978a; § 7.12). This utilised the Monte Carlo method referred to in § 2. 2. The formula for R includes terms

to account for overvoltage and backscatter coefficient.

$$R = 1 - \eta \left[I(U_o) + \eta\, G(U_o) \right]^{1.67}$$

where $I(U_o) = 0.33148\ \ln U_o + 0.05596\ (\ln U_o)^2 - 0.06339\ (\ln U_o)^3$

$$+ 0.00947\ (\ln U_o)^4$$

and $G(U_o) = \frac{1}{U_o} \left[2.8789\ \ln U_o - 1.51307\ (\ln U_o)^2 + 0.81312 (\ln U_o)^3 - 0.08241 (\ln U_o)^4 \right]$

Hence by selecting η values which are appropriate to the kilovoltage being used the expression can be applied to any probe excitation energy. An additional advantage of the method is that it may be used for targets at non-normal incidence. This is because the R factor for an inclined target will be the same as that for a specimen normal to the electron beam with the same η value as the inclined specimen. Thus R for any sample inclination may be calculated directly providing the correct value of η is inserted into the formula. There is no difficulty in carrying this out in practice because Darlington (1975) has provided an expression to calculate backscatter coefficients for inclined specimens if η at normal incidence is known.

2.3 Evaluation of the New Correction Procedure

The atomic number correction described in § 2.2 and the Bishop absorption correction incorporating the new expression for the mean depth of X-ray emission have been combined to form a complete correction procedure. Also included is the characteristic fluorescence correction of Reed (1965).

Before this model could be used in practice it was necessary to

derive an analytical expression for the backscatter coefficient, η, since this parameter is incorporated in the formulae for the backscatter factor, R, and the mean depth of X-ray generation, $\overline{\rho z}$. This was accomplished by applying a regression analysis technique to data of Seidel (cited in Darlington 1975) which covered a wide range of atomic number (4 - 92) and electron energies (9 - 100 keV).

The following expression was obtained

$$\eta = f_1(Z)\ (1 + f_2(Z)\ \ln\ (E_o/20)) \text{ where}$$

$$f_1(Z) = (-\ 52.3791 + 150.4837\ Z - 1.6737\ Z^2 + 0.00716\ Z^3)\ \times\ 10^{-4}$$

$$\text{and } f_2(Z) = (-\ 1112.8 + 30.298\ Z - 0.15498\ Z^2)\ \times\ 10^{-4}$$

Values of η calculated using the above equation were compared to the original data of Seidel and it was found that the RMS error was 2.3% (Love and Scott 1978; § 7.14) which is as good as the precision of the original measurements. Hence the expression may be used with confidence for incident electron energies in the range 10 - 100 keV. It should however be pointed out that the equation will be less reliable for low electron energies (< 5 keV) since the backscatter coefficient no longer varies smoothly with atomic number (Darlington and Cosslett 1976) and therefore cannot be adequately represented by a polynominal.

The new correction procedure has been applied to the 430 microanalysis measurements described in Love and Scott, 1978 (§ 7.14). It was found that the model was superior to methods which incorporate either of the two Philibert absorption corrections. It is considered that the improvement achieved by the new model is mainly associated with a more accurate absorption correction because absorption is usually the single largest correction factor. To test the accuracy of the new atomic number correction only low absorbing systems ($f(\chi) > 0.8$) were used in the assessment. Comparison of the data corrected by the new model and the

established method (Duncumb and Reed atomic number correction and simplified Philibert absorption correction) again shows that a higher degree of accuracy may be achieved when using the former approach. This indicates that our atomic number correction is better than the Duncumb and Reed approach.

Finally, the new correction model is applied to light element results obtained on oxide systems (Love et al 1974a, § 7.3). Again a higher degree of precision is obtained than achieved previously (see table 3 in Love and Scott 1978; § 7.14) but the number of corrected data lying within 2½% of the true value is only 38% compared with 46% obtained when using the Duncumb and Reed atomic number correction and the full Philibert absorption correction. However, it should also be pointed (see Love et al 1975b; § 7.6) that the full Philibert model gives worse results than the simplified Philibert method when applied to heavy element systems and is, therefore, of limited value in quantitative electron probe microanalysis.

It is considered that errors associated with the 430 binary alloy systems are largely responsible for the 5.3% standard deviation obtained with the new correction model and that new, more reliable, microanalysis data must be collated in order to assess the absolute accuracy of the method.

3. Some Related Quantitative Electron Microscopy Studies

3.1 Oxidation of Orlon Fibres

In section 1 researches into problems involved in the electron probe microanalysis of oxygen in ceramic specimens were described. Studies have also been undertaken on light element microanalysis in polymeric materials and in Love et al 1975a (§ 7.5) a study of the oxidation of polyacrylonitrile fibres is discussed. These fibres are employed as precursors in carbon fibre production and a pre-oxidation treatment is used to raise the softening temperature above the decomposition temperature, thereby preventing fibres sticking together during the subsequent pyrolosis. Microscopic examination of cross-sections of certain grades of fibre (Courtelle) after oxidation had revealed a zoned structure, the extent of the zoning being associated with the length of the oxidation treatment. Commercial fibres of Orlon showed however, no evidence of zoning after similar oxidation treatments.

The objective of subsequent work was to discover whether an oxidation gradient existed across these two types of fibre. Because of the fibre's small cross section ($\sim 2 \times 10^{-4}$ mm^2) determination of diffusion profiles may be best achieved by electron probe microanalysis. A suitable method of specimen preparation for polymers had first to be devised, since these materials are poor thermal and electrical conductors and are often damaged by electron beam irradiation. Several methods were tried, and eventually it was found that thin, 1 μm thick, sections prepared by microtomy gave the best results. These sections were supported on a thin carbon film which in turn was mounted upon a copper grid. The specimen was then coated with 100 Å layer of gold to provide a conducting path for the electrons. Oxygen detection was carried out using a low electron accelerating voltage in order to maximise detection efficiency (Love 1975) and a small specimen current (50 nA) to reduce any specimen damage. The effect of variation of thickness across the fibre section

upon the oxygen emission was minimised by comparing oxygen peak intensity with the continuous background radiation.

From the investigation it was evident that the zoned structure was indeed indicative of a change in oxygen concentration across the section and a mechanism to account for the absence of zoning in Orlon fibres under normal oxidation conditions was proposed.

The study described above was performed by means of wavelength dispersive analysis but a much more extensive study of polymeric materials would be possible if the specimen current could be reduced by an order of magnitude, since in most cases this would solve the problem of beam induced damage. Small specimen currents are adequate for energy dispersive analysis (EDS) and we have carried out a preliminary study on oxygen and carbon analysis of Courtelle fibres using a new form of EDS detector with a removable window. The assessment, which was performed in the United States working in collaboration with Dr Russ, showed that this technique was capable of distinguishing between oxygen levels in the cored and zoned regions (reference to G. Love in Russ 1977).

3.2 Oxide Layers Formed on Metals

Scanning electron microscopy and electron probe microanalysis studies have also been concerned with high temperature oxidation studies on metals and alloys. This research programme was carried out by Dr Cox and my own contribution has been concerned with the characterisation of microstructures. In particular, electron probe microanalysis has been used to investigate the distribution in the oxide scale of different alloying additions in steel (Cox, Love, McEnaney and Scott 1973, § 7.2). This study led to a new theory of element partitioning in oxide scales (Cox, McEnaney and Scott 1972) which is believed to have more universal application than previous theories. Other aspects of metal oxidation have involved investigations

of both preferential intergranular oxidation and oxygen distributions in stripped films. The work highlighted the importance of scanning transmission (STEM) studies since it was found that 50 keV STEM images obtained in the electron probe microanalyser provided more information about the duplex oxide film than similar images obtained using 100 keV electrons in the conventional transmission microscope.

3.3 Structural Analysis of Avian Eggshells

Another study involving electron optical techniques was carried out in collaboration with Dr R Board of the School of Biological Sciences and concerned a detailed structural analysis of avian eggshells (Tullett, Board, Love, Perrott and Scott, 1976; § 7.9). The shell itself is composed of calcium carbonate which takes the form of calcite columns growing from a number of nucleation sites on the membrane, radially outwards. The external layer of the shell is, however, different in structure. In the case of the domestic fowl, guinea fowl and greater flamingo it consists of organic material, but in sea birds it was found to be mainly vaterite, another crystalline form of calcium carbonate.

Quantitative electron probe microanalysis in conjunction with wet chemical analysis indicated that the phosphorus levels were higher in the external layer for all shells studied although the effect was not as marked for sea birds. From the results it was proposed that phosphorus poisoning could account for the change in structure of the external layers. In the case of the domestic fowl, guinea fowl and greater flamingo the amount of phosphorus, in the form of phosphate, is sufficient to terminate further growth of calcium carbonate. In the eggshells of sea birds, however, the smaller amount of phosphate can be incorporated into the calcium carbonate lattice although this results in vaterite rather than calcite becoming the stable structure. From this investigation it has been

shown that the presence of vaterite may be related to the physiology of the birds.

3.4 Methods of Foil Thickness Measurement in the TEM

Many of our recent studies using transmission microscopy have been concerned with measurement of defect densities or precipitate populations (Miller and Scott 1978). Although established methods, such as the analysis of extinction contours or measurement of slip traces, are limited in their range of application the addition of STEM and EDS facilities to the conventional transmission microscope have provided techniques of foil thickness measurement which may be more suitable and more accurate for such work. Methods which are being assessed include contamination spot and convergent beam techniques, which may be regarded as absolute methods, and the use of X-ray emission measurements which involve calibration (Love et al 1977; § 7.11).

Specimens of Al-Mg-Zn containing a fine dispersion of precipitates have been employed in this study. From a comparison of the thickness data with corresponding micrographs the accuracy of the various thickness determinations were assessed by plotting the number of precipitates visible in unit area of foil versus foil thickness.

The results showed that the contamination spot technique appeared to overestimate the foil thickness but in the case of Al-Mg-Zn specimens some, if not all, of the discrepancy could be explained on the basis of surface oxidation.

The convergent beam technique is, in principle, the most precise but, from the limited number of measurements we have carried out, a considerable disparity appears to exist between the two sets of data obtained using the convergent beam and contamination methods. In addition extinction distances calculated for aluminium appear to be at variance with those available in the literature.

The relative accuracy of characteristic X-ray measurements seemed to be good ($\sim$ 5%) over a foil thickness range $\sim$ 1000 Å - 3000 Å but the absolute accuracy will, of course, depend upon the calibration method adopted.

From this preliminary study it has been possible to compare the various techniques and to assess the potential areas of application (see table Love et al, 1977; § 7.11). Further work recommended in this area is referred to in a following section (§ 4.2).

3.5 Characterisation of the Prism Surfaces of Kaolinite Microcrystals

The study of Kaolinite microcrystals was carried out in collaboration with Dr Flegmann of the School of Biological Sciences. Kaolinite is a common constituent of soils and the surface chemistry of the constituent particles is of interest because it affects the ability of the soil to retain plant nutrients. It was therefore necessary to establish the crystal indices of the particles' prism surfaces so that this could be related to the surface activity.

Because of the size of the crystals ($\sim$ 0.5 μm) electron diffraction was undertaken to achieve this objective (Flegmann, Love and Scott, 1971; § 7.1). The resulting electron diffraction patterns were complicated by the presence of 'extra' spots but this could be satisfactorily explained by postulating that the crystals consisted of several superimposed thin-layers displaced relative to one another by a fraction of the a or b parameter. This would result in an extension of the reciprocal lattice points into relrods and provide additional intersections of the reciprocal lattice with the Ewald sphere, thus accounting for the extra spots. From the analysis of the diffraction pattern the indices of the prism faces of the crystallites could then be indexed as (010), ($1\bar{1}0$) and (110).

4. Conclusions

A thorough examination of absorption correction models used in electron probe microanalysis has been made. It was shown that on theoretical grounds the most frequently used correction procedure, that due to Philibert (1963), is limited in its range of application and is unsuitable for light element analysis. This was confirmed when the model was applied to soft X-ray data. The more rigorous full Phillibert model was found to work reasonably well for light element analysis but, rather surprisingly, was inferior to the simplified Philibert approach for correcting heavy element data. Optimisation of the h and σ parameters incorporated in each of the models was performed using regression analyses and it was shown that although improvements could be made to the full and simplified Philibert absorption corrections, the basic limitations of both still remain.

Development of a new correction devised by Bishop (1974) was next undertaken. Application of this model to experimental microanalysis data revealed that its range of operation was greater than either of the two Philibert methods. However it was felt that further improvement could be achieved if a more precise expression for the mean depth of X-ray generation could be obtained.

This was done by developing a Monte-Carlo programme which simulates electron interactions in solids. In addition to providing information regarding the mean depth, the model was used to obtain data on the surface ionisation function $\Phi(0)$, a parameter of particular significance in light element analysis, and also on the backscatter factor. An analytical expression has now been developed to represent the backscatter factor in terms of over-voltage and backscatter coefficient. This, together with a new equation to represent the rate of energy loss in a solid, has enabled a new atomic number correction to be constructed. It has several advantages over existing methods since it avoids some of the approximations made in the Duncumb and

Reed (1968) approach and in principle it may be applied to specimens inclined with respect to the incident electron beam.

This atomic number correction has been combined with the Bishop absorption model which incorporates the new equation for the mean depth determined from the Monte Carlo data. The complete correction procedure has been tested by applying it to existing experimental microanalysis data. It was found to be better than any method which incorporated either of the Philibert absorption corrections. Moreover the adoption of the new atomic number correction was found to signifciantly improve the accuracy of the corrected data.

It should also be pointed out that the new model is more fundamental than other correction procedures which incorporate parameters specifically optimised to give the best fit to experimental results.

Studies on the application of quantitative electron probe microanalysis and related techniques such asscanning and transmission electron microscopy have also been described. It has been shown that these methods provide important new information in the fields of both materials and bioligical science.

In additon to the above mentioned studies a detailed assessment of methods of foil thickness measurement has been undertaken. The work carried out to date suggests that recent developments in this area may lead to ways of measuring the thickness of foils more precisely, which in turn would enable measurements on defect populations and precipitate densities to be made more accurately.

5. Recommendations for Further Work

It is suggested that developments in the research should proceed along the following lines in the areas of (a) improved correction theories in electron probe microanalysis and (b) quantitative microstructural analysis in the transmission electron microscope.

5.1 Quantitative Electron Probe Microanalysis

It is possible to use the Monte-Carlo methods developed in this research in order to establish how the mean depth of X-ray generation depends upon the orientation of the specimen with respect to the direction of the incident electron beam. If the dependence can be adequately represented in terms of a simple analytical expression it could be readily incorporated into the Bishop absorption model. The modified model when combined with the new atomic number correction (Love et al, 1978a; § 7.12) would then be capable of coping with any specimen geometry.

Before the proposed correction procedure could be recommended for general use, however, its accuracy would have to be established for a wide range of experimental conditions. In order to achieve this objective it will be necessary to obtain new experimental data by, for example, making measurements on a series of well characterised binary specimens tilted with respect to the incident electron beam.

These measurements would be best carried out using an energy dispersive X-ray analyser for the following reasons:

(a) experimental errors introduced in positioning the specimen would be small whereas wavelength dispersive analysis is extremely sensitive to specimen height variations.

(b) the research would provide information about the precision of analysis achievable with an SEM-EDS combination.

Light element work using an EDS system presents difficulties due to the relatively poor spectral resolution of the analyser and to pulse

pile-up effects. However, our earlier work on polyacrylonitrile fibres has shown that the EDS technique is feasible for soft X-ray studies and warrants further investigation. A pre-requisite for any quantitative light element analysis is an accurate method of background subtraction and existing techniques, such as frequency filtering, which have been successfully employed at higher X-ray energies (> 1 keV) will have to be assessed. This could be achieved by making comparisons between data obtained using both EDS and WDS methods on identical specimens. If successful, such research holds out the prospect of light element analysis on beam sensitive materials and the wider use of EDS systems for soft X-ray measurement.

It is desirable, when analysing for soft X-rays, to minimise the absorption correction in order to reduce errors introduced when using the unreliable mass absorption coefficients presently available. This may be achieved either by tilting the specimen towards the detector or by reducing the energy of the incident electron beam. In many microanalysers there is no facility for tilting specimens in the required direction and hence the latter method must be adopted. Unfortunately from the study on oxide systems it is apparent that there are large errors in the corrected data obtained at these low energies (Love 1975). This suggests that either the atomic number correction is inadequate here or that the conducting coatings used are markedly affecting the electron behaviour in the sample. It is therefore proposed to carry out further measurements using several different coating materials (carbon, aluminium, copper and gold) and a range of coating thicknesses (100 Å - 500 Å). Complementary studies would be carried out using Monte-Carlo methods to obtain a clearer understanding of the effect ofsurface coatings on electron-solid interactions. It is hoped that such an investigation will enable positive recommendations regarding the selection of coating material and thickness to be made. Any defect in the atomic number correction at low

electron energies is likely to arise from the breakdown of the continuous energy loss approximation and here again the effects of this may be determined by recourse to Monte Carlo methods.

As discussed previously in this section much of the proposed research programme on quantitative electron probe microanalysis concerns the development of the Bishop absorption correction for use with tilted specimen geometry. However, the absolute accuracy of the model for normal electron incidence has not been established at this juncture because errors in the raw data employed in its assessment were almost certainly responsible for the 5.3% RMS error obtained (Love and Scott 1978; § 7.14). The extensive new set of experimental measurements obtained from the foregoing investigation should provide data which will enable a more stringent test of the absorption method to be made. If a more exact model proves desirable, which may be the case in view of the simplistic shape function employed in the Bishop correction procedure, the method outlined by Love (1975) could be investigated. This should, in principle, be superior to that of Bishop since the $\Phi(\rho z)$ curve is more accurately represented. The model requires a total of four input parameters, these being $\Phi(max)$, the mass depth corresponding to $\Phi(max)$, the surface ionisation function and the mean depth. Development of this model is being undertaken and expressions for the mean depth (Love et al 1977; § 7.10) and the surface ionisation function (Love et al 1978b; § 7.13) are available. All that is now needed are equations to represent the remaining two parameters in terms of the backscatter coefficient and overvoltage and this can be accomplished using existing Monte-Carlo methods. It should be stressed that the 'triangular model' would not replace the Bishop procedure entirely since it could not be readily modified to deal with specimens at non-normal electron incidence.

5.2 Quantitative Microstructural Analysis

Some useful data on defect populations in thin foils have been obtained but the accuracy of film thickness measurement must be further improved before the information can be used to develop appropriate theoretical models. Thus the film thickness techniques employed need to be refined and their reliability assessed.

The difficulty with the contamination spot method lies in locating corresponding points of contamination on top and bottom of the foil which give the correct measurement of spot separation; practical difficulties are increased because the two spots have different geometry. Experiments should therefore be carried out to analyse the profile of the spot as a function of the electron beam conditions (diameter and electron dose) and foil characteristics (thickness and atomic number). Direct information could be obtained by examining the spots, before and after heavy metal shadowing using scanning/transmission microscopy. The substrate materials might include aluminium, copper and gold, vacuum deposited as thin films of accurately known thickness.

Experiments involving the convergent beam method should be designed to investigate the anomolous effects found with aluminium foil containing precipitates, i.e. the inconsistency between calculated and published extinction distances and the discrepancy with thickness data obtained by the alternative absolute method. Work could be carried out in pure aluminium foils and samples of aluminium alloy at different stages in the precipitation sequence. In addition to solid-solution and precipitation effects, the possible influence of defects and strain in the crystal lattice might be examined.

Research on the characteristic X-ray method of determining foil thickness should be aimed at establishing, firstly, the relative efficiencies of X-ray generation for all elements of interest (Nasir 1972; Cliff and Lorimer 1972), since then a single standard foil of known thickness

may be used for calibration. This information would also allow extension of the method to multiphase materials where compositional changes have to be accounted for, thereby overcoming limitations inherent in the original technique. Secondly, corrections would be developed to compensate for X-ray absorption, electron scattering and changes in ionisation cross section (Jacobs and Baboroviska 1972), factors which become more significant with increase in foil thickness. This programme of work would facilitate the development of a procedure for quantitative microanalysis of specimen composition which does not require standards.

An evaluation of the continuum X-ray method is also proposed since it may have advantages compared with the characteristic X-ray method for studying those systems in which characteristic X-rays are heavily absorbed.

As a final point, this quantitative study could involve the development of an on-line data reduction system for rapid processing of X-ray information such that foil thickness and composition data become available while the specimen is still being examined in the electron microscope. This instant feedback would enable the microscopist to select the most suitable foil areas for quantitative microstructural analysis.

6. References

Andersen, C.A. and Wittry, D.B., 1968, J. Phys. D.: Appl. Phys. 1, 529.

Bethe, H.A. 1930, Ann. Phys. Leipz. 5, 325.

Bishop, H.E., 1966, X-ray Optics and Microanalysis eds. R. Castaing, P. Deschamps and J. Philibert (Paris : Hermann), p.153.

Bishop, H.E., 1974, J. Phys.D.: Appl. Phys., 7, 2009.

Bothe, W., 1929, Z. Phys., 54, 161.

Castaing, R., 1960, Adv. Electronics, 13, 17,

Cliff, G. and Lorimer, G.W., 1972, Electron Microscopy 1972, (London : Inst. of Phys.), 140.

Cox, M.G.C., Love, G., McEnaney, B. and Scott, V.D., 1973, Scanning Electron Microscopy : Systems and Applications, p.282.

Cox, M.G.C., McEnaney, B. and Scott, V.D., 1972, Phil. Mag., 26, 839.

Curgenven, L. and Duncumb, P., 1971, T.I. Research Lab. Rep. No.303.

Darlington, E.H., 1975, J. Phys. D.: Appl. Phys., 8, 85.

Darlington, E.H. and Cosslett, V.E., 1972, J. Phys. D. : Appl. Phys., 5, 1969.

Duncumb, P. and Da Casa, 1967, Conference on Electron Probe Microanalysis, Institute of Physics and Physical Society, London.

Duncumb, P. and Melford, D.A., 1966, X-ray Optics and Microanalysis, eds. R. Castaing, P. Deschamps and J. Philibert, (Paris : Hermann) p.240.

Duncumb, P. and Reed, S.J.B., 1968, Quantitative Electron Probe Miroanalysis : Nat. Bur. Stands Spec. Publ. 298, ed. K.F.J. Heinrich, (Washington : U.S. Dept. of Commerce) p.133.

Flegmann, A.W., Love, G. and Scott, V.D., 1971, Clay Minerals, 9, 245.

Green, M., 1963, X-ray Optics and Microanalysis eds. H.H. Pattee, V.E. Cosslett and A. Engström (New York : Academic Press), p.361.

Green, M., and Cosslett, V.E., 1961, Proc. Phys. Soc. 78, 1206.

Heinrich, K.F.J., 1967, Trans. of Second Nat. Conf. on Electron Probe Microanalysis, Boston, USA, Paper No.7.

Jacobs, M.H., and Baborovska, J., 1972, Electron Microscopy, (London : Inst. of Phys.), 136.

Love, G., 1975, M.Sc. Thesis, University of Bath.

Love, G. and Scott, V.D., 1978, J. Phys. D. : Appl. Phys. accepted for publication.

Love, G., Cox, M.G.C. and Scott, V.D., 1974a, J. Phys. D. : Appl. Phys., 7, 2131.

Love, G., Cox, M.G.C. and Scott, V.D., 1974b, J. Phys. D. : Appl. Phys., 7, 2142.

Love, G., Cox, M.G.C., Scott, V.D., 1975a, Materials Research Bulletin, 10, 815.

Love, G., Cox, M.G.C. and Scott, V.D., 1975b, J. Phys. D. : Appl. Phys., 8, 1686.

Love, G., Cox., M.G.C. and Scott, V.D., 1976a, J. Phys. D. : Appl. Phys., 9, 7.

Love, G., Cox, M.G.C. and Scott, V.D., 1976b, Developments in Electron Microscopy and Analysis, ed. J.A. Venables, (London : Academic Press), p.145.

Love, G., Cox, M.G.C. and Scott, V.D., 1977a, J. Phys. D. : Appl. Phys., 10, 7.

Love, G., Cox, M.G.C., and Scott, V.D., 1977b, Developments in Electron Microscopy and Analysis 1977, ed. D.L. Misell (Bristol : Inst. of Phys.) Inst. Phys. Conf. Ser. No. 36, p.347.

Love, G., Cox, M.G.C. and Scott, V.D., 1978a, J. Phys. D. : Appl. Phys., 11, 7.

Love, G., Cox, M.G.C. and Scott, V.D., 1978b, J. Phys. D. : Appl. Phys., 11, 23.

Miller, W.S. and Scott, V.D., 1978, Met. Sci. J., 12.

Nasir, M.J., Electron Microscopy 1972, (London : Inst. of Phys.), 142.

Philibert, J. 1963, X-ray Optics and Microanalysis, eds. H.H. Pattee, V.E. Cosslett and A. Engstrom, (New York : Academic Press) p.379.

Philibert, J. and Tixier, R., 1968, Quantitative Electron Probe Microanalysis, Nat. Bur. Stands. Spec. Publ. 298 ed. K.F.J. Heinrich (Washington : U.S. Dept. of Commerce) p.13.

Reed, S.J.B., 1965, Brit. J. Appl. Phys., 16, 913.

Reed, S.J.B., 1975, Electron Microprobe Analysis (Cambridge : Cambridge Univ. Press) p.320.

Russ, J.C., 1977, EDAX Editor, 7, No.2, 6.

Salter, W.J.M., 1970, A Manual of Quantitative Electron Probe Microanalysis (London : Structural Publications Ltd), p.79.

Springer, G., 1967, Neues Jahrb. Mineral, Abhandl, 106, 241.

Tullett, S.G., Board, R.G., Love, G., Perrott, H.R. and Scott, V.D., 1976, Acta Zoologica. (Stockh.), 57, 79.

7. Reprints of Papers

7.1 Electron-Optical Study of the Prism Surfaces of Kaolinite Microcrystals

A.W. Flegmann, G. Love and V.D. Scott,

1971, Clay Minerals, 9, 245.

Clay Minerals (1971) 9, 245.

NOTES

ELECTRON-OPTICAL STUDY OF THE PRISM SURFACES OF KAOLINITE MICROCRYSTALS

The microcrystals of kaolinite, like those of other layer silicate minerals, possess two types of crystallographically different surfaces (Van Olphen, 1963). This crystal form can account for various rheological and ion adsorption characteristics of kaolinite in aqueous suspension (Flegmann, Goodwin & Ottewill, 1969). While the basal surfaces of the plate-like crystallites are recognized as being of the (001) type, the indices of the prism surfaces have not so far been reported. Selected area electron diffraction combined with electron microscopy were used here to determine the crystal indices of the external prism surfaces of kaolinite microcrystals.

The kaolinite, a selected Cornish clay kindly given by English China Clays, St Austell, was first converted into the sodium form and the electrolyte-free clay was suspended in 10^{-4}M cetyl-trimethyl ammonium bromide solution. Droplets of the dilute suspension were deposited onto carbon coated copper grids, dried and then examined in an A.E.I. EM802 electron microscope operating at 100 kV. Diffraction spot patterns from 20 single crystals were obtained using a 25 μm selected area aperture. The camera constant was determined by evaporating a thin layer of silver onto some of the grids to provide an internal standard. Complementary X-ray diffraction measurements on a random powder preparation were also carried out, the d-spacings obtained agreeing with those of Brindley & Robinson (1946).

A typical crystal is shown in the electron micrograph, Plate 1(a). The corresponding electron diffraction pattern, Plate 1(b), consists of a hexagonal array of spots, and is reproduced in the appropriate orientation, having allowed for image rotation in the electron microscope. The spot patterns were measured and d-spacings calculated by reference to the diffraction rings from the internal standard.

In order to index the diffraction patterns, sections of the reciprocal lattice for kaolinite were constructed (Figs 1 and 2) using Brindley & Robinson's (1946) data. In Fig 1, the b-axis is perpendicular to the plane of the diagram, while in Fig 2 the a-axis is so oriented. In both diagrams the direction of the beam is shown parallel to c*, the case for crystals oriented with their ab planes perpendicular to the electron beam.

For a crystal in this orientation, the full circles shown in Figs 1 and 2 are seen to lie on the Ewald sphere, giving rise to the hk$l$ diffractions with $h = 3\bar{l}$ represented, again as full circles, in Fig 3. Comparison of this set of spots with those of the observed diffraction pattern (Plate 1(b)) shows, however, that the latter contains a number of additional diffractions which may be indexed according to $h = 3l + 1$.

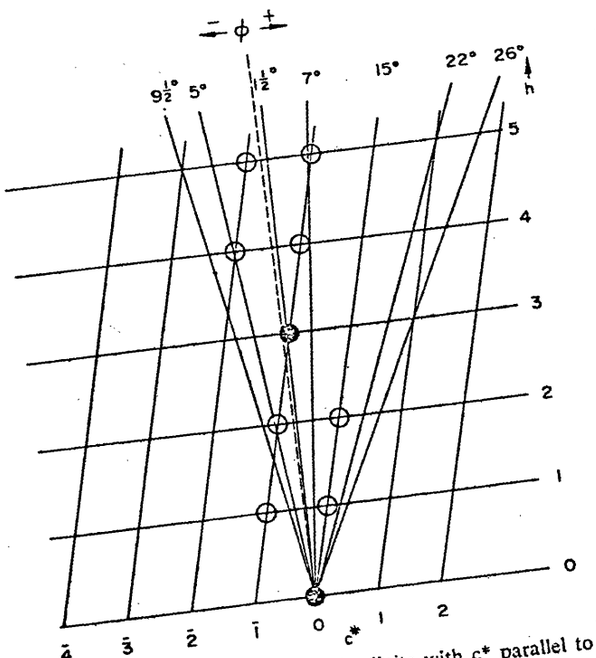

FIG. 1. Reciprocal lattice construction for kaolinite with c* parallel to the electron beam; b-axis perpendicular to the plane of the diagram.

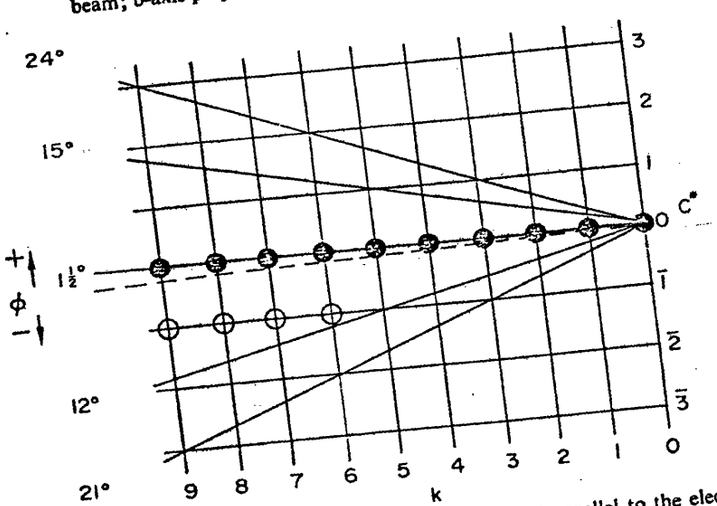

FIG. 2. Reciprocal lattice construction for kaolinite with c* parallel to the electron beam; a-axis perpendicular to the plane of the diagram.

PLATE 1

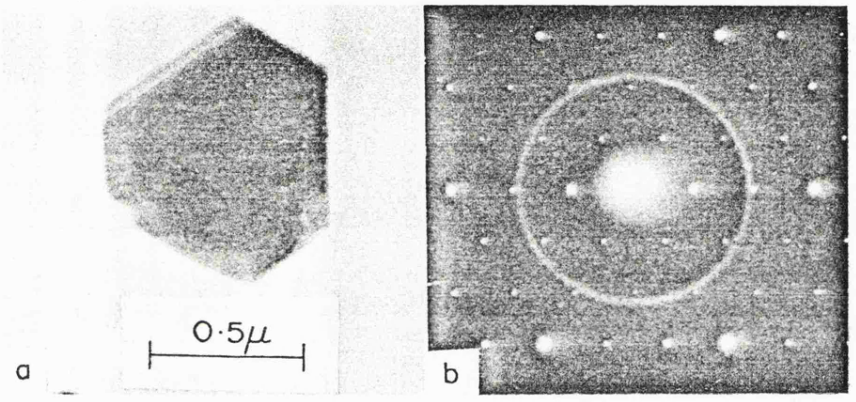

(*a*) Electron micrograph of a kaolinite microcrystal. (*b*) Electron diffraction pattern in corresponding orientation showing kaolinite spot pattern and silver calibration rings.

To face page 246

Any explanation for the extra spots based on mosaicity in individual crystals is unacceptable, since it implies that regions of the crystals must be rotated by about 15° around the crystal axes; no diffraction contrast of the type expected from such tilt boundaries was found in the electron micrographs.

The observed diffraction pattern may, however, be satisfactorily interpreted if each reciprocal lattice point is considered as being extended into rods or spikes ('relrods'). For the plate-like kaolinite crystals these relrods would be perpendicular to c*, providing additional intersections of the reciprocal lattice with the Ewald sphere and would thus account for the extra spots. These reciprocal lattice points are shown as open circles in Figs 1, 2 and 3. Crystals would have to be no more than a few unit layers thick to satisfy this condition, but estimates indicate that even the thinnest crystals used in the present investigation consist of ten or more unit layers. If, however, the crystals consisted of several superimposed thin layers displaced relative to one another by a fraction of either the a or b parameter (analogous to a stacking fault), then sufficient extension of the reciprocal lattice points would occur.

Having indexed a diffraction pattern (see Fig 3), the a and b lattice parameters may be calculated using the appropriate geometrical relationship for the kaolinite triclinic lattice (Andrews *et al.*, 1967). The d-spacing for 020 was found to be

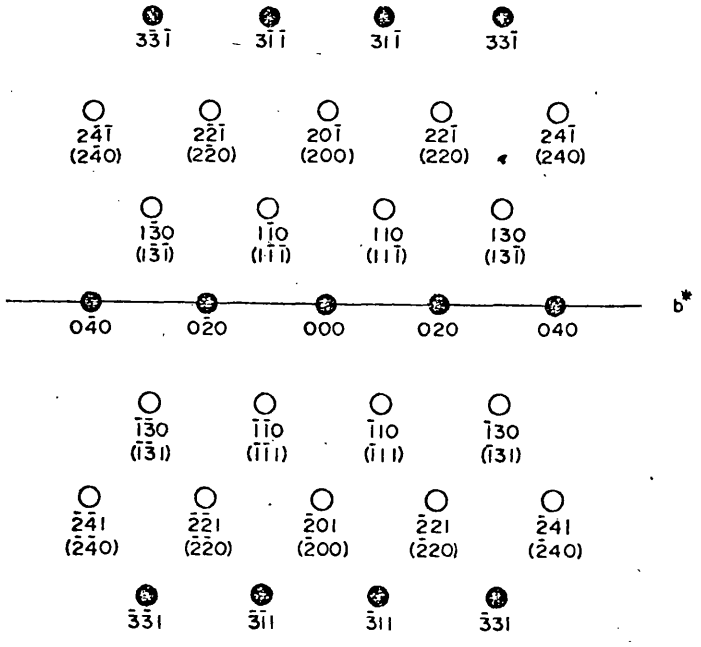

FIG. 3. Indexed diffraction pattern. ●, diffractions from the $31k\bar{1}$ planes; ○, additional diffractions associated with streaking of the reciprocal lattice (relrods).

4·48 ± 0·02 Å which gives a b-parameter of 8·96 ± 0·04 Å, close to the published value of 8·95 Å.

Determination of the a-parameter may be accomplished by measurement of an h00 diffraction. Using the 200 spot and computing the d-spacing from the simplified relationship $\frac{1}{d} = \frac{h}{a} \frac{1}{\sin \beta}$ (taking $\alpha = 90°$) gave an a parameter of 5·28 ± 0·04, much higher than the accepted value of 5·14 Å. Since, however, [200] is inclined to the Ewald sphere, this value needs to be multiplied by sin β, restoring it to 5·12 ± 0·04 Å, in good agreement with the published figure of 5·15 Å. This value would be obtained by measurement of the 200 spot directly from the diffraction pattern which follows of course, from the fact that the a and b axes of crystallites lying perpendicular to the electron beam must themselves lie in the Ewald sphere.

It should be pointed out, that since crystals will not always be accurately perpendicular to the beam due to unevenness of the carbon support film, relrods may intersect the Ewald sphere at positions corresponding to different spacings and would thus account for some of the scatter in the results. Also in this connection, the X-ray diffraction study on a large number of randomly oriented crystals showed the line broadening which might be expected from relrods. Such line broadening has been attributed (Murray & Lyons, 1956) to b-axis disorder with displacements of about $-\frac{a}{3}$ between successive layers of the crystallites, the type of lattice faulting which would account for the observed two-dimensional electron diffraction effects. These effects would be absent for perfectly crystalline material.

Referring to Plate 1(a) and 1(b) the prism faces of the crystals may now be indexed. The prism faces of the crystal are seen to be parallel to [100], [130] and [1$\bar{3}$0], forming the characteristic hexagonal shape of the particles; it follows that the indices of the prism faces of the crystallites are (010), (1$\bar{1}$0) and (110). Accurate measurement of the diffraction patterns enables the 020 reflection (4·48 ± 0·42) Å to be distinguished from the other two, allowing the prism plane indices to be correctly assigned to the crystal. Inspection of the diffraction intensities also facilitates identification, since rows of strong reflections (full circles, h=3$\bar{1}$) lie parallel to [010].

Acknowledgments. The authors are indebted to Dr J. A. Gard for helpful comments on the interpretation of the results and to Dr R. A. L. Sullivan for the X-ray measurements.

A. W. Flegmann*
G. Love†
V. D. Scott†

*School of Biological Sciences,
†School of Materials Sciences,
The University, Claverton Down, Bath.
26 May 1971.

REFERENCES

ANDREWS K.W., DYSON D.J. & KEOWN S.R. (1967) *Interpretation of Electron Diffraction patterns*, p. 72. Hilger and Watts Ltd., London.

BRINDLEY G.W. & ROBINSON K. (1946) *Miner. Mag.* 27, 242.

FLEGMANN A.W., GOODWIN J.W. & OTTEWILL R.H. (1969) *Proc. Brit. Cer. Soc.* 13, p. 31.

MURRAY M.H. & LYONS S.C. (1956) *Clays and Clay Minerals* (A. Swineford, ed.) p. 31. Publication 456. Nat. Acad. Sci. – Nat. Res. Counc., Washington.

OLPHEN H. VAN (1963) *An Introduction to Clay Colloid Chemistry*, p. 93. Wiley, New York.

7.2 Studies in the SEM of Oxide Layers Formed on Metals.

M.G.C. Cox, G. Love, B. McEnaney and V.D. Scott

1973 Scanning Electron Microscopy:

Systems and Applications, p.282.

Scanning electron microscopy: systems and applications 1973

STUDIES IN THE SEM OF OXIDE LAYERS FORMED ON METALS

by M.G.C. Cox, G. Love, B. McEnaney and V.D. Scott

School of Materials Science, University of Bath, Bath, UK.

Recent developments in accessories and in analytical techniques for the scanning electron microscope have produced an instrument now capable of providing quantitative information on the structure of solids. This paper shows how data obtained using the microanalysis attachment have enabled a new interpretation of the structure and growth of oxide layers on metals to be made. Illustrations are taken from our work on the oxidation of Fe-Cr alloys at 400-600°C. in CO_2-based gas, where the effect of factors such as alloy composition and oxidation environment upon the formation of thin films in early stages of oxidation and upon the subsequent development of thicker scales are of particular interest. Detailed structural analysis of the metal and of the solid oxidation products is carried out using a number of complementary techniques including a JXA-50A scanning electron probe microanalyser fitted with two crystal spectrometers. The information is related to kinetic data obtained with a sensitive microbalance by continuous weighing of samples undergoing oxidation.

A typical fracture section through oxidised metal (a Fe-5% Cr alloy oxidised for 150 hours at 600°C) is illustrated in Fig. 1. This shows a duplex scale with vestigial polishing scratches at the oxide/oxide interface, indicating that this was the original metal surface. It may be deduced that a two-way diffusion process is occurring during oxidation; the outer oxide is formed by outward flow of metal cations through the oxide scale to react at the gas/oxide interface and the inner layer by inward movement of oxidising species to the metal/oxide interface. The EPMA profiles, Fig. 2, show that the outer scale is essentially iron oxide and that chromium is concentrated within the inner layer. Although such partitioning of alloying elements within oxide scales has been reported in the literature on alloy oxidation, Pfeil (1929) refering to the phenomenon as long ago as 1929, no satisfactory explanation had been put forward. We have accounted for partitioning by relating cation mobility to the energetics of movement through the oxide sub-lattice via interstitial sites (Cox, McEnaney and Scott, 1972) as follows.

The structure of both oxide layers formed on the Fe-Cr alloys was spinel. Spinels possess a cubic unit cell consisting of a close-packed arrangement of 32 oxygen anions and containing 32 octahedral and 64 tetrahedral interstices; the 24 metal cations are distributed over 16 octahedral and 8 tetrahedral sites. Cation diffusion through this lattice occurs (Azaroff, 1961) by successive movement from an octahedral site to an adjacent unoccupied tetrahedral site and then to the next unoccupied octahedral interstice. Octahedral and tetrahedral site preference energies for cations may be calculated using crystal field theory, from which it can be shown that Cr^{3+} has a high octahedral site preference energy, Ep, while Fe^{2+} has low preference energy and Fe^{3+} has no preference.

A ranking order for cation mobility may be established from the magnitude of the octahedral site preference energy, Ep, as follows:-

$$Fe^{3+} > V^{3+} > Mn^{3+} > Cr^{3+} \quad \text{(trivalent ions)}$$

$$Mn^{2+} > Fe^{2+} > Co^{3+} > Ni^{2+} \quad \text{(divalent ions)}$$

Support for the proposed relation between Ep and the kinetics of oxidation is given by the correlation observed between Ep and k, the parabolic oxidation rate constant for some first row transition metals (Cox et al, 1972). For Fe-Cr

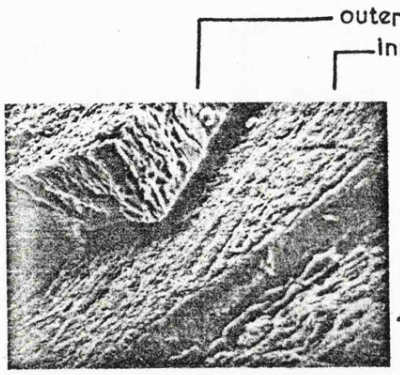

Figure 1 Fracture section through Fe-5% Cr alloy oxidised at 600°C for 100 hours. SEM x350

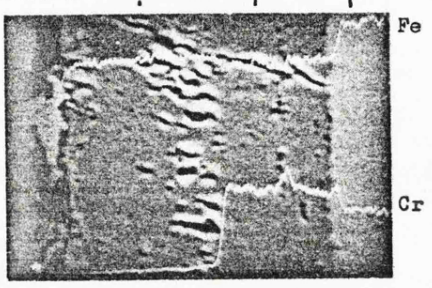

Figure 2 As Fig. 1. Polished section through oxide scale showing concentration profiles for iron and chromium. x 600

alloys it follows that Cr^{3+}, with its high octahedral site preference energy, will diffuse much more slowly than Fe^{3+} through close-packed oxides and therefore only iron will reach the gas/oxide interface, forming the outer layer of Fe_3O_4. The growth of the inner spinel layer, $(Fe_{3-x}\ Cr_x)O_4$ results from penetration of oxidant through voids and fissures in the scale (Cox, McEnaney and Scott, 1973), x being related to alloy composition. Since the reaction is controlled by the rate of outward movement of iron cations through the oxide scales, the oxidation rate constant is found to be substantially independent of alloy composition, in accord with the above model. Many similar observations on partitioning of elements in oxide scales on alloys can be explained using these principles.

This data, of course, could be obtained using an electron-probe microanalyser without SEM capability. However, notwithstanding the limitation on x-ray spatial resolution imposed by diffusion within the sample, high electron probe resolution and picture quality are essential for unambiguously locating and recognising microfeatures prior to microanalysis. This is particularly important when, as is usually the case, oxide films are not homogeneous. They may vary in thickness, contain voids or fine second-phase dispersions, or some local enhanced oxide growth may occur at grain boundaries and inclusions in the metal. Fig. 3 shows local development of haematite whiskers which is associated with the introduction of very small traces of oxygen into the gas stream and is a sensitive indicator of leaks in the oxidation apparatus.

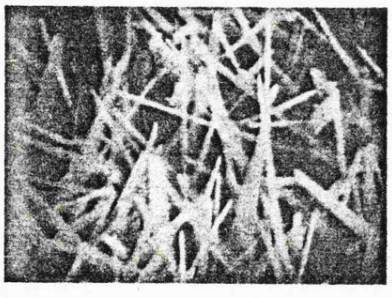

Figure 3 Local growth of haematite whiskers on Fe-Cr alloy, SEM x6000

Another form of local attack, possibly at inclusions in the metal, is illustrated in an extraction replica, Fig. 4.

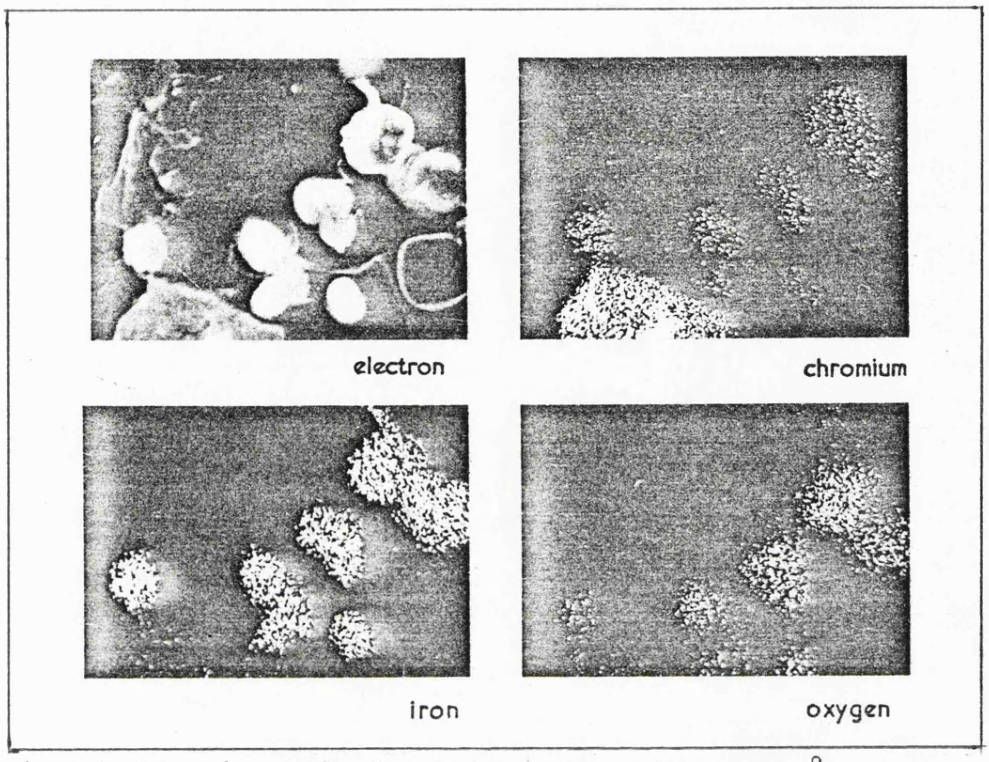

Figure 4 Extraction replica from Fe-20% Cr alloy oxidised at 600°C for ~100 hours, showing distribution of chromium, iron and oxygen in the particles. x3000.

The flake-like particles are mainly Cr_2O_3, while the spherical particles contain, in addition, much iron. The spherical particles are believed to be amorphous, since they gave no crystalline diffractions even in a 1 Mev transmission electron microscope; although their shape suggests that surface tension forces have played a part in their formation, their occurrence remains unexplained. Fig. 4 is of additional interest since it shows that good electron-probe resolution (~500Å) can be achieved using probe currents sufficient to give satisfactory scanning x-ray pictures (40 secs. exposure) in our microanalyser. High sensitivity x-ray spectrometers (or energy dispersive systems) are essential for studying these thin films, since they are severely damaged by specimen currents $>10^{-8}$A.

Another example of non-uniform oxide film is shown in Fig. 5, taken from a chemically stripped film using the SEM and STEM imaging modes respectively. The more transparent regions revealed in the STEM image are rhombohedral oxide, the opaque oxide is spinel. We have noted that STEM images can be produced at 50kV from oxide layers which are nearly opaque to 100 keV electrons in the CTEM mode. Special attention is being paid to such films formed in the early stages of oxidation. Different oxides may be characterised not only by their crystal structure but by octahedral and tetrahedral site filling requirements determined by crystal field theory and by the thermodynamics of the oxidation

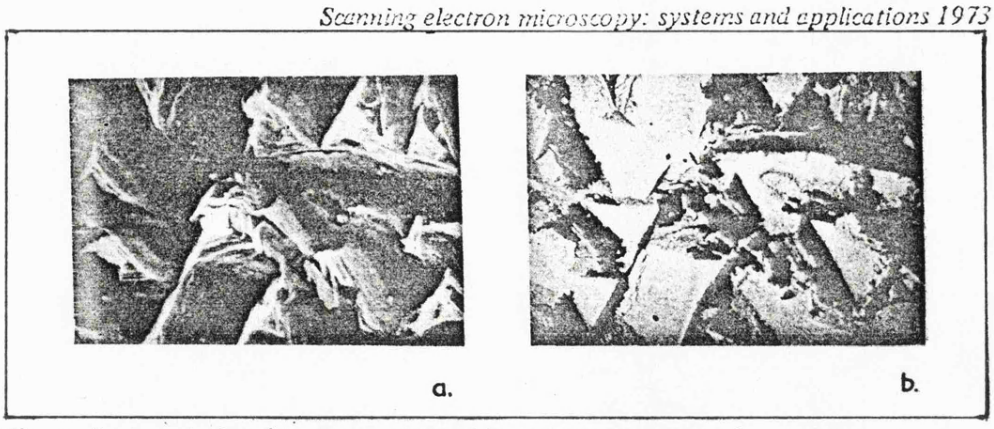

Figure 5 Detached oxide from oxidised Fe-20% Cr alloy showing thin rhombohedral film with local thicker spinel growth (a)SEM, (b) STEM. x 5000

reaction. In this way we are able to account for the growth and stability ranges of thin oxide films as well as the thicker duplex scales described above. For example, in rhombohedral, α-M_2O_3, oxides all the cations are in octahedral positions and this structure is stable for all values of the Cr/Fe ratio in $(Fe,Cr)_2O_3$. In the cubic spinel structure, however, the crystal field approach suggests that there is a maximum chromium content when Cr^{3+} ions occupy all the octahedral sites; i.e. at a composition corresponding to

$$Fe_8^{tet}\ Cr_{16}^{oct}\ O_{32}\ (Cr/Fe\ ratio - 1.86).$$

With chromium-rich Fe-Cr alloys (>15% Cr), a film of Cr_2O_3 forms first due to the higher affinity of chromium for oxygen. Any cation diffusion through this oxide will be slow since, due to the high Ep value for Cr^{3+}, Cr^{3+} in octahedral sites effectively blocks the Azaroff diffusion path and the film will remain stable and protective. Eventually, however, as the reaction continues the Cr_2O_3 layer will become diluted with iron and, when the Cr/Fe ratio falls below 1.86, spinel can form. This view is supported by careful microanalysis experiments which show that spinel is formed only when the Cr/Fe ratio is below the value of 1.86. Local growth of spinel oxide at an early stage is illustrated at metal grain boundaries in Fig. 6a and at asperities on the metal surface in Fig. 6b. The remainder of the surface is

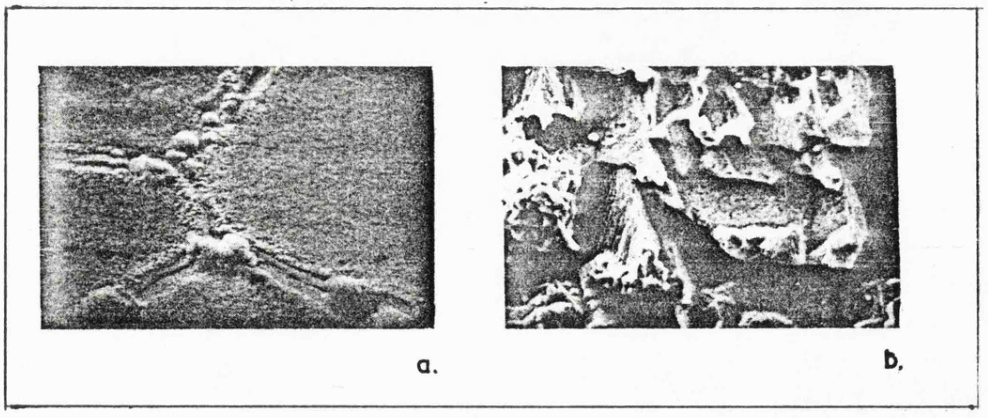

Figure 6 Local growth of spinel oxide at (a) grain boundaries and (b) surface asperities. SEM x 1500.

still covered with chromium-rich rhombohedral oxide which is protective; see also detached film, Fig. 5. Eventually the spinel spreads across the entire surface, forming the duplex scale structure shown in Fig. 1, and the oxidation rate markedly increases (Cox et al, 1973).

Much of our work on oxidation involves the use of soft x-rays for microanalysis and, while this is essential for oxygen measurement and for distinguishing between oxide and carbide formation, it is also of value when analysing metallic elements. By recording L x-ray lines, low probe voltages can be used, thereby reducing electron penetration and x-ray diffusion in the sample (~3000Å at 5kV). Sensitivity to surface segregation effects is improved, which is useful when oxides are difficult to strip, and differences in chemical composition may be discerned between the two surfaces of stripped oxide layers. A parallel research programme on light element analysis is aimed at quantitative interpretation of raw x-ray data which, it is hoped, will establish the extent to which quantitative microanalysis of oxide films is practicable.

Acknowledgements

To C.E.G.B., Berkeley for their support of some of this work.

References

Azaroff, L.V. 1961, J. Appl. Phys., 32, 1638
Cox, M.G.C., McEnaney, B. and Scott, V.D., 1972, Phil. Mag., 26, 839
Cox, M.G.C., McEnaney, B. and Scott, V.D., 1973, Phil. Mag., 27 (in press)
Pfeil, L.B., 1929, J. Iron Steel Inst., 119, 501

7.3 Electron Probe Microanalysis Using Oxygen X-rays: I Mass Absorption Coefficients

G. Love, M.G.C. Cox and V.D. Scott, 1974a, J. Phys. D. : Appl. Phys. 7, 2131.

J. Phys. D: Appl. Phys., Vol. 7, 1974. Printed in Great Britain. © 1974

Electron probe microanalysis using oxygen x-rays: I. Mass absorption coefficients

G Love, M G C Cox and V D Scott
School of Materials Science, University of Bath, Claverton Down, Bath BA2 7AY

Received 22 March 1974, in final form 15 May 1974

Abstract. Electron probe microanalysis of oxygen in a range of binary and ternary oxides is described. Experimental data are presented for a range of electron accelerating voltages and for two different take-off angle instruments. The ratio of oxygen K emission from specimen and standard is found to reach a limiting value, the same for each instrument, as the applied voltage is increased. The observations are shown to support the thin-film model (Duncumb and Melford 1966) proposed for quantitative analysis of light elements and also to enable its range of applicability to be established in terms of specimen characteristics and experimental conditions. The model is used together with chemical composition data for the oxides, and a consistent set of mass absorption coefficients are calculated which are considered to be accurate within 10%. These new data are discussed and compared with previously published values.

1. Introduction

Correction models for converting microanalysis measurements into quantitative data have been investigated by many workers in the field (see reviews by Martin and Poole 1971, Beaman and Isasi 1972), but, while it appears that suitable procedures have been established for the analysis of elements with characteristic wavelengths < 10 Å, their extension into the light-element region has been much less successful. Difficulties arise here not only because the physical bases of models may be inappropriate for light-element analysis but also because reliable input data such as x-ray mass absorption coefficients are lacking. For light-element systems atomic number effects may be relatively large, involving corrections typically $\sim 20\%$, but absorption corrections may be very much greater, up to several 100% in certain cases. This fact coupled with the considerable uncertainty attached to published mass absorption coefficients in the soft x-ray region, quoted values commonly differing by a factor of two or more, may lead to errors in the absorption correction which outweigh those due to other effects. The manner in which any error in chosen values for coefficients is proportionately related to the accuracy of final corrected data may be demonstrated by considering a much favoured absorption correction, the simple Philibert (1963) formula:

$$f(\chi) = \frac{1+h}{(1+\chi/\sigma)\,[1+h\,(1+\chi/\sigma)]}$$

with: $h = 1{\cdot}2\,A/Z^2$, where A is atomic weight and Z is atomic number; $\chi = \mu/\rho \operatorname{cosec} \theta$, where μ/ρ is the mass absorption coefficient and θ the x-ray take-off angle; σ the Lenard

coefficient $= 2{\cdot}39 \times 10^5/(E_0^{1{\cdot}5} - E_c 1{\cdot}5)$, where E_0 is the probe voltage and E_c is the x-ray excitation voltage (Duncumb and Shields 1966).

The relative error is obtained by differentiating (Heinrich and Yakowitz 1969):

$$\frac{\Delta f(\chi)}{f(\chi)} = \frac{1+2h(1+\chi/\sigma)}{1+h(1+\chi/\sigma)} \frac{\Delta\chi}{\sigma+\chi}.$$

The limiting case for heavy absorbers, $\chi/\sigma \gg 1$, is then,

$$\lim_{\chi/\sigma\to\infty} \frac{\Delta f(\chi)}{f(\chi)} = 2\frac{\Delta\chi}{\chi}.$$

When $\chi/\sigma = 1$

$$\frac{\Delta f(\chi)}{f(\chi)} = \frac{1+4h}{2(1+2h)} \frac{\Delta\chi}{\chi}$$

which reduces to $\frac{1}{2}\,\Delta\chi/\chi$ for small h and to $\Delta\chi/\chi$ for large h. Hence in the soft x-ray region, where typically $\chi/\sigma \geqslant 1$, $\frac{1}{2}\,\Delta\chi/\chi < \Delta f(\chi)/f(\chi) < 2\,\Delta\chi/\chi$, and errors in μ/ρ will produce errors of corresponding magnitude in $f(\chi)$. Thus it follows that evaluation of proposed correction models may be rendered valueless unless the mass absorption coefficients are known with a precision commensurate with the accuracy of experimental measurement.

Values of mass absorption coefficients for soft x-rays have been reviewed by Weisweiler (1970). Absolute values of μ/ρ obtained by an x-ray reflection technique (Ershov *et al* 1967) as well as by absorption measurements in thin films of material (Lukirski *et al* 1964, Ershov 1967) are reported, and, although reproducibilities approaching 10% were claimed, discrepancies between the two sets of data sometimes reached 50%. The results of Henke *et al* (1967) using gaseous absorbers are likely to be the most reliable data available, mass absorption coefficients for oxygen radiation in a range of other elements up to argon ($Z = 18$) being estimated by interpolation. Absolute values for μ/ρ beyond the L edge ($Z > 21$) are either lacking or imprecise, apart from those for the gases krypton and xenon (Henke *et al* 1967). Mass absorption coefficients have often been calculated from microanalysis measurements, but these should always be treated cautiously since the values would reflect any inadequacy in the physical basis of the correction model and input parameters such as h, σ, etc.

This paper focuses attention on mass absorption coefficients in the light-element region. Results are described for the measurement of oxygen K x-rays in a range of binary and ternary oxides. A treatment of the distribution of x-ray generation with depth in these materials is given which leads to an assessment of the applicability of the 'thin-film approximation' proposed by Duncumb and Melford (1966) for quantitative light element microanalysis. This simple approach requires no separate atomic number correction and, since fluorescence effects can be neglected in this region of the x-ray spectrum, the experimental data is used to establish a criterion for its validity. In addition, since specimen compositions are accurately known, the results are applied in conjunction with the absolute μ/ρ data of Henke *et al* (1967) to determine mass absorption coefficients for oxygen K x-rays in a large number of elements.

2. Experimental details

A range of binary oxides (A_xO_z) and ternary oxides ($A_xB_yO_z$) in the form of high-purity single crystals were obtained from a variety of sources for this investigation,

(see table 2); to these was added vitreous arsenic oxide (As_2O_3) made in the laboratory by sublimation on to a hot surface.

Each specimen was mounted and prepared simultaneously with an aluminium oxide (Al_2O_3) standard. Smooth and flat surfaces were achieved by mechanical polishing on successively finer grades of abrasive down to 1 μm diamond. The samples were made conducting by coating with a thin layer (< 100 Å) of copper and then inserted into the microanalyser. This procedure minimized possible errors due to small variations in coating thickness and to any slight misalignment of the specimen when positioned under the electron probe.

Measurements were carried out on two types of electron probe microanalyser, a Cambridge Scientific Instruments Ltd. Microscan 1 (x-ray take-off angle 20°) and a JEOL JXA-50A (x-ray take-off angle 35°). For soft x-ray work the Microscan 1 was fitted with lead stearate and clinochlore crystals, while a window consisting of several thin layers of formvar supported on a nickel mesh and coated with a thin (~20 Å) layer of aluminium was affixed to the proportional counter. A cold stage was incorporated (Ranzetta and Scott 1966) to reduce build-up of contamination on the sample. The JXA-50A was a standard commercial instrument fitted with a cold stage and two crystal spectrometers, one containing a stearate crystal and a thin window proportional counter. A clinochlore analysing crystal was added for this study, and the electron trap was modified to operate up to 5 kV in order to reduce background due to scattered electrons entering the counter; the modification was necessary for analysis of specimens at high kV.

Two procedures were used for x-ray intensity measurements:

(i) The spectrometer system was slowly scanned through the appropriate range of Bragg angle, and the whole of the oxygen K emission band plotted using a pen recorder. Peak intensity was obtained from the recorder chart and a value for the background to be subtracted was estimated by interpolation of measurements taken either side of the peak.

(ii) The spectrometer system was slowly scanned through the whole of the oxygen K emission band while integrating the x-ray counts, the background correction being estimated as before.

Each experimental value involved a minimum of five measurements on each sample, the specimen being repositioned on each occasion. Reproducibility was found to be within ±3% of the mean value with the exception of results on lead oxide (PbO) where the peak-to-background ratio was very low. Measurements were carried out using probe voltages within the range 5–40 kV, and the microanalysis data are presented in this paper as the intensity ratio $k = I_{\text{specimen}}/I_{\text{standard}}$.

3. Experimental results

Table 1 lists recorded intensity ratios k using peak height and peak intensity measurements for both stearate and clinochlore analysing crystals. They were obtained on MgO, Cr_2O_3 and Fe_2O_3 (Al_2O_3 standard) using the JXA-50A operating at 15 kV probe voltage.

With the exception of the clinochlore peak height measurements, k values for each specimen are closely similar. The difference in the former set of data may be attributed to changes in peak shape of the oxygen K emission due to valence band effects, a feature which is revealed with the clinochlore crystal (see figure 1) but not with the lower-resolution stearate crystal. To reduce possible errors arising from valence band effects,

Table 1. Intensity ratios k using different methods of measurement: A peak heights, clinochlore; B integrated peaks, clinochlore; C peak heights, stearate; D integrated peaks, stearate: JXA-50A, 15 kV

Specimens	k values			
	A	B	C	D
MgO	1·17	0·96	0·91	0·93
Cr_2O_3	0·84	1·08	1·06	1·05
Fe_2O_3	0·67	0·88	0·89	0·89

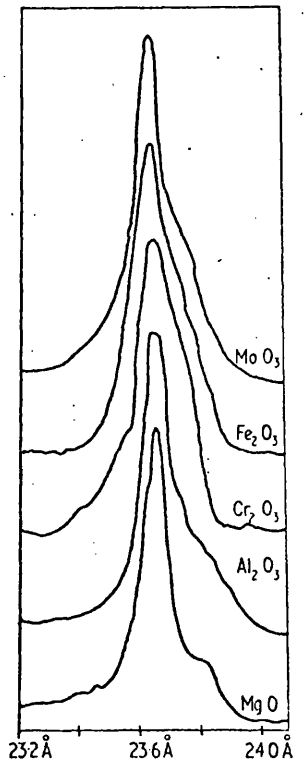

Figure 1. Oxygen K x-ray emission bands for a selection of oxides, obtained using a clinochlore analysing crystal.

integrated peak intensities were measured when using clinochlore. With stearate, however, peak height measurements were preferred, since the background corrections required in integrated peak measurements were high, and consequently the method became either more time consuming or less precise. A selection of measured k ratios for oxides are plotted in figure 2 as a function of probe voltage. All curves show voltage dependence, the effect being more marked for some oxides than others. It is clear that oxide systems with a mean mass absorption coefficient for oxygen x-rays less than that of the Al_2O_3 standard, for example Cr_2O_3, show an increase in k with increase in probe voltage, whereas those with a mean μ/ρ greater than that of the standard show a decrease in k, for example ZrO_2. At high probe voltages k values are virtually independent of kV. The limiting value for a particular system was found to be the same for both JXA-50A and Microscan 1 measurements, although there were significant differences between the

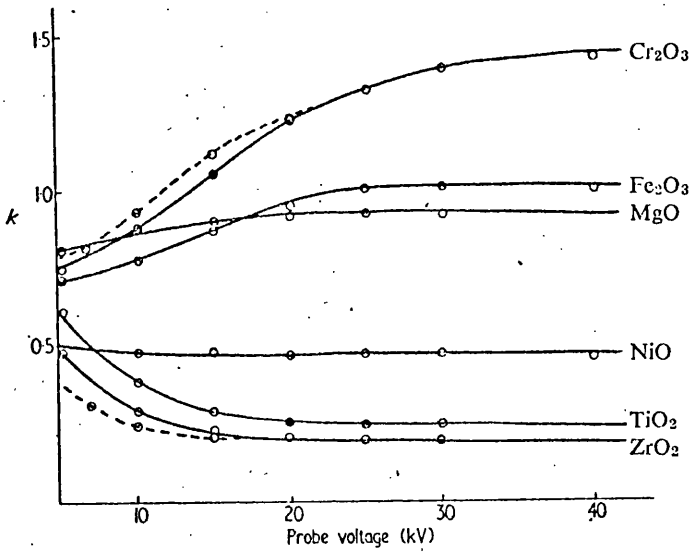

Figure 2. Intensity ratios for selection of oxide systems plotted as a function of probe voltage; Al_2O_3 standard: broken curves refer to Microscan 1 results.

two sets of data at lower probe voltages. Typical Microscan 1 results are illustrated by the dotted lines in figure 2, as obtained on Cr_2O_3 and ZrO_2. Limiting values for k for every oxide system studied are collated in table 2.

Table 2. List of specimens studied

Specimens	$\phi(0)$ values	Limiting k-values	Source
Al_2O_3	1·34	1·00	RRE Malvern
SiO_2	1·35	0·91	Metals Research
TiO_2	1·51	0·261	Metals Research
Cr_2O_3	1·58	1·450	Metals Research
Fe_2O_3	1·61	1·020	Metals Research
MgO	1·33	0·92	Oxford University
NiO	1·69	0·497	Oxford University
ZrO_2	1·82	0·211	Oxford University
MoO_3	1·78	0·253	Oxford University
PbO	2·28	0·071	Oxford University
As_2O_3	1·75	0·371	Prepared in the laboratory
Fe_2TiO_5	1·58	0·464	Oxford University
$NiTiO_3$	1·60	0·315	Oxford University
$CaSiO_3$	1·43	0·330	Sheffield University
$CaZrO_3$	1·73	0·185	W C Spicer
$MgCr_2O_4$	1·53	1·283	Imperial College
$MgAl_2O_4$	1·34	0·992	RRE Malvern
$PbMoO_4$	2·09	0·144	RRE Malvern

4. Discussion

The physical basis of any correction procedure for electron probe microanalysis involves a knowledge of the distribution of x-ray production with depth. This information is

usually given in the form of $\phi(\rho z)$ curves (figure 3) where $\phi(\rho z)$ is the ratio of x-rays generated in a thin layer of mass thickness $d(\rho z)$ at a depth ρz in a bulk specimen to those generated in an isolated thin film of the same mass thickness. The value of $\phi(\rho z)$ rises from $\phi(0)$ in surface regions to a maximum; this is due to (*a*) the increase in electron path length in each layer $d(\rho z)$ as the electrons diffuse into the sample, and (*b*) the increase in ionization cross section for x-rays as the electron energy approaches the critical

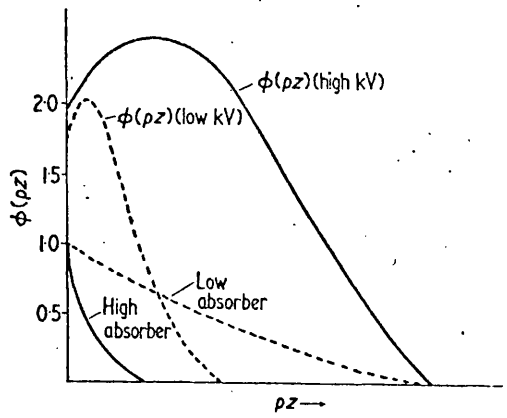

Figure 3. Curves of $\phi(\rho z)$ against ρz, showing distribution of x-ray production with depth at a high and a low probe voltage: also shown are x-ray transmission curves for a high and a low absorber. The pair of full curves indicate conditions for the thin-film approximation to be valid.

ionization potential. $\phi(\rho z)$ subsequently decreases with increase in ρz as fewer electrons reach the deeper layers. Two $\phi(\rho z)$ curves are included in figure 3 to show the greater mean depth of x-ray production at a higher probe voltage. On their way out of the sample the generated x-rays will be attenuated due to absorption, and also shown in figure 3 are two x-ray transmission curves, one for a highly absorbing specimen and one for a low absorber. The emitted x-ray intensity is thus given by

$$I=\int_0^\infty \phi(\rho z)\exp(-\chi\rho z)\,d(\rho z).$$

The $\phi(\rho z)$ curves indicate that as χ tends to infinity, the emitted x-rays originate from only the immediate surface regions of the sample and, in this situation, the emitted intensity may be written

$$I=\phi(0)\int_0^\infty \exp(-\chi\rho z)\,d(\rho z)=\frac{\phi(0)}{\chi}.$$

Now for a specimen of composition AB, producing $n_{AB}^{A}\,d(\rho z)$ ionizations per unit area from element A in the surface region, the emergent intensity is given by $I_{AB}^{A}=n_{AB}^{A}/\chi_{AB}^{A}$. Since, by definition

$$\phi(0)=\lim_{d\rho z\to 0}\frac{n\,d(\rho z)}{n(0)\,d(\rho z)},$$

where $n(0)d(\rho z)$ is the number of ionizations per unit area produced in the same mass thickness of an isolated layer of the same material,

$$I_{AB}^{A}=\phi(0)_{AB}^{A}\,n(0)_{AB}^{A}\,\frac{1}{\chi_{AB}^{A}}.$$

In a layer of AB of mass thickness $d(\rho z)$ the weight per unit area of element A is $C^A_{AB}\,d(\rho z)$, and hence the number of A atoms per unit area is $C^A_{AB}\,(N/A_A)\,d(\rho z)$, where N is Avogadro's number and A_A is the atomic weight of element A. Thus the number of ionizations $n(0)^A_{AB}$ occurring per unit area in this layer is $C^A_{AB}\,(N/A_A)\,\psi(E)\,d(\rho z)$, where $\psi(E)$ is the ionization cross section. Since now the electron energy loss is zero for an infinitely thin film, $\psi(E)$ may be replaced by $\psi(E_0)$, where E_0 is the incident electron energy, and the emergent intensity becomes

$$I^A_{AB}=\frac{\phi(0)^A_{AB}}{\chi^A_{AB}}\,C^A_{AB}\,\frac{N}{A_A}\,\psi(E_0)\,d(\rho z).$$

For two specimens of composition AB and AC the intensity ratio k is

$$k=\frac{I^A_{AB}}{I^A_{AC}}=\frac{\phi(0)^A_{AB}\,\chi^A_{AC}\,C^A_{AB}}{\phi(0)^A_{AC}\,\chi^A_{AB}\,C^A_{AC}}$$

$$=\frac{\phi(0)^A_{AB}\,(\mu/\rho)^A_{AC}\,C^A_{AB}}{\phi(0)^A_{AC}\,(\mu/\rho)^A_{AB}\,C^A_{AC}}.$$

This is the expression for the 'thin-film approximation' (Duncumb and Melford 1966) and it is important to note that it involves no separate atomic number correction. Values for $\phi(0)$ are available in the literature; those given by Duncumb (Martin and Poole 1971) were obtained theoretically from backscattering results of Bishop (1966), while Reuter (1972) gave values based directly on thin-film experiments. To convert backscattering data into $\phi(0)$ values requires, however, knowledge of the ionization cross section $\psi(E)$, and unfortunately the exact form of ψ as a function of overvoltage E_0/E_c is not well established especially at low (<2) overvoltages. This is evident from the comparison made by Reuter (1972) and his empirical relationship for $\phi(0)$ shown below is therefore preferred:

$$\phi(0)=1+2{\cdot}8\,(1-0{\cdot}9\,E_c/E_0)\,\eta$$

where η is the backscattered fraction of electrons and depends upon atomic number. The expression indicates that $\phi(0)$ becomes substantially independent of probe voltage when $E_0>40\,E_c$, which agrees with present findings that k tends to a limiting value as E_0 is increased. The previous equation for the intensity ratio k also predicts that the limiting value of k is independent of x-ray take-off angle θ in accord with present experimental data on 20° and 35° take-off angle instruments and adding further support to the validity of the 'thin-film' approach.

Values of $\phi(0)$ listed in table 2 for the different oxides were calculated by weight-averaging η-values for the constituent elements. This method is preferable (Bishop 1966, 1968) to the alternative of first weight-averaging Z for the oxide and then determining $\phi(0)$, although differences between the two methods are generally small (~3% for the worst case studied) at overvoltages corresponding to limiting k-values. As is usual practice, μ/ρ for the sample may be calculated from data for the constituent elements according to $\mu/\rho=\sum_{i=1}^{i=n} C_i\,(\mu/\rho)_i$.

The criteria for the range of applicability of the 'thin-film approximation' in quantitative microanalysis may now be deduced. For the model to be valid the mean depth of x-ray generation $\overline{\rho z_g}$ must be greater than the mean depth of x-ray escape $\overline{\rho z_E}$ from the specimen. The mean depth of x-ray generation may be determined from $\phi(\rho z)$ curves, but, for present purposes, the Lenard law $j=j_0\exp(-\sigma\rho z)$ will be used as a first approximation: this gives $\overline{\rho z_g}$ as $1/\sigma$. Similarly the x-ray absorption profile is given by

$I = I_0 \exp(-\chi\rho z)$, and $\overline{\rho z}_E = 1/\chi$. Hence the criterion for validity may be written

$$\overline{\rho z}_g > \overline{\rho z}_E, \quad \text{ie} \quad \chi/\sigma > 1.$$

In agreement with this, the experimental data (figure 2) taken in conjunction with published values for σ (Salter 1970) indicate that $\chi/\sigma > 3$ for the 'thin-film' model to apply. Figure 2 also shows that k-values for the most heavily absorbing oxides (ZrO_2 and TiO_2) become dependent upon probe voltage below ~25 kV, an effect attributed to breakdown of the model for the Al_2O_3 standard ($\chi/\sigma \sim 3$ at 25 kV) rather than for the more heavily absorbing oxides. The use of oxide standards with lower mean μ/ρ than Al_2O_3 (eg Cr_2O_3 or BeO) should therefore be avoided in quantitative work with the 'thin-film' model unless very high probe voltages are available. Bishop (1974) has proposed a more stringent applicability criterion for the thin-film model, $f(\chi) < 0{\cdot}01$, ie $\chi/\sigma > 50$, which is of course more difficult to comply with in most practical microanalysis work. However, while Bishop's criterion may be important when considering x-ray intensities, it is suggested that the practice of taking intensity ratios would keep discrepancies in estimating limiting values for k within 5% for most of the results reported here.

Table 3. Calculated mass absorption coefficients for oxygen K x-rays: broken lines indicate absorption edges

Element	Z	μ/ρ	Element	Z	μ/ρ
O	8	1300	Fe	26	3630
F	9	1850	Co	27	4220
Ne	10	2750	Ni	28	5120
Na	11	3630	Cu	29	5660
Mg	12	4950	Zn	30	6380
Al	13	6230	Ga	31	7170
Si	14	8140	Ge	32	8030
P	15	9820	As	33	9000
S	16	12400	Se	34	9830
Cl	17	14300	Br	35	11100
A	18	16100	Kr	36	12100
K	19	20500	Rb	37	13400
Ca	20	24600	Sr	38	14700
Sc	21	26800	Y	39	16300
Ti	22	23200	Zr	40	17800
V	23	(26000)	Nb	41	19500
Cr	24	2470	Mo	42	21000
Mn	25	2960	Pb	82	15600

Once the range of applicability of the 'thin-film' approach has been established, mass absorption coefficients may be calculated from the experimental data. Since the only factors required, k and $\phi(0)$, may be deduced with an accuracy of ~5% and 3% respectively, such estimates should involve less uncertainty than previously published data. A suggested relationship between mass absorption coefficient and atomic number has been expressed as $\mu/\rho\,(A/N) = a\lambda^3 Z^4 + bZ^2$, where λ is the x-ray wavelength and a and b are constants between particular absorption edges (Compton and Allison 1935). By using this equation together with present results and Henke's directly measured absorption data for oxygen K x-rays, μ/ρ-values for a wide range of elements were calculated (table 3). The analysis was carried out using a least-squares regression technique; the

standard deviation from the regression line of these new data was 3%, the same as the experimental reproducibility, indicating that the regression equation used was satisfactory. The value for vanadium is considered to be less reliable, since it was estimated graphically by assuming the line passing through the titanium point lies parallel to the regression line between the K and LI edges; unfortunately this value could not be experimentally substantiated because of the proximity of the vanadium L and oxygen K bands (separation ~4 eV).

To reduce the complexity of mathematical analysis, $CaZrO_3$, Fe_2TiO_5, $PbMoO_4$, $NiTiO_3$ and $MgCr_2O_4$ were excluded, since the metallic elements in each of these compounds lay on different regression lines. The mean mass absorption coefficient for each of these oxides was subsequently calculated from data in table 3. Limiting k-values were then predicted and compared with experiment (table 4), the two sets of values showing good agreement.

Table 4. Comparison of predicted and measured limiting k-values for compounds excluded from regression analysis

Specimen	Predicted k_{11m}	Measured k_{11m}
$CaZrO_3$	0·192	0·185
Fe_2TiO_5	0·481	0·464
$PbMoO_4$	0·155	0·144
$NiTiO_3$	0·322	0·315
$MgCr_2O_3$	1·310	1·280

Absolute errors will, of course, depend upon the absolute accuracy of Henke's data which were measured from the attenuation of a collimated beam of x-rays. The absorption situation might be different in x-ray microanalysis where the x-ray source is divergent, although Henke considers that the scattering contribution $(\mu/\rho)_s$ to the absorption coefficient $\mu/\rho=(\mu/\rho)_s+(\mu/\rho)_p$, where $(\mu/\rho)_p$ is the photoelectric contribution, is small for the systems studied.

Computed values for μ/ρ (table 3) are illustrated graphically in figure 4, a plot of $\log(\mu/\rho)(A/Z)$ against $\log Z$, in order to facilitate comparison with other data. It should be noted that, apart from Henke's directly measured data, the present values are generally different from those often quoted in the literature (Weisweiler 1970); this is particularly the case for elements whose absorption edges are close to the energy of oxygen K x-rays. Data derived from microanalysis measurements (Kohlhaas and Scheiding 1970) clearly disagree for high values of μ/ρ. However, since these workers used the simple Philibert correction, which breaks down at high χ and overcorrects for absorption, calculated χ values would be expected to be low in such a treatment. It is also apparent that their μ/ρ results do not conform to a simple power law with Z, but, since no mention is made of the type of analysing crystal used nor how x-ray intensities were recorded, these data are difficult to assess; certainly there is no justification for their bending the line to pass through points for calcium and titanium as these elements lie on different sides of the LI absorption edge. Some measure of agreement with present results is evident in the interpolated values given by Gray and Wert (1969) (see figure 4).

Before concluding, the work of Shiraiwa and Fujino (1970) on oxygen analysis in oxides merits comment. These workers used the simple Philibert absorption formula together with an atomic number correction proposed by Poole and Thomas (1961–2) and claimed satisfactory agreement between theory and experiment when choosing the

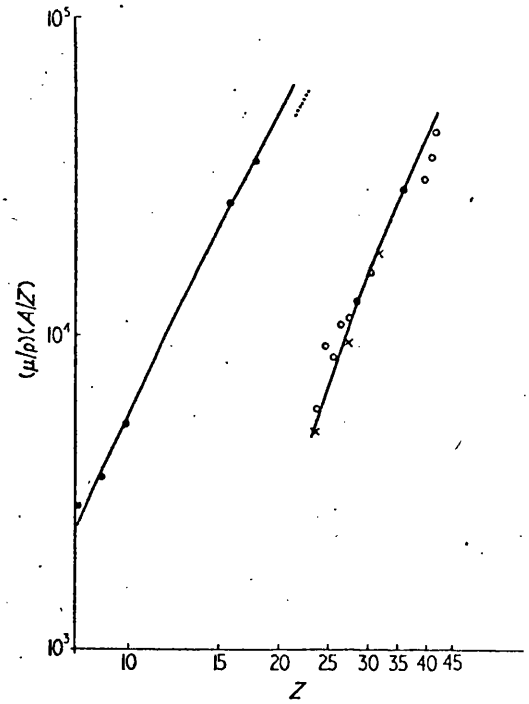

Figure 4. Plot of log $(\mu/\rho)(A/Z)$ against log Z. Data calculated from present results are shown as a continuous curve: broken curve between LI and LII edges is drawn through the titanium point and parallel to the line between the K and LI edges: ● Henke's direct measurements on gases; ○ Kohlhaas and Scheiding's data from microanalysis measurements; × Gray and Wert.

following mass absorption coefficients: Al (7000), Ti (19 500), Cr (3700), Fe (4700), Ni (5900), etc. Unfortunately, insufficient experimental information is given for detailed comparison with the present work, although it may be noted that their chosen μ/ρ-values are consistently higher for lower absorbers (eg chromium) and lower for higher absorbers (eg titanium) than coefficients listed in table 3. The application of this correction procedure and also other proposed models to quantitative light element microanalysis will be the subject of a later paper.

5. Conclusions

It has been shown that quantitative light-element microanalysis of oxygen may be achieved using a simple correction model whenever experimental conditions for analysis and specimen absorption characteristics are appropriate. These conditions are interrelated and a criterion for the range of applicability of the model has been determined. The approach is particularly suitable for analysing light elements, provided that sufficiently high probe voltages can be used. This restriction may, however, be serious in much practical light-element work since generally element detection sensitivities are considerably worse at higher kV where x-ray attenuation by absorption together with high background intensities reduce peak-to-background ratios.

Experimental results satisfying the applicability criterion have been used to determine mass absorption coefficients for oxygen K x-rays in a wide range of elements.

Following an assessment of experimental errors and of parameters contained in the theoretical treatment for x-ray emission intensities from solids, the accuracy of the method has been evaluated, and it is considered that these new data are more reliable than many others used by previous workers.

Acknowledgments

Thanks are due to Dr C W Haworth, Dr P Suddaby, Dr S E R Hiscocks and Mrs B Wanklin for provision of oxide crystals, to Dr L Hailes for the clinochlore, and to the SRC for support.

References

Beaman D R and Isasi J A 1972 *Electron Beam Microanalysis: ASTM Spec. Publ.* 506
Bishop H E 1966 *PhD Thesis*, University of Cambridge
—— 1968 *J. Phys.* D: *Appl. Phys.* 1 673–84
—— 1974 *J. Phys.* D: *Appl. Phys.* 7 2009–20
Compton A H and Allison S K 1935 *X-rays in Theory and Experiment*, 2nd edn (New York: Van Nostrand)
Duncumb P and Melford D A 1966 *X-ray Optics and Microanalysis* ed R Castaing, P Deschamps and J Philibert (Paris: Hermann) pp 240–53
Duncumb P and Shields P K 1966 *The Electron Microprobe* ed T D McKinley, K F J Heinrich and D A Wittry (New York: Wiley) pp 284–95
Ershov O A 1967 *Optics Spectrosc., Wash.* 22 252–4
Ershov O A, Brytov I A and Lukirski A P 1967 *Optics Spectrosc., Wash.* 22 66–9
Gray L S and Wert C A 1969 *Advances in X-ray Analysis* ed C S Barrett, J B Newkirk and G R Mallett (New York: Plenum Press) 12 563–78
Heinrich K F J and Yakowitz H 1969 *X-ray Optics and Microanalysis* ed G Möllenstedt and K H Gaukler (Berlin: Springer-Verlag) pp 151–9
Henke B L, Elgin R L, Lent R E and Ledingham R B 1967 *Norelco Reptr* 14 112–31
Kohlhaas E and Scheiding F 1970 *Arch. Eisenhüttenwes.* 41 97–101
Lukirski A P, Savinov E P, Ershov O A and Shepelev Yu F 1964 *Optics Spectrosc., Wash.* 16 168–72
Martin P M and Poole D M 1971 *Metall. Rev.* 150 ref. 137
Philibert J 1963 *X-ray Optics and Microanalysis* ed H H Pattee, V E Cosslett and E Engström (New York: Academic Press) p 379.
Poole D M and Thomas P M 1961–2 *J. Inst. Metals* 90 228
Ranzetta G V T and Scott V D 1966 *J. Sci. Instrum.* 43 816–9
Reuter W 1972 *X-ray Optics and Microanalysis* ed G Shinoda, K Kohra and T Ishinokawa (Tokyo: Tokyo UP) pp 121–30
Salter W M 1970 *Quantitative Electron Probe Microanalysis* (London: Structural Publication)
Shiraiwa T. and Fujino N 1970 *Jap. J. Appl. Phys.* 9 976–82
Weisweiler W 1970 *Microchim. Acta* 744–64

7.4 Electron Probe Microanalysis Using Oxygen X-rays: II Absorption Correction Models

G. Love, M.G.C. Cox and V.D. Scott,

1974b, J. Phys. D : Appl. Phys.

7, 2142

J. Phys. D: Appl. Phys., Vol. 7, 1974. Printed in Great Britain. © 1974

Electron probe microanalysis using oxygen x-rays: II. Absorption correction models

G Love, M G C Cox and V D Scott
School of Materials Science, University of Bath, Claverton Down, Bath, BA2 7AY

Received 1 May 1974, in final form 20 June 1974

Abstract. Proposed absorption correction methods for quantitative electron probe microanalysis are evaluated with reference to oxygen analysis of oxides. Three established absorption correction procedures, the Andersen–Wittry, simple Philibert and full Philibert models, are considered and their predictions compared with experimental measurements. The findings are discussed in relation to the x-ray distribution with depth in the target as given by the different models. It is shown that the full Philibert treatment gives best agreement, although none of the models provides a satisfactory absorption correction for practical light-element microanalysis.

1. Introduction

Much previous published work on quantitative light-element ($Z < 10$) microanalysis has employed reference standards of composition similar to the specimen or to the constituent being analysed. By this means the corrections which have to be applied to convert raw experimental data into quantitative results may be minimized, reducing in turn the likely errors caused by inaccurate correction models. While the method may be regarded as satisfactory it is generally inconvenient because of the large number of complex standards required, and a more comprehensive solution to the problem, which utilises a suitably accurate and well-tested correction model, is therefore preferable.

Although considerable information is available in the literature (see reviews by Martin and Poole 1971, Beaman and Isasi 1972) on correction procedures for quantitative electron probe microanalysis of heavy elements, their extension into the light-element region has received relatively little attention. The problems that can arise here have been referred to by a number of workers. For example, it has been argued that the physical basis of the respective models may be inappropriate for light-element microanalysis and also that input data such as x-ray mass absorption coefficients are unreliable. Ranzetta and Scott (1964, 1966) have discussed the use of the calculations of Archard and Mulvey (1963) and of Philibert (1963) in light-element studies, while Duncumb and Melford (1966) and Andersen (1967) have compared the Philibert treatment with the Monte Carlo calculations of Bishop (1966) in measurements of carbon K x-ray emission in carbon and carbides. Although these researches indicated that the simple Philibert expression was inappropriate for x-ray absorption corrections in the light-element region, Shiraiwa and coworkers claimed that it worked satisfactorily when applied, together with an atomic number correction proposed by Poole and Thomas (1961–2), to the analysis of carbon, boron (Shiraiwa *et al* 1972) and oxygen (Shiraiwa and Fujino 1970) in a number of compounds. While this difference of opinion may seem perhaps surprising, it should be

noted that Shiraiwa was selective about the choice of mass absorption coefficients and in some cases made adjustments to values given in the literature. In this connection, a new set of mass absorption coefficients for oxygen x-rays has recently been published (Love *et al* 1974); these are substantially different from the data used by Shiraiwa and Fujino and cast some doubt on the validity of their work on oxygen analysis. Application of both the simple and full Philibert expressions, in conjunction with an atomic number correction (Duncumb and Reed 1968) and a fluorescence correction (Reed 1965), to the analysis of titanium carbides was discussed by Gray and Wert (1969), who concluded that the absorption and the atomic number corrections were in error. The simple Philibert correction was used also by Kohlhaas and Scheiding (1969, 1970) in carbon and oxygen analyses but this work concentrated on deriving mass absorption coefficients from microanalysis measurements. A simple correction model, the thin-film approximation proposed specifically for light-element microanalysis by Duncumb and Melford (1966), was studied by Love *et al* (1974) with reference to the analysis of oxygen in oxides. Love established criteria for the range of applicability of this simple model and concluded that it could not be widely used in practical microanalysis.

In the present paper, three established absorption correction procedures, the Andersen-Wittry (Andersen and Wittry 1968), the simple Philibert and the full Philibert (1963) models are investigated with particular reference to quantitative microanalysis of oxygen in oxides; for present purposes the Duncumb and Reed (1968) atomic number correction has been used. Experimental measurements have been made over a range of probe voltages using two instruments with different x-ray take-off angles. The results are compared with calculated values for x-ray intensity ratios and are discussed in relation to the x-ray distribution with depth in the target as predicted by each model.

2. Experimental details

The range of binary and ternary oxides used in the investigation have been listed previously (Love *et al* 1974); in addition the methods employed for sample preparation and for x-ray intensity measurements were described. The study also produced a new set of mass absorption coefficients for oxygen x-rays which are considered more reliable than previous data; they have been used in evaluating the following, more comprehensive models.

Experimental data is presented here using electron probe voltages within the range 5–30 kV and the information is given as an intensity ratio, $k = I_{\text{specimen}}/I_{\text{standard}}$, the standard being alumina. Results were obtained on two different microanalysers, a JEOL JXA-50A with an x-ray take-off angle of 35° and a Cambridge Microscan I with a take-off angle of 20°. Reproducibility was found to be within $\pm 3\%$ for the first and $\pm 5\%$ for the second instrument, with the exception of PbO results ($\pm 10\%$) where the peak-to-background ratio was very low. The probe voltages quoted were found to be accurate to within 0·2 kV by measuring the short wavelength limit of continuous x-ray emission from a gold target.

3. Experimental results

Recorded x-ray intensity ratios k for the oxides studied are listed as a function of kV in table 1(*a* and *b*); the two sets of data refer to measurements made using the JEOL

Table 1. Experimental intensity ratios obtained using (*a*) the JXA 50A instrument (take-off angle 35°), (*b*) the Microscan I instrument (take-off angle 20°). Al_2O_3 standard in both cases.

(*a*)

Oxide formula	Probe voltage (kV) 5	10	15	20	25	30
MgO	0·812	0·876	0·913	0·915	0·927	0·920
Cr_2O_3	0·753	0·886	1·06	1·24	1·34	1·41
TiO_2	0·611	0·384	0·296	0·263	0·256	0·261
Fe_2O_3	0·723	0·782	0·887	0·960	1·02	1·03
NiO	0·502	0·484	0·496	0·488	0·486	0·488
PbO	—	—	0·085	0·085	0·080	0·071
MoO_3	0·541	0·351	0·271	0·264	0·263	0·253
ZrO_2	0·483	0·299	0·233	0·212	0·208	0·211
SiO_2	1·04	0·980	0·935	0·912	0·882	0·903
$MgAl_2O_4$	0·961	0·972	0·978	0·986	0·988	0·992
$MgCr_2O_4$	0·799	0·892	1·06	1·19	1·21	1·22
Fe_2TiO_5	0·672	0·550	0·500	0·473	0·451	0·464
$NiTiO_3$	0·586	0·423	0·346	0·323	0·315	0·315
$PbMoO_4$	0·363	0·222	0·181	0·167	0·152	0·144
$CaZrO_3$	0·457	0·262	0·214	0·195	0·188	0·185
$CaSiO_3$	0·683	0·425	0·365	0·322	0·330	0·330

(*b*)

Oxide formula	Probe voltage (kV) 6·5	10	15	20	25	30
MgO	0·849	0·887	0·946	0·966	0·957	0·930
Cr_2O_3	0·788	0·903	1·10	1·25	1·36	1·39
TiO_2	0·409	0·290	0·261	0·254	0·255	0·253
Fe_2O_3	0·722	0·810	0·905	0·936	0·987	1·012
NiO	0·501	0·464	0·452	0·458	0·469	0·480
PbO	0·125	0·093	0·101	0·092	0·101	0·091
MoO_3	0·405	0·288	0·251	0·250	0·255	0·260
ZrO_2	0·332	0·241	0·208	0·207	0·208	0·210
SiO_2	1·03	0·970	0·950	0·920	0·929	0·927
$MgAl_2O_4$	0·932	0·949	0·959	0·968	0·976	0·950
$MgCr_2O_4$	0·753	0·905	1·09	1·19	1·25	1·29
Fe_2TiO_5	0·586	0·498	0·450	0·461	0·454	0·460
$NiTiO_3$	0·433	0·333	0·286	0·299	0·289	0·295
$PbMoO_4$	0·228	0·179	0·156	0·155	0·155	0·173
$CaZrO_3$	0·338	0·230	0·197	0·194	0·193	0·196
$CaSiO_3$	0·543	0·402	0·336	0·323	0·345	0·347

JXA-50A and Cambridge Microscan I respectively. Proposed absorption correction models have been evaluated in conjunction with the atomic number correction given by Duncumb and Reed (1968) by comparing measured intensity ratios k with values k' predicted from the different models using the known compositions of oxide specimens. No fluorescence corrections have been applied in this study since in this region of the x-ray spectrum fluorescent yields are very small and the effect may be neglected (Duncumb and Melford 1966).

4. Discussion

4.1. X-ray distribution with depth

The accuracy of any proposed correction model depends upon its ability to predict correctly the x-ray distribution in the specimen. The x-ray production profile is usually given as curves showing the variation of $\phi(\rho z)$ with mass depth ρz, where $\phi(\rho z)$ is the ratio of x-rays generated in an infinitely thin layer of mass thickness $\mathrm{d}(\rho z)$ at mass depth ρz in a bulk specimen to those generated in an isolated film of the same mass thickness. On their way out of the sample, the generated x-rays suffer absorption and the intensity emerging at an angle θ to the surface may be written as

$$I=\int_0^\infty \phi(\rho z)\exp(-\chi\rho z)\,\mathrm{d}(\rho z),$$

where

$$\chi=(\mu/\rho)\operatorname{cosec}\theta$$

and μ/ρ is the mass absorption coefficient, or as

$$I=f(\chi)\int_0^\infty \phi(\rho z)\,\mathrm{d}(\rho z)$$

where $f(\chi)$ represents the fraction of the generated intensity $\int_0^\infty \phi(\rho z)\,\mathrm{d}(\rho z)$ reaching the x-ray detector. In quantitative microanalysis the x-ray intensity from the specimen is compared with that from a standard under identical analysis conditions to give the ratio

$$k'=\frac{I}{I_{\mathrm{STD}}}=\frac{C}{C_{\mathrm{STD}}}\,\frac{f(\chi)}{f(\chi)_{\mathrm{STD}}}\,\frac{\int_0^\infty \phi(\rho z)\,\mathrm{d}(\rho z)}{\int_0^\infty \phi(\rho z)_{\mathrm{STD}}\,\mathrm{d}(\rho z)}.$$

The last quotient in the above equation is termed the atomic number correction and is usually calculated separately from the absorption term $f(\chi)/f(\chi)_{\mathrm{STD}}$.

In the present study, the atomic number correction proposed by Duncumb and Reed (1968) has been used; values of the mean ionization potential of the target J are calculated from $J/Z=14[1-\exp(-0{\cdot}1Z)]+75{\cdot}5Z^{-Z/7{\cdot}5}-Z/(100+Z)$ where Z is the

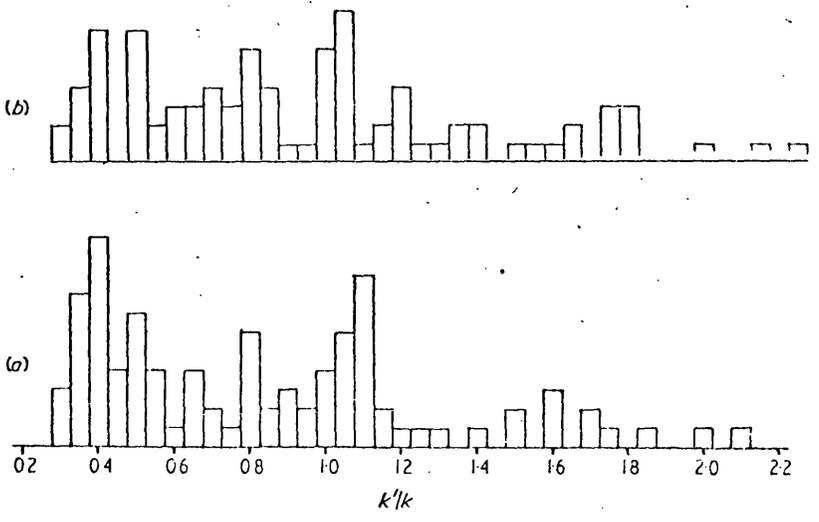

Figure 1. Histograms of oxygen microanalysis data, k'/k. (*a*) uncorrected measurements, (*b*) incorporating atomic number correction (Duncumb and Reed 1968) only.

atomic number (Duncumb *et al* 1969). This treatment has been previously tested for a wide range of systems and found to give satisfactory results (Poole 1968, Philibert 1969), although it has been suggested (Heinrich and Yakowitz 1970) that some uncertainties (several per cent in cases) are associated with the method. Such errors are, however, considered to be the lesser problem at this stage of the investigation since absorption corrections are generally very much greater than atomic number corrections in light-element microanalysis. This may be seen by comparing the effect of applying solely an atomic number correction to the present results, see figure 1(*a* and *b*), with data which includes both atomic number and absorption corrections, see for example figure 4.

There have been a number of approaches for deriving the absorption correction. Ideally the appropriate $f(\chi)$ values should be determined directly from experimental $\phi(\rho z)$ curves, but owing to a paucity of data, particularly in the light-element region, most treatments have involved semi-empirical approaches to the problem. The form of the $\phi(\rho z)$ curve is shown schematically in figure 2 and any successful model should predict

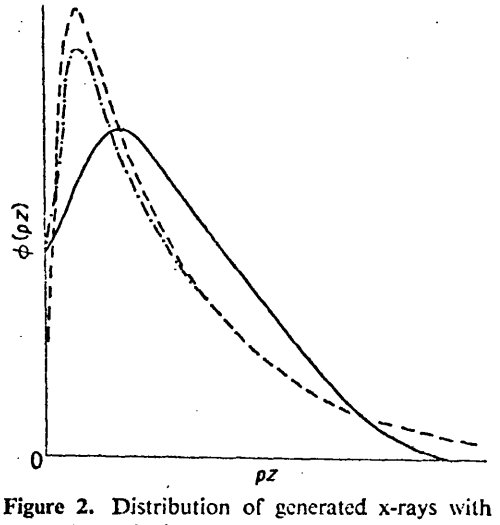

Figure 2. Distribution of generated x-rays with depth in target as deduced from: —— Monte Carlo (Bishop 1974); —·—·— full Philibert and - - - - simple Philibert treatments.

firstly the correct mean depth of ionization $\overline{\rho z}$ and secondly an appropriate shape function. For high values of $f(\chi)$, say $>0{\cdot}7$, the mean depth is the more important parameter but for lower values of $f(\chi)$, as in soft x-ray microanalysis, the shape function becomes increasingly significant (Bishop 1974). In the present study values of $f(\chi)$ range from 0·84 (Cr_2O_3, 5 kV, 35° take-off angle) to 0·02 (TiO_2, 30 kV, 20° take-off angle)—see also table 2.

4.2. Andersen–Wittry method

The absorption correction proposed by Andersen and Wittry (1968) is based upon a graphical procedure for obtaining $f(\chi)$ values. Essentially the method assumes that $f(\chi)$ is a function only of the mean depth of ionization and χ. By plotting $f(\chi)$ against $\chi\rho z'$, where $\rho z'$ is the effective mean depth of ionization, figure 3, it was shown that a single calibration curve could be produced using experimental data given by Castaing and Descamps (1955), Green (1963) and Castaing and Henoc (1966) on systems where

Table 2. Some relevant correction factors for selected oxide systems, see figure 6.
(1) Atomic number correction (Duncumb and Reed 1968); alumina standard.
(2) $f(\chi)$ values; full Philibert model; 35° take-off angle.
(3) $f(\chi)$ values; full Philibert model; 20° take-off angle.

Oxide formula		Probe voltage (kV) 5	6·5	10	15	20	25	30
	(1)	1·000	1·000	1·000	1·000	1·000	1·000	1·000
Al_2O_3	(2)	0·728	—	0·465	0·308	0·215	0·158	0·121
	(3)	—	0·503	0·331	0·200	0·133	0·095	0·072
	(1)	0·973	0·973	0·974	0·976	0·974	0·975	0·977
MgO	(2)	0·749	—	0·495	0·334	0·236	0·175	0·135
	(3)	—	0·532	0·358	0·220	0·147	0·106	0·080
	(1)	1·161	1·143	1·120	1·104	1·092	1·087	1·080
Cr_2O_3	(2)	0·843	—	0·643	0·485	0·371	0·289	0·231
	(3)	—	0·676	0·511	0·350	0·250	0·186	0·143
	(1)	1·121	1·107	1·092	1·082	1·073	1·069	1·064
TiO_2	(2)	0·412	—	0·177	0·097	0·062	0·043	0·033
	(3)	—	0·201	0·107	0·057	0·036	0·025	0·019
	(1)	1·344	1·297	1·241	1·202	1·175	1·161	1·149
ZrO_2	(2)	0·452	—	0·206	0·115	0·074	0·052	0·039
	(3)	—	0·232	0·126	0·067	0·043	0·030	0·022

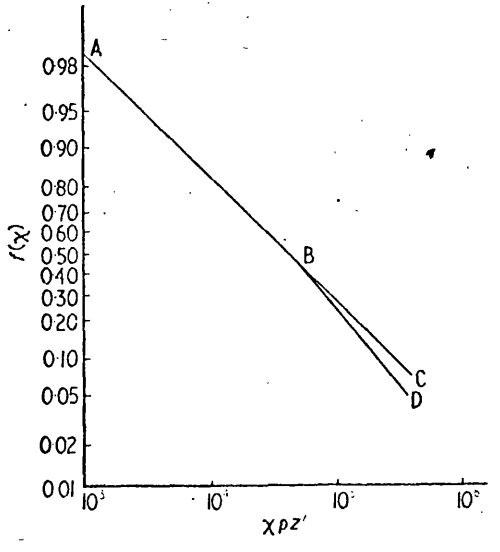

Figure 3. Universal $f(\chi)$ curve from Andersen and Wittry (1968).

$f(\chi) > 0{\cdot}5$ (figure 3, curve AB). For values of $f(\chi) < 0{\cdot}5$, however, the data given for lighter elements such as aluminium diverge from that for heavier systems (Cu, Au). Following Andersen's recommendation the curve for aluminium (figure 3, curve BD) has been used where the mean atomic number of the specimen is less than 26 and the Cu–Au curve (figure 3, curve BC) for samples of higher mean atomic number. Values for $\rho z'$ were

calculated from their equation

$$\rho z' = \frac{1}{Z^{1/3}} \frac{A}{Z} \left(\frac{E_0^{1.8}}{1.8 \ln (174 E_0/Z)} - \frac{E_c^{1.8}}{1.8 \ln (174 E_c/Z)} \right)$$

where E_0 is the applied voltage and E_c is the critical excitation potential of the element being analysed. Their account does not make it clear which averaging procedure should be adopted for A and Z, but present calculations have used weight-averaging. Many of the microanalysis results on oxide systems could not be included in evaluating the Andersen–Wittry method, since their calibration curves do not extend below $f(\chi) \sim 0{\cdot}1$; hence only 35° take-off angle results are discussed. Calculated intensity ratios, k' are compared with experimental intensity ratios k in the histogram, figure 4. The data ($\sim 80\%$ of the 35° take-off angle results) are seen to be grouped around $k'/k = 1$, with an RMS error of $\sim 9\%$; by rejecting all systems with $f(\chi) < 0{\cdot}5$ ($\sim 60\%$ of the results), the RMS error could be improved to $\sim 7\%$.

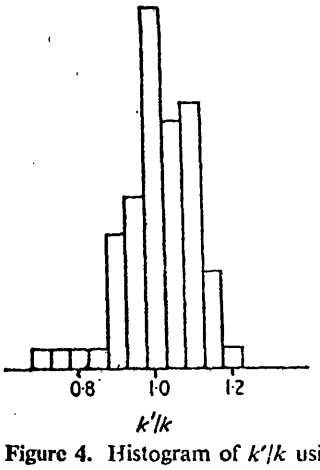

Figure 4. Histogram of k'/k using the Andersen–Wittry method: k' is the calculated and k is the experimental intensity ratio; 35° x-ray take-off angle results only.

4.3. Full Philibert model

Using a simplified model for electron scattering in solids, Philibert (1963) proposed a form for $\phi(\rho z)$ which may be written as

$$\phi(\rho z) = \xi \exp(-\sigma \rho z) - [\xi - \phi(0)] \exp[-(1 + 1/h)\, \sigma \rho z] \cdot \qquad (1)$$

where ξ represents the scattering function at a depth greater than the depth of complete diffusion and theoretically ~ 4, σ is the Lenard coefficient, and σ/h represents the variation in electron scattering with atomic number and has been evaluated using the Bothe theory of multiple scattering (Bothe 1929).

Hence integrating and putting $\xi = 4$ gives

$$f(\chi) = \frac{1 + \dfrac{\phi(0) h}{4 + \phi(0) h} \dfrac{\chi}{\sigma}}{\left(1 + \dfrac{\chi}{\sigma}\right)\left(1 + \dfrac{h}{1+h} \dfrac{\chi}{\sigma}\right)}.$$

In applying the full Philibert model to the present results, the following values for σ and h, obtained from a best-fit analysis to Green's $f(\chi)$ data (Green 1963), were used (Duncumb

and Melford 1966):

$$\sigma = \frac{2{\cdot}54 \times 10^5}{E_0^{1{\cdot}5} - E_c^{1{\cdot}5}}, \qquad h = 4{\cdot}5\, A/Z^2.$$

h was determined for the oxides by weight-averaging A and Z separately, although alternative averaging methods have been adopted by other workers (see Martin and Poole 1971, Beaman and Isasi 1972). $\phi(0)$ was calculated from an expression given by Reuter (1972), $\phi(0) = 1 + 2{\cdot}8\,(1 - 0{\cdot}9\, E_c/E_0)\eta$, where η is the backscatter coefficient given by

$$\eta = \sum_{i=0}^{n} C_i \eta_i.$$

Calculated and experimental intensity ratios are compared in figure 5(*a* and *b*) for 35° and 20° take-off angle geometries respectively. Both histograms show a slight positive bias (~1·5%), the RMS error from unity being 6% for the first set of data and 11% for the second. Even after taking into account the poorer experimental reproducibility

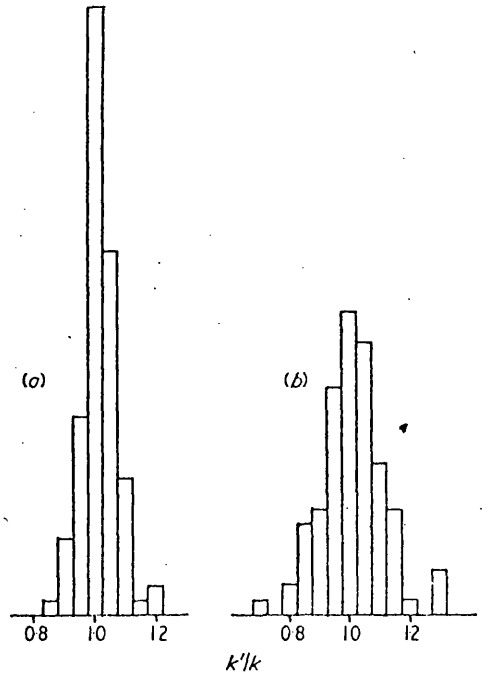

Figure 5. Histograms of k'/k using full Philibert model: (*a*) 35°, and (*b*) 20° x-ray take-off angle results.

for the lower take-off angle results, figure 5(*b*), it may be seen that the full Philibert correction is less satisfactory when applied to these data, ie where the magnitude of the absorption correction is greater. When values for k'/k are plotted, figure 6, as a function of kV for a typical selection of systems (MgO, Cr_2O_3, TiO_2 and ZrO_2, see table 2), it is apparent that the general shape of the curves is not changed substantially by reducing the take-off angle but that the discrepancies are greater. Since the atomic number effect would be the same for both geometries this is further evidence that the absorption correction is unsatisfactory. It would be useful to re-examine the expression for σ used in the absorption correction and to investigate whether the constants can be optimized

to improve the model for use over a much wider range of probe voltages, since values chosen by previous workers have been based on data with a bias towards operating voltages in the range 20–30 kV. Certainly evidence exists which would indicate that a square law (ie $\sigma \propto E_0^{-2}$) may be more appropriate (Philibert *et al* 1972). Hence it is not possible at this stage to decide the extent to which the atomic number correction may also be in error, although the large discrepancies ($\sim 20\%$) in Cr_2O_3 data at low kV, where absorption is relatively small in both specimen, $f(\chi) \sim 0{\cdot}8$, and standard $f(\chi) \sim 0{\cdot}7$, would suggest that it may be deficient particularly when applied to low-probe-voltage results, in accord with the conclusions of Gray and Wert (1969).

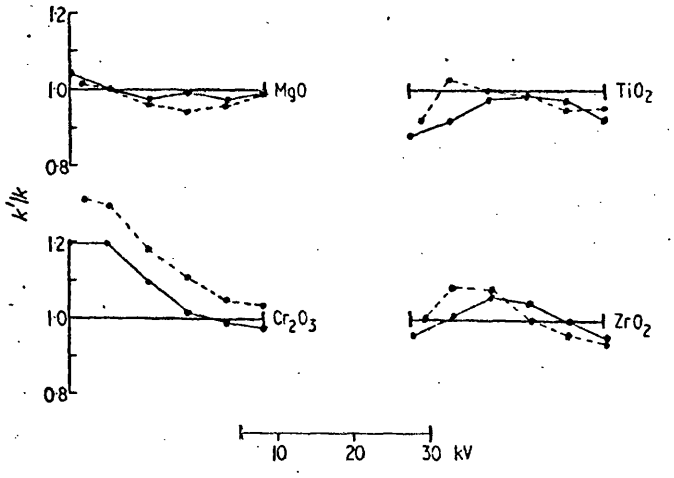

Figure 6. Plots of k'/k using full Philibert model for MgO, Cr_2O_3, TiO_2 and ZrO_2: full curve, 35°, and broken curve, 20° x-ray take-off angle results.

4.4. Simple Philibert model

Based upon experimental information available for the hard x-ray region, Philibert (1963) proposed a drastic simplification to the treatment described in the preceding section. He noted that good agreement with experiment was possible by neglecting $\phi(0)$ provided that h was suitably adjusted. The expression for $f(\chi)$ then becomes

$$f(\chi) = \left[\left(1+\frac{\chi}{\sigma}\right)\left(1+\frac{h}{1+h}\frac{\chi}{\sigma}\right)\right]^{-1} \qquad (2)$$

where h is now given by $h = 1{\cdot}2\ A/Z^2$. Both Heinrich (1968) and Duncumb *et al* (1969) have examined the applicability of the expression and concluded the optimum value for σ was given by

$$\frac{4{\cdot}5 \times 10^5}{E_0^{1{\cdot}65} - E_c^{1{\cdot}65}}.$$

These equations for h and σ are used in the present treatment, h being averaged as described in §4.3.

The calculated intensity ratios k' are compared with experimental data in figure 7(*a* and *b*). As with the full Philibert treatment both sets of results show a small positive bias of $\sim 1{\cdot}5\%$. Each distribution exhibits a skew character, most of which arises from results at high probe voltages. The greater spread in figure 7(*b*) (RMS error of $\sim 19\%$) compared with figure 7(*a*) (11%) is indicative of an inaccurate absorption correction, far

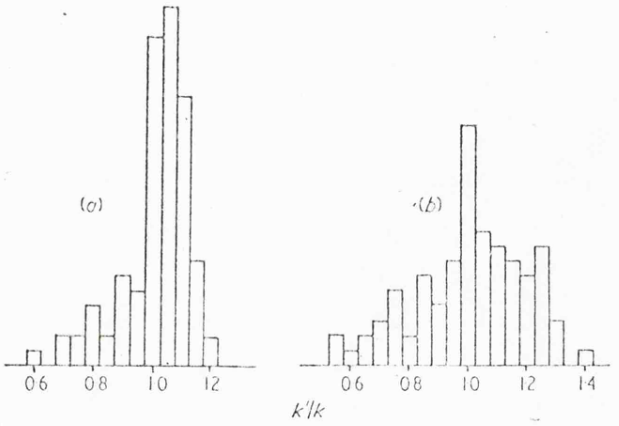

Figure 7. Histograms of k'/k using simple Philibert model: (*a*) 35°, and (*b*) 20° x-ray take-off angle results.

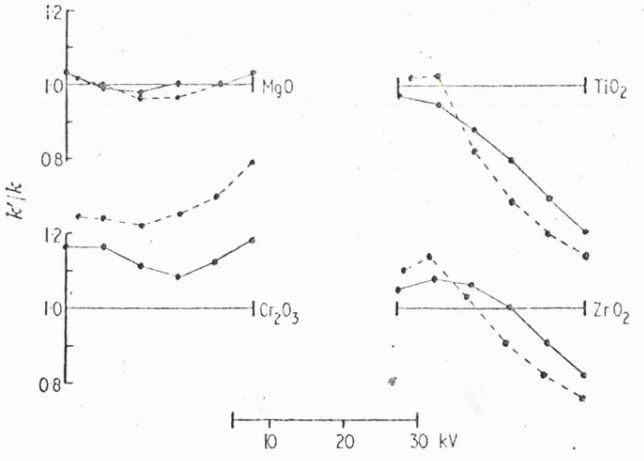

Figure 8. Plots of k'/k using simple Philibert model for MgO, Cr_2O_3, TiO_2 and ZrO_2: full curve, 35°, and broken curve, 20° x-ray take-off angle results.

worse than for the full Philibert procedure. The plots of k'/k against kV figure 8, show clearly that the simple Philibert treatment overcorrects for absorption at low $f(\chi)$ values. Hence when the specimen is more highly absorbing than the alumina standard, eg TiO_2 and ZrO_2, very low values of k'/k are obtained at the higher kV, whereas for less absorbing specimens, eg Cr_2O_3, k'/k is too high. Only when absorption characteristics for specimen and standard are similar, eg MgO, is the simple correction anywhere near satisfactory for light-element microanalysis.

4.5. Comparison of absorption correction methods

In the analysis of systems containing light elements, correct values of both the mean depth of ionization and the shape function are important and, depending upon the nature of the correction model and the probe voltage used, either or both of these parameters may be significantly in error. The expression for the mean depth in each of the three models tested involves a power function of the accelerating voltage which has been

optimized empirically using experimental values of $f(\chi)$ for microanalysis data obtained mostly in the 20–30 kV range. Hence it would not be surprising to find discrepancies present when operating outside this voltage range, as has been mentioned earlier.

The shape function assumed in the Andersen–Wittry method studied here is independent of overvoltage and atomic number. Thus when, below $f(\chi) \sim 0{\cdot}5$, the shape function becomes increasingly important, the method becomes correspondingly less accurate, as is borne out from data used by these authors and from the present oxygen microanalysis results. In an appendix to their paper Andersen and Wittry proposed the use of an analytical expression which assumes a Gaussian distribution for $\phi(\rho z)$ characterized by the median depth and standard deviation, but insufficient $\phi(\rho z)$ data are available for evaluating these parameters for a wide range of systems. It should also be noted that, while this assumption of a symmetrical Gaussian function for $\phi(\rho z)$ may allow the correct peak position and width to be predicted, such a model cannot be adjusted to give simultaneously the correct value for $\phi(0)$. The modifications recommended by Kyser (1972), who introduced an additional exponential term into the equation for $\phi(\rho z)$ to enable the correct value of $\phi(0)$ to be used, may improve the analytical expression of Andersen and Wittry, but neither of these two approaches has yet been tested.

It is clear that the simple Philibert model cannot be extended into the soft x-ray region where $f(\chi)$ is usually less than $\sim 0{\cdot}6$. A major criticism of the model is that ionization in the surface regions $\phi(0)$ has been assumed zero, and, consequently, incorrect limiting behaviour is predicted, ie from equation (2) as $\chi/\sigma \rightarrow \infty$

$$f(\chi) \approx \frac{1+h}{h} \frac{\sigma^2}{\chi^2} \propto \frac{1}{\chi^2}.$$

The correct limiting value for $f(\chi)$ may be obtained from the thin-film model (Duncumb and Melford 1966):

$$f(\chi) = \frac{\phi(0)}{\int_0^\infty \phi(\rho z)\, \mathrm{d}(\rho z)} \frac{1}{\chi} \propto \frac{1}{\chi}.$$

Thus the simple Philibert approach would increasingly overcorrect for absorption as χ takes larger values, in accord with the experimental observations on oxides. Some degree of compensation for the loss of ionization near the surface is achieved by distorting the true shape of the $\phi(\rho z)$ curve, ie adjusting the height and position of the maximum to give the correct mean depth, see figure 2, but this provides no comprehensive solution to the problem.

The full Philibert model provides a better representation of the x-ray distribution with depth, see figure 2, and it can be shown that the limit for $f(\chi)$ as $\chi/\sigma \rightarrow \infty$ is given by

$$f(\chi) \approx \frac{\phi(0)\,(1+h)}{4+\phi(0)\,h} \frac{\sigma}{\chi};$$

ie the correct limiting behaviour is predicted for highly absorbing systems. One criticism levelled at the full Philibert model is that the exponential decrease in $\phi(\rho z)$ at large mass depths is inappropriate, and, since it can be reasonably assumed that the value used for the mean depth of ionization is satisfactory, the ionization near the surface as described by the model may be correspondingly in error (see Duncumb and Melford 1966). Such a discrepancy would be particularly important in soft x-ray microanalysis where most of the detected x-rays originate close to the specimen surface. The mass depth ρz^* where the maximum value for $\phi(\rho z)$ occurs may be determined as follows in terms of the parameters $\phi(0)$, h, ξ and σ.

Differentiating equation (1) with respect to ρz and equating to zero gives

$$\rho z^* = \frac{h}{\sigma} \ln pq, \text{ where } p = 1 - \frac{\phi(0)}{\xi} \text{ and } q = \frac{h+1}{h}.$$

Now the mean mass depth $\overline{\rho z}$ is given by

$$\overline{\rho z} = \frac{\int_0^\infty \rho z \phi(\rho z)\, \mathrm{d}(\rho z)}{\int_0^\infty \phi(\rho z)\, \mathrm{d}(\rho z)}$$

and from equation (1) we may write

$$\overline{\rho z} = \frac{1}{\sigma} \frac{q^2 - p}{q^2 - pq}$$

Hence

$$\frac{\rho z^*}{\overline{\rho z}} = h \frac{q^2 - pq}{q^2 - p} \ln pq$$

Plots of $\rho z^*/\overline{\rho z}$ against h taking $\phi(0)/\xi$ values for carbon as 0·3 and for copper as 0·4 are given in figure 9. Both curves show broad maxima at $h \sim 0{\cdot}5$ and 0·4 with corresponding $\rho z^*/\overline{\rho z}$ values of 0·3 and 0·25 respectively. It is instructive to compare these deductions with predictions from the Monte Carlo calculations of Bishop (1966). Bishop concluded

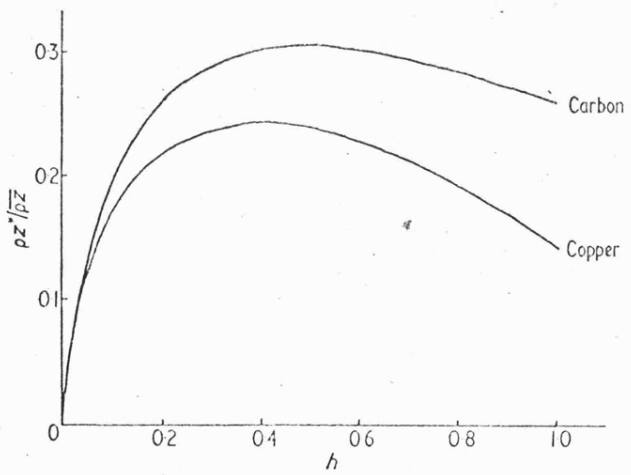

Figure 9. Plots of $\rho z^*/\overline{\rho z}$ against h for carbon and copper using full Philibert model: ρz^* is mass depth corresponding to maximum $\phi(\rho z)$ and $\overline{\rho z}$ is mean mass depth. $E_0/E_c = 10$.

that the Monte Carlo model gave a good representation of the shape of the $\phi(\rho z)$ curve on the basis of a comparison with the experimental data of Castaing and Descamps (1955), a view which was substantiated by Duncumb and Melford (1966) and Andersen (1967) in their studies of carbon K x-ray emission from carbon and carbides. From the calculations Bishop (1974) has deduced that, with $E_0/E_c = 10$, $\rho z^*/\overline{\rho z}$ is $\sim 0{\cdot}5$ for copper but for light elements can greatly exceed this value; for example, for carbon $\rho z^*/\overline{\rho z} \sim 1$. Hence while there is some agreement between the positions of the maxima deduced from the Monte Carlo and the full Philibert treatments for heavier elements such as copper, they differ considerably for light-element systems. In fact no amount of adjustment of h

in the Philibert expression will produce the correct shape function at the high overvoltages used in light-element work.

5. Conclusions

Correction procedures for quantitative electron probe microanalysis have been investigated with reference to their extension into the soft x-ray region. Since it has been argued that possible discrepancies in the x-ray absorption correction may far outweigh any error in the atomic number correction, attention has been focused on the applicability of three established absorption corrections: the Andersen–Wittry, full Philibert, and simple Philibert models. Each has been evaluated using experimental data obtained by oxygen x-ray analysis of well characterized binary and ternary oxides.

The present results have indicated that none of the three methods gives a satisfactory absorption correction which may be applied over a sufficiently wide range of experimental situations. Furthermore, while discrepancies may be unacceptably large in present studies using a compound standard of Al_2O_3, it is emphasized that agreement may be even worse if elemental standards are used (eg in the microanalysis of carbon and boron compounds).

The Andersen–Wittry empirical approach is severely limited since the concept of a universal $f(\chi)$ curve cannot be extended to highly absorbing systems; the method cannot therefore be recommended as useful for practical light-element microanalysis. The simple Philibert model is also restricted in its use and it has been shown that significant discrepancies occur between calculated and experimental results as a consequence of the assumption that $\phi(0)$ is zero. The full Philibert treatment was generally in best accord with experimental data but even here discrepancies, particularly at low kV, may be regarded as unacceptably large.

It may be concluded, therefore, that alternative correction procedures for absorption in quantitative light-element microanalysis must be sought and a future paper will discuss possible modifications to the full Philibert expression as well as evaluating the square model proposed by Bishop and Poole (1973). Finally, while it is considered that the Duncumb and Reed atomic number correction used in the present study may be the lesser problem at this stage, it is nevertheless believed that an improved atomic number correction may prove to be necessary in light-element microanalysis.

Acknowledgments

Thanks are due to the SRC for support of this work.

References

Andersen C A 1967 *Br. J. Appl. Phys.* **18** 1033–43
Andersen C A and Wittry D B 1968 *J. Phys.* D: *Appl. Phys.* **1** 529–40
Archard G D and Mulvey T 1963 *Br. J. Appl. Phys.* **14** 626–34
Beaman D R and Isasi J A 1972 *Electron Beam Microanalysis* ASTM STP 506
Bishop H E 1966 *PhD Thesis*, University of Cambridge
—— 1974 *J. Phys.* D: *Appl. Phys.* **7** 2009–20
Bishop H E and Poole D M 1973 *J. Phys.* D: *Appl. Phys.* **6** 1142–58

Bothe W 1929 *Z. Phys.* 54 161–78
Castaing R and Descamps J 1955 *J. Phys. Rad.* 16 304
Castaing R and Henoc J 1966 *X-ray Optics and Microanalysis* ed R Castaing, P Deschamps and J Philibert (Paris: Hermann) pp 120–6
Duncumb P and Melford D A 1966 *X-ray Optics and Microanalysis* ed R Castaing, P Deschamps and J Philibert (Paris: Hermann) pp 240–53
Duncumb P and Reed S J B 1968 *Quantitative Electron Probe Microanalysis* ed K F J Heinrich *NBS Spec. Publ.* 298 pp 133–54
Duncumb P, Shields-Mason P K and Da Casa C 1969 *X-ray Optics and Microanalysis* ed G Möllenstedt and K H Gaukler (Berlin: Springer-Verlag) pp 146–50
Gray L S and Wert C A 1969 *Advances in X-ray Analysis* ed C S Barrett, J B Newkirk and G R Mallett (New York: Plenum Press) 12 563–78
Green M 1963 *PhD Thesis*, University of Cambridge
Heinrich K F J 1968 *Advances in X-ray Analysis* ed J B Newkirk, G Mallett and H G Pfeiffer (New York: Plenum Press) 11 40–55
Heinrich K F J and Yakowitz H 1970 *Microchim. Acta* 123–34
Kohlhaas E and Scheiding F 1969 *X-ray Optics and Microanalysis* ed G Möllenstedt and K H Gaukler (Berlin: Springer-Verlag) pp 193–7
—— 1970 *Archiv. Eisenh.* 41 97–101
Kyser D F 1972 *X-ray Optics and Microanalysis* ed G Shinada, K Kohra and T Ishinokawa (Tokyo: Tokyo UP) pp 147–56
Love G, Cox M G C and Scott V D 1974 *J. Phys.* D: *Appl. Phys.* 7 2131–41
Martin P M and Poole D M 1971 *Metall. Rev.* 150
Philibert J 1963 *X-ray Optics and Microanalysis* ed H H Pattee, V E Cosslett and E Engström (New York: Academic Press) pp 379–92
——1969 *X-ray Optics and Microanalysis* ed G Möllenstedt and K H Gaukler (Berlin: Springer-Verlag) pp 114–31
Philibert J, Bryckaert D and Tixier R 1972 *X-ray Optics and Microanalysis* ed G Shinoda, K Kohra and T Ishinokawa (Tokyo: Tokyo UP) pp 157–62
Poole D M 1968 *Quantitative Electron Probe Microanalysis* ed K F J Heinrich *NBS Spec. Publ.* 298 pp 93–131
Poole D M and Thomas P M 1961–2 *J. Inst. Metals* 90 228–33
Ranzetta G V T and Scott V D 1964 *Br. J. Appl. Phys.* 15 263–74
—— 1966 *X-ray Optics and Microanalysis* ed R Castaing, P Deschamps and J Philibert (Paris: Hermann) pp 254–62
Reed S J B 1965 *Br. J. Appl. Phys.* 16 913
Reuter W 1972 *X-ray Optics and Microanalysis* ed G Shinoda, K Kohra and T Ishinokawa (Tokyo: Tokyo UP) pp 121–30
Shiraiwa T and Fujino N 1970 *Jap. J. Appl. Phys.* 9 976–82
Shiraiwa T, Fumino N and Murayama J 1972 *X-ray Optics and Microanalysis* ed G Shinoda, K Kohra and T Ishinokawa (Tokyo: Tokyo UP) pp 213–8

7.5 Electron Probe Microanalysis of Oxygen in Heat Treated Orlon Fibres.

G. Love, M.G.C. Cox and V.D. Scott, 1975a Materials Research Bulletin 10, 815.

Mat. Res. Bull. Vol. 10, pp. 815-818, 1975. Pergamon Press, Inc. Printed in the United States.

ELECTRON-PROBE MICROANALYSIS OF OXYGEN IN HEAT-TREATED ORLON FIBRES

G. Love, M.G.C. Cox and V.D. Scott,
School of Materials Science,
University of Bath, U.K.

(Received May 28, 1975; Refereed)

ABSTRACT

A method of using electron probe microanalysis to measure oxygen contents of heat treated Orlon fibres is described. The method utilizes specimens in the form of thin sections (~ 1 μm thick) which are coated with a thin layer of gold prior to analysis. It is shown that by comparing oxygen X-ray spectra obtained from inner and outer regions of certain heat-treated fibres the presence of oxygen gradients may be established. The findings are discussed in relation to rate controlling processes occurring during oxidation.

Carbon fibres are produced from certain types of filamentary polymers, notably polyacrylonitrile (PAN), by thermal treatment. The heat treatment schedule for PAN is critical and must be optimised for each size and commercial grade of precursor in order to achieve a satisfactory yield of carbon fibre with the desired mechanical properties. An important stage in the process (1) involves heating the polymer fibres in air under tension prior to pyrolysis. This oxidation reaction raises the softening temperature above the decomposition temperature and thus prevents fibres sticking together during subsequent pyrolysis.

Watt and Johnson (1) showed that 3 denier (2.65×10^{-4} mm^2 cross section) Courtelle (a circular PAN fibre containing 6% methyl acrylate comonomer and acid comonomer) gave an optimum yield of carbon fibres after oxidation in air for 6 hours at 220°C, the oxygen uptake of the fibres being estimated as 9% using a Coleman oxygen analyser. A limiting oxygen uptake of 12 wt % was found after prolonged oxidation at 220°C but such extended treatments, while tending to increase the elastic modulus of the carbon fibre, were found to give lower yields. Microscopic examination of sections through Courtelle fibres heat-treated in air for times shorter than the optimum revealed a dark outer zone. The extent of this zone was found to increase with oxidation time and was therefore believed to be associated with oxygen uptake. However, a zone structure was not usually evident in oxidised Orlon (a bean shaped PAN fibre containing 6% methyl acrylate only) unless heat treated in vacuo prior to oxidation (2). There is thus considerable interest in establishing if a zone structure is indicative of an oxygen gradient across the fibre and how this may affect the carbon fibre production process. Because of the small cross section of

the PAN fibres, however, chemical analysis of zoned regions is difficult. In this paper the use of electron-probe microanalysis to study the oxygen distribution in oxidised Orlon fibres is described. Some preliminary results are given and discussed in relation to the oxidation mechanism.

Two samples of 1.8 denier Orlon (1.65×10^{-4} mm^2 cross section) fibres were selected for this study, batch A having been heated in air for 1 hour at 240°C and batch B for 1 hour in vacuum at 230°C prior to treatment in air at 230°C. A JEOL JXA 50A electron probe microanalyser with a stearate crystal for oxygen analysis was used. Experiments were carried out on polished sections through fibres mounted in various compounds and also on thin sections prepared by ultra-microtomy. Cold setting resins were unsuitable for mounting specimens because they contain oxygen and are poor thermal and electrical conductors. Mounting in Woods metal was also unsatisfactory because wetting of the fibres did not occur, resulting in poor electrical and thermal contact. Thin sections mounted on polished beryllium and coated with carbon gave better results but background radiation was high because of specular reflection of soft X-rays. The method finally adopted was to mount 1µm sections on a carbon film supported on copper microscope grids; these were then coated with 100 Å of gold. Specimen damage due to electron irradiation, while frequently a problem in polymer analysis, did not prevent useful information being obtained on heat-treated Orlon samples; it was noted, however, that untreated material was much less stable during electron bombardment. Probe conditions were set at 10 kV with a current as measured on a bulk copper standard of 50 nA; this gave a probe size of ~5000 Å. Oxygen X-ray measurements were carried out by positioning the probe on a selected feature of the specimen and rotating the spectrometer system through the oxygen peak. Peak and background measurements were read from the spectral trace recorded on a chart. X-ray analysis recordings were made from three regions on each fibre section (indicated typically by a, b and c in Figs 1 and 2).

An optical micrograph taken in transmitted light from sections cut from batch A is illustrated in Fig 1; these sections possessed a uniform brown colour.

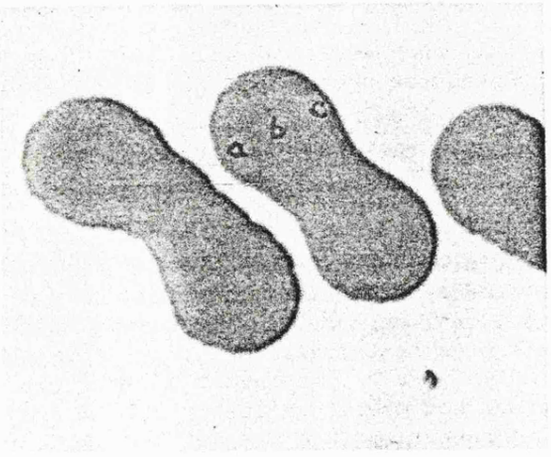

FIG 1.
1.8 denier Orlon. Heated 1 hr. in air at 240°C (batch A) Optical micrograph x2000.

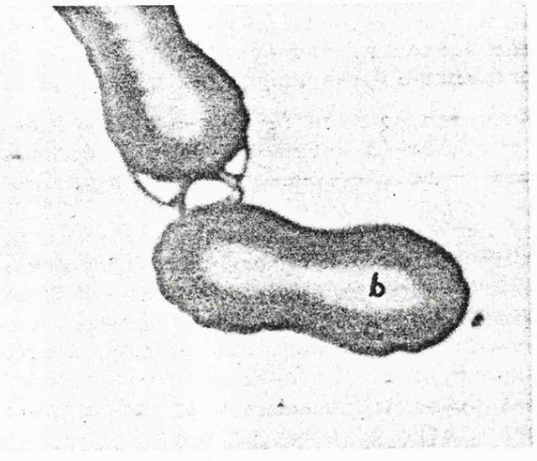

FIG 2.
1.8 denier Orlon. Heated 1 hr. in vacuum at 230°C, then 1 hr. in air at 230°C (batch B). Optical micrograph x2000.

The microanalysis results from three such sections are given in Table 1 as counts/sec for peak (P) and background (B). Values for $\frac{P-B}{B}$ are also given in the table; these are more reliable for comparison purposes since, as Hall has shown (3), effects due to thickness differences between sections are minimised. Sections cut from batch B showed a zone structure on optical examination, Fig 2; they were brown on the outside and yellow on the inside. The relevant microanalysis data are given in Table 2.

TABLE 1

Sections from batch A. Orlon fibre heated in air for 1 hour at 240°C.

	Section 1			Section 2			Section 3		
	a	b	c	a	b	c	a	b	c
P	60	65	60	73	77	92	45	74	60
B	47	57	47	54	54	65	34	53	44
$\frac{P}{B}$	1.28	1.27	1.28	1.37	1.42	1.42	1.32	1.40	1.36
$\frac{P-B}{B}$	0.28	0.27	0.28	0.37	0.42	0.42	0.32	0.40	0.36

TABLE 2

Sections from batch B. Orlon fibre heated in vacuum for 1 hour at 230°C and then in air for 1 hour at 230°C.

	Section 1			Section 2			Section 3		
	a	b	c	a	b	c	a	b	c
P	67	53	60	41	58	41	35	33	29
B	41	39	39	28	55	32	28	30	24
$\frac{P}{B}$	1.64	1.36	1.54	1.46	1.08	1.28	1.25	1.10	1.21
$\frac{P-B}{B}$	0.64	0.36	0.54	0.46	0.08	0.28	0.25	0.10	0.21

The above results show that oxygen can be detected by electron probe microanalysis in heat-treated Orlon fibres. In batch A (see Fig 1), no significant difference was found in oxygen concentration across the fibre, the small differences in the $\frac{(P-B)}{B}$ figure lying within the experimental error. In batch B (see zone structure in Fig 2), it was possible to detect differences in oxygen concentration across the fibre, the oxygen level being significantly higher in the outer regions than in the core. It may be noted from Table 2, that the apparent concentration profiles differed from one section to another; this effect, which may be attributed to specimen thickness variations and to non-normal incidence of the electron beam, has been minimised by taking $\frac{(P-B)}{B}$ values. It may be inferred from these data that in batch A the rate controlling process is the oxidation reaction and that the effect of vacuum heat treatment prior to oxidation is to change the rate controlling

process to oxygen diffusion. Previous work (4) has shown vacuum heat treatment of the linear polyacrylonitrile polymer causes conversion to a ladder polymer. This process is initiated at acidic sites on the polymer chain. The ladder polymer oxidises more readily than the initial linear polymer due to the formation of activated methylene groups at positions flanked by $-\underset{\underset{CN}{|}}{CH}-$ groups (5). Hence during oxidation of batch B the high rate constant for the oxidation ensures that the reaction is diffusion limited and therefore zoning occurs. For batch A given no prior heat treatment in vacuum the rate of reaction is determined by the rate at which ladder polymer is formed. This is a slow process relative to the oxidation reaction and, consequently, oxygen may diffuse through the specimen sufficiently fast to oxidise all the ladder polymer as it forms. Thus no zoning occurs in batch A. This mechanism also accounts for the zone structure observed in Courtelle fibres which have not been given prior heat treatment in vacuum (1) since the addition of acid comonomer causes a faster conversion to ladder polymer.

Thanks are due to Messrs. W. Watt, and W. Johnson of Materials Department, R.A.E. Farnborough for helpful discussions and provision of specimens and micrographs.

References

1. W. Watt and J. Johnson, Conference on Industrial Carbon and Graphites. Soc. Chem. Ind. London, 417 (1970).
2. W. Watt, Private Communication.
3. T. Hall, Quantitative Electron Probe Microanalysis ed. Heinrich,N.B.S. Spec. Pub. 298, 269 (1968).
4. N. Grassie and J. Hay, J. Polymer Sci. 56, 189 (1962).
5. J. Brandrup and L. H. Peebles, Macromolecules, 1, 64 (1968).

7.6 Assessment of Philibert's Absorption Correction Models in Electron Probe Microanalysis.

G. Love, M.G.C. Cox and V.D. Scott, 1975b, J. Phys. D : Appl. Phys., 8, 1686.

J. Phys. D: Appl. Phys., Vol. 8, 1975. Printed in Great Britain. © 1975

Assessment of Philibert's absorption correction models in electron-probe microanalysis

G Love, M G C Cox and V D Scott
School of Materials Science, University of Bath, Bath BA2 7AY

Received 12 March 1975, in final form 2 May 1975

Abstract. The values of the constants in the expression for h and σ, employed in the full and simple Philibert absorption correction procedures, have been optimized by making use of extensive experimental microanalysis data on binary systems. New values are proposed which differ substantially from previously accepted constants and which, for most systems, improve the accuracy of these absorption corrections. However, both Philibert models are still inadequate when applied to soft x-ray measurements. Based upon the present findings, some comments are made with reference to methods of averaging h for multicomponent systems and also to atomic number corrections.

1. Introduction

The absorption correction most widely used in quantitative electron-probe microanalysis is based upon the formula given by Philibert (1963) which may be written as

$$f(\chi)=\frac{1+h}{(1+\chi/\sigma)\,[1+h\,(1+\chi/\sigma)]}. \tag{1}$$

$\chi=(\mu/\rho)\,\mathrm{cosec}\,\theta$, where μ/ρ is the mass absorption coefficient and θ is the x-ray take-off angle; $h=1{\cdot}2\,A/Z^2$ is a parameter which accounts for electron-scattering behaviour in the specimen, where A is atomic weight and Z is the atomic number; σ is the Lenard coefficient which is tabulated by Philibert as a function of kilovoltage.

After examination of the $f(\chi)$ curves of Castaing and Descamps (1955) and Green (1963), Duncumb and Shields (1966) suggested the use of

$$\sigma=2{\cdot}39\times10^5/(E_0^{1{\cdot}5}-E_c^{1/5})$$

where E_0 is the probe voltage and E_c is the critical x-ray excitation voltage, while Heinrich (1967) proposed that the accuracy of the correction could be further improved by using

$$\sigma=4{\cdot}5\times10^5/(E_0^{1{\cdot}65}-E_c^{1{\cdot}65}).$$

This was later confirmed by Duncumb *et al* (1969) from analysis of a large number of practical microanalysis data. A criticism of the above work is, however, that the expression was derived from microanalysis data obtained mainly at high probe voltages (greater than 15 kV), and therefore its applicability to lower kV is uncertain.

Equation (1) is, in effect, a simplification of the full expression given by Philibert (1963)

$$f(\chi)=\frac{1+[\phi\,(0).h/(4+\phi\,(0).h)]\,(\chi/\sigma)}{(1+\chi/\sigma)\,(1+h\chi/(1+h)\,\sigma)}. \tag{2}$$

$\phi(0)$ is the ratio of x-rays generated in a thin layer of mass thickness $d(\rho z)$ at the surface of a bulk specimen to those generated in an isolated film of the same mass thickness. Philibert suggested that h should be taken as $3{\cdot}5\,A/Z^2$ but gave little indication of the appropriate σ values to be used, while from a study of $f(\chi)$ curves (Castaing 1960, Green 1963) Duncumb and Melford (1966) proposed values of $4{\cdot}5\,A/Z^2$ for h and $2{\cdot}54\times10^5/(E_0^{1{\cdot}5}-E_c^{1{\cdot}5})$ for σ. No rigorous test of this expression has, however, been carried out using experimental microanalysis data.

In the present paper, microanalysis results obtained over a wide range of probe voltages are evaluated in detail, and revised values of h and σ for both the full and simple Philibert models are put forward. The present findings are also discussed with reference to methods proposed for averaging h for multicomponent systems and to the use of these correction models in light element work.

2. Microanalysis data

A survey of published microanalysis measurements on binary systems was carried out. Data were excluded where there were substantial differences between the mass absorption coefficients quoted by Theisen and Vollath (1967) and Heinrich (1966). The final selection of data comprised 471 microanalysis measurements (table 1). These have been plotted as c_i/k_i in a histogram (figure 1) in order to give an indication of the magnitude of the correction factors required; c_i is the actual concentration and k_i is the measured intensity ratio. The correction methods described below were applied using a computer program.

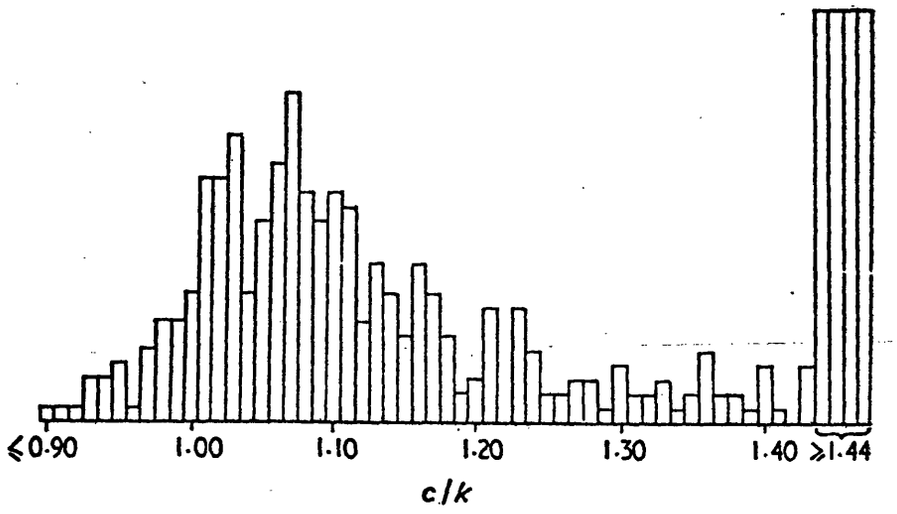

Figure 1. Histogram of uncorrected microanalysis data; data in block on right of diagram includes results where c/k ranges from 1·44 to ~15.

3. Correction procedures

3.1. Fluorescence corrections

The fluorescence correction proposed by Reed (1965) to account for excitation by characteristic x-ray radiation was applied; it was found to be less than 1% for the majority

Table 1. Summary of microanalysis data and important constants for 471 binary systems. (1) refers to the element being analysed and (2) pertains to the other binary constitutent. Fluor code takes a value of 1 or 0 according to whether a characteristic fluorescence correction has been applied or not.

The system numbers have the following references: 1–220, Poole (1968); 221–240, Friskney and Haworth (1968); 241–243, Brown (1964); 244–249, Yakowitz *et al* (1969); 250–255, Shimizu *et al* (1972); 256–313, Peisker (1967); 314–422, Thoma (1970); 423–437, Springer (1966); 438–471, Beaman and Solosky (1972).

System number	Atomic number (1)	Atomic number (2)	Mass absorption coefficient (1)	Mass absorption coefficient (2)	Critical exit energy (1)	Weight fraction (1)	Int. ratio (1)	Probe voltage	Take-off angle	Fluor code
1	28	78	58·80	242·00	8·33	0·551	0·560	30·00	15·50	1
2	28	78	58·80	242·00	8·33	0·297	0·305	30·00	15·50	1
3	28	78	58·80	242·00	8·33	0·164	0·166	30·00	15·50	1
4	28	78	58·80	242·00	8·33	0·065	0·067	30·00	15·50	1
5	78	28	131·80	242·40	11·56	0·449	0·345	30·00	15·50	0
6	78	28	131·80	242·40	11·56	0·703	0·580	30·00	15·50	0
7	78	28	131·80	242·40	11·56	0·836	0·775	30·00	15·50	0
8	78	28	131·80	242·40	11·56	0·935	0·884	30·00	15·50	0
9	29	79	53·60	217·50	8·98	0·794	0·789	30·00	15·50	1
10	29	79	53·60	217·50	8·98	0·598	0·585	30·00	15·50	1
11	29	79	53·60	217·50	8·98	0·399	0·386	30·00	15·50	1
12	29	79	53·60	217·50	8·98	0·201	0·194	30·00	15·50	1
13	79	29	127·50	245·50	11·92	0·206	0·152	30·00	15·50	0
14	79	29	127·50	245·50	11·92	0·402	0·324	30·00	15·50	0
15	79	29	127·50	245·50	11·92	0·601	0·505	30·00	15·50	0
16	79	29	127·50	245·50	11·92	0·799	0·730	30·00	15·50	0
17	30	47	48·80	179·20	9·66	0·075	0·061	30·00	15·50	0
18	30	47	48·80	179·20	9·66	0·146	0·128	30·00	15·50	0
19	79	47	127·50	130·30	11·92	0·199	0·186	30·00	15·50	1
20	79	47	127·50	130·30	11·92	0·405	0·399	30·00	15·50	1
21	79	47	127·50	130·30	11·92	0·594	0·593	30·00	15·50	1
22	79	47	127·50	130·30	11·92	0·804	0·780	30·00	15·50	1
23	44	73	633·80	2734·20	2·84	0·835	0·614	30·00	15·50	1
24	44	73	633·80	2734·20	2·84	0·691	0·431	30·00	15·50	1
25	44	73	633·80	2734·20	2·84	0·566	0·282	30·00	15·50	1
26	44	73	633·80	2734·20	2·84	0·456	0·197	30·00	15·50	1
27	44	73	633·80	2734·20	2·84	0·358	0·140	30·00	15·50	1
28	44	73	633·80	2734·20	2·84	0·193	0·067	30·00	15·50	1
29	44	73	633·80	2734·20	2·84	0·059	0·017	30·00	15·50	1
30	73	44	156·30	174·30	9·88	0·165	0·160	30·00	15·50	1
31	73	44	156·30	174·30	9·88	0·309	0·289	30·00	15·50	1
32	73	44	156·30	174·30	9·88	0·434	0·414	30·00	15·50	1
33	73	44	156·30	174·30	9·88	0·544	0·532	30·00	15·50	1
34	73	44	156·30	174·30	9·88	0·642	0·635	30·00	15·50	1
35	73	44	156·30	174·30	9·88	0·807	0·800	30·00	15·50	1
36	73	44	156·30	174·30	9·88	0·941	0·960	30·00	15·50	1
37	74	44	150·80	160·30	10·20	0·168	0·180	30·00	15·50	1
38	74	44	150·80	160·30	10·20	0·438	0·444	30·00	15·50	1
39	74	44	150·80	160·30	10·20	0·645	0·655	30·00	15·50	1
40	74	44	150·80	160·30	10·20	0·809	0·825	30·00	15·50	1
41	74	44	150·80	160·30	10·20	0·942	0·965	30·00	15·50	1
42	45	74	593·70	2489·20	3·00	0·911	0·776	30·00	15·50	1
43	45	74	593·70	2489·20	3·00	0·688	0·425	30·00	15·50	1
44	45	74	593·70	2489·20	3·00	0·564	0·293	30·00	15·50	1
45	45	74	593·70	2489·20	3·00	0·410	0·185	30·00	15·50	1
46	45	74	593·70	2489·20	3·00	0·153	0·069	30·00	15·50	1
47	45	74	593·70	2489·20	3·00	0·024	0·008	30·00	15·50	1
48	74	45	150·80	171·00	10·20	0·089	0·088	30·00	15·50	1
49	74	45	150·80	171·00	10·20	0·312	0·306	30·00	15·50	1
50	74	45	150·80	171·00	10·20	0·436	0·423	30·00	15·50	1
51	74	45	150·80	171·00	10·20	0·590	0·556	30·00	15·50	1
52	74	45	150·80	171·00	10·20	0·847	0·814	30·00	15·50	1
53	74	45	150·80	171·00	10·20	0·976	0·970	30·00	15·50	1
54	92	8	94·30	2·70	17·16	0·881	0·826	30·00	15·50	0
55	92	6	94·30	1·10	17·16	0·952	0·924	30·00	15·50	0
56	92	8	94·30	2·70	17·16	0·882	0·837	28·50	15·20	0
57	92	13	94·30	11·50	17·16	0·815	0·725	28·50	15·20	0
58	92	13	695·40	662·50	3·55	0·815	0·728	11·00	15·40	0
59	29	13	53·60	49·90	8·98	0·536	0·496	28·50	16·00	0
60	40	14	22·10	9·50	17·99	0·620	0·544	28·50	15·00	0
61	40	14	22·10	9·50	17·99	0·796	0·748	28·50	15·00	0
62	40	13	22·10	7·70	17·99	0·530	0·472	28·50	15·00	0
63	40	8	22·10	1·70	17·99	0·945	0·920	28·50	15·00	0
64	12	39	459·10	2759·80	1·30	0·406	0·274	16·50	17·50	1
65	79	25	127·80	168·20	11·92	0·766	0·683	28·50	17·30	0
66	79	31	127·80	39·00	11·92	0·739	0·718	28·50	17·30	0
67	79	47	127·80	130·10	11·92	0·500	0·470	30·00	17·30	1
68	79	47	127·80	130·10	11·92	0·500	0·450	19·40	17·30	0
69	79	29	127·80	244·50	11·92	0·238	0·174	28·50	17·30	0
70	79	29	127·80	244·50	11·92	0·527	0·433	28·50	17·30	0
71	79	29	127·80	244·50	11·92	0·600	0·502	33·90	17·30	0
72	79	29	127·80	244·50	11·92	0·600	0·510	28·20	17·30	0
73	79	29	127·80	244·50	11·92	0·600	0·514	22·50	17·30	0
74	79	29	127·80	244·50	11·92	0·600	0·500	19·80	17·30	0
75	79	29	127·80	244·50	11·92	0·600	0·498	16·80	17·30	0
76	79	29	127·80	244·50	11·92	0·200	0·140	33·90	17·30	0
77	79	29	127·80	244·50	11·92	0·200	0·146	28·20	17·30	0
78	79	29	127·80	244·50	11·92	0·200	0·147	22·50	17·30	0
79	79	29	127·80	244·50	11·92	0·200	0·145	19·80	17·30	0

Table 1.—*Continued*

System number	Atomic number (1)	Atomic number (2)	Mass absorption coefficient (1)	Mass absorption coefficient (2)	Critical exit energy (1)	Weight fraction (1)	Int. Ratio (1)	Probe voltage	Take-off angle	Fluor code
80	79	29	127·80	244·50	11·92	0·200	0·147	16·80	17·30	0
81	79	29	127·80	244·50	11·92	0·400	0·310	28·20	17·30	0
82	79	29	127·80	244·50	11·92	0·025	0·016	28·20	17·30	0
83	79	29	127·80	244·50	11·92	0·800	0·737	28·20	17·30	0
84	79	29	127·80	244·50	11·92	0·050	0·035	28·20	17·30	0
85	79	29	127·80	244·50	11·92	0·010	0·007	28·20	17·30	0
86	79	29	127·80	244·50	11·92	0·100	0·064	28·20	17·30	0
87	79	29	127·80	244·50	11·92	0·005	0·003	28·20	17·30	0
88	29	79	53·60	209·10	8·98	0·762	0·758	28·50	16·00	1
89	29	79	53·60	209·10	8·98	0·473	0·470	28·50	16·00	1
90	29	79	53·60	209·10	8·98	0·400	0·362	33·90	17·10	1
91	29	79	53·60	209·10	8·98	0·400	0·398	28·20	17·10	1
92	29	79	53·60	209·10	8·98	0·400	0·426	22·50	16·00	1
93	29	79	53·60	209·10	8·98	0·400	0·456	16·80	16·00	1
94	29	79	53·60	209·10	8·98	0·800	0·798	16·80	16·00	1
95	28	13	58·80	61·10	8·33	0·421	0·360	10·00	16·20	0
96	28	13	58·80	61·10	8·33	0·421	0·370	15·00	16·20	0
97	28	13	58·80	61·10	8·33	0·421	0·380	20·00	16·20	0
98	28	13	58·80	61·10	8·33	0·421	0·385	25·00	16·20	0
99	28	13	58·80	61·10	8·33	0·421	0·385	30·00	16·20	0
100	28	13	58·80	61·10	8·33	0·421	0·385	35·00	16·20	0
101	28	13	58·80	61·10	8·33	0·592	0·525	10·00	16·20	0
102	28	13	58·80	61·10	8·33	0·592	0·540	15·00	16·20	0
103	28	13	58·80	61·10	8·33	0·592	0·555	20·00	16·20	0
104	28	13	58·80	61·10	8·33	0·592	0·560	25·00	16·20	0
105	28	13	58·80	61·10	8·33	0·592	0·560	30·00	16·20	0
106	28	13	58·80	61·10	8·33	0·592	0·560	35·00	16·20	0
107	26	13	71·50	94·00	7·11	0·408	0·360	10·00	16·50	0
108	26	13	71·50	94·00	7·11	0·408	0·362	15·00	16·50	0
109	26	13	71·50	94·00	7·11	0·408	0·365	20·00	16·50	0
110	26	13	71·50	94·00	7·11	0·408	0·367	25·00	16·50	0
111	26	13	71·50	94·00	7·11	0·408	0·370	30·00	16·50	0
112	26	13	71·50	94·00	7·11	0·408	0·370	35·00	16·50	0
113	22	13	110·00	248·50	4·96	0·372	0·320	10·00	17·30	0
114	22	13	110·00	248·50	4·96	0·372	0·317	15·00	17·30	0
115	22	13	110·00	248·50	4·96	0·372	0·307	20·00	17·30	0
116	22	13	110·00	248·50	4·96	0·372	0·295	25·00	17·30	0
117	22	13	110·00	248·50	4·96	0·372	0·280	30·00	17·30	0
118	22	13	110·00	248·50	4·96	0·372	0·265	35·00	17·30	0
119	92	13	94·30	11·50	17·60	0·746	0·644	31·50	15·60	0
120	92	13	94·30	11·50	17·60	0·688	0·578	31·50	15·60	0
121	92	6	94·30	1·10	17·60	0·952	0·920	31·50	15·60	0
122	92	6	94·30	1·10	17·60	0·908	0·866	31·50	15·60	0
123	92	28	94·30	89·80	17·60	0·670	0·580	31·50	15·60	0
124	92	28	94·30	89·80	17·60	0·448	0·353	31·50	15·60	0
125	92	26	94·30	74·30	17·60	0·681	0·586	31·50	15·60	0
126	92	22	94·30	48·30	17·60	0·554	0·474	31·50	15·60	0
127	92	22	94·30	48·30	17·60	0·833	0·779	31·50	15·60	0
128	92	22	94·30	48·30	17·60	0·952	0·937	31·50	15·60	0
129	92	29	94·30	98·20	17·60	0·428	0·343	31·50	15·60	0
130	92	32	94·30	126·20	17·60	0·522	0·436	31·50	15·60	0
131	92	50	94·30	62·00	17·60	0·401	0·371	31·50	15·60	0
132	92	77	94·30	199·70	17·60	0·381	0·313	31·50	15·60	0
133	26	8	71·50	22·30	7·11	0·697	0·642	12·00	40·00	0
134	26	8	71·50	22·30	7·11	0·697	0·647	15·00	40·00	0
135	26	8	71·50	22·30	7·11	0·697	0·654	20·00	40·00	0
136	26	8	71·50	22·30	7·11	0·697	0·661	25·00	40·00	0
137	26	8	71·50	22·30	7·11	0·697	0·665	29·00	40·00	0
138	26	8	71·50	22·30	7·11	0·700	0·649	29·00	20·00	0
139	29	13	53·60	49·90	8·98	0·041	0·039	28·50	20·00	0
140	29	13	53·60	49·90	8·98	0·041	0·038	16·80	20·00	0
141	29	13	53·60	49·90	8·98	0·041	0·033	12·20	20·00	0
142	13	28	385·50	4838·60	1·56	0·578	0·385	10·00	17·00	1
143	13	28	385·50	4838·60	1·56	0·578	0·240	15·00	17·00	1
144	13	28	385·50	4838·60	1·56	0·578	0·175	20·00	17·00	1
145	13	28	385·50	4838·60	1·56	0·578	0·145	25·00	17·00	1
146	13	28	385·50	4838·60	1·56	0·578	0·127	30·00	17·00	1
147	13	28	385·50	4838·60	1·56	0·578	0·115	35·00	17·00	1
148	13	28	385·50	4838·60	1·56	0·408	0·247	10·00	17·00	1
149	13	28	385·50	4838·60	1·56	0·408	0·160	15·00	17·00	1
150	13	28	385·50	4838·60	1·56	0·408	0·102	20·00	17·00	1
151	13	28	385·50	4838·60	1·56	0·408	0·080	25·00	17·00	1
152	13	28	385·50	4838·60	1·56	0·408	0·070	30·00	17·00	1
153	13	28	385·50	4838·60	1·56	0·408	0·065	35·00	17·00	1
154	13	26	385·50	3852·30	1·56	0·592	0·446	10·00	17·00	1
155	13	26	385·50	3852·30	1·56	0·592	0·335	15·00	17·00	1
156	13	26	385·50	3852·30	1·56	0·592	0·263	20·00	17·00	1
157	13	26	385·50	3852·30	1·56	0·592	0·211	25·00	17·00	1
158	13	26	385·50	3852·30	1·56	0·592	0·182	30·00	17·00	1
159	13	26	385·50	3852·30	1·56	0·592	0·159	35·00	17·00	1
160	13	22	385·50	2276·80	1·56	0·628	0·511	10·00	17·00	1
161	13	22	385·50	2276·80	1·56	0·628	0·420	15·00	17·00	1
162	13	22	385·50	2276·80	1·56	0·628	0·332	20·00	17·00	1
163	13	22	385·50	2276·80	1·56	0·628	0·267	25·00	17·00	1
164	13	22	385·50	2276·80	1·56	0·628	0·230	30·00	17·00	1
165	13	22	385·50	2276·80	1·56	0·628	0·215	35·00	17·00	1
166	39	12	908·10	2139·30	2·40	0·594	0·443	16·50	16·50	0
167	13	25	385·50	3515·60	1·56	0·746	0·640	10·00	20·00	1
168	13	25	385·50	3515·60	1·56	0·746	0·534	15·00	20·00	1
169	13	25	385·50	3515·60	1·56	0·746	0·381	29·00	20·00	1
170	13	26	385·50	3852·30	1·56	0·610	0·459	10·00	20·00	1

Table 1.—*Continued*

System number	Atomic number (1)	Atomic number (2)	Mass absorption coefficient (1)	Mass absorption coefficient (2)	Critical exit energy (1)	Weight fraction (1)	Int. ratio (1)	Probe voltage	Take-off angle	Fluor code
171	13	26	385·50	3852·30	1·56	0·610	0·355	15·00	20·00	1
172	13	26	385·50	3852·30	1·56	0·610	0·194	29·00	20·00	1
173	13	27	385·50	4328·30	1·56	0·673	0·541	10·00	20·00	1
174	13	27	385·50	4328·30	1·56	0·673	0·430	15·00	20·00	1
175	13	27	385·50	4328·30	1·56	0·673	0·230	29·00	20·00	1
176	13	28	385·50	4838·60	1·56	0·580	0·415	10·00	20·00	1
177	13	28	385·50	4838·60	1·56	0·580	0·300	15·00	20·00	1
178	13	28	385·50	4838·60	1·56	0·580	0·144	29·00	20·00	1
179	13	12	385·50	4375·60	1·56	0·624	0·460	10·00	20·00	0
180	13	12	385·50	4375·60	1·56	0·624	0·350	15·00	20·00	0
181	13	12	385·50	4375·60	1·56	0·624	0·212	29·00	20·00	0
182	13	29	385·50	5383·70	1·56	0·460	0·310	10·00	20·00	1
183	13	29	385·50	5383·70	1·56	0·460	0·205	15·00	20·00	1
184	13	29	385·50	5383·70	1·56	0·460	0·092	29·00	20·00	1
185	92	6	620·70	56·70	3·72	0·908	0·855	10·00	52·50	0
186	92	6	620·70	56·70	3·72	0·908	0·868	15·00	52·50	0
187	92	6	620·70	56·70	3·72	0·908	0·878	20·00	52·50	0
188	92	6	620·70	56·70	3·72	0·908	0·889	25·00	52·50	0
189	92	6	620·70	56·70	3·72	0·908	0·898	30·00	52·50	0
190	92	6	620·70	56·70	3·72	0·908	0·907	35·00	52·50	0
191	92	7	620·70	92·40	3·72	0·944	0·909	10·00	52·50	0
192	92	7	620·70	92·40	3·72	0·944	0·918	15·00	52·50	0
193	92	7	620·70	92·40	3·72	0·944	0·926	20·00	52·50	0
194	92	7	620·70	92·40	3·72	0·944	0·933	25·00	52·50	0
195	92	7	620·70	92·40	3·72	0·944	0·938	30·00	52·50	0
196	92	7	620·70	92·40	3·72	0·944	0·943	35·00	52·50	0
197	92	14	620·70	703·50	3·72	0·962	0·939	10·00	52·50	0
198	92	14	620·70	703·50	3·72	0·962	0·943	15·00	52·50	0
199	92	14	620·70	703·50	3·72	0·962	0·946	20·00	52·50	0
200	92	14	620·70	703·50	3·72	0·962	0·948	25·00	52·50	0
201	92	14	620·70	703·50	3·72	0·962	0·949	30·00	52·50	0
202	92	14	620·70	703·50	3·72	0·962	0·950	35·00	52·50	0
203	92	15	620·70	846·60	3·72	0·884	0·822	10·00	52·50	0
204	92	15	620·70	846·60	3·72	0·884	0·831	15·00	52·50	0
205	92	15	620·70	846·60	3·72	0·884	0·838	20·00	52·50	0
206	92	15	620·70	846·60	3·72	0·884	0·843	25·00	52·50	0
207	92	15	620·70	846·60	3·72	0·884	0·845	30·00	52·50	0
208	92	15	620·70	846·60	3·72	0·884	0·847	35·00	52·50	0
209	92	16	620·70	1004·00	3·72	0·881	0·814	10·00	52·50	0
210	92	16	620·70	1004·00	3·72	0·881	0·821	15·00	52·50	0
211	92	16	620·70	1004·00	3·72	0·881	0·827	20·00	52·50	0
212	92	16	620·70	1004·00	3·72	0·881	0·829	25·00	52·50	0
213	92	16	620·70	1004·00	3·72	0·881	0·829	30·00	52·50	0
214	92	16	620·70	1004·00	3·72	0·881	0·827	35·00	52·50	0
215	92	26	620·70	423·60	3·72	0·962	0·944	10·00	52·50	0
216	92	26	620·70	423·60	3·72	0·962	0·949	15·00	52·50	0
217	92	26	620·70	423·60	3·72	0·962	0·953	20·00	52·50	0
218	92	26	620·70	423·60	3·72	0·962	0·956	25·00	52·50	0
219	92	26	620·70	423·60	3·72	0·962	0·958	30·00	52·50	0
220	92	26	620·70	423·60	3·72	0·962	0·960	35·00	52·50	0
221	12	8	463·60	2432·80	1·30	0·603	0·285	25·00	20·00	0
222	12	8	463·60	2432·80	1·30	0·603	0·499	10·00	20·00	0
223	13	8	385·00	1503·30	1·56	0·529	0·325	25·00	20·00	0
224	13	8	385·00	1503·30	1·56	0·529	0·460	10·00	20·00	0
225	14	8	327·90	965·60	1·84	0·467	0·311	25·00	20·00	0
226	14	8	327·90	965·60	1·84	0·467	0·389	10·00	20·00	0
227	14	6	327·90	356·80	1·84	0·701	0·680	10·00	20·00	0
228	22	8	110·60	65·70	4·96	0·599	0·582	30·00	20·00	0
229	24	8	88·20	39·40	5·99	0·684	0·664	40·00	20·00	0
230	24	8	88·20	39·40	5·99	0·684	0·639	30·00	20·00	0
231	24	8	88·20	39·40	5·99	0·684	0·639	20·00	20·00	0
232	26	8	71·40	24·50	7·11	0·699	0·653	40·00	20·00	0
233	26	8	71·40	24·50	7·11	0·699	0·653	30·00	20·00	0
234	26	8	71·40	24·50	7·11	0·699	0·653	20·00	20·00	0
235	26	8	71·40	24·50	7·11	0·699	0·624	10·00	20·00	0
236	40	8	845·80	614·30	2·22	0·740	0·649	20·00	20·00	0
237	40	8	845·80	614·30	2·22	0·740	0·643	10·00	20·00	0
238	48	16	491·50	1201·70	3·54	0·778	0·643	30·00	20·00	0
239	48	16	491·50	1201·70	3·54	0·778	0·665	20·00	20·00	0
240	48	16	491·50	1201·70	3·54	0·778	0·671	10·00	20·00	0
241	28	23	58·90	278·00	8·33	0·200	0·164	30·00	30·00	0
242	28	47	58·90	265·30	8·33	0·200	0·173	30·00	30·00	1
243	28	80	58·90	263·10	8·33	0·200	0·177	30·00	30·00	1
244	74	42	150·80	139·80	10·20	0·800	0·772	20·00	52·50	0
245	74	42	150·80	139·80	10·20	0·800	0·742	15·00	52·50	0
246	74	42	1465·60	1416·30	2·80	0·800	0·726	10·00	52·50	0
247	42	74	728·00	3145·20	2·52	0·200	0·143	20·00	52·50	1
248	42	74	728·00	3145·20	2·52	0·200	0·164	15·00	52·50	1
249	42	74	728·00	3145·20	2·52	0·200	0·212	10·00	52·50	0
250	13	26	385·70	3840·60	1·56	0·241	0·083	30·00	52·50	1
251	13	26	385·70	3840·60	1·56	0·241	0·098	25·00	52·50	1
252	13	26	385·70	3840·60	1·56	0·241	0·124	20·00	52·50	1
253	26	13	71·40	93·40	7·11	0·759	0·748	30·00	52·50	0
254	26	13	71·40	93·40	7·11	0·759	0·742	25·00	52·50	0
255	26	13	71·40	93·40	7·11	0·759	0·736	20·00	52·50	0
256	14	42	327·90	1493·00	1·84	0·369	0·399	5·00	20·00	1
257	14	42	327·90	1493·00	1·84	0·369	0·340	10·00	20·00	1
258	14	42	327·90	1493·00	1·84	0·369	0·284	15·00	20·00	1
259	14	42	327·90	1493·00	1·84	0·369	0·241	20·00	20·00	1
260	14	42	327·90	1493·00	1·84	0·369	0·198	25·00	20·00	1
261	14	42	327·90	1493·00	1·84	0·369	0·176	30·00	20·00	1

Table 1.—*Continued*

System number	Atomic number (1)	Atomic number (2)	Mass absorption coefficient (1)	Mass absorption coefficient (2)	Critical exit energy (1)	Weight fraction (1)	Int. ratio (1)	Probe voltage	Take-off angle	Fluor code
262	14	42	327·90	1493·00	1·84	0·369	0·159	35·00	20·00	1
263	25	51	79·50	626·60	6·53	0·474	0·460	15·00	20·00	0
264	25	51	79·50	626·60	6·53	0·474	0·421	20·00	20·00	0
265	25	51	79·50	626·60	6·53	0·474	0·385	25·00	20·00	0
266	25	51	79·50	626·60	6·53	0·474	0·350	30·00	20·00	0
267	33	31	37·80	232·60	11·86	0·518	0·492	15·00	20·00	0
268	33	31	37·80	232·60	11·86	0·518	0·477	20·00	20·00	0
269	33	31	37·80	232·60	11·86	0·518	0·465	25·00	20·00	0
270	33	31	37·80	232·60	11·86	0·518	0·446	30·00	20·00	0
271	33	31	37·80	232·60	11·86	0·518	0·428	35·00	20·00	0
272	33	49	37·80	117·40	11·86	0·395	0·418	15·00	20·00	0
273	33	49	37·80	117·40	11·86	0·395	0·405	20·00	20·00	0
274	33	49	37·80	117·40	11·86	0·395	0·394	25·00	20·00	0
275	33	49	37·80	117·40	11·86	0·395	0·385	30·00	20·00	0
276	33	49	37·80	117·40	11·86	0·395	0·377	35·00	20·00	1
277	42	14	19·10	7·20	20·00	0·631	0·560	30·00	20·00	1
278	42	14	19·10	7·20	20·00	0·631	0·567	35·00	20·00	0
279	42	14	728·00	1982·60	2·52	0·631	0·485	10·00	20·00	0
280	42	14	728·00	1982·60	2·52	0·631	0·454	15·00	20·00	0
281	42	14	728·00	1982·60	2·52	0·631	0·413	20·00	20·00	0
282	42	14	728·00	1982·60	2·52	0·631	0·377	25·00	20·00	0
283	42	14	728·00	1982·60	2·52	0·631	0·354	30·00	20·00	0
284	49	15	463·20	889·80	3·73	0·787	0·718	10·00	20·00	0
285	49	15	463·20	889·80	3·73	0·787	0·717	15·00	20·00	0
286	49	15	463·20	889·80	3·73	0·787	0·709	20·00	20·00	0
287	49	15	463·20	889·80	3·73	0·787	0·691	25·00	20·00	0
288	49	15	463·20	889·80	3·73	0·787	0·677	30·00	20·00	0
289	49	15	463·20	889·80	3·73	0·787	0·674	35·00	20·00	0
290	49	33	463·20	909·40	3·73	0·605	0·569	10·00	20·00	0
291	49	33	463·20	909·40	3·73	0·605	0·563	15·00	20·00	1
292	49	33	463·20	909·40	3·73	0·605	0·539	20·00	20·00	1
293	49	33	463·20	909·40	3·73	0·605	0·521	25·00	20·00	1
294	49	33	463·20	909·40	3·73	0·605	0·498	30·00	20·00	1
295	49	33	463·20	909·40	3·73	0·605	0·500	35·00	20·00	1
296	49	51	463·20	525·70	3·73	0·485	0·492	10·00	20·00	1
297	49	51	463·20	525·70	3·73	0·485	0·499	20·00	20·00	1
298	49	51	463·20	525·70	3·73	0·485	0·494	30·00	20·00	1
299	51	25	413·40	304·50	4·13	0·526	0·498	10·00	20·00	1
300	51	25	413·40	304·50	4·13	0·526	0·530	15·00	20·00	1
301	51	25	413·40	304·50	4·13	0·526	0·534	20·00	20·00	1
302	51	25	413·40	304·50	4·13	0·526	0·551	25·00	20·00	1
303	51	25	413·40	304·50	4·13	0·526	0·574	30·00	20·00	1
304	51	25	413·40	304·50	4·13	0·526	0·579	35·00	20·00	1
305	51	31	413·40	588·60	4·13	0·636	0·599	10·00	20·00	0
306	51	31	413·40	588·60	4·13	0·636	0·598	15·00	20·00	1
307	51	31	413·40	588·60	4·13	0·636	0·594	20·00	20·00	1
308	51	31	413·40	588·60	4·13	0·636	0·580	25·00	20·00	1
309	51	31	413·40	588·60	4·13	0·636	0·571	30·00	20·00	1
310	51	31	413·40	588·60	4·13	0·636	0·571	35·00	20·00	1
311	51	49	413·40	364·30	4·13	0·515	0·530	10·00	20·00	0
312	51	49	413·40	364·30	4·13	0·515	0·541	20·00	20·00	0
313	51	49	413·40	364·30	4·13	0·515	0·543	30·00	20·00	1
314	28	26	58·90	379·60	8·33	0·098	0·097	10·00	75·00	0
315	28	26	58·90	379·60	8·33	0·098	0·092	15·00	75·00	0
316	28	26	58·90	379·60	8·33	0·098	0·089	20·00	75·00	0
317	28	26	58·90	379·60	8·33	0·098	0·086	25·00	75·00	0
318	28	26	58·90	379·60	8·33	0·098	0·084	30·00	75·00	0
319	28	26	58·90	379·60	8·33	0·098	0·078	35·00	75·00	0
320	28	26	58·90	379·60	8·33	0·098	0·075	40·00	75·00	0
321	28	26	58·90	379·60	8·33	0·098	0·098	10·00	20·00	0
322	28	26	58·90	379·60	8·33	0·098	0·080	15·00	20·00	0
323	28	26	58·90	379·60	8·33	0·098	0·080	20·00	20·00	0
324	28	26	58·90	379·60	8·33	0·098	0·074	25·00	20·00	0
325	28	26	58·90	379·60	8·33	0·098	0·066	30·00	20·00	0
326	28	26	58·90	379·60	8·33	0·098	0·057	35·00	20·00	0
327	28	26	58·90	379·60	8·33	0·098	0·048	40·00	20·00	0
328	13	12	385·70	4376·50	1·56	0·091	0·066	10·00	75·00	0
329	13	12	385·70	4376·50	1·56	0·091	0·047	15·00	75·00	0
330	13	12	385·70	4376·50	1·56	0·091	0·035	20·00	75·00	0
331	13	12	385·70	4376·50	1·56	0·091	0·026	25·00	75·00	0
332	13	12	385·70	4376·50	1·56	0·091	0·019	30·00	75·00	0
333	13	12	385·70	4376·50	1·56	0·091	0·015	35·00	75·00	0
334	13	12	385·70	4376·50	1·56	0·091	0·013	40·00	75·00	0
335	13	12	385·70	4376·50	1·56	0·091	0·060	10·00	52·50	0
336	13	12	385·70	4376·50	1·56	0·091	0·042	15·00	52·50	0
337	13	12	385·70	4376·50	1·56	0·091	0·028	20·00	52·50	0
338	13	12	385·70	4376·50	1·56	0·091	0·022	25·00	52·50	0
339	13	12	385·70	4376·50	1·56	0·091	0·017	30·00	52·50	0
340	13	12	385·70	4376·50	1·56	0·091	0·039	10·00	20·00	0
341	13	12	385·70	4376·50	1·56	0·091	0·023	15·00	20·00	0
342	13	12	385·70	4376·50	1·56	0·091	0·014	20·00	20·00	0
343	13	12	385·70	4376·50	1·56	0·091	0·012	25·00	20·00	0
344	13	12	385·70	4376·50	1·56	0·091	0·009	30·00	20·00	0
345	13	12	385·70	4376·50	1·56	0·091	0·008	35·00	20·00	0
346	13	12	385·70	4376·50	1·56	0·091	0·006	40·00	20·00	0
347	13	26	385·70	3840·60	1·56	0·100	0·087	10·00	75·00	1
348	13	26	385·70	3840·60	1·56	0·100	0·069	15·00	75·00	1
349	13	26	385·70	3840·60	1·56	0·100	0·054	20·00	75·00	1
350	13	26	385·70	3840·60	1·56	0·100	0·041	25·00	75·00	1
351	13	26	385·70	3840·60	1·56	0·100	0·033	30·00	75·00	1
352	13	26	385·70	3840·60	1·56	0·100	0·027	35·00	75·00	1

Table 1.—*Continued*

System number	Atomic number (1)	(2)	Mass absorption coefficient (1)	(2)	Critical exit energy (1)	Weight fraction (1)	Int. ratio (1)	Probe voltage	Take-off angle	Fluor code
353	13	26	385·70	3840·60	1·56	0·100	0·022	40·00	75·00	1
354	13	26	385·70	3840·60	1·56	0·100	0·076	10·00	52·50	1
355	13	26	385·70	3840·60	1·56	0·100	0·059	15·00	52·50	1
356	13	26	385·70	3840·60	1·56	0·100	0·043	20·00	52·50	1
357	13	26	385·70	3840·60	1·56	0·100	0·033	25·00	52·50	1
358	13	26	385·70	3840·60	1·56	0·100	0·027	30·00	52·50	1
359	13	26	385·70	3840·60	1·56	0·100	0·053	10·00	20·00	1
360	13	26	385·70	3840·60	1·56	0·100	0·035	15·00	20·00	1
361	13	26	385·70	3840·60	1·56	0·100	0·025	20·00	20·00	1
362	13	26	385·70	3840·60	1·56	0·100	0·016	25·00	20·00	1
363	13	26	385·70	3840·60	1·56	0·100	0·015	30·00	20·00	1
364	13	26	385·70	3840·60	1·56	0·100	0·014	35·00	20·00	1
365	13	26	385·70	3840·60	1·56	0·100	0·011	40·00	20·00	1
366	14	26	327·90	2502·10	1·84	0·086	0·084	10·00	75·00	1
367	14	26	327·90	2502·10	1·84	0·086	0·073	15·00	75·00	1
368	14	26	327·90	2502·10	1·84	0·086	0·061	20·00	75·00	1
369	14	26	327·90	2502·10	1·84	0·086	0·050	25·00	75·00	1
370	14	26	327·90	2502·10	1·84	0·086	0·044	30·00	75·00	1
371	14	26	327·90	2502·10	1·84	0·086	0·035	35·00	75·00	1
372	14	26	327·90	2502·10	1·84	0·086	0·027	40·00	75·00	1
373	14	26	327·90	2502·10	1·84	0·086	0·082	10·00	52·50	1
374	14	26	327·90	2502·10	1·84	0·086	0·067	15·00	52·50	1
375	14	26	327·90	2502·10	1·84	0·086	0·053	20·00	52·50	1
376	14	26	327·90	2502·10	1·84	0·086	0·044	25·00	52·50	1
377	14	26	327·90	2502·10	1·84	0·086	0·035	30·00	52·50	1
378	14	26	327·90	2502·10	1·84	0·086	0·066	10·00	20·00	1
379	14	26	327·90	2502·10	1·84	0·086	0·044	15·00	20·00	1
380	14	26	327·90	2502·10	1·84	0·096	0·036	20·00	20·00	1
381	14	26	327·90	2502·10	1·84	0·086	0·025	25·00	20·00	1
382	14	26	327·90	2502·10	1·84	0·086	0·018	30·00	20·00	1
383	14	26	327·90	2502·10	1·84	0·086	0·019	35·00	20·00	1
384	14	26	327·90	2502·10	1·84	0·086	0·016	40·00	20·00	1
385	23	14	98·30	235·20	5·46	0·470	0·440	10·00	75·00	0
386	23	14	98·30	235·20	5·46	0·470	0·431	15·00	75·00	1
387	23	14	98·30	235·20	5·46	0·470	0·436	20·00	75·00	0
388	23	14	98·30	235·20	5·46	0·470	0·430	25·00	75·00	0
389	23	14	98·30	235·20	5·46	0·470	0·431	30·00	75·00	0
390	23	14	98·30	235·20	5·46	0·470	0·433	35·00	75·00	0
391	23	14	98·30	235·20	5·46	0·470	0·415	40·00	75·00	0
392	23	14	98·30	235·20	5·46	0·470	0·447	10·00	52·50	0
393	23	14	98·30	235·20	5·46	0·470	0·442	15·00	52·50	0
394	23	14	98·30	235·20	5·46	0·470	0·433	20·00	52·50	0
395	23	14	98·30	235·20	5·46	0·470	0·427	25·00	52·50	0
396	23	14	98·30	235·20	5·46	0·470	0·408	30·00	52·50	0
397	23	14	98·30	235·20	5·46	0·470	0·431	10·00	20·00	0
398	23	14	98·30	235·20	5·46	0·470	0·408	15·00	20·00	0
399	23	14	98·30	235·20	5·46	0·470	0·405	20·00	20·00	0
400	23	14	98·30	235·20	5·46	0·470	0·414	25·00	20·00	0
401	23	14	98·30	235·20	5·46	0·470	0·384	30·00	20·00	0
402	23	14	98·30	235·20	5·46	0·470	0·378	35·00	20·00	0
403	23	14	98·30	235·20	5·46	0·470	0·358	40·00	20·00	0
404	41	23	783·00	939·10	2·37	0·080	0·073	10·00	75·00	1
405	41	23	783·00	939·10	2·37	0·080	0·075	15·00	75·00	1
406	41	23	783·00	939·10	2·37	0·080	0·072	20·00	75·00	1
407	41	23	783·00	939·10	2·37	0·080	0·073	25·00	75·00	1
408	41	23	783·00	939·10	2·37	0·080	0·071	30·00	75·00	1
409	41	23	783·00	939·10	2·37	0·080	0·071	35·00	75·00	1
410	41	23	783·00	939·10	2·37	0·080	0·068	40·00	75·00	1
411	41	23	783·00	939·10	2·37	0·080	0·074	10·00	52·50	1
412	41	23	783·00	939·10	2·37	0·080	0·077	15·00	52·50	1
413	41	23	783·00	939·10	2·37	0·080	0·073	20·00	52·50	1
414	41	23	783·00	939·10	2·37	0·080	0·070	25·00	52·50	1
415	41	23	783·00	939·10	2·37	0·080	0·065	30·00	52·50	1
416	41	23	783·00	939·10	2·37	0·080	0·070	10·00	20·00	1
417	41	23	783·00	939·10	2·37	0·080	0·068	15·00	20·00	1
418	41	23	783·00	939·10	2·37	0·080	0·068	20·00	20·00	1
419	41	23	783·00	939·10	2·37	0·080	0·063	25·00	20·00	1
420	41	23	783·00	939·10	2·37	0·080	0·064	30·00	20·00	1
421	41	23	783·00	939·10	2·37	0·080	0·056	35·00	20·00	1
422	41	23	783·00	939·10	2·37	0·080	0·053	40·00	20·00	1
423	82	16	116·60	42·10	13·04	0·866	0·807	20·00	75·00	0
424	82	16	116·60	42·10	13·04	0·866	0·809	25·00	75·00	0
425	82	16	116·60	42·10	13·04	0·866	0·813	30·00	75·00	0
426	82	16	116·60	42·10	13·04	0·866	0·818	35·00	75·00	0
427	82	16	116·60	42·10	13·04	0·866	0·826	40·00	75·00	0
428	26	16	71·40	167·40	7·11	0·466	0·406	10·00	75·00	0
429	26	16	71·40	167·40	7·11	0·466	0·421	12·00	75·00	0
430	26	16	71·40	167·40	7·11	0·466	0·425	15·00	75·00	0
431	26	16	71·40	167·40	7·11	0·466	0·425	20·00	75·00	0
432	26	16	71·40	167·40	7·11	0·466	0·422	25·00	75·00	0
433	26	16	71·40	167·40	7·11	0·466	0·419	30·00	75·00	0
434	30	16	49·00	73·30	9·66	0·671	0·620	15·00	75·00	0
435	30	16	49·00	73·30	9·66	0·671	0·620	20·00	75·00	0
436	30	16	49·00	73·30	9·66	0·671	0·626	25·00	75·00	0
437	30	16	49·00	73·30	9·66	0·671	0·628	30·00	75·00	0
438	48	12	491·50	546·80	3·54	0·550	0·454	30·00	52·50	0
439	48	12	491·50	546·80	3·54	0·720	0·639	30·00	52·50	0
440	29	79	53·70	208·60	8·98	0·199	0·213	25·00	18·00	1
441	29	79	53·70	208·60	8·98	0·396	0·417	25·00	18·00	1
442	29	79	53·70	208·60	8·98	0·599	0·620	25·00	18·00	1
443	29	79	53·70	208·60	8·98	0·790	0·807	25·00	18·00	1

Table 1.—*Continued*

System number	Atomic number (1)	(2)	Mass absorption coefficient (1)	(2)	Critical energy (1)	Weight fraction (1)	Int. Ratio (1)	Probe voltage	Take-off angle	Fluor code
444	79	29	127·50	245·40	11·92	0·201	0·149	25·00	18·00	0
445	79	29	127·50	245·40	11·92	0·401	0·314	25·00	18·00	0
446	79	29	127·50	245·40	11·92	0·604	0·513	25·00	18·00	0
447	79	29	127·50	245·40	11·92	0·801	0·741	25·00	18·00	0
448	29	30	53·70	59·50	8·98	0·729	0·730	25·00	18·00	0
449	30	29	49·00	44·20	9·66	0·271	0·273	25·00	18·00	0
450	22	41	110·60	718·70	4·96	0·350	0·241	25·00	18·00	1
451	41	22	783·00	819·60	2·37	0·650	0·599	25·00	18·00	1
452	74	42	150·80	139·80	10·20	0·785	0·764	30·00	18·00	1
453	74	42	1465·60	1416·30	1·80	0·785	0·764	5·00	18·00	0
454	42	74	728·00	3145·20	2·52	0·215	0·230	5·00	18·00	0
455	26	24	71·40	474·20	7·11	0·902	0·870	20·00	18·00	0
456	26	24	71·40	474·20	7·11	0·902	0·887	10·00	18·00	0
457	73	6	156·30	4·50	9·88	0·938	0·912	20·00	18·00	0
458	73	6	1548·70	374·90	1·72	0·938	0·914	7·00	18·00	0
459	41	6	783·00	191·50	2·37	0·886	0·868	7·00	18·00	0
460	14	12	327·90	2824·60	1·84	0·366	0·316	5·00	18·00	0
461	28	26	58·90	379·60	8·33	0·051	0·040	20·00	18·00	0
462	28	26	58·90	379·60	8·33	0·563	0·507	20·00	18·00	0
463	28	26	58·90	379·60	8·33	0·630	0·568	20·00	18·00	0
464	28	26	58·90	379·60	8·33	0·895	0·869	20·00	18·00	0
465	28	26	58·90	379·60	8·33	0·100	0·079	20·00	18·00	0
466	28	26	58·90	379·60	8·33	0·200	0·161	20·00	18·00	0
467	28	26	58·90	379·60	8·33	0·198	0·161	20·00	18·00	0
468	79	47	127·50	130·30	11·92	0·800	0·767	20·00	18·00	0
469	79	47	127·50	130·30	11·92	0·601	0·559	20·00	18·00	0
470	79	47	127·50	130·30	11·92	0·400	0·359	20·00	18·00	0
471	79	47	127·50	130·30	11·92	0·224	0·199	20·00	18·00	0

(90%) of cases studied and was rarely greater than 5%. No correction for fluorescence by the continuum was included in the computer program; this omission may produce both small positive or negative contributions (Springer and Rosner 1969), resulting in a slight increase in standard deviation of corrected data but little change in the optimum values obtained below for σ and h.

3.2. Atomic number correction

Two atomic number correction procedures have been studied, the method of Duncumb and Reed (1968) and the more rigorous approach of Philibert and Tixier (1968). It was found that each method gave substantially the same result (within 1% relative) for the 471 systems studied, in accord with the findings of Philibert (1969). Since the first method was simpler to apply this was used in the subsequent examination of the absorption correction.

3.3. Absorption correction

Mass absorption coefficient data provided by Heinrich (1966) have been employed. A computer program was written to study the effect on the Philibert absorption corrections of varying the parameters B, C and n in the expressions $h=B.A/Z^2$ and $\sigma=C/(E_0{}^n-E_c{}^n)$ (see equations 1 and 2). $\phi(0)$ values given by Reuter (1972) have been used together with a weight averaging method for

$$h=B\sum_{i=1}^{i=j} c_i.A_i/Z_i{}^2 \qquad (3)$$

where j is the number of constituent elements in the sample.

Although a higher proportion of low voltage data were used in this analysis than in previous investigations (e.g. Poole 1968) the majority (354 of the 471) were measurements >15 kV (see table 1). In order to minimize bias of the analysis towards high kV results,

the data were separated into two groups, >15 kV and $\leqslant 15$ kV, and the mean square deviation δ calculated separately for each group using

$$\delta = \frac{1}{m}\sum_{i=1}^{i=m}(1-k_i'/k_i)^2.$$

k_i' is the intensity ratio predicted by a particular correction procedure, k_i is the measured intensity ratio and m is the number of systems in the group. The sum Δ of the two mean square deviations was then used to assess the effect of varying the parameters B, C and n.

4. Optimization of parameters in the absorption correction

4.1. Full Philibert model

Calculated Δ values are plotted against C (solid lines) for $B=1{\cdot}5$ and for different values of n in figure 2; curves (not shown) were also plotted for $B=1{\cdot}0$, $2{\cdot}0$, $2{\cdot}5$, $4{\cdot}0$ and $5{\cdot}0$.

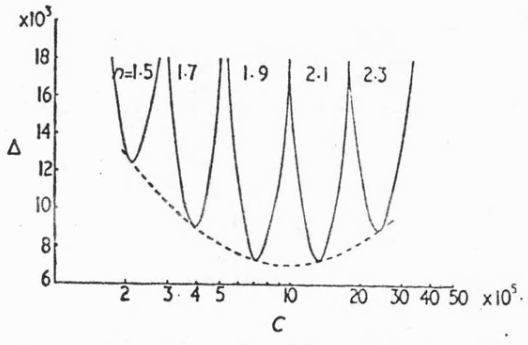

Figure 2. Plot of Δ against C for values of $n=1{\cdot}5$, $1{\cdot}7$, $1{\cdot}9$, $2{\cdot}1$ and $2{\cdot}3$; full Philibert expression with $B=1{\cdot}5$. Dotted line shows locus of minima.

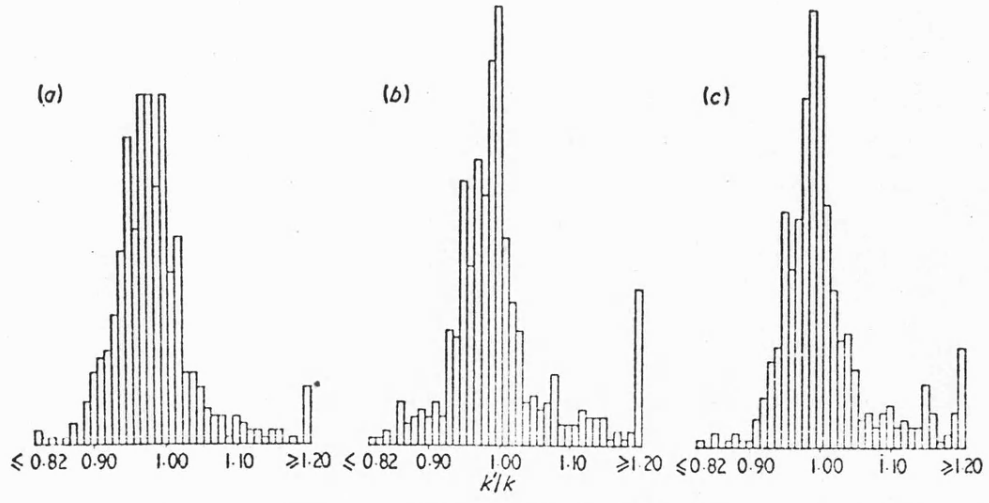

Figure 3. Histograms of data corrected using full Philibert expression: (*a*) New constants, Δ-optimized; (*b*) Duncumb and Melford's constants; (*c*) Alternative optimization method with $B=2{\cdot}2$, $C=10{\cdot}35\times10^3$ and $n=1{\cdot}95$.

Each solid curve has a minimum, and the loci of all minima (e.g. broken curve in figure 2) indicate that Δ is smallest ($7{\cdot}0\times10^{-3}$) when $B=1{\cdot}5$, $C=9{\cdot}5\times10^5$ and $n=1{\cdot}99$.

A histogram of results corrected using these optimum figures is given in figure 3(*a*); for comparison purposes, data corrected with constants proposed earlier by Duncumb and Melford are illustrated in figure 3(*b*). The revised values have significantly narrowed the distribution, improving the standard deviation from 9·2% to 6·3%, but the corrected data are distributed about $k'/k=0{\cdot}99$.

Since in the foregoing analysis a relatively small number of results with large discrepancies may have a disproportionate effect on the findings, a second method of assessment was examined based upon maximizing the number of predicted results which lay within $\pm5\%$ of the true intensity ratio. This did not, however, produce a unique set of optimized values of B, C and n, and in table 2 are listed four sets which all appeared to give the same accuracy of correction. The histogram (figure 3*c*) illustrates the effect of using one set ($B=2{\cdot}2$, $C=10{\cdot}35\times10^5$ and $n=1{\cdot}95$).

Table 2. Sets of values for constants B, C and n giving the maximum probability of results lying with 5%

B	C (10^5)	n
2·2	10·4	1·95
2·2	8·8	1·90
2·3	6·6	1·80
2·4	6·6	1·80

A skew distribution is still apparent and the spread in the results is greater than that shown in figure 3(*a*) using constants deduced by the Δ-optimization method (7·7% compared to 6·3% standard deviation) but the standard deviation is again smaller than that obtained (9·2%) using Duncumb and Melford's values.

Both methods of assessment were repeated by using mass absorption coefficients of Theisen and Vollath (1967) and different values for B, C and n were obtained. The mass absorption coefficients used gave a significantly greater mean square error than Heinrich's data, which suggests they may be less accurate. This view differs from that of Martin and Poole (1971) who believe Theisen and Vollath's values are possibly more accurate. However, in this study Theisen's values have not been employed further.

4.2. Simple Philibert model

Only one assessment criterion, Δ-optimization, has been used for investigating the simple Philibert model. The optimum values were found to be $B=0{\cdot}85$, $C=6{\cdot}8\times10^5$ and $n=1{\cdot}86$, and corrected data are shown in figure 4(*a*). The same microanalysis results corrected using Heinrich's constants are given in figure 4(*b*). Respective standard deviations are 5·9% and 7·4%, the revised constants mainly improving corrections for systems with errors greater than 10%, but reducing slightly the height of the histogram peak and the number of results lying within 5% (357 with Heinrich's constants and 338 with the new values).

4.3. Averaging of h for multicomponent systems

In Philibert's treatment, Bothe's scattering law (Bothe 1929) is used for electron scattering in solids and this expression may be written in terms of the standard deviation of the

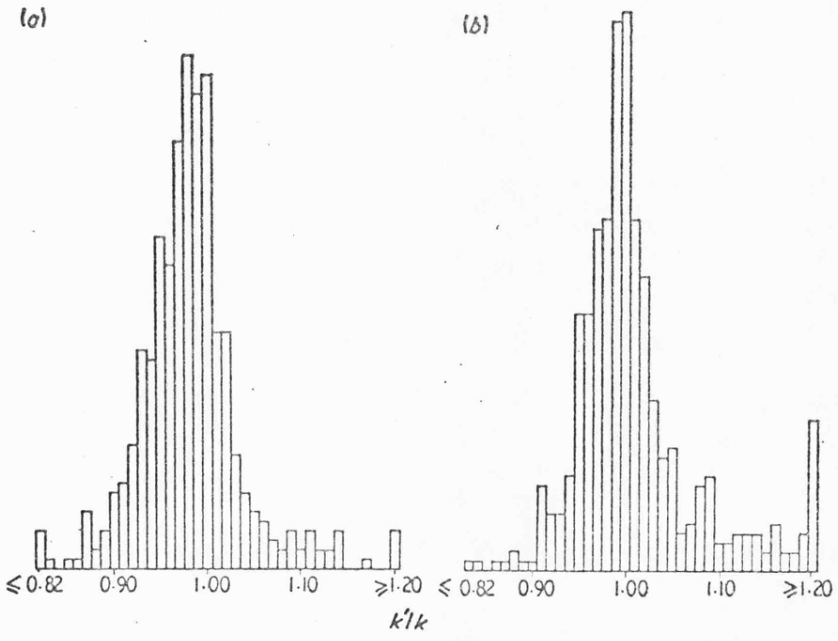

Figure 4. Histograms of data corrected using simple Philibert expression: (*a*) New constants, Δ-optimized; (*b*) Heinrich's constants.

angle ω that the electron is deflected from its original, incident direction and the mass depth ρz.

$$\omega = (400/E_0).(Z^2\ \rho z/A)^{1/2}.$$

Now the variance ω^2 is additive for multicomponent systems $\omega^2 = \Sigma\omega_i^2$

$$\omega^2 = \left(\frac{400}{E_0}\right)^2 \sum \frac{Z_i^2}{A_i}\,(\rho z)_i.$$

Hence, since $(\rho z)_i$ can be interpreted as the mass per unit area of the ith component it may be expressed as $(\rho z)_i = c_i \rho z$.

Therefore

$$\omega^2 = \left(\frac{400}{E_0}\right)^2 \rho z \sum c_i\, Z_i^2/A_i$$

and

$$\omega = (400/E_0)\ (\rho z)^{1/2}\ [\Sigma\ (c_i Z_i^2/A_i)]^{1/2}.$$

It is assumed (Philibert 1963) that electrons are fully scattered at mass depth ρz_m when $\omega = \pi/4$, where

$$\rho z_m = \frac{4 \times 10^{-6}\ E_0^2}{\Sigma\ c_i\, Z_i^2/A_i}.$$

Consequently it would be reasonable to assume that the appropriate method for averaging h in multicomponent systems is

$$h = \frac{B}{\Sigma\ c_i Z_i^2/A_i} = \frac{1}{\Sigma\ c_i/h_i}. \tag{4}$$

This expression can be shown to be equivalent to

$$h=\frac{B\,\Sigma a_i\,A_i}{\Sigma a_i(Z_i)^2}$$

an averaging method suggested by Martin and Poole (1971) which is written in terms of atomic concentration a_i.

The application of this second averaging method (equation 4) to the full Philibert treatment gave a different set of optimum constants ($B=1{\cdot}5$, $C=9{\cdot}75\times10^5$, $n=2{\cdot}00$) from the first method ($B=1{\cdot}5$, $C=9{\cdot}5$, $n=1{\cdot}99$), although similar standard deviations were obtained (optimum $\Delta=6{\cdot}35\%$ and $6{\cdot}33\%$ respectively).

5. Oxygen analysis in oxides

The Δ-optimized constants deduced from the analysis of 471 systems were then applied to some oxygen microanalysis results published previously (Love *et al* 1974b). The work had included measurements over a range of probe voltages (5–30 kV) on a number of binary and ternary oxides using an instrument with a 35° take-off angle. Duncumb and Reed's atomic number correction was used together with μ/ρ data given by Love *et al* (1974a). In the case of the full Philibert treatment it was found that using the revised constants increased the RMS error from 6% to 7·5%; this was mainly due to increased errors in data obtained at low kV (< 15 kV). For the simple Philibert model, the RMS error was increased from 11% to 14%, but it should be noted that this method has previously been criticized as inappropriate for light element microanalysis (see, for example, Love *et al* 1974b).

The two averaging methods for h discussed earlier gave almost the same standard deviation for the respective models, which is surprising since it would be expected that the accuracy of the absorption correction in systems comprising light elements would be more sensitive to the averaging method adopted. The inadequacy of the correction model, however, precludes further comment.

6. Discussion

Results of this detailed study of 471 systems have shown that the overall accuracy of the absorption corrections proposed by Philibert may be improved by adopting revised values for the constants B, C and n in the expressions for σ and h. In particular, it is proposed that the power n of the voltage dependence be increased. These adjustments improve the accuracy of those results which previously had large errors and/or those data obtained at lower probe voltages.

For the full Philibert correction, the revised value for n was 1·99, as compared with 1·5 suggested by Duncumb and Melford. An even higher power, $n=2{\cdot}3$, was put forward by Matteudi and Ruste (1973) but this value cannot be regarded as generally applicable since it was deduced from studies on a single system B_4C. The following, based upon the present investigation, may be used with advantage:

$$\sigma=9{\cdot}5\times10^5/(E_0^2-E_c^2); \qquad h=1{\cdot}5\,A/Z^2.$$

In the case of the simple Philibert model, a revised value for n of 1·86 is proposed. This is higher than the 1·65 recommended by Heinrich, although it is interesting to note that the results published by Duncumb *et al* (1969) may be interpreted as indicating $n > 1{\cdot}65$. Indeed, Philibert *et al* (1972), in their work on x-ray emission characteristics from pure elements, suggest an even higher-power law $n \simeq 2$, while Lenard's original work (see for example Philibert 1963) indicates $n \sim 2$–3, depending upon kV. Present results indicate that the following expressions should be used:

$$\sigma = 6{\cdot}8 \times 10^5/(E_0^{1{\cdot}86} - E_c^{1{\cdot}86}); \qquad h = 0{\cdot}85\, A/Z^2.$$

The effect of introducing the revised sets of constants into Philibert's absorption correction may be demonstrated by plotting the ratio of calculated $f(\chi)$ to experimental $f(\chi)$, against χ. This has been done in figure 5 for aluminium K_α radiation in aluminium at 20 kV, the experimental measurements being taken from Castaing and Henoc (1966). The diagram indicates that the new values improve both the full and simple Philibert absorption corrections for highly absorbing systems; for the former they are preferable over almost the entire $f(\chi)$ range, while for the latter they are better where $f(\chi) > 0{\cdot}03$.

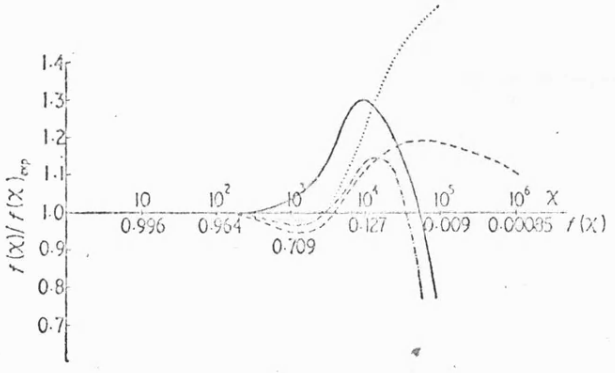

Figure 5. Plot of ratios of calculated $f(\chi)$ to experimental $f(\chi)$ of Castaing and Henoc (1966) for aluminium at 20 kV. —— Using full Philibert with Duncumb and Melford's constants; —·— As —— curve but with Δ-optimized constants; ..... Using simple Philibert with Heinrich's constants; — — — As ... curve with Δ-optimized constants.

It is also instructive to examine the relevant $\phi(\rho z)$ curves. In figure 6(*a*), for aluminium at 20 kV, peak heights using the revised constants correspond more closely to the experimental curve (Castaing and Henoc 1966) than the $\phi(\rho z)$ curves calculated using previous constants. However, the new values have not substantially altered the position of the peak. A similar set of $\phi(\rho z)$ curves at 10 kV (figure 6*b*) shows that both peak position and height are incorrect when using the revised constants; in fact, the Philibert models give better agreement with the experimental $\phi(\rho z)$ data if the original constants are introduced. It may be concluded, therefore, that neither of the Philibert models can be adjusted to give accurate results covering a wide range of experimental conditions. This point has also been made by Bishop (Bishop 1974) in a theoretical treatment.

Heinrich and Yakowitz (1969) have shown that, by choosing, where possible, conditions to satisfy the criterion $f(\chi) > 0{\cdot}8$, absorption errors may be reduced to $\sim 1\%$ in most cases and if, therefore, data obtained only on low absorbing systems ($f(\chi) > 0{\cdot}8$)

are examined, it may be possible to assess the accuracy of the atomic number correction of Duncumb and Reed (1968). Figure 7 shows these data after applying the Duncumb and Reed atomic number correction, the full Philibert absorption correction with revised constants, and a correction for fluorescence by characteristic radiation. Close examination

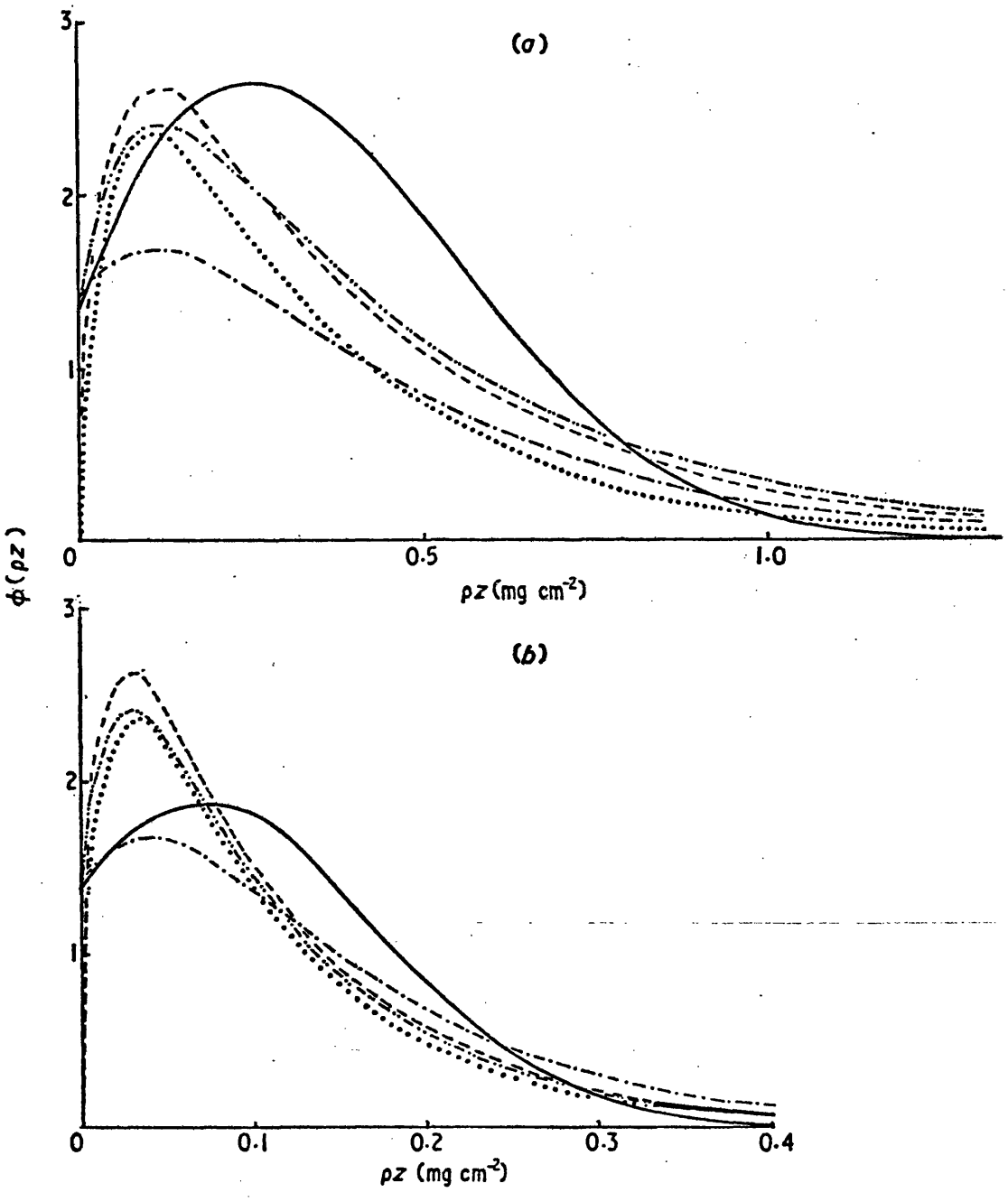

Figure 6. Comparison of calculated $\phi(\rho z)$ with experimental curves: (*a*) Aluminium at 20 kV; (*b*) Aluminium at 10 kV. ·—·— Using full Philibert with Duncumb and Melford's constants; ——··—— As ·—·— but with Δ-optimized constants; ..... Using simple Philibert but with Heinrich's constants; - - - - - As ..... curve but with Δ-optimized constants; ——— Experimental (Castaing and Henoc 1966).

of this information indicates that the corrected results are dependent upon the overvoltage U. Results at low overvoltages ($U<2$) have been filled in in the histogram and clearly show a displacement of the peak relative to the complete set of data in the diagram; similarly, results at high overvoltages show a displacement in the opposite sense.

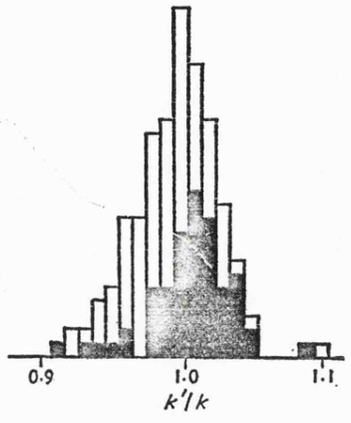

Figure 7. Histogram of corrected data on low absorbing systems ($f(\chi)>0{\cdot}8$), using full Philibert with Δ-optimized constants. Low overvoltage results ($U<2$) are filled; note the displacement of the peak relative to complete set of data, indicating some overcorrection.

Since, as mentioned above, absorption errors are of the order of 1% in most cases and furthermore any error in the small fluorescence contribution from characteristic x-rays is insignificant it may be concluded that either the continuous fluorescence or atomic number correction is in error, or perhaps both.

7. Conclusions

The full and simple Philibert absorption corrections have been evaluated using a large number of microanalysis data (471 systems). New values of constants to be used in the expressions for h and σ are proposed for both models which differ substantially from previously accepted values. They are shown to improve the accuracy and range of applicability of both corrections but the simple Philibert model with the new h and σ gives the greater precision. However, the new values are inappropriate for oxygen analysis and tend particularly to increase errors in low kV data; the full Philibert model with Duncumb and Melford's constants might be considered preferable here.

It was shown that both the value for h and the method of averaging for multicomponent systems does not sensitively affect correction accuracy.

The atomic number correction of Duncumb and Reed (1968) and Philibert and Tixier (1968) have also been compared and in none of the cases examined did they differ by more than 1%. Their applicability to light element systems will be assessed in a later paper.

Finally, it is considered that the magnitude of uncertainties in both published microanalysis data and mass absorption coefficients may be a limiting factor in assessing correction procedures for quantitative work. While this does not invalidate the present

investigation, since a marked decrease in the RMS error has been achieved, further refinements of correction methods may become increasingly difficult.

Acknowledgments

Thanks are due to the Bath University Computer Unit under the direction of Dr A W Nichol and particularly to Miss G M Venner for assistance with programming.

References

Beaman D R and Solosky L F 1972 *Anal. Chem.* **44** 1598–1610
Bishop H E 1974 *J. Phys.* D: *Appl. Phys.* **7** 2009–20
Bothe W 1929 *Z. Phys.* **54** 161–78
Brown J D 1964 *Advances in X-ray Analysis* vol 7 eds W M Mueller, G R Mallett and M Fay (New York: Plenum Press) pp 340–52
Castaing R 1960 *Advances in Electronics and Electron Physics* vol 13 (New York: Academic Press) p 317
Castaing R and Descamps J 1955 *J. Phys. Rad.* **16** 304
Castaing R and Henoc J 1966 *X-ray Optics and Microanalysis* eds R Castaing, P Deschamps and J Philibert (Paris: Hermann) pp 120–6
Duncumb P and Melford D A 1966 *X-ray Optics and Microanalysis* eds R Castaing, P Deschamps and J Philibert (Paris: Hermann) pp 240–53
Duncumb P and Reed S J B 1968 *Quantitative Electron Probe Microanalysis* ed K F J Heinrich *NBS. Spec. Publ.* 298 pp 133–54
Duncumb P and Shields P K 1966 *The Electron Microprobe* eds T D McKinley, K F J Heinrich and D A Wittry (New York: Wiley) pp 284–95
Duncumb P, Shields-Mason P K and da Casa C 1969 *X-ray Optics and Microanalysis* eds G Möllenstedt and K H Gaukler (Berlin: Springer-Verlag) pp 146–50
Friskney C A and Haworth C W 1968 *J. Phys.* D: *Appl. Phys.* **1** 873–9
Green M 1963 *X-ray Optics and Microanalysis* eds H H Pattee V E Cosslett and E Engström (New York: Academic Press) pp 361–77
Heinrich K F J 1966 *The Electron Microprobe* eds T D McKinley K F J Heinrich and D A Wittry (New York: Wiley) pp 296–377
—— 1967 *2nd Natn. Conf. on Electron Microprobe Analysis*, Electron Probe Analysis Society of America, Boston, Mass.
Heinrich K F J and Yakowitz H 1969 *X-ray Optics and Microanalysis* eds G Möllenstedt and K H Gaukler (Berlin: Springer-Verlag) pp 151–9
Love G, Cox M G C and Scott V D 1974a *J. Phys.* D: *Appl. Phys.* **7** 2131–41
—— 1974b *J. Phys.* D: *Appl. Phys.* **7** 2142–55
Martin P M and Poole D M 1971 *Metall. Rev.* **150**
Matteudi G and Ruste J 1973 *Rev. Phys. Appl.* **8** 27–32
Peissker E 1967 *Mikrochim. Acta, Suppl.* **II** 156–72
Philibert J 1963 *X-ray Optics and Microanalysis* eds H H Pattee, V E Cosslett and E Engström (New York: Academic Press) pp 379–92
—— 1969 *X-ray Optics, Optics and Microanalysis* eds G Mollenstedt and K H Gaukler (Berlin: Springer-Verlag) pp 114–31
Philibert J, Bryckaert D and Tixier R 1972 *X-ray Optics and Microanalysis* eds G Shinoda, K Kohra and T Ishinokawa (Tokyo: Tokyo UP) pp 157–62
Philibert J and Tixier R 1968 *Quantitative Electron Probe Microanalysis* ed K F J Heinrich *NBS Spec. Publ.* 298 pp 13–33
Poole D M 1968 *Quantitative Electron Probe Microanalysis* ed K F J Heinrich *NBS Spec. Publ.* 298 pp 93–131
Reed S J B 1965 *Br. J. Appl. Phys.* **16** 913–26
Reuter W 1972 *X-ray Optics and Microanalysis* eds G Shinoda, K Kohra and T Ishinokawa (Tokyo: Tokyo UP) pp 121–30

Shimizu R, Nishigori N and Murata K 1972 *X-ray Optics and Microanalysis* eds G Shinoda, K Kohra and T Ishinokawa (Tokyo: Tokyo UP) pp 95–104

Springer G 1966 *X-ray Optics and Microanalysis* eds R Castaing, P Deschamps and J Philibert (Paris: Hermann) pp 296–304

Springer G and Rosner B 1969 *X-ray Optics and Microanalysis* eds G Möllendstedt and G H Gaukler (Berlin: Springer-Verlag) pp 170–5

Theisen R and Vollath D 1967 *Tabellen der Massenschwachungskoeffizienten von Rontgenlinien* (Dusseldorf: Verlag Stahleisen)

Thoma C 1970 *Mikrochim. Acta. Suppl* IV 102–13

Yakowitz H, Michaelis R E and Vieth D L 1969 *Advances in X-ray Analysis* vol 12 eds C S Barratt, J B Newkirk and G R Mallet (New York: Plenum Press) pp 418–38

7.7 Assessment of Bishop's Absorption Correction Model in Electron Probe Microanalysis

G. Love, M.G.C. Cox and V.D. Scott,

1976a, J. Phys. D : Appl. Phys. 9, 7.

J. Phys. D: Appl. Phys., Vol. 9, 1976. Printed in Great Britain. © 1976

Assessment of Bishop's absorption correction model in electron probe microanalysis

G Love, M G C Cox and V D Scott
School of Materials Science, University of Bath, Claverton Down, Bath, Avon, BA2 7AY

Received 8 August 1975

Abstract. The absorption correction model proposed recently by Bishop is evaluated by making use of a large number of published microanalysis results. From a best-fit analysis on these data, constants are derived for use in the expression for the mean mass depth of x-ray generation. Miroanalysis results corrected using the Bishop model are compared with those obtained by applying the more widely used Philibert equations. It is shown that Bishop's method combines the best features of both the full Philibert model for elements with $Z<12$ and the simplified Philibert treatment where $Z\geqslant 12$. In addition, methods of averaging h, a parameter accounting for the effect of atomic number on absorption, are discussed.

1. Introduction

The most widely used correction procedures for converting raw microanalysis data into elemental concentrations involve separately correcting for the effects of atomic number, x-ray absorption and fluorescence.

Whilst the magnitudes of the atomic number and fluorescence corrections are seldom greater than 20%, the absorption correction can amount to a percentage of several hundreds. Thus, the precision of quantitative analysis is likely to be affected most by an unsatisfactory absorption correction, that is, by the validity of the empirical model used and the accuracy of input parameters.

The analytical expression proposed by Philibert (1963) to account for the effects of absorption in the target may be written as

$$f(\chi)=\frac{1+[\phi(0).h/(4+\phi(0).h)]\,(\chi/\sigma)}{(1+\chi/\sigma)\,[1+h\chi/(1+h)\,\sigma]} \tag{1}$$

$f(\chi)$ is the fractional transmission of the target for x-rays which are emitted in the direction of the spectrometer i.e. at an angle θ to the specimen surface; $\chi=\mu/\rho$ cosec θ, μ/ρ being the mass absorption coefficient of the measured radiation in the target; σ and h are parameters to account for the variation of $f(\chi)$ with electron energy E_0 and atomic number Z respectively; $\Phi(0)$ is the ratio of the number of x-rays generated in an infinitely thin layer at the surface of a massive target to the number generated in an isolated thin layer of the same thickness and composition. This equation is usually simplified (Philibert 1963) by putting $\Phi(0)$ equal to zero, which then gives

$$f(\chi)=\frac{1}{(1+\chi/\sigma)\,[1+h\chi/(1+h)\,\sigma]}. \tag{2}$$

Philibert proposed $h=1{\cdot}2\,A/Z^2$, where A is the atomic weight of the target, and tabulated σ as a function of E_0. Duncumb and Shields (1966) modified σ to account for the effect of overvoltage and suggested

$$\sigma=\frac{2{\cdot}39\times10^5}{E_0^{1{\cdot}5}-E_c^{1{\cdot}5}}$$

where E_c is the critical excitation potential for the radiation being considered. This was later changed by Heinrich (1967) to

$$\sigma=\frac{4{\cdot}5\times10^5}{E_0^{1{\cdot}65}-E_c^{1{\cdot}65}},$$

an alteration confirmed by Duncumb *et al* (1969) from an evaluation using experimental microanalysis data. Recently the expressions used for σ and h have been further refined by Love *et al* (1975) and, following a three-parameter regression analysis on a more extensive range of microanalysis data, the following equations were recommended:

$$\sigma=\frac{6{\cdot}8\times10^5}{E_0^{1{\cdot}86}-E_c^{1{\cdot}86}} \qquad \text{and } h=0{\cdot}85\,\frac{A}{Z^2}.$$

These workers also showed that the simplified Philibert formula (equation 2) provided a better correction than the full expression (equation 1) for microanalysis using hard x-rays ($\lambda<10$ Å) but that the latter approach was superior for soft-x-ray studies.

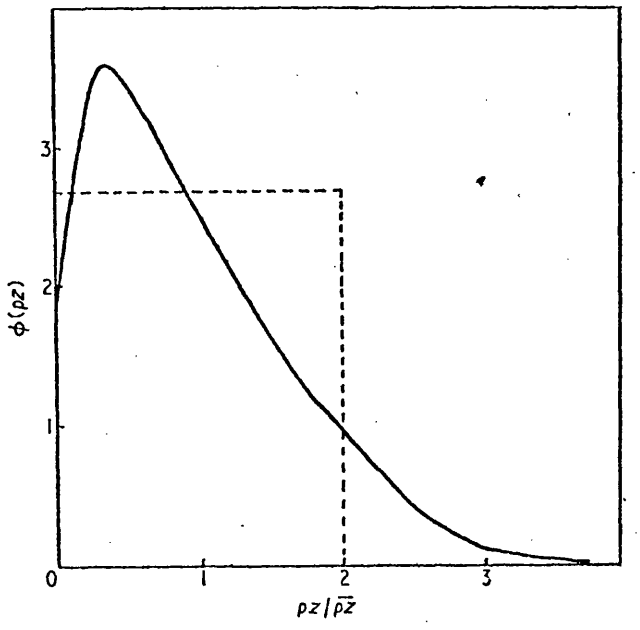

Figure 1. X-ray distribution with mass depth of gold $L\alpha$ radiation for 30 keV electrons: ——— Monte Carlo calculation; - - - - approximation of Bishop.

A new absorption correction has been proposed by Bishop (1974) in which x-ray distribution with depth is approximated to a rectangle, see figure 1. The value for $f(\chi)$ is given by $[1-\exp(-2\chi\overline{\rho z})]/2\chi\overline{\rho z}$ and for the mean mass depth of x-ray generation, $\overline{\rho z}$, Bishop suggested that values deduced from the simplified Philibert model could be

used:

$$\overline{\rho z}=[(1+2h)/(1+h)]/\sigma.$$

In this paper the Bishop model is evaluated and compared with the Philibert absorption corrections using a large number of experimental microanalysis data. From the study a new set of constants to be used in the expression for $\overline{\rho z}$ is proposed and Bishop's model is discussed in relation to light-element microanalysis. Some comments are also made regarding the method of averaging h for multi-component systems.

2. Correction procedures

In a previous paper, (Love *et al* 1975) a table was presented of microanalysis measurements selected from a survey of published data on binary systems. For the present analysis 430 of these results have been used, the remainder being excluded because they are now considered to be unreliable (see Appendix).

Corrections due to Reed (1965) for characteristic fluorescence and to Duncumb and Reed (1968) for atomic number have been applied in conjunction with the absorption corrections listed in table 1. Heinrich's mass absorption coefficients (Heinrich 1966) have been employed throughout except in the case of the soft-x-ray data described later. The models of Bishop and Philibert (simplified version) are compared for two methods of averaging h for multi-component systems; the approach favoured by most workers, namely $h=\Sigma(c_i h_i)$, is indicated in this table by I, and II refers to averaging based upon $h=1/\Sigma(c_i/h_i)$ (Love *et al* 1975).

Table 1. Absorption correction methods evaluated by making use of 430 microanalysis data

Method	Model	h average	n	$C(10^5)$	B	SRM error (%)
1	Simplified Philibert	I	1·65	4·50	1·20	6·8
2		II	1·65	4·50	1·20	7·1
3†		I	1·84	6·58	0·84	5·3
4†		II	1·82	6·41	0·99	5·3
5	Bishop	I	1·65	4·50	1·20	5·9
6		II	1·65	4·50	1·20	5·8
7†		I	1·77	6·80	0·72	5·3
8†		II	1·77	7·05	1·06	5·3

(I) $h=\Sigma(c_i h_i)$; (II) $h=1/\Sigma(c_i/h_i)$
† Δ-optimized constants, n, C and B.

In addition to using values for n, B and C suggested by other workers in $\sigma=C/(E_0^n-E_c^n)$ and $h=BA/Z^2$ (see table 1), the result of using constants derived from a Δ-optimization procedure (Love *et al* 1975) based upon the analysis of 430 binary systems is examined.

3. Results

The optimized values of n, B and C are given in table 1. Corrected data using absorption correction methods 1–8 are summarized in the bar chart figure 2 which shows the per-

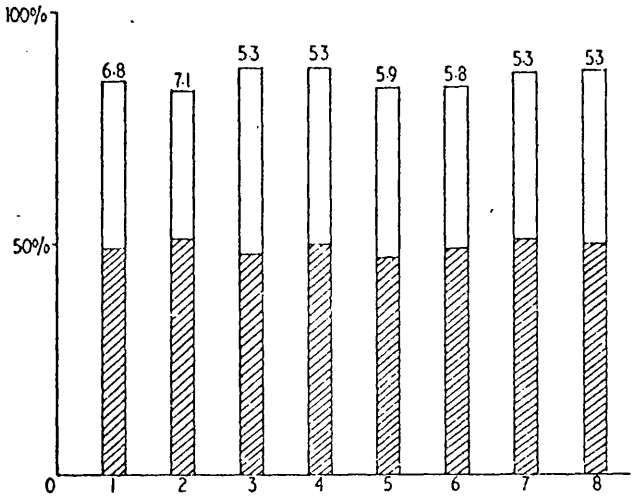

Figure 2. Bar chart summarizing data corrected using absorption correction methods 1–8. The height of each bar corresponds to the percentage of corrected data within 7½% of $k'/k=1$ and hatching indicates percentage within 2½%. RMS errors in (%) are indicated numerically above each bar.

centage of results within 7½% and within 2½% (hatched); the respective RMS errors are included (see also table 1).

4. Comparison of correction methods

Examination of the RMS errors would suggest that, firstly, the method of averaging h is unimportant and, secondly, the Bishop model with optimized constants gives similar results to the simplified Philibert correction with optimized constants (each 5·3%). Hence, from a practical point of view it would appear that there is little to choose between the two approaches. If, however, the distribution of corrected data as indicated by the symmetry of histograms (not shown) is taken into account, some differences are apparent. The ideal model would give, firstly, the smallest RMS error and, secondly, the greatest degree of symmetry in the corrected results, the distribution of these reflecting merely random errors in the input data. This asymmetry may be expressed as the ratio of the number of results lying below to those lying above $k'/k=1$, where k' is the calculated ratio of intensities from specimen and standard and k is the measured ratio. For method 4 the asymmetry ratio is 2·1 and for method 8 it is 1·6, indicating that the Bishop model with optimized constants is superior to the simplified Philibert treatment. Furthermore, the corresponding ratios for methods 3 and 7 ($h=\Sigma c_i h_i$) are 2·46 and 1·96 respectively, which suggests that h should be written as $h=1/\Sigma(c_i/h_i)$ for multi-component systems.

5. Application to oxygen analysis in oxides

Microanalysis measurements of oxygen over a range of probe voltages on binary and ternary oxides have been published previously (Love *et al* 1974b). Four absorption correction methods have been applied to these results together with Duncumb and Reed's atomic number correction. Mass absorption coefficients were taken from Love

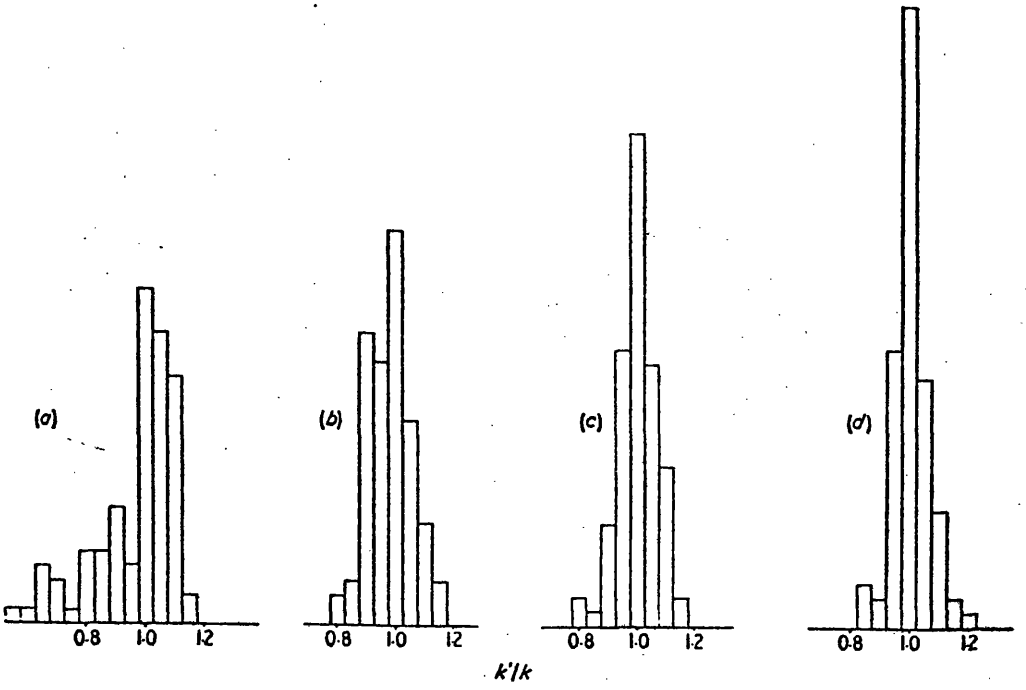

Figure 3. Histograms of oxide data corrected using (*a*) method 1, (*b*) method 5, (*c*) method 8 and (*d*) the full Philibert model.

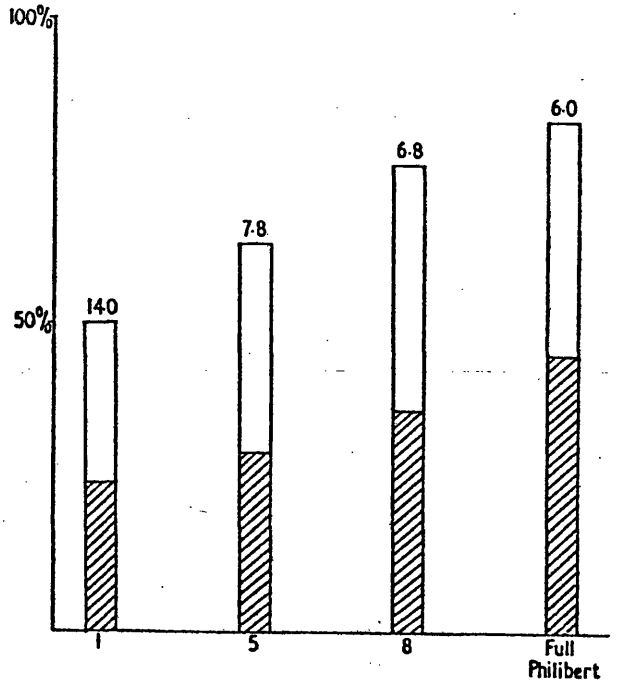

Figure 4. Bar chart summarizing information given in figure 3. The height of each bar corresponds to the percentage of corrected data within 7½% of $k'/k=1$ and hatching indicates percentage within 2½%. RMS errors (%) are indicated numerically above each bar.

et al (1974a). Only one method using the simplified Philibert absorption correction is given here since it has been shown earlier (Love *et al* 1975) that it is inappropriate where absorption is large, e.g. in light-element analysis. Hence the simplified Philibert with Heinrich's constants (method 1) is included only for comparison purposes. The approach suggested by Bishop (method 5) is evaluated, as well as method 8 which uses $h=1/\Sigma(c_i/h_i)$ together with the appropriate optimized constants. Finally, the full expression proposed by Philibert (equation 1) is included, incorporating constants of Duncumb and Melford (1966), $\Phi(0)$ values of Reuter (1972) and taking $h=$ Å c_i/h_i.

Corrected results using these four methods are illustrated in the histograms, figures 3(*a*)–(*d*), and in the bar chart, figure 4. Also included in figure 4 are the respective RMS errors. The results show clearly that the full Philibert model is best for correcting these light-element data and that the simplified Philibert approach is worst. Furthermore, the procedure suggested by Bishop (method 5) is markedly better than the simplified Philibert correction (method 1) and can be significantly improved by using the Δ-optimized constants (method 8). Indeed, method 8 results in a fairly symmetrical distribution of data about $k'/k=1$ and in this respect compares very favourably with the full Philibert absorption correction.

6. Conclusions

Based upon an evaluation of 430 microanalysis results where elements $Z>12$ are being analysed, it is shown that the absorption correction proposed by Bishop is comparable with the commonly used simplified Philibert method. It is also apparent that Bishop's model can be significantly improved by using constants which have been derived from an optimization programme based upon a best-fit analysis. The following expressions for σ and h are recommended: $\sigma=7{\cdot}05\times10^5/(E^{1{\cdot}77}-E_c^{1{\cdot}77})$ and $h=1{\cdot}06\ A/Z^2$ in conjunction with the method of averaging h described in an earlier paper (Love *et al* 1975).

In systems where the absorption correction factor is large, such as the oxygen analysis results discussed here, Bishop's method is clearly superior to the simplified Philibert method. Indeed, it gives similar RMS errors to the full Philibert absorption correction and has the advantage of being simpler to carry out. Thus, the range of applicability of existing computer correction programmes can be readily extended to include analysis of light elements by replacing the simplified Philibert expression with the equation of Bishop.

Present results also suggest that any further refinement of correction models may be restricted by the lack of accurately proven input data and that much of the residual RMS error in the corrected data given here could be associated with experimental uncertainties in the microanalysis measurements. The possibility too that the present findings may be affected by the choice of mass absorption coefficients should not be overlooked.

Acknowledgments

Thanks are due to Bath University Computer Unit, under the direction of Dr A W Nichol, for assistance with programming.

Appendix

The original table of collated data comprised 471 systems and is detailed as table 1 in a previous paper (Love *et al* 1975). Although many published data had already been

rejected in drawing up this list it was thought that further improvements could be made by being even more selective. For example, where a set of data exists containing only one variable, such as composition or probe voltage, the experimental points should lie on a smooth, monotonic curve and any significant deviation indicates unsatisfactory data (Heinrich 1968). In the present study data were rejected where this deviation exceeded 5%, and the whole data set was rejected where it was impossible to decide which particular results were in error. In all, 41 systems were discarded (see table 2) leaving a total of 430 systems, although it should be recognized that some grossly inaccurate data may still remain since the above tests could not always be applied.

Table 2. Systems excluded from the present analysis. (For a complete list of the 471 systems to which the table refers, see table 1 of Love *et al* 1975.)

System numbers					
17	49	86	322	381	417
18	50	87	342	382	418
24	51	139	345	383	419
29	52	140	346	384	420
37	53	141	378	411	421
46	84	165	379	412	422
48	85	243	380	416	

References

Bishop H E 1974 *J. Phys. D: Appl. Phys.* 7 2009–20

Duncumb P and Melford D A 1966 *X-ray Optics and Microanalysis* ed R Castaing, P Deschamps and J Philibert (Paris: Herman) pp 240–53

Duncumb P and Reed S J B 1968 *Quantitative Electron Probe Microanalysis* ed K F J Heinrich (NBS Spec. Publ. 298) pp 133–54

Duncumb P and Shields P K 1966. *The Electron Microbe* ed T D McKinley, K F J Heinrich and D B Wittry (New York: Wiley) pp 284–95

Duncumb P, Shields-Mason P K and da Casa C 1969 *X-ray Optics and Microanalysis* ed G Mollenstedt and K H Gaukler (Berlin: Springer-Verlag) pp 146–50

Heinrich K F J 1966. *The Electron Microprobe* ed T D McKinley, K F J Heinrich and D B Wittry (New York: Wiley) pp 296–377

—— 1967 *Trans. 2nd Natn. Conf. Electron Probe Microanalysis, Boston, USA* (Boston: Electron Probe Analysis Society of America) Paper No. 7

—— 1968 *Advances in X-ray Analysis* ed J B Newkirk, G Mallett and H G Pfeiffer (New York: Plenum Press) 11 40–55

Love G, Cox M G C and Scott V D 1974a *J. Phys. D: Appl. Phys.* 7 2131–41

—— 1974b *J. Phys. D: Appl. Phys.* 7 2142–55

—— 1975 *J. Phys. D: Appl. Phys.* 8 1686–1702

Philibert J 1963 *X-ray Optics and X-ray Microanalysis* ed H H Pattee, V E Cosslett and A Engström (New York: Academic Press) pp 379–92

Reed S J B 1965 *Br. J. Appl. Phys.* 16 913

Reuter W 1972 *X-ray Optics and Microanalysis* ed G Shinoda, K Kohra and T Ishikonawa (Tokyo: University Press) pp 121–30

7.8 Absorption Corrections in Quantitative Light Element Analysis.

G. Love, M.G.C. Cox and V.D. Scott, 1976b, Developments in Electron Microscopy and Analysis, ed. J.A. Venables, (Academic Press; London), p.145.

ABSORPTION CORRECTIONS IN QUANTITATIVE LIGHT ELEMENT MICROANALYSIS

G. Love, M.G.C. Cox and V.D. Scott

School of Materials Science, University of Bath,

Claverton Down, Bath BA2 7AY

Introduction. Correction procedures for quantitative electron probe microanalysis of elements $Z \geqslant 12$ are well established, but extension of these techniques to light elements has received much less attention. Difficulties may arise here because the physical bases of correction models, such as the laws describing electron scattering in solids, are not well understood and certain input parameters such as mass absorption coefficients are unreliable. Hence it is not surprising to find that much published work on quantitative analysis of the light elements has employed standards of composition similar to the material being analysed in order to minimise the magnitude of the correction. However, while the method may be satisfactory in some cases, it is generally inconvenient due to the large number of standards required and a better procedure would incorporate an accurate correction model together with only a limited number of standards.

In light element microanalysis the absorption correction, which can amount to several hundreds of per cent, is often much larger than either the atomic number effect or fluorescence contribution. Thus the precision of analysis is likely to be affected most by an unsatisfactory absorption model. In the present paper the absorption correction proposed by Bishop (1974) is evaluated and compared with the more frequently used Philibert (1963) expressions.

The absorption correction of Bishop. Bishop (1974) has discussed the characteristics of a good absorption correction and shown that provided absorption is small $f(\chi)$ is given by

$$\underset{\chi \to 0}{f(\chi)} = \left(1 - \chi \overline{\rho z}\right) ,$$

where $f(\chi)$ is the fractional transmission of the target for x-rays emerging in the direction of the spectrometer, i.e. at angle θ to the surface of the target; $\overline{\rho z}$ is the mean mass depth of x-ray generation and $\chi = \mu/\rho \operatorname{Cosec} \theta$ where μ/ρ is the mass absorption coefficient of the x-ray of interest in the target. With increasing absorption the shape of the x-ray distribution with depth, $\phi(\rho z)$, becomes more important and finally for very high absorption the value of $\phi(\rho z)$ at the surface, $\phi(0)$, determines the magnitude of the absorption correction.

Bishop has suggested a rectangular profile to represent the x-ray distribution with depth, the assumption being that $\phi(\rho z)$ has a constant finite value for $0 \leqslant \rho z \leqslant 2\overline{\rho z}$ whilst outside these limits $\phi(\rho z) = 0$. On this basis $f(\chi)$ is given by

$$f(\chi) = \frac{1}{2\chi\overline{\rho z}} \left[1 - \exp\left(-2\chi\overline{\rho z}\right)\right]$$

An expression for $\overline{\rho z}$ can be extracted from the simplified Philibert equation,

$$f(\chi) = \left[\left(1 + \chi/\sigma\right)\left(1 + \frac{h}{1+h}\cdot\chi/\sigma\right)\right]^{-1} , \quad \text{given by} \quad \overline{\rho z} = \left(\frac{1+2h}{1+h}\right)\frac{1}{\sigma} \quad \ldots (1)$$

$h = B\,\frac{A}{Z^2}$ where B is a constant and A and Z are the atomic weight and number of the target respectively; σ varies with the incident electron energy, E_o, and with the excitation potential of the x-radiation, E_c, and is expressed as

$$\sigma = \frac{C}{E_o^n - E_c^n}, \qquad C \text{ and } n \text{ being}$$

constants. The use of equation (1) can be justified since the form of the variation of $\overline{\rho z}$ with both Z and E_o accords reasonably with that calculated by Monte Carlo methods (Bishop 1966). Since the constants B, C and n normally used in the Philibert expression (e.g. those of Heinrich (1967) and Duncumb, Shields-Mason and Da Casa (1969)) are semi empirical, there is no a priori justification for their use in the Bishop method. Consequently alternative values of B, C and n for Bishop's method have been established by the Δ-optimisation procedure of Love, Cox and Scott (1975) using microanalysis data covering a wide range of systems.

Optimisation of constants B, C and n.

430 microanalysis results have been compiled and used in the present work to establish optimised values for B, C and n (see table 1). These data include analysis of elements with $12 \leq Z \leq 92$ at incident electron energies in the range 5 - 40 kV.

Table 1. Values of constants for use in equations for h and σ

Method	B	C	n
1	0.72	6.80×10^5	1.77
2(a)	1.2	4.50×10^5	1.65
2(b)	0.84	6.58×10^5	1.84
3	4.5	2.54×10^5	1.50

1. Bishop's absorption method, Δ-optimised constants.
2. Simplified Philibert method
$$f(\chi) = \left[\left(1+\chi/\sigma\right)\left(1+\frac{h}{1+h}\chi/\sigma\right)\right]^{-1}$$
   (a) Heinrich's (1967) constants
   (b) Δ-optimised constants
3. Full Philibert method
$$f(\chi) = \left(1+\frac{\phi(0)h}{4+\phi(0)h}\cdot\chi/\sigma\right)\left[\left(1+\chi/\sigma\right)\left(1+\frac{h}{1+h}\cdot\chi/\sigma\right)\right]^{-1}$$
   Duncumb and Melford's (1966) constants - Reuters (1972) $\phi(0)$ values

In the Δ-optimisation the Duncumb, Shields-Mason and da Casa (1969) atomic number, Reed's (1965) characteristic fluorescences and Bishop's absorption correction have been used in conjunction with mass absorption coefficients tabulated by Heinrich (1966). Values of h were calculated using $h = \Sigma_i c_i h_i$ where c_i is the weight fraction of the i th element.

Assessment of absorption corrections. These optimised values of B, C and n have been used to calculate the oxygen intensity ratio, k', relative to an alumina standard for a series of binary and ternary oxides (for details of oxide systems see Love et al 1974b). The calculations have been carried out using the mass absorption coefficients of Love et al (1974a). The ratio of k' to the measured intensity ratio k, was plotted in histogram Fig.1a. and the RMS deviation from 1.00 was found to be 7.4%.

These results have been compared with the simplified (method 2a) and full (method 3) Philibert models, see histograms Fig.1(b) and 1(c). It should be noted that the distribution of results for the simplified Philibert method (RMS deviation 14%) is clearly inferior to that shown in Fig.1(a). This may be attributed to the systematic failure of this model at low values of $f(\chi)$ resulting from the approximation $\phi(0) = 0$. Comparison with the full Philibert results Fig.1(c) indicates that the Bishop model is only marginally inferior for light element analysis, the RMS deviations being 6.0% and 7.4% respectively. This difference probably results from the inadequacy of the x-ray depth distribution of the Bishop model in the immediate surface regions of the target.

The Bishop model has also been applied to the 430 microanalysis measurements described earlier and these results are presented in a histogram Fig.2a(RMS deviation 5.3%). To facilitate comparison, these measurements have been corrected using the simplified Philibert method with both Heinrich's constants Fig.2(b) (RMS deviation 6.8%) and constants derived by a Δ-optimisation procedure Fig.2(c) (RMS deviation 5.3%). It is apparent that for hard x-ray analysis there is little to choose between the Bishop and simplified Philibert methods providing the appropriate optimised constants are used in each case.

Conclusions. In a previous paper (Love et al 1975) it has been shown that the simplified Philibert method is superior to the full Philibert correction for analysis of elements where $Z \geqslant 12$. Using this information and that supplied in the present paper it is evident that Bishop's approach combines the best features of both Philibert methods and has a wider range of application than either.

While values of B, C and n have been recommended for use in the Bishop absorption correction these have been derived using Heinrich's mass absorption coefficients; the adoption of alternative μ/ρ data may necessitate revision of the constants.

Finally, it should be noted that further progress in the experimental refinement of absorption correction models will be restricted by the lack of microanalysis measurements and mass absorption coefficients of sufficient accuracy.

References

Bishop H.E. 1966 X-ray Optics and Microanalysis eds. R. Castaing, P. Deschamps and J. Philibert (Paris : Hermann) p.112.

Bishop H.E. 1974 J. Phys. D. : Appl. Phys. 7, 2009.

Duncumb P. and Melford D.A. 1966, X-ray Optics and Microanalysis eds. R. Castaing, P. Deschamps and J. Philibert (Paris : Hermann) p.240.

Duncumb P., Shields-Mason P.K. and da Casa C. 1969 X-ray Optics and Microanalysis eds. G. Möllenstedt and K.H. Gaukler (Berlin : Springer-Verlag) p.146

Heinrich K.F.J. 1966 The Electron Microprobe eds. T.D. McKinley, K.F.J. Heinrich and D.A. Wittry (New York : Wiley) p.296.

Heinrich K.F.J. 1967 2nd Natn. Conf. on Electron Microprobe Analysis, Electron Probe Analysis Society of America, , Boston, Mass.

Love G., Cox, M.G.C. and Scott, V.D. 1974a J. Phys.D. : Appl. Phys. 7, 2131-41.

Love G., Cox M.G.C. and Scott V.D. 1974b J. Phys. D. : Appl. Phys. 7, 2142-55.

Love G., Cox M.G.C. and Scott V.D. 1975 J. Phys. D. : Appl. Phys. In Press.

Philibert J. 1963 X-ray Optics and X-ray Microanalysis eds. H.H. Pattec, V.E. Cosslett and A. Engström (New York : Academic Press) p.379.

Reed S.J.B 1965 Br. J. Appl. Phys. 16, 913.

Reuter W. 1972 X-ray Optics and Microanalysis eds. G. Shinoda, K. Kohra and T. Ishinokawa (Tokyo U.P.) p.121.

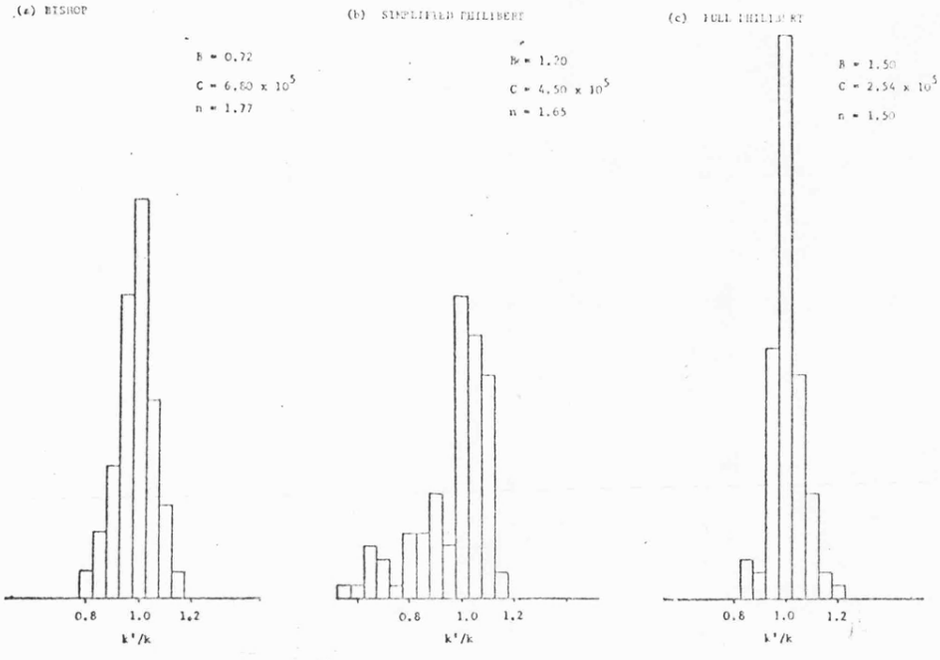

Fig. 1

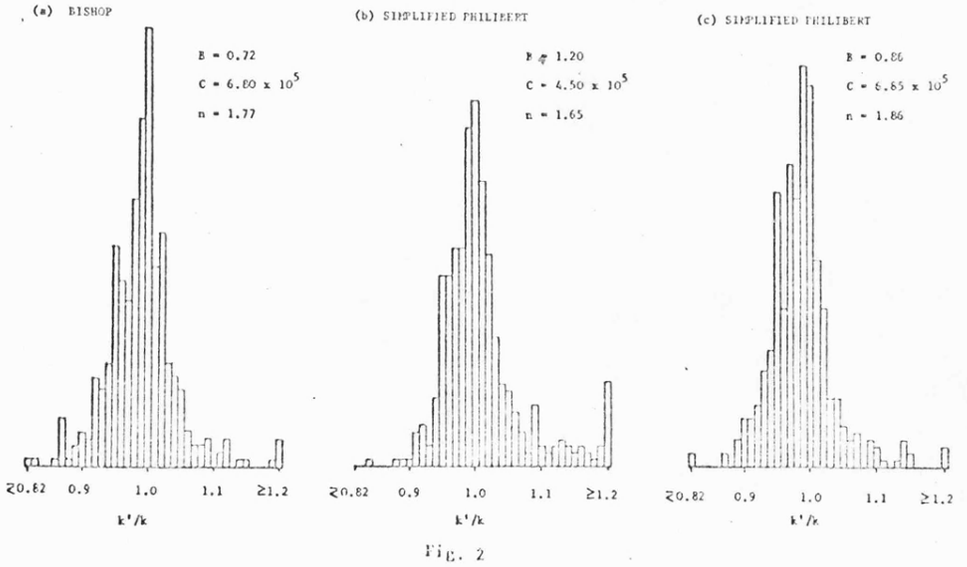

Fig. 2

7.9 Vaterite Deposition During Eggshell Formation in the Comorant, Gannet and Shag and in the "Shell-less" Eggs of the Domestic Fowl.

S.G. Tullett, R.G. Board, G. Love, H.R. Perrott and V.D. Scott.,

1976c, Acta Zoologica, (Stockh.), 57, 79.

Vaterite Deposition During Eggshell Formation in the Cormorant, Gannet and Shag, and in 'Shell-less' Eggs of the Domestic Fowl.

S. G. Tullett, R. G. Board*, G. Love, H. R. Perrott and V. D. Scott*

School of Biological Sciences* and School of Materials Science, University of Bath, Claverton Down, Bath, England
(Accepted October 15, 1975)

Abstract

The eggshells of the cormorant (*Phalacrocorax carbo*), domestic fowl (*Gallus domesticus*), gannet (*Sula bassana*), guinea fowl (*Numida meleagris*), greater flamingo (*Phoenicopterus ruber*), and shag (*Phalacrocorax aristotelis*) have been separated into two groups on the basis of the composition of their outer stratum. In the domestic fowl, guinea fowl and greater flamingo the outer stratum is an organic cuticle while in the sea-birds it is an inorganic cover rich in vaterite. The calcareous deposits on the membranes of eggs of the domestic fowl which are shell-less at oviposition have been shown to consist essentially of the vaterite form of calcium carbonate. Reasons for the occurrence of this polymorph of calcium carbonate are discussed with relation to the physiology of the birds.

Introduction

The avian eggshell is composed essentially of calcium carbonate in the form of calcite columns. In the case of the domestic fowl the true shell is covered externally by a thin organic cuticle. This cuticle has a vesicular structure (Simons and Wiertz 1966) and consists of protein, fat and polysaccharides or sugars (Tyler and Simkiss 1958, Cooke and Balch 1970, Wedral et al. 1974). In the eggs of birds belonging to the Phalacrocoridae and Podicepidae (Tyler 1966) the external layer has a chalky appearance, is rich in inorganic material and is more appropriately termed a cover (after Schmidt 1958) rather than a cuticle. Despite these observations no reasons have been given for these differences in structure nor has any suggestion been given of their role in nature.

This paper presents results obtained during a survey of avian eggshells. A detailed study has been carried out using scanning electron microscopy, X-ray diffraction and electron probe microanalysis which has provided new information on the morphology, crystal structure and chemical composition of various types of eggshell. It is shown that the formation of the two basic types of eggshell discussed may be related to the physiology and life-style of the bird. A model is proposed for the formation of the normal eggshell in the domestic fowl and an explanation offered to account for eggs which are shell-less at oviposition.

Materials and Methods

Sources of eggs. Fragments of cormorant eggshell were obtained from Regent's Park; domestic fowl eggs, some of which were shell-less at oviposition, were from commercial laying stock; fragments of gannet eggshell were from Monk's Wood Experimental Station, Abbots Ripton; greater flamingo eggshells from The Wildfowl Trust, Slimbridge; guinea fowl eggs from birds kept in cages or free range and fragments of shag eggshells from Bardsey Island Bird Observatory.

Methods of examination. (a) Scanning electron microscopy: Outer surfaces and sections of radially fractured eggshells were examined. For this purpose specimens of shell were cemented onto aluminium stubs with DAG 915 (Acheson Colloids Co., Prince Rock, Plymouth) and coated under vacuum with a thin (30 nm thickness) layer of gold: palladium alloy. A Stereoscan S4 (Cambridge Scientific Instruments Ltd.) operating at an accelerating voltage of 10 kV was used.

(b) Electron probe microanalysis: Pieces of eggshell were embedded in Plastiecraft (Turner Research Ltd., Leeds) using a vacuum impregnation technique to ensure complete infiltration of the shell (Board & Tullett, 1975). Radial sections through the shell were prepared by polishing on successively finer grades of diamond paste down to a 1 μm finish. They were coated under vacuum with a thin layer (30 nm thickness) of gold and examined in a JEOL JXA-50A electron probe microanalyser.

c) Chemical assay: The phosporus content of the different eggshell samples was calculated from phosphate determinations obtained using a modified Fiske-Subbarow (1925) method. Samples of organic cuticles (10 mg), crystalline covers (50 mg) and outer shell (50 mg) were obtained by scraping the eggshell with a scalpel. These samples as well as the inner shell (100 mg) remaining from such a process and whole true shells (100 mg) were analysed. The material was dissolved in 0.5 ml HCl (A.R.) and maintained at 100 °C for 5 min. The solution was made up to 6 ml with water and a dilution series prepared from this for analysis. Phosphate was assayed by addition of 1 ml 2.5 % ammonium molybdate followed by 1 ml reducing agent (3 % $NaHSO_3$, 1 % Elon (Kodak Ltd, London)) and reading, after 20 min., the optical density at 660 nm.

(d) Flame photometry and atomic absorptiometry: Samples of eggshell were dissolved as above and made up to a volume of 10 ml. Sodium and potassium levels were measured using a flame photometer (E.E.L. Instruments, Essex) and magnesium using an atomic absorptiometer (Unicam SP 90A Series 2, Pye Instruments, Cambridge).

(e) X-ray diffraction: The crystal structure of the shell specimens was examined by the Debye-Scherrer method using copper K_α-radiation at 40 kV and 20 m. amp with a nickel filter.

Results

Scanning electron micrographs taken from a radial section through the eggshell of a greater flamingo (total thickness 0.70 mm) are illustrated in Figs. 1 a and b. These show an abrupt change from the columnar crystals of the true shell to a vesicular cuticle of about 0.07 mm thickness. The columnar crystals were found by X-ray diffraction to be calcite. The material forming the cuticle had a chalky appearance. However, it gave no X-ray diffraction pattern and, moreover, dissolved in boiling sodium hydroxide (5 % w/v) which suggested that it was organic in nature.

Electron probe microanalysis on polished radial sections of the greater flamingo eggshell showed a marked increase in the phosphorus level from the shell (0.15 wt%) to the cuticle (4.0 wt%) as illustrated in the line scan in Fig. 1 c. The cuticle was estimated to contain around 15 % by weight of calcium calculated on the assumption that the shell ($CaCO_3$) contained about 36 wt%. A number of other elements including chlorine, magnesium, potassium and sodium were detected but these were in much lower concentrations (usually < 0.1 wt%) and, due to the nature of the samples, concentration changes across the section were difficult to ascertain. A small increase in the sulphur level was detected from the outer shell (0.1 wt%) to the cuticle (0.5 wt%). Chemical analyses confirmed these data and indicated a marked difference in the phosphorus content between the shell and cuticle (Table 1).

The shell of domestic fowl eggs, which are known to have an organic cuticle (Tyler and Simkiss 1958, Cooke and Balch 1970, Wedral et al. 1974), and those of the guinea fowl gave, apart from the absence of calcium in the cuticle, essentially similar results to those of the greater flamingo (Table 1).

Scanning electron micrographs taken from a radial section through the eggshell of a gannet (total thickness 0.45 mm) are illustrated in Figs. 1 d and e. An abrupt change from columnar crystals to a spherulitic cover of about 0.06 mm thickness can be seen. A notable difference between Figs. 1 e and b is that the particles forming the cover are larger (0.35—3.40 μm cf. 0.01—0.05 μm diameter) than those of the cuticle. In the gannet eggshell the columnar crystals were found by X-ray diffraction to be calcite (Fig. 3 a). The cover gave a clear X-ray diffraction pattern (Fig. 3 b) and was identified with vaterite, the third polymorph of calcium carbonate.

Electron probe microanalysis on polished sections of gannet eggshells showed there was a much smaller difference in phosphorus levels between the shell (< 0.1 wt%) and cover (0.4 wt%) than with eggs having a cuticle. Traces of chlorine, magnesium, potassium, sodium and sulphur were found (< 0.1 wt%), with indications of slightly more chlorine, magnesium and sulphur towards the outer layers. The above data are in general agreement with results obtained by chemical assay (Table 1).

The eggs of two other sea-birds, cormorant and shag, were similar to that of the gannet in having a crystalline cover of vaterite over the true shell of calcite. Certain of the larger spheres possessed a dimpled appearance as shown in

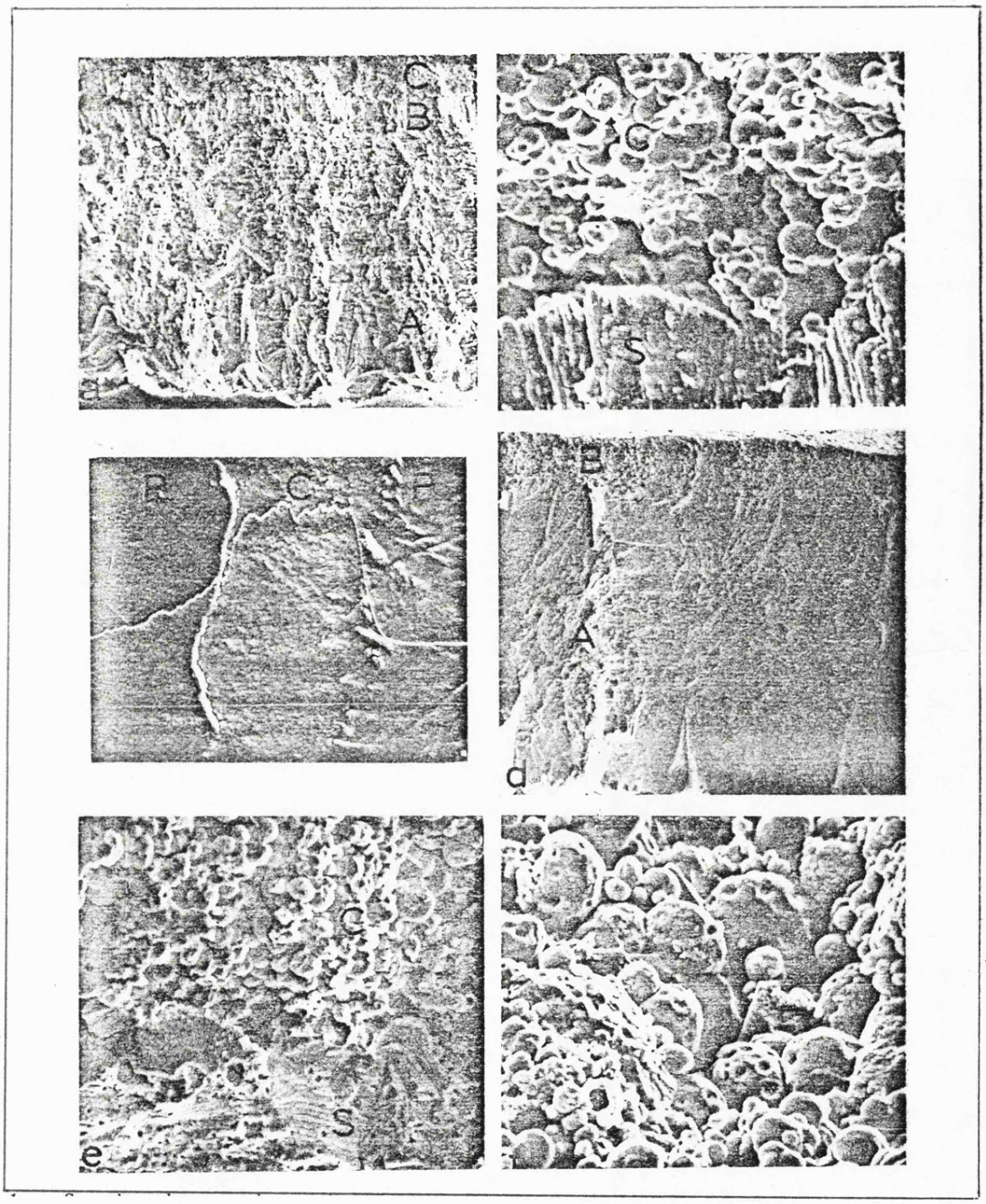

Fig. 1. a. Scanning electron micrograph (SEM of a radially fractured greater flamingo eggshell showing the regions (*A* inner shell, *B* outer shell, *C* cuticle) analysed in the study. *b.* High magnification of 1 a showing abrupt change from columnar crystals of true shell (*S*) to the vesicular organic cuticle. (*C*). *c.* Line scan for phosphorus across the outer strata of a greater flamingo eggshell. The micrograph shows the increasing level of phosphorus from the outer shell (*B*) to the cuticle (*C*) and its absence in the embedding plastic (*P*). The horizontal line indicates the location of the scan on the specimen. *d.* SEM of a radially fractured gannet eggshell showing the regions (*A* true shell, *B* cover) analysed in the study. *e.* High magnification of 1 d showing change from the true shell (*S*) to the cover (*C*). The outer shell layer is less ordered compared to the greater flamingo and many pit-like holes are present in the shell—a feature of many sea-bird eggs we have examined. *f.* Outer surface of a shag eggshell showing the spherulitic deposits forming the cover. *a* 75×, *b* 3575×, *c* 250×, *d* 125×, *e* 1435×, *f* 3260×.

Table 1. *Elemental composition (wt%) of avian eggshells*

Eggs with an organic cuticle					Eggs with a vaterite cover			
Species	Element	A	B	C	Species	Element	A	B
Domestic Fowl	P	0.08—0.09	1.60—2.80	2.50—2.80	Cormorant	P	0.07—0.09	0.50—0.55
	Mg	0.43—0.48	1.50	1.63—1.67		Mg	0.09	0.14
	Na	0.04	0.04	0.02		Na	0.05	0.04
	K	0.01	0.03	0.02		K	0.03	0.08
Greater Flamingo	P	0.13—0.15	1.70—2.30	3.00—4.00	Gannet	P	0.05—0.06	0.35—0.40
	Mg	0.16—0.18		0.13—0.17		Mg	0.15	0.10
	Na	0.05		0.02		Na	0.05	0.04
	K	0.02		0.30		K	0.03	0.08
Guinea Fowl	P	0.04—0.08	0.70—2.30	5.00—6.40	Shag	P	0.04—0.05	0.35—0.40
	Mg	0.42—0.45	0.70—0.75	2.19—2.80		Mg	0.14	0.09
	Na	0.05	0.06	0.01		Na	0.05	0.05
	K	0.02	0.03	0.20		K	0.03	0.08
					Shell-less Domestic Fowl	P	—	0.11—0.13
						Mg	—	0.24
						Na	—	0.05
						K	—	0.08

Note: Itoh and Hatano (1964) have shown increases in the P and Mg levels between the inner and outer shell of the eggs of domestic fowl. The outer shell values quoted in this table also reflect the presence of a "cuticular" component as, owing to the nature of preparation of the samples, pore plugs would be present. A, B, C, see Fig. 1.

Fig. 1 f. The chemical composition data were also similar to those obtained for the gannet eggshell (Table 1).

A scanning electron micrograph of the surface of a domestic fowl egg that was shell-less at oviposition is illustrated in Fig. 2 a and shows the spherular nature of the deposits on the outer shell membrane. Eggs on which the deposits were thicker (Fig. 2 b) resembled surface views of the gannet eggshell. The deposits on shell-less eggs were found to consist essentially of vaterite (Fig. 3 c). Chemical analysis showed that the sodium levels were similar, magnesium levels lower and phosphorus and potassium levels slightly higher than those found in the inner shell of normal eggs of the domestic fowl. Hence, these deposits resemble more closely the cover of the sea-birds studied than the normal shell of the domestic fowl.

An Aylesbury duck egg which was formed normally but due to antiperistalsis had been moved back up the oviduct was found to be overlain with albumen and two shell membranes. Calcium carbonate was crystallised upon the outer shell membrane as a mixture of calcite and vaterite (Fig. 3 d).

Discussion

The present study on the eggshells of the domestic fowl, guinea fowl, greater flamingo, cormorant, gannet and shag has shown that they may be separated into two categories. The eggs of the domestic fowl, guinea fowl and greater flamingo consist of the true shell of calcite covered on its external surface with cuticle. The eggs of the sea-birds comprise a true shell of calcite covered externally by a layer of vaterite.

The work has also demonstrated that the calcium carbonate laid down on the outer shell membrane of domestic fowl eggs which are shell-less at oviposition consist essentially of particles of vaterite. Hence, these deposits resemble the cover of certain sea-birds rather than the normal mammillary knobs laid down during the formation of domestic fowl eggshells which have been shown by Fujii and Tamura (1971). It is noteworthy that as long ago as 1869 von Nathusius had shown

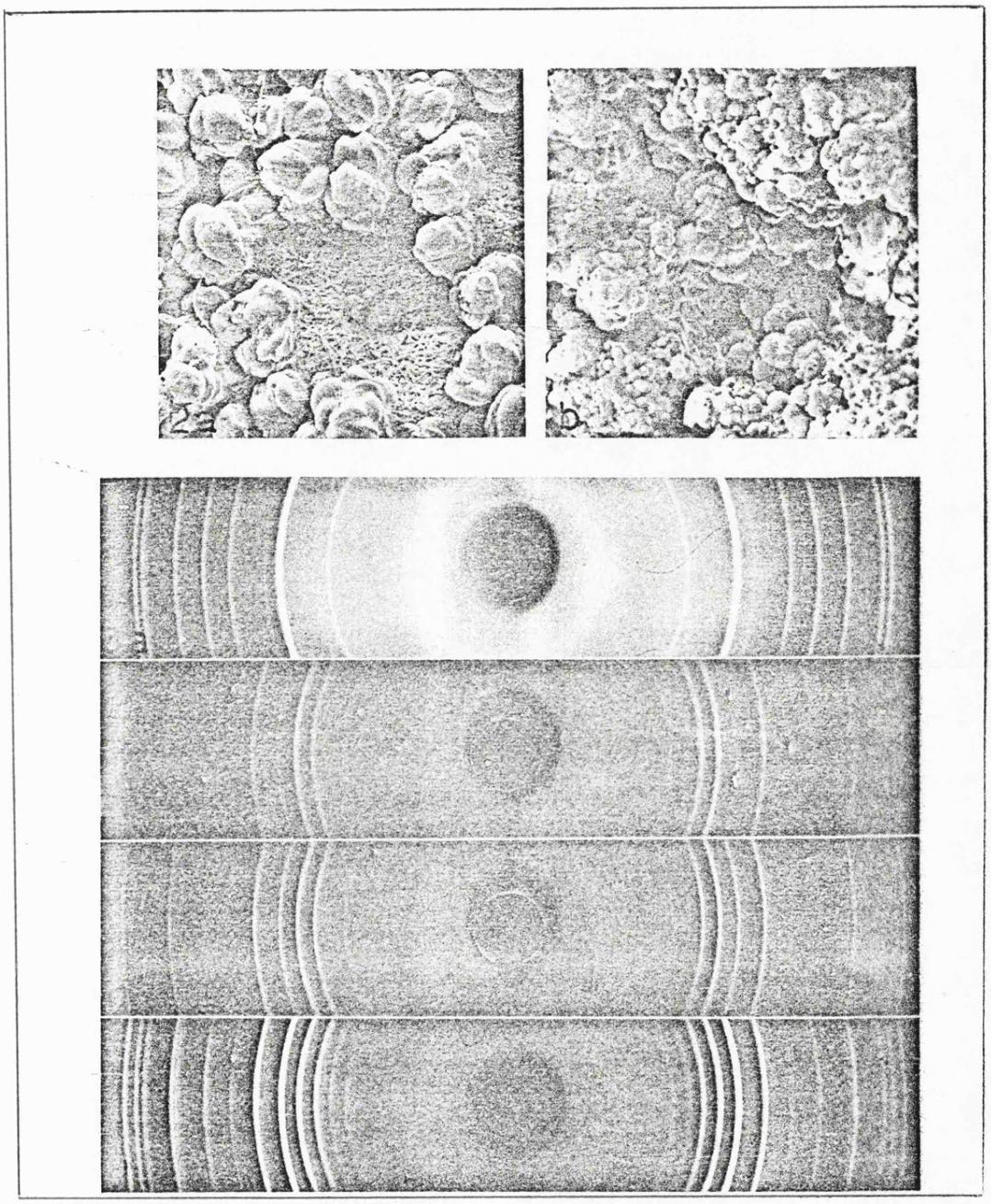

Fig. 2. a. Surface view of a "shell-less" domestic fowl egg. A little crystallisation has occurred forming unusual nodular mamillary knobs on the surface of the outer shell membrane. *b.* Surface view of a "shell-less" domestic fowl egg with more advanced crystallisation. *a* 125×, *b* 310×.

Fig. 3. X-ray diffraction patterns from: *a.* Powdered inner shell layers from a gannet egg. The pattern is characteristic of calcite. *b.* Powdered cover from a gannet eggshell. This pattern is that of vaterite. The prominent calcite line from Fig. 3 a is also represented as a series of spots indicating that a little shell calcite must have been removed as the cover was scraped from the egg. *c.* Powdered deposits from a "shell-less" domestic fowl egg. Traces of calcite are present but the predominant pattern is of vaterite. *d.* Pattern for the outer soft shell of a "double-shelled" Aylesbury duck egg. This "shell" is crystallised as a mixture of calcite and vaterite.

an unusual mammillary structure in a soft-shelled turkey egg. This consisted of nodules of shell material resting on the outer shell membrane. Since previous work (Buckner et al. 1922) has shown that lack of calcium is not the causative factor in the production of shell-less eggs some other change at the crystallisation site must be responsible. The present evidence indicates that alterations in the phosphorus levels, present as phosphates derived from the blood, may cause the change from calcite to vaterite in eggshells having a crystalline cover and terminate eggshell formation in eggs having an organic cuticle. The latter possibility has been intimated by Simkiss (1964) who discussed phosphates as poisons of calcification and by Simons (1971) who suggested they may help terminate eggshell formation.

The avian eggshell is elaborated from raw materials removed from the blood at the shell gland. The calcium and carbonate ions are assembled sandwich style. It is postulated that there is an equilibrium between phosphates that are bound to carriers in the blood and do not cross the shell gland wall and phosphates which are free to cross the wall. Phosphate which enters the shell gland may then substitute for carbonate ions in the calcite lattice. It is suggested that while a small amount of phosphate (equivalent to 0.1 wt% phosphorus) can be incorporated into the calcite lattice, too much may render this structure unstable. According to Raistrick (1949), phosphate ions may remove the electrostatic potential for the absorption of a further layer of calcium ions.

In the case of the domestic fowl, guinea fowl and greater flamingo the phosphate levels increase to such an extent (incorporation rate of above about 2.5 wt%) as to terminate all crystallisation. The organic cuticle is then added.

In the case of the sea-birds the phosphorus content was 0.33—0.55 wt% in the cover compared with <0.1 wt% in the calcitic shell. The phosphorus level of 0.33—0.55 wt% is not sufficiently high to terminate crystallisation but incorporation of this amount of phosphorus as phosphates in the calcium carbonate lattice results in vaterite becoming the stable structure rather than calcite. Vaterite has only previously been found once to our knowledge in eggshells (Gould 1972) and only rarely occurs in biological systems, for example, in biliary calculi (Bogren and Larsson 1963), on experimental regeneration of the shells of certain molluscs and the alga *Coccolithus huxleyi* (Wilbur and Watabe 1963), as an accompanying mineral in calcite kidney stones in horses (Gruenberg 1971), and in the reproductive systems of certain snails (Watabe et al. 1973).

The vaterite crystals are seen in this study to adopt a spherulitic form. This morphology suggests that fresh calcium carbonate crystals are being nucleated but, probably due to the level of phosphate (equivalent to 0.33—0.55 wt%), are not allowed to develop into large crystals characteristic of the growth of the inner layers of calcite. It is not possible at this stage in the work to say what material forms the nucleation sites but it is probably connected with the natural secretions of the oviduct.

The next question to be answered is why, in the final stages of shell formation, higher levels of phosphate are present in the domestic fowl, guinea fowl and greater flamingo than in the seabirds? The sudden increase in the phosphorus level from the outer shell to the cuticle in the eggs of the domestic fowl, guinea fowl and greater flamingo probably reflects a switch from crystallisation of the true shell to the secretion of the organic cuticle within the shell gland. The situation in the sea-birds is more complex and the smaller rise in phosphorus content between the shell and outer cover must be associated with a change in the source of calcium for eggshell crystallisation from one having a high Ca:P ratio to one having a low Ca:P ratio. Indeed, two types of calcium reserve have been identified in the domestic fowl (Common and Hale 1942, Black and Tyler 1944) which may be used when the dietary intake is insufficient to provide all the shell calcium. One is a readily mobilised reserve which these authors suggest is probably used at the beginning of shell formation and has a relatively high Ca:P ratio while the other is a less readily mobilised reserve which is used towards the end of shell formation and has a low Ca:P ratio. It is interesting to speculate what these two reserves are and what their relevance is to egg production in the birds studied.

It is known that calcium for eggshell formation is drawn from a special reserve known as medullary bone laid down in the marrow cavities of the limb bones at the onset of the reproductive period. The breakdown of medullary bone results in a concommitant release of phosphate which is excreted (see Simkiss 1967). Thus several, not mutually exclusive, possibilities present themselves towards the end of shell formation. First, the diet and/or the initial medullary bone store (calcium store 1) is sufficient to provide all the calcium for shell formation. Secondly, this store

may become depleted and the bird then has to draw on a calcium store (2) which may be formed either of secondary medullary bone formed during depletion of Store 1, or it may be the skeletal bone itself. In the case of the domestic fowl, guinea fowl and greater flamingo calcium store 1 is presumably sufficient to provide all the shell calcium and the increase in phosphorus towards the end of shell formation reflects, as suggested previously, a switch from crystallisation to cuticle secretion rather than a switch in the source of calcium. Calcium store 2 probably does not become operational in such birds until the final eggs in a protracted clutch.

It is suggested that the birds which have to fly out to sea for food, eg. the cormorant and shag, avoid a large increase in body weight during the breeding season by laying down only a small medullary bone store. The gannet, which plunges into the water for food from heights of 50 feet and more has, among other shock-absorbing features, a strengthened skeleton to withstand impact with the water (Beazley 1974). Here again the scope for medullary bone storage may be limited. Hence, a switch from calcium store 1 to store 2 is likely to be made before shell formation is complete. This switch it is suggested may lead to an increase in the phosphate concentration to levels which favour vaterite rather than calcite formation.

The eggs of the greater flamingo are interesting in two further respects. Firstly, the proposed switch from crystallisation to cuticle secretion does not appear to close down the incorporation of calcium into the shell. Hence, the cuticle contains a high proportion of calcium but, again possibly due to the high phosphate concentrations, this is not crystallised and no X-ray diffraction pattern is obtained from specimens of cuticle. Secondly, the inner shell of the greater flamingo had the highest phosphorus content of any of the eggs studied. This must be related to the fact that the greater flamingo and its close relative the lesser flamingo inhabit eutrophic waters (Brown 1959) which are naturally rich in phosphorus (Middlebrooks et al. 1974) and their diet includes phosphate-rich blue-green algae.

The proposed mechanism of eggshell formation can be extended to explain certain unusual features of eggshell structure, for example, the vaterite form of the calcium deposits laid down on the outer shell membrane of domestic fowl eggs which are shell-less at oviposition. Such eggs occur regularly within laying flocks and observations at a local poultry farm suggest they are laid only a few hours after a normal egg rather than the usual 24.5 hour interval. This suggests that two oocytes may have been ovulated simultaneously or within a short interval. The first receives a normal calcite shell covered with a phosphate-rich cuticle. The second egg enters the shell gland as the phosphate levels are falling after the cuticle secretion for the first egg. The level is, however sufficiently high to impede calcite growth and, in consequence, vaterite becomes the more stable form. Further evidence for this mechanism has been provided by a normal Aylesbury duck egg which just prior to oviposition was moved back up the oviduct. The coating of albumen received by this egg indicates that it moved up as far as the magnum—hence on the basis of figures presented by Gilbert (1971) it would be about three hours before it re-entered the shell gland. This is a longer interval than that occuring between the proposed exit of egg 1 and the entry of egg 2 in the production of shell-less eggs. It would be expected, therefore, that the phosphate levels would have fallen lower than those permitting only vaterite production. Indeed, the membranes of the "outer" egg had received calcareous deposits consisting of a mixture of calcite and vaterite. The formation of weak eggshells may also be explained similarly although in this case it is suggested that the shell gland fluid composition recovers to favour normal calcite deposition upon an abnormal cone layer. This view is supported by the studies of King and Robinson (1972) who published micrographs of weak eggshells showing an unusual cone layer composed of spherular units. Unfortunately, no data as to its chemical composition are available.

The conditions necessary for vaterite formation appear to be present at some time during each egg laying cycle. Of the birds studied, only the sea-birds seem to have made use of this feature to provide a vaterite cover for the egg. This cover must have intrinsic properties favourable to the successful development of the embryo. One possible function that has been suggested (Board et al. 1976) is it helps keep the egg clean.

Vaterite has been identified in eggshells only once previously (Gould 1972) in the case of the brown pelican. Unfortunately whole shells were analysed and the location of the vaterite within the eggshell was therefore not apparent. However, it seems reasonable to assume that the pelicans, which are close allies of the cormorant, gannet and shag, have a similar shell structure to these birds. The fact that a relatively thin shell in

Gould's study had an infinitely high calcite to vaterite ratio (supposedly as a result of the effects of the metabolites of DDT) may indicate that the egg was coverless—a situation akin to cuticle-less eggs in the domestic fowl discussed by Board (1975). One of the functions of the vaterite cover must be as a mechanical defence against microbial penetration of the shell (see Board and Fuller, 1974). Therefore if the coverless state is a result of the effects of the metabolites of persistent pesticides this introduces the question of egg losses through addling in addition to the usual losses through breakage discussed by Ratcliffe (1970).

Acknowledgements

One of us (S.G.T.) would like to thank the British Egg Marketing Board Research and Education Trust for a scholarship. Thanks are due to the S.R.C. for the original provision of a scanning electron microscope and to people who supplied material for study; Mr. and Mrs. H. F. Hoddinott (domestic fowl), Mr. G. Tucker (guinea fowl), Prof. G. V. T. Matthews (greater flamingo), Mr. M. Peacock (shag), Mr. P. J. Olney (cormorant) and Dr. J. L. F. Parslow (gannet). Thanks are also due to Mr. B. Chapman for production of the X-ray diffraction patterns.

References

Beazely, M. 1974. *World Atlas of Birds.* Mitchell Beazely Publishers Ltd., London.

Black, D. J. G., Tyler, C. 1944. Fluctuations in the porosity of eggshells. *Nature,* Lond. *153:* 682—683.

Board, R. G. 1975. The microstructure of the cuticle-less shell of the eggs of the domestic hen. *Br. Poult. Sci. 16:* 89—93.

— *Tullett, S. G.* 1975. The pore arrangement in the emu (*Dromaius novachollandiae*) as shown by plastic models. *J. Microscopy 103:* 281—284.

— — *Perrott, H. R.* 1976. A classification of pore systems in avian eggshells. *J. Zool. London.*

Bogren, H., Larsson, K. 1963. Crystalline components of biliary calculi. *Scand. J. Clin. Lab. Invest. 15:* 457—462.

Brown, L. H. 1959. *The Mystery of the Flamingoes.* Country Life, London.

Buckner, G. D., Martin, J. H., Pierce, W. C., Peter, A. M. 1922. Calcium in eggshell formation. *J. Biol. Chem. 51:* 51—54.

Common, R. H., Hale, R. W. 1941. Observations on the mineral metabolism of pullets. VI. The mobilization of body calcium for shell formation. *J. Agric. Sci. 31:* 415—437.

Cooke, A. S., Balch, D. A. 1970. Studies of membrane, mammillary cores and cuticle of the hen eggshell. *Br. Poult. Sci. 11:* 345—352.

Fiske, C., Subbarow, Y. 1925. The colorimetric determination of phosphorus. *J. Biol. Chem. 66:* 375—400.

Fujii, S., Tamura, T. 1970. Scanning electron microscopy of shell formation in the hens egg. *J. Fac. Fish. Anim. Husb.,* Hiroshima Univ. *9:* 65—81.

Gilbert, A. B. 1971. Transport of the egg through the oviduct and oviposition. In *Physiology and Biochemistry of the Domestic Fowl.* Vol. 3. (Bell, D. J., Freemen, B. M., eds.), Academic Press, London.

Gould, R. W. 1972. Brown pelican eggshells: X-ray diffraction studies. *Bull. Environ. Cont. and Tox. 8:* 84—88.

Gruenberg, W. 1971. Karbonat-Harnsteine herbivorer Säugetiere. *Zentralbl. Veterinärmed. Reihe A. 18:* 767—823.

Itoh, H., Hatano, T. 1964. Variation of magnesium and phosphorus deposition rates during egg shell formation. *Poult. Sci. 43:* 77—80.

King, N. R., Robinson, D. S. 1972. The use of the scanning electron microscope for comparing the structure of weak and strong egg shells. *J. Microscopy 95:* 437—443.

Middlebrooks, E. J., Falkenborg, D. H., Maloney, T. E. 1974. *Modelling the Eutrophication Process.* Ann Arbor Science Publins, Michigan.

Nathusius, N. von. 1869. Nachtrage zu der Arbeit "Über die Hüllen, welche den Dotter des Vogeleies umgeben". *Z. wiss. Zool. 19:* 322—348.

Raistrick, B. 1949. The influence of foreign ions on crystal growth from solution. I. The stabilization of the supersaturation of calcium carbonate solutions by anions possessing O-P-O-P-O chains. *Disc. Faraday Soc. 5:* 234—237.

Ratcliffe, D. A. 1970. Changes attributable to pesticides in egg breakage frequency and eggshell thickness in some British birds. *J. appl. Ecol. 7:* 67—115.

Schmidt, W. J. 1968. Schleim-, Kalk- und Farbstoff-Ablagerungen auf der Kalkschale von Vogeleiern. *Z. Zellforsch. 47:* 251—268.

Simkiss, K. 1964. Phosphates as crystal poisons of calcification. *Biol. Rev. 39:* 487—505.

— 1971. *Calcium in Reproductive Physiology.* Chapman and Hall Ltd., London.

Simons, P. C. M. 1971. Ultrastructure of the hen eggshell and its physiological interpretation. *Comm. No. 175.* Central Institute for Poultry Research. Beekbergen, the Netherlands.

— *Wiertz, G.* 1966. The ultrastructure of the surface of the cuticle of the hens egg in relation to egg cleaning. *Poultry. 45:* 1153—1162.

Tyler, C. 1969. A study of the egg shell of the

gaviiformes, procellariformes, podicipitoformes and pelicaniformes. *J. Zool. Lond. 158:* 395—412.

— *Simkiss, K.* 1958. Studies on egg shells. VIII. The determination of membrane-, pore- and matrix-protein—a reassessment. *J. Sci. Fd. Agric. 9:* 375—380.

Watabe, N., Meenakshi, V. R., Blackwelder, P. L., Dunkelberger, D. G. 1973. Distribution of vaterite crystals in reproductive systems of ampullarid snails. *Am. Zoolog. 13:* 1334.

Wedral, E. M., Vadehra, D. V., Baker, R. C. 1974. Chemical composition of the cuticle, and the inner and outer shell membranes from eggs of *Gallus gallus. Comp. Biochem. Physiol. 47B:* 631—640.

Wilbur, K. M., Watabe, N. 1963. Experimental studies on calcification in molluscs and the alga *Coccolithus huxleyi. Ann. N. Y. Acad. Sci. 109,* Art 1, 82—112.

Dr. S. G. Tullett
School of Biological Sciences
University of Bath
Claverton Down, Bath BA2 7AY
England

7.10 A Simple Monte Carlo Method for Simulating Electron-Solid Interactions and its Application to Electron Probe Microanalysis.

G. Love, M.G.C. Cox and V.D. Scott,

1977a, J. Phys. D _ Appl. Phys.,

10, 7.

J. Phys. D: Appl. Phys., Vol. 10, 1977. Printed in Great Britain. © 1977

A simple Monte Carlo method for simulating electron–solid interactions and its application to electron probe microanalysis

G Love, M G C Cox and V D Scott
School of Materials Science, University of Bath, Claverton Down, Bath, Avon, BA2 7AY

Received 13 August 1976

Abstract. A Monte Carlo method based on Curgenven and Duncumb's treatment is described. It is shown that the predictions of the model agree well with experimental backscattered electron energy distributions and $\phi(\rho z)$ curves. The model is used to generate $\phi(\rho z)$ curves for a wide range of analytical conditions. Based on these data an examination is carried out of the way in which the mean depth of x-ray production varies with electron accelerating voltage, overvoltage and atomic number of the target. An expression for the mean depth is deduced; the form of this expression is compared with that predicted by the Philibert model.

1. Introduction

Correction factors for converting the intensity of characteristic x-rays excited by electron bombardment into elemental concentrations depend upon the distribution with depth of primary x-rays in the target. If this distribution, usually represented as the function $\phi(\rho z)$, is known accurately, it is possible to calculate rigorously correction factors for atomic number, absorption and fluorescence effects and hence achieve quantitative analysis.

The function $\phi(\rho z)$ may be determined experimentally (e.g., Castaing and Descamps 1955, Schmitz *et al* 1969) but such measurements are difficult to carry out, except for a restricted range of experimental conditions, and the results are not always reliable.

An alternative method of obtaining $\phi(\rho z)$ data involves the development of theoretical models which are based upon the physics of electron–target interactions. The essential requirement is to obtain a realistic picture of the electrons in the target in terms of their energy, position and direction; $\phi(\rho z)$ data may then be determined using an appropriate ionization cross-section. The calculation may be carried out either by employing a collective electron model based upon solution of the Boltzmann transport equation (Brown 1968, Brown *et al* 1969) or by simulating individual electron trajectories using Monte Carlo techniques (Green 1962, Bishop 1965, Shimizu *et al* 1966); both methods produce data which accord well with some experimentally determined $\phi(\rho z)$ curves as well as with backscattered electron energy distributions.

A simplified Monte Carlo approach has been suggested by Curgenven and Duncumb (1971) who, in their treatment of electron scattering, chose firstly to neglect the nuclear screening effects of the orbital electrons, and secondly to assume that all angular scattering was caused by elastic interactions. These simplifications were then partially com-

pensated for by trial and error adjustments of the impact parameter used in the scattering model such that the predicted backscatter coefficients fitted experimental data. This novel approach removed the need to know the scattering parameters accurately and permitted the programme to be run on a mini-computer. The model has been found to adequately represent both continuum x-ray generation (Statham 1975) and magnetic contrast in the scanning electron microscope (Newbury *et al* 1973). However, it has not been tested thoroughly by comparison with experimental backscattered electron energy distributions and $\phi(\rho z)$ data.

A computer programme has been written, based upon the approach of Curgenven and Duncumb, which incorporates new developments facilitating its use over a wide range of conditions. In the present paper it is used to generate backscattered electron energy and $\phi(\rho z)$ distributions and the programme is evaluated by comparing these data with experimental results. The importance of the mean depth of x-ray generation in practical microanalysis is stressed, and an analytical expression is deduced which shows how this parameter depends on atomic number, overvoltage and excitation energy. Finally the form of the calculated results is compared with predictions of the Philibert (1963) model.

2. The Monte Carlo model

The scattering that an electron suffers when it penetrates a solid arises from interactions with both the nuclei and orbital electrons of the target. Interaction with the nucleus results in very little energy transfer because of the much greater mass of the nucleus compared with the electron, but this elastic process is almost entirely responsible for the large-angle scattering which occurs. Interaction of the moving electron with the orbital electrons of the target atoms, however, results in considerable energy transfer and the energy lost subsequently reappears as continuous x-radiation, characteristic x-radiation, light, secondary electrons and heat.

In the Monte Carlo method, the electron trajectory is divided into a number of steps and the energy, position and direction of the electron is computed at the end of each step. This information together with knowledge of the ionization cross-section enables the characteristic x-ray production at a particular depth in the specimen to be calculated.

As mentioned earlier, the Monte Carlo method adopted in this paper is based almost exclusively on the treatment of Curgenven and Duncumb (1971), but some simplification has been possible since the two-dimensional plots for electron and x-ray distributions produced by these workers were not required. In addition the following treatment incorporates minor changes to some of the mathematical techniques.

2.1. Electron energy loss

Following usual practice it is assumed that the electron loses energy continuously rather than in discrete amounts. The expression of Bethe (1930) is normally used to describe the rate of energy loss, i.e.

$$\frac{dE}{d(\rho s)} = -\frac{78\,500}{E}\frac{Z}{A}\ln\left(\frac{1{\cdot}166\,E}{J}\right) \tag{1}$$

where Z is the atomic number, A is the atomic weight, ρs is the distance along the electron trajectory, E is the electron energy, and J is the mean ionization potential (i.e. the average

energy loss per inelastic event). Most workers have assumed that J is constant in the above equation for all electron energies, but this leads to physically unrealistic results at low electron energies since equation (1) then predicts that the rate of energy loss becomes zero when $E=J/1{\cdot}166$, and hence the electron would never be stopped by the target. In reality J is constant only at high energies since, as the electron energy falls, high-energy excitations can no longer contribute to the energy loss process (Cosslett 1966, Rao-Sahib and Wittry 1974). Thus as E decreases J decreases at a faster rate and $\mathrm{d}E/\mathrm{d}(\rho s)$ increases continuously until the electron has lost all its energy.

In the present work, equation (1) with a constant value of J has been used at high energies. At low energies, however, where the variation of J with E is unknown, a simple parabolic extrapolation of the Bethe expression from its inflexion at $E/J=6{\cdot}338$ to the origin (see figure 1) has been employed, viz

$$\frac{\mathrm{d}E}{\mathrm{d}(\rho s)}=-\frac{62\,360}{E^{1/2}}\frac{Z}{A}\frac{1}{J^{1/2}}. \tag{2}$$

This empirical modification to equation (1), first suggested by Rao-Sahib and Wittry (1974), predicts the correct limiting behaviour of $\mathrm{d}E/\mathrm{d}(\rho s)$ as $E\rightarrow 0$.

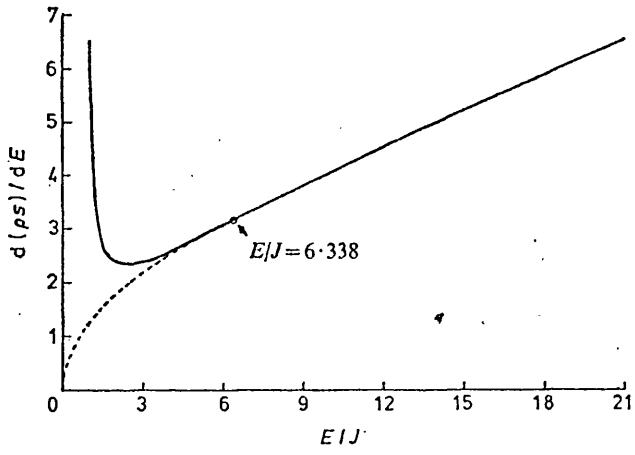

Figure 1. Plot of $\mathrm{d}(\rho s)/\mathrm{d}E$ (arbitrary units) vs E/J showing the behaviour of the Bethe expression (——) at low energies; note the steep rise as $E\rightarrow J/1{\cdot}166$. Also shown is the parabolic extrapolation (– – –) which is adopted in the present work for $E<6{\cdot}338J$.

It is somewhat simpler to select the appropriate J value for a particular element since it is approximately proportional to the atomic number Z. Although a number of equations have been proposed to take into account minor departures from a linear relationship (Duncumb *et al* 1969; Berger and Seltzer 1964, Zeller cited by Ruste and Gantois 1975), these are inconsistent one to another and we have chosen instead to adopt a single J/Z value of 0·0135 keV. This choice is based upon the following facts:

(1) An average of all the J/Z data reviewed by Ruste and Gantois is 0·0131 keV.
(2) The ionization potential of hydrogen is 0·0136 keV.
(3) 0·0135 keV is in close agreement with Duncumb *et al*'s J/Z data for high-atomic-number elements.
(4) The value accords with the theoretical predictions of Bloch (1933).

As a final point it was observed when carrying out Monte Carlo calculations that the mean depth of x-ray generation was insensitive to the precise values adopted for J/Z.

The first part of the Monte Carlo programme calculates the total electron path length ρs_m. This is given by

$$\rho s_m = -\int_0^{E_0} \frac{1}{\mathrm{d}E/\mathrm{d}(\rho s)}\,\mathrm{d}E$$

where E_0 is the incident electron energy and $\mathrm{d}E/\mathrm{d}(\rho s)$ is obtained from equation (1) for $E > 6{\cdot}338$ J and from equation (2) for $E \leq 6{\cdot}338$ J. The integration is performed numerically using Simpson's rule.

It was decided to subdivide the electron range into 100 equal steps of length $\Delta(\rho s)$, since 25 steps are known to be insufficient for accurate representation of electron trajectories in heavy targets such as gold (Bishop 1974). The energy of the electron at the lth step is then expressed as

$$E_l = E_{l-1} - \int_{(\rho s)_{l-1}}^{(\rho s)_l} \frac{\mathrm{d}E}{\mathrm{d}(\rho s)}\,\mathrm{d}(\rho s) \tag{3}$$

which is evaluated numerically using a fourth-order Runge Kutta method.

2.2. Angular scattering of electrons

In common with many other Monte Carlo methods, angular scattering of the electron within the specimen is deduced using the Rutherford scattering equation:

$$\cot(\beta/2) = 2P/b \tag{4}$$

where β is the scattering angle, P is the impact parameter (i.e. the closest distance of the approach in Å of the electron to the nucleus if no deflection of the electron was to occur), and $b = 0{\cdot}0144\,Z/E$ in Å when E is in keV. In writing b as $0{\cdot}0144\,Z/E$ we have followed Curgenven and Duncumb in ignoring nuclear screening by orbital electrons. It should be noted that the Rutherford equation is applicable to single scattering, whereas for the step lengths used in most Monte Carlo programmes a plural scattering treatment would be more appropriate.

The errors introduced—firstly by the use of a Rutherford single-scattering law, secondly by treating all angular scattering events as elastic and thirdly by ignoring the screening factor—are reduced by adjusting the expression for the impact parameter such that the Monte Carlo calculation gives the correct backscatter coefficient. Comparison with backscatter coefficients is chosen because these data are known accurately for a wide range of experimental conditions (Bishop 1966, Heinrich 1966, Darlington 1971, Drescher *et al* 1970).

2.3. Structure of the programme

A typical electron trajectory is shown in figure 2. At each step in the programme, E is calculated using equation (3) and a value for the impact parameter P is selected such that

$$P = P_0\,(YFL)^{1/2}$$

where YFL is a pseudo random number in the range 0–1. Electrons are assumed to arrive randomly over a circle radius P_0 and the square root allows for the greater probability of large P values. P_0, the maximum impact parameter, is selected such that the

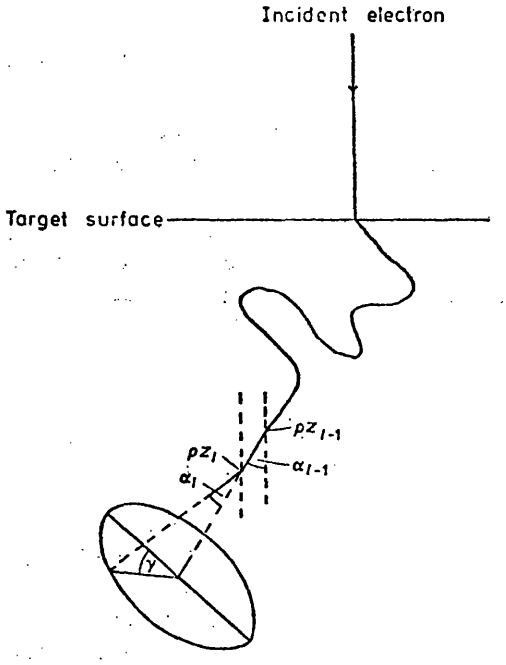

Figure 2. Typical electron trajectory in a solid.

Monte Carlo programme yields the correct backscatter coefficient. The values of P and E are then substituted in equation (4) to give β. The azimuthal scattering angle γ, determined using a second random number, is given by $\gamma=2\pi YFL$ since all azimuths are equally probable. It can be shown from the geometry of an electron trajectory that at the lth step the mass depth is given by

$$(\rho z)_l=(\rho z)_{l-1}+\Delta(\rho s)\cos\alpha_{l-1}$$

and the angle α the electron makes with the surface normal may be expressed by

$$\cos\alpha_l=\cos\alpha_{l-1}\cos\beta-\sin\alpha_{l-1}\sin\beta\cos\gamma.$$

Successive steps of the electron in the specimen are calculated until the electron has either lost all its energy (i.e. 100 steps have been calculated) or has escaped from the specimen (i.e. $\rho z<0$). The number of x-rays produced is then determined using the ionization cross-section $\psi(U)$. The expression of Worthington and Tomlin (1956)

$$\psi(U)=(\text{const}/U)\ln U$$

is adopted in the present work when $U\geq 1$, where U is the overvoltage E/E_c, E_c being the critical excitation potential of the x-ray line of interest. For overvoltages less than unity, ψ takes a value of zero.

Several thousand such trajectories are calculated in order that the average behaviour of electrons may be simulated. The backscattered electron energy distribution is obtained by recording the number of incident electrons which subsequently leave the specimen together with their residual energy. The number of x-rays produced at each depth in the specimen is summed for all trajectories and compared with the number of x-rays that would be generated in a thin film of thickness $\Delta(\rho s)$ by the incident electron beam. This then gives the normalized form of the distribution of x-rays with depth $\phi(\rho z)$ proposed by Castaing and Descamps (1955).

2.4. Adjustment using backscatter coefficients

The maximum impact parameter P_0 is a function of Z and E, and in order to utilize the Monte Carlo programme for a wide range of experimental situations it is necessary to choose *a priori* P_0 values which give the correct backscatter coefficient η. Curgenven and Duncumb's original work is not particularly informative here since only four values of P_0 are listed.†

The number of electrons backscattered must depend only on the value of cot $(\beta/2)$ determined at each of the 100 steps constituting the electron trajectory. Cot $(\beta/2)$ is related to both YFL and the energy of the electron by equation (4), which may be rewritten as

$$\cot(\beta/2) = 2P_0E(YFL)^{1/2}/0{\cdot}0144\,Z \tag{5}$$

and we may define $\cot(\beta_0/2) = 2P_0E_0/0{\cdot}0144Z$ where β_0 is the minimum scattering angle for the incident electron with energy E_0. Hence we obtain

$$\cot(\beta/2) = \cot(\beta_0/2)\,(E/E_0)\,(YFL)^{1/2}.$$

Now, since firstly the variation of E/E_0 along the electron trajectory is substantially independent of Z (being only slightly dependent through the $\ln(1{\cdot}166E/J)$ term of Bethe's equation) and, secondly, YFL averages to a constant value when a large number of trajectories are considered, it follows that η must depend only upon cot $(\beta_0/2)$. In order to verify this, values of P_0 for a wide range of Z and E were selected by trial and error such that the backscatter coefficients calculated by the Monte Carlo programme were close to the experimental values of Bishop (1966). Values of tan $\beta_0/2$ were determined from P_0, and these are plotted against calculated backscatter coefficients in figure 3 which shows them to be well represented by a single curve irrespective of electron energy,

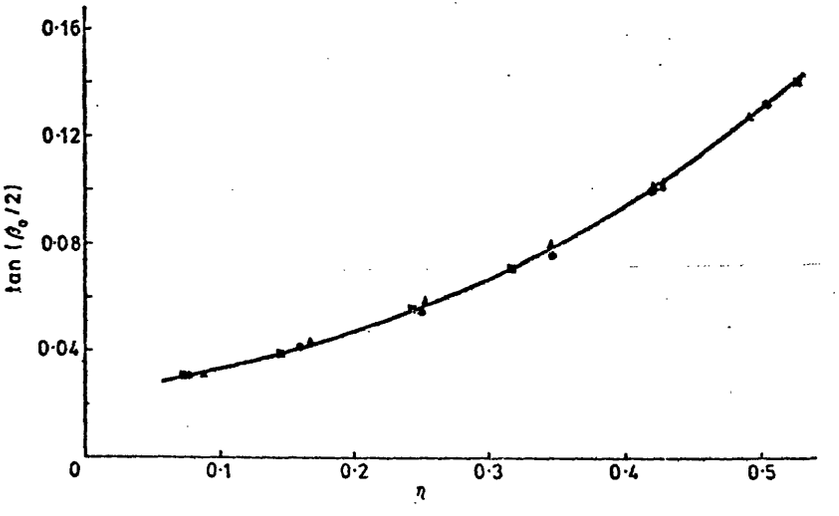

Figure 3. Plot of tan $(\beta_0/2)$ vs η for incident electron energies of (▲) 5 kV, (●) 10 kV and (■) 30 kV. Note that all the data are well represented by a single curve irrespective of electron energy.

† P Duncumb (private communication) has suggested that P_0 may be approximately expressed as $P_0 = (0{\cdot}82\,Z^{0{\cdot}4})/E$. This equation does not relate P_0 specifically to η and is hence considered less fundamental than the corresponding expression suggested in this paper.

any small departures being well within the statistics of the Monte Carlo simulation. Least-squares analysis of these data gave

$$\tan(\beta_0/2) = 0{\cdot}02209 + 0{\cdot}10716\eta + 0{\cdot}03009\eta^2 + 0{\cdot}37555\eta^3.$$

This expression was incorporated into the Monte Carlo programme, thus eliminating P_0 and leaving as input requirements only readily available parameters η, E_0, E_c, Z, A and the number of electron trajectories N. Output from the programme includes values for the calculated backscatter coefficient, the backscattered electron energy distribution, the x-ray distribution with depth and the mean mass depth of x-ray generation. The reliability of the regression may be checked after each Monte Carlo calculation by comparing the input parameter η with that calculated in the programme. In no case studied to date has the difference between these values been significant.

3. Results

3.1. Energy distribution of backscattered electrons

Backscattered electron energy distributions have been calculated for a range of targets of differing atomic number. Agreement with experimental results is good as may be seen from, for example, figure 4 in which Monte Carlo calculations for Al, Cu and Au

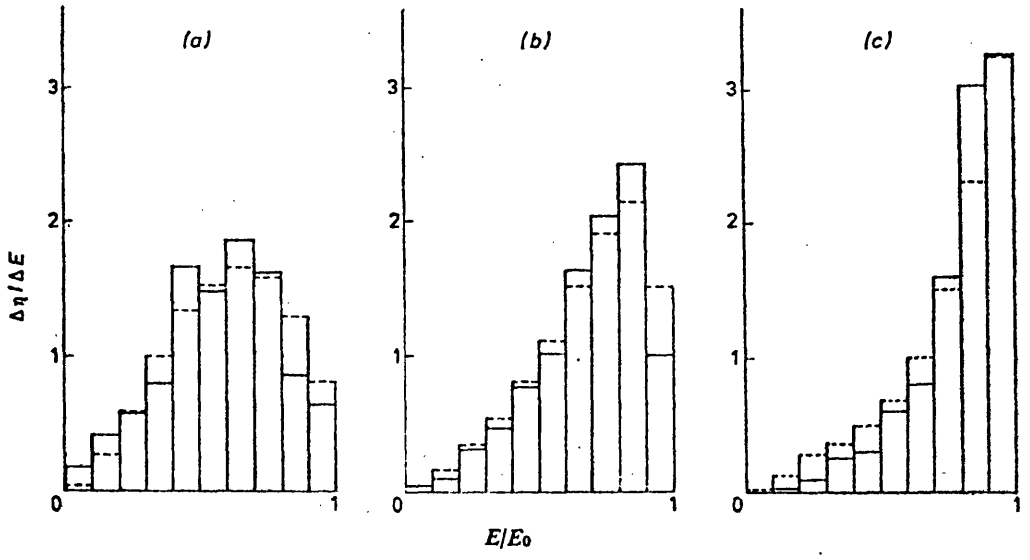

Figure 4. Backscattered electron energy distributions at 30 kV for (*a*) aluminium, (*b*) copper, (*c*) gold: — Monte Carlo results; - - - experimental results of Darlington (1971).

at 30 kV are compared with the data of Darlington (1971). It may be inferred that since the electron energy distribution at the surface is predicted correctly, the electron energy distribution predicted at all depths in the target is also likely to be satisfactory.

3.2. Distribution of x-rays with depth

Figure 5 illustrates experimental $\phi(\rho z)$ data obtained, using a tracer technique, for aluminium at 10, 20 and 29 kV (Castaing and Henoc 1966) together with results from the Monte Carlo programme. Whilst the Monte Carlo results are satisfactory at 20 and

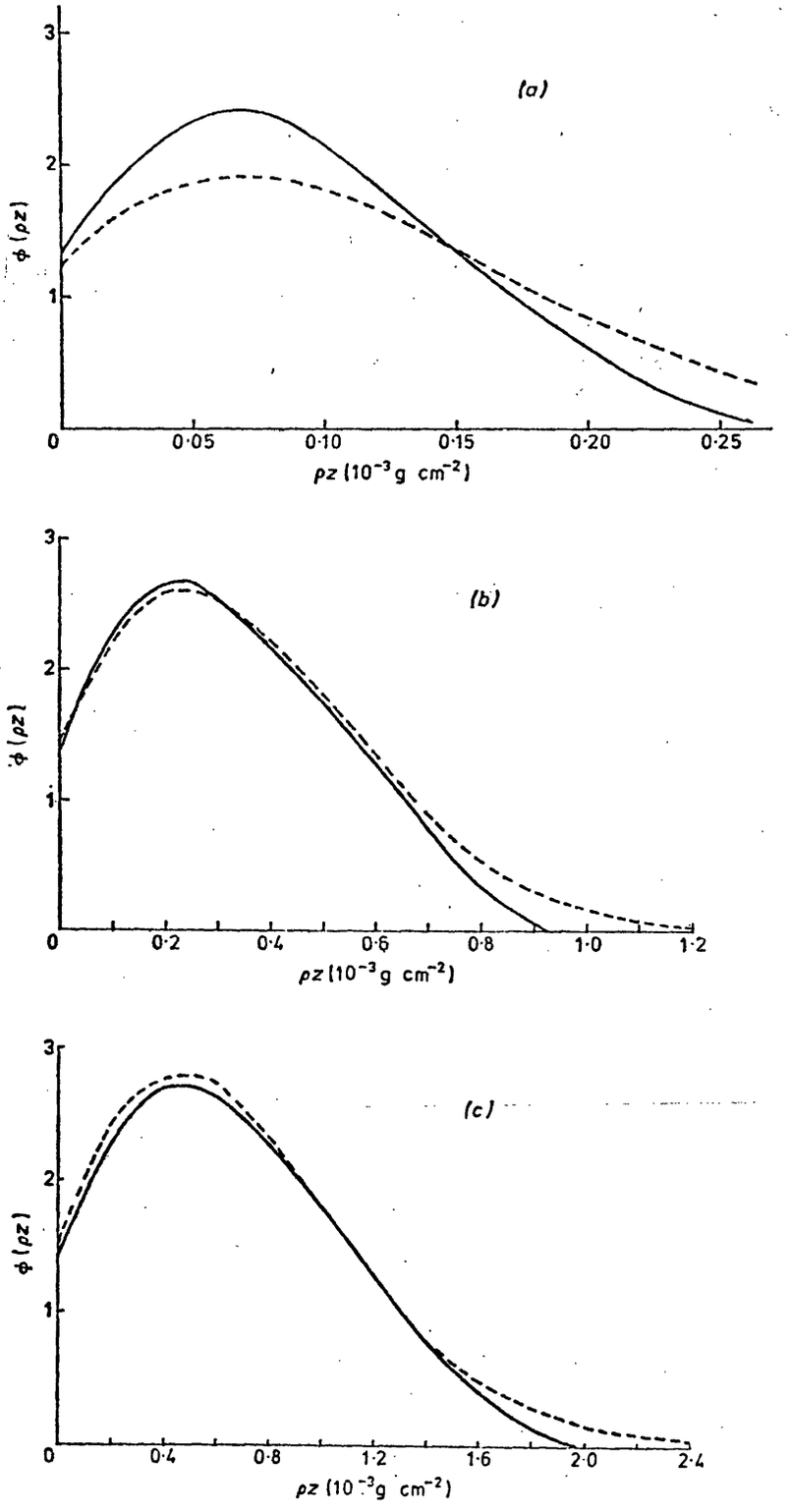

Figure 5. $\phi(\rho z)$ distributions for aluminium at (*a*) 10 kV, (*b*) 20 kV (*c*) 29 kV: —— Monte Carlo results; – – – experimental results of Castaing and Henoc (1966).

29 kV there is some discrepancy between calculated and experimental data at 10 kV. However, at the lower kilovoltage the thickness of tracer element may no longer be regarded as insignificant compared with the mean depth of x-ray excitation and some flattening of the experimental distribution is to be expected.

A $\phi(\rho z)$ curve calculated for copper at 30 kV is illustrated in figure 6. In this case it has been compared with the experimental results of Schmitz *et al* (1969) as well with those of Castaing and Descamps (1955) since it is difficult to decide which is the more reliable. The Monte Carlo data agrees well with the former set of measurements.

A calculated $\phi(\rho z)$ curve for lead at 29 kV is given in figure 7, but in this case there

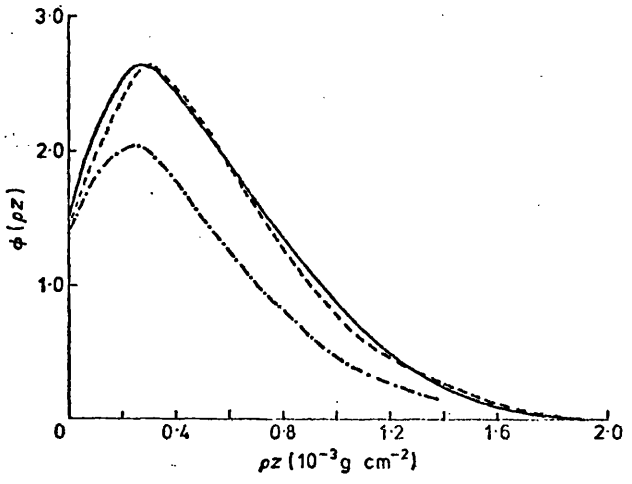

Figure 6. $\phi(\rho z)$ distributions for copper: —— Monte Carlo results at 30 kV; – – – experimental data of Schmitz *et al* (1969) at 30 kV; —·— experimental data of Castaing and Descamps (1955) at 29 kV.

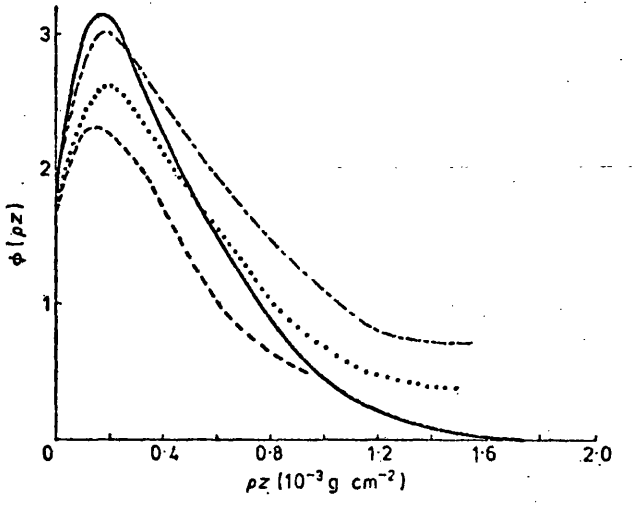

Figure 7. $\phi(\rho z)$ distributions for lead and gold. Monte Carlo results for (——) lead at 29 kV; experimental resuls of Vignes and Dez (1968) for (. . .) lead at 29 kV and for (— – —) lead at 33 kV; experimental results of Castaing and Descamps (1955) for (– – –) gold at 29 kV.

appears to be even greater difficulty in choosing experimental data for assessment purposes. To illustrate this point results obtained by Vignes and Dez (1968) at 29 kV and at 33 kV have been included but, since the difference between the two curves is much greater than expected from the relatively small change in voltage, it is difficult to decide which, if either of them, is correct. Castaing and Descamp's measurements on gold at 29 kV are also included in figure 7, which further underlines the problem of obtaining reliable experimental $\phi(\rho z)$ data on heavy elements. Such data will, in any case, be somewhat distorted due to x-ray fluorescence by the continuum; this results in a long exponential tail to the experimental $\phi(\rho z)$ distribution.

In view of the limited agreement between existing sets of experimental $\phi(\rho z)$ data it was concluded that there was little justification in attempting to refine the present treatment further by including more sophisticated models for elastic scattering (e.g. Bolon and Lifshin 1973) and inelastic scattering (e.g. Henoc and Maurice 1975). The present treatment is capable of predicting $\phi(\rho z)$ with an accuracy at least comparable with existing experimental determinations and should therefore be capable of producing x-ray depth distributions for a range of situations where experimental data either has not been or cannot be obtained. This versatility is exploited in the following section in a discussion of factors which affect the mean depth of x-ray generation.

3.3. Mean depth of x-ray generation

The fraction $f(\chi)$ of generated x-rays, emitted into the solid angle subtended by the spectrometer, which are not absorbed by the specimen is given by

$$f(\chi)=\frac{\int_0^\infty \phi(\rho z)\exp(-\chi\rho z)\,\mathrm{d}(\rho z)}{\int_0^\infty \phi(\rho z)\,\mathrm{d}(\rho z)}.$$

$\chi=\mu/\rho$ cosec θ, where μ/ρ is the mass absorption coefficient of the target and θ is the x-ray take-off angle. Expanding the exponential term in this equation gives

$$f(\chi)=\frac{\int_0^\infty \phi(\rho z)\,\mathrm{d}(\rho z)}{\int_0^\infty \phi(\rho z)\,\mathrm{d}(\rho z)}-\frac{\chi\int_0^\infty \phi(\rho z)\,(\rho z)\,\mathrm{d}(\rho z)}{\int_0^\infty \phi(\rho z)\,\mathrm{d}(\rho z)}\quad\cdots\quad\frac{(-\chi)^n\int_0^\infty \phi(\rho z)\,(\rho z)^n\,\mathrm{d}(\rho z)}{n!\int_0^\infty \phi(\rho z)\,\mathrm{d}(\rho z)}.$$

The high-order terms are important when absorption is large (i.e. when $f(\chi)<0{\cdot}5$), but when absorption is small

$$f(\chi)=1-\chi\frac{\int_0^\infty \phi(\rho z)\,(\rho z)\,\mathrm{d}(\rho z)}{\int_0^\infty \phi(\rho z)\,\mathrm{d}(\rho z)}.$$

It should be noted that the ratio of the integrals in this equation is, by definition, the mean depth of x-ray generation $\overline{\rho z}$. Thus the mean depth is an important parameter which controls to a very large extent the magnitude of the absorption correction and is included explicitly or implicitly in all absorption correction formulae. In this section, an empirical expression for the mean depth is deduced which is an accurate representation of the Monte Carlo data in giving the correct energy, atomic number and overvoltage dependence.

Clearly the mean depth will depend upon: (*a*) the total distance ρs_m travelled by the electron; (*b*) the degree to which electrons are scattered along their trajectories; and (*c*) the variation of ionization cross-section along the path of the electron as it progressively loses energy. Hence for constant overvoltage U_0, the ratio of the mean depth of x-ray generation $\overline{\rho z}$ to the total path length ρs_m should be a function of the degree of scattering only, i.e. the ratio will be a function of the backscatter coefficient η. This was substantiated by carrying out a series of Monte Carlo calculations for the elements C, Al, Ti, Cu, Ag and Au at electron probe voltages of 5, 10, 30 kV. The mean depths were deduced at overvoltages of 1·5, 2, 3, 10 and 100. Results are plotted in figure 8 as $\overline{\rho z}/\rho s_m$ vs η. The diagram demonstrates that $\overline{\rho z}/\rho s_m$ at constant overvoltage is a continuous function of η and is independent of the incident electron energy.

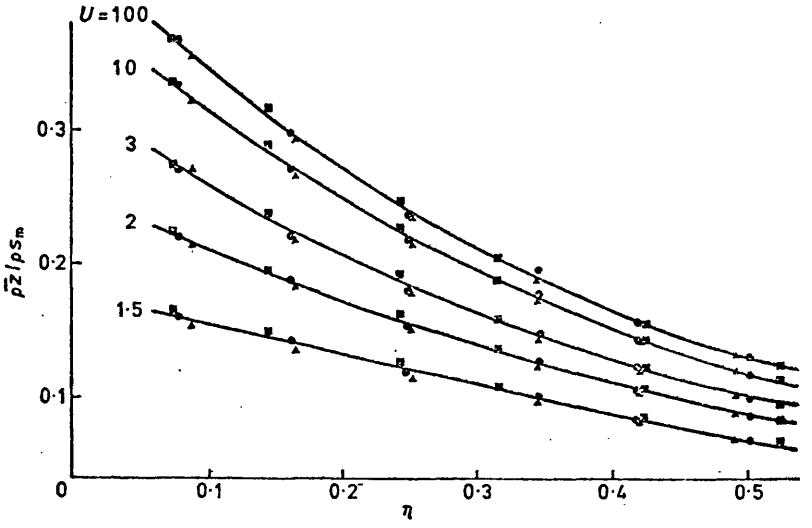

Figure 8. Plot of $\overline{\rho z}/\rho s_m$ vs η at $U_0 = 1{\cdot}5$, 2, 3, 10 and 100. Results obtained at incident electron energies of (▲) 5 kV, (⊖) 10 kV and (⊠) 30 kV are shown. Note that at constant overvoltage the $\overline{\rho z}/\rho s_m$ is almost independent of electron energy.

It can be shown (see Appendix) that the mean depth is expected to be a function of overvoltage with the form

$$\frac{\overline{\rho z}}{\rho s_m} = \left(\frac{\overline{\rho z}}{\rho s_m}\right)_{U_0 \to \infty} \frac{\ln U_0}{\ln U_0 + q} \tag{6}$$

where q is a constant for a particular element. Hence a plot of $\rho s_m/\overline{\rho z}$ vs $1/\ln U_0$ should give a straight line of slope $q(\rho s_m/\overline{\rho z})_{U_0 \to \infty}$ and intercept $(\rho s_m/\overline{\rho z})_{U_0 \to \infty}$. Such a plot is illustrated in figure 9 for an incident electron energy of 30 kV. The relationship (equation 6) has been found to be quite general and represents accurately the Monte Carlo data over a wide range of overvoltages ($1{\cdot}5 < U_0 < 100$) and also incident electron energies (5 kV $< E_0 <$ 30 kV).

The constant q was found to be almost independent of energy but was a function of η:

$$q = 0{\cdot}70256 - 1{\cdot}09865\,\eta + 1{\cdot}00460\,\eta^2. \tag{7}$$

The values of $(\overline{\rho z}/\rho s_m)_{U_0 \to \infty}$ deduced from equation (6) are independent of energy and were also found to be a function of η only, which is to be expected from the form of the

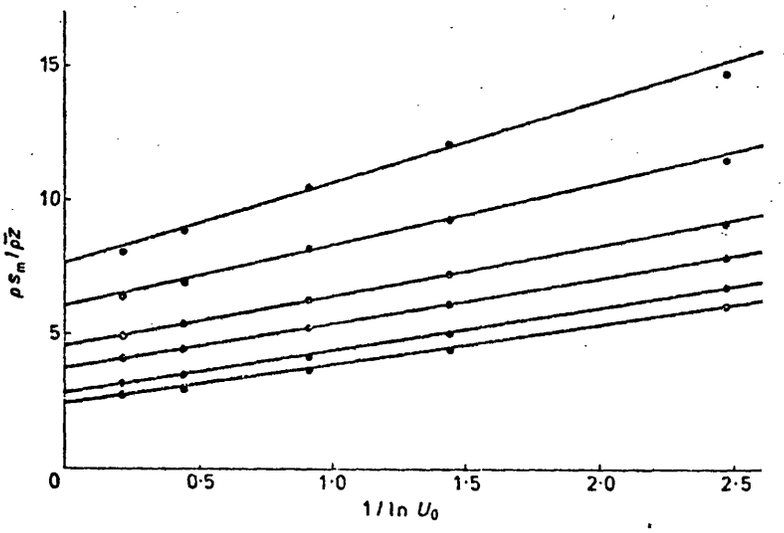

Figure 9. Plot of $\rho s_m/\bar{\rho z}$ vs $1/\ln U_0$ at 30 kV for the elements C, Al, Ti, Cu, Ag and Au.

results illustrated in figure 8. Using a least-squares analysis the following relationship was deduced:

$$\left(\frac{\bar{\rho z}}{\rho s_m}\right)_{U_0 \to \infty} = 0{\cdot}49269 - 1{\cdot}09870\,\eta + 0{\cdot}78557\,\eta^2. \tag{8}$$

Substituting equation (7) and (8) in equation (6) leads to an analytical expression for the mean depth of x-ray generation given by

$$\bar{\rho z} = \frac{\rho s_m (0{\cdot}49269 - 1{\cdot}09870\,\eta + 0{\cdot}78557\,\eta^2) \ln U_0}{(0{\cdot}70256 - 1{\cdot}09865\,\eta + 1{\cdot}00460\,\eta^2) + \ln U_0}.$$

The total path length of the electron ρs_m may be easily evaluated by numerical integration of equations (1) and (2) (see §2.1).

3.4. The Philibert model

The only other available equation for the mean depth was that derived from the Philibert (1963) model by Bishop (1974):

$$\bar{\rho z} = \frac{(1+2h)}{(1+h)} E_0^n \frac{(1-1/U_0^m)}{c}. \tag{9}$$

The power n in the energy-dependent term is a constant and different workers have proposed values in the range 1·5–2. The power m in the overvoltage-dependent term conventionally takes the same value as n. c is another constant, and again various values have been proposed for this, ranging from 2×10^5 to 10^6. The term $(1+2h)/(1+h)$ in equation (9) is meant to take into account the effect of the target material on electron scattering, and h is normally expressed as $1{\cdot}2A/Z^2$.

To assess the validity of the energy-dependent term, equation (9) may be rewritten

$$\lg \bar{\rho z} = \lg\left(\frac{1+2h}{1+h}\,\frac{(1-1/U_0^m)}{c}\right) + n \lg E_0.$$

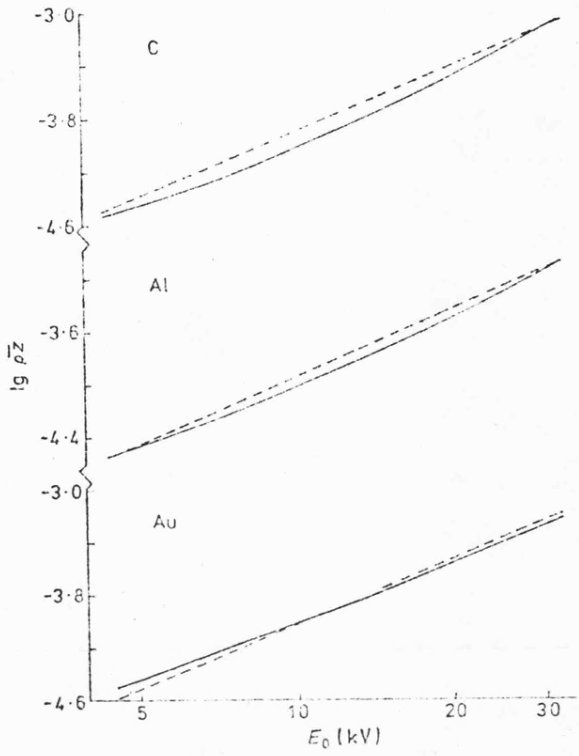

Figure 10. Plot of log ρz vs E_0 (log scale) for C, Al and Au for $U_0=10$: —— Monte Carlo results; – – – results calculated using Philibert's absorption model.

Values calculated for this equation are plotted in figure 10 as lg $\bar{\rho z}$ vs lg E_0 for the elements C, Al and Au ($U_0=10$); Heinrich's (1967) constants ($n=1{\cdot}65$ and $c=4{\cdot}5\times10^5$) were adopted. Also included in figure 10 are data deduced using the Monte Carlo model, and these show that n is not constant with Z or with E_0; for example, n varies for carbon from $\sim1{\cdot}5$ at 10 kV to ~2 at 30 kV. Hence the different values which have been suggested for n in the Philibert expression of 1·5 (Duncumb and Shields 1966), 1·65 (Heinrich 1967, Duncumb *et al* 1969), 1·86 (Love *et al* 1975) and 1·77 (Love *et al* 1976) can be rationalized since the different groups of workers have based their optimum values of n upon different sets of experimental data. Clearly no single value of n is adequate for all conditions encountered in microanalysis.

The overvoltage dependence of the mean depth in both the Philibert model and the Monte Carlo model is compared in figure 11, where $\ln U_0/(\ln U_0+q)$ is plotted against $(1-1/U_0^{1{\cdot}65})$; $m=1{\cdot}65$ has been chosen since this is the value most commonly used in the Philibert model. The curves for C, Al and Au were obtained by putting $q=0{\cdot}623$, 0·537 and 0·381 respectively. It may be seen from these results that there is an approximately linear relationship over the range of overvoltages used in practical microanalysis. Furthermore, these data indicate that the overvoltage-dependent parameters in equations (6) and (9) are related, since

$$f(Z).\left(1-\frac{1}{U_0^{1{\cdot}65}}\right)\approx\frac{\ln U_0}{\ln U_0+q}$$

where $f(Z)$ is a function of atomic number. It may be concluded therefore that, since $f(Z)$ may be included in other terms in equation (9) such as $(1+2)/(1+h)$ and c, the

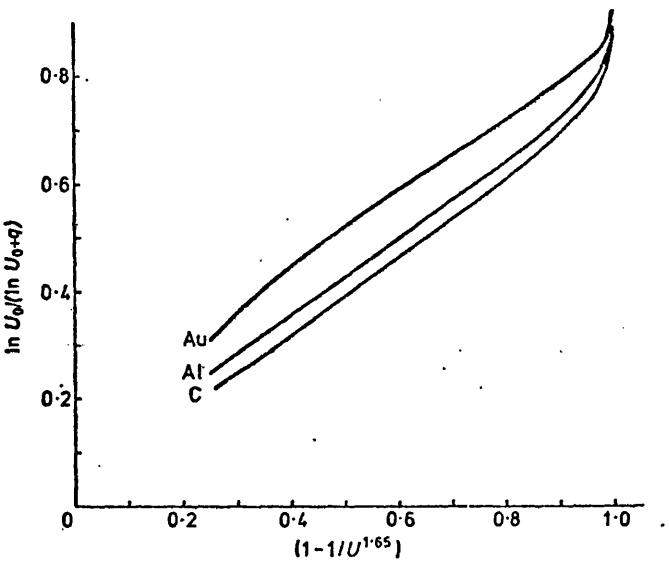

Figure 11. Plot of ln $U_0/(\ln U_0+q)$ vs $(1-1/U_0^{1\cdot65})$ for C, Al and Au for $1\cdot5 < U_0 < 100$. Note the approximate linearity of the curves over a wide range of overvoltages.

Philibert expression may approximately represent the overvoltage dependence over the range encountered in normal microanalysis work.

Before concluding it was decided to examine the effect of using different values of m in the overvoltage dependent term. Bishop (1974) has suggested on the basis of the Thompson–Whiddington energy loss expression that a power of 2 would be more appropriate here. However our findings show that this is less satisfactory than the use of $m=1\cdot65$; in fact $m=1\cdot5$ might be better than either.

4. Conclusions

A Monte Carlo treatment based on Curgenven and Duncumb's method has been developed which is simple to use since the trial and error approach for optimizing electron scattering parameters has been eliminated. The new model works well as evidenced by the close agreement between calculated data and experimental information on backscattered electron energy distributions. The model is used to generate $\phi(\rho z)$ curves for a wide range of experimental conditions as experienced in practical microanalysis and agreement with available experimental $\phi(\rho z)$ curves is satisfactory.

From the Monte Carlo data, an analysis has been carried out of the way in which the mean depth of x-ray production varies with electron accelerating voltage, overvoltage and atomic number of the target material; this enabled an analytical expression for the mean depth to be deduced. It has also been shown that the mean depth predicted by the Philibert model is wrong since it does not give the correct form of electron energy dependence, which also implies that the Philibert absorption correction used in microanalysis is inappropriate.

Future work will be concerned with the use of the new expression for mean depth in a practical microanalysis correction procedure. A new atomic number correction will also be proposed based upon data produced by the present Monte Carlo approach.

Acknowledgments

Thanks are due to Dr P Duncumb for making available a copy of *Tube Investments Report 303* describing Curgenven and Duncumb's Monte Carlo treatment and for his helpful comments on the present paper. The cooperation of the University Computer Unit under the direction of Dr A W Nicol is also acknowledged.

Appendix. Variation of mean depth with overvoltage

A form for the dependence of mean depth on overvoltage may be derived by considering the variation of ionization cross-section along the trajectory. The ionization cross-section may be expressed as (Worthington and Tomlin 1956)

$$\psi(U)=\frac{\text{const}}{U}\ln U$$

and thus the mean overvoltage $\bar{U}$ for a complete trajectory is by definition

$$\bar{U}=\frac{\int_1^{U_0}\psi(U)\,U\,\mathrm{d}U}{\int_1^{U_0}\psi(U)\,\mathrm{d}U}.$$

Hence

$$\frac{\bar{U}}{U_0}=\frac{2}{U_0}\left(\frac{U_0\ln U_0-(U_0-1)}{(\ln U_0)^2}\right).$$

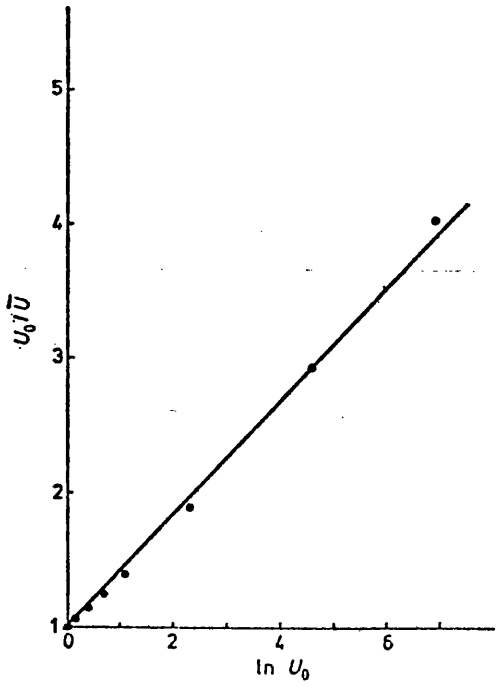

Figure 12. Plot of U_0/U vs ln U_0 for $1 < U_0 < 1000$.

This equation was evaluated over the range $1 < U_0 < 1000$, and it was found that $U_0/\bar{U}$ was almost a linear function of $\ln U_0$ (see figure 12). Thus $\bar{U}/U_0$ may be represented by

$$\frac{\bar{U}}{U_0} = \frac{1}{1+g \ln U_0}$$

where g is a constant. Now assuming that the electron loses energy according to a simple power law (Dekker 1958, Whiddington 1914) we may write

$$\left(\frac{E}{E_0}\right)^p = 1 - \frac{\rho s}{\rho s_m}$$

and substituting $U = E/E_c$ gives

$$\frac{\rho s}{\rho s_m} = 1 - \left(\frac{U}{U_0}\right)^p.$$

Hence

$$\frac{\rho s}{\rho s_m} = 1 - \left(\frac{1}{1+g \ln U_0}\right)^p$$

$$\simeq 1 - \frac{1}{1+gp \ln U_0}$$

$$= \frac{gp \ln U_0}{1+gp \ln U_0}$$

$$= \frac{\ln U_0}{\ln U_0 + 1/gp}.$$

This expression gives the fraction of the trajectory traversed to reach the mean overvoltage. We would expect $\overline{\rho z}$ to be some fraction t of ρs, i.e.

$$\overline{\rho z} = t \rho s.$$

Thus

$$\frac{\overline{\rho z}}{\rho s_m} = t \frac{\ln U_0}{\ln U_0 + 1/gp}$$

and as $U_0 \to \infty$

$$\left(\frac{\overline{\rho z}}{\rho s_m}\right)_{U_0 \to \infty} = t.$$

Therefore

$$\frac{\overline{\rho z}}{\rho s_m} = \left(\frac{\overline{\rho z}}{\rho s_m}\right)_{U_0 \to \alpha} \frac{\ln U_0}{\ln U_0 + q}$$

where the constant $1/gp$ has been replaced by q giving the form used in the text.

References

Berger M J and Seltzer S M 1964 *Nucl. Ser. Rep. No.* 39, *NAS-NRC Pub. No.* 1133 (Washington DC: Nat. Acad. Sci.) pp 205–68

Bethe H A 1930 *Ann. Phys., Lpz.* 5 325–400

Bishop H E 1965 *PhD Thesis*, University of Cambridge
—— 1966 *X-ray Optics and Microanalysis* ed. R Castaing, P Deschamps and J Philibert (Paris: Hermann) pp 153–8
Bishop H E 1974 *J. Phys. D: Appl. Phys.* 7 2009–20
Bloch F 1933 *Z. Phys.* 81 363–78
Bolon R B and Lifshin E 1973 *Scanning Electron Microscopy*, 1973 (Chicago: IITRI) pp 286–92
Brown D B 1968 *Quantitative Electron Probe Microanalysis: NBS Spec. Publ.* 298 ed. K F J Heinrich pp 63–80
Brown D B, Wittry D B and Kyser D F 1969 *J. Appl. Phys.* 40 1627–36
Castaing R and Descamps J 1955 *J. Phys. Radium* 16 304–17
Castaing R and Henoc J 1966 *X-ray Optics and Microanalysis* eds R Castaing, P Deschamps and J Philibert (Paris: Hermann) pp 120–6
Cosslett V E 1966 *X-ray Optics and Microanalysis* eds R Castaing, P Deschamps and J Philibert (Paris: Hermann) pp 85–96
Curgenven L and Duncumb P 1971 *Tube Investments Res: Rep. No.* 303
Darlington E H 1971 *PhD Thesis*, University of Cambridge
Dekker A 1958 *Solid St. Phys.* 6 251–311
Drescher H, Reimer L and Seidel H 1970 *Z. Angew. Phys.* 29 331–6
Duncumb P and Shields P K 1966 *The Electron Microprobe* eds T D McKinley, K F J Heinrich and D B Wittry (New York: John Wiley) pp 284–95
Duncumb P, Shields-Mason P K and da Casa C 1969 *X-ray Optics and Microanalysis* eds G Mollenstedt and K H Gaukler (Berlin: Springer-Verlag) pp 146–50
Green M 1962 *PhD Thesis*, University of Cambridge
Heinrich K F J 1966 *X-ray Optics and Microanalysis* eds R Castaing, P Deschamps and J Philibert (Paris: Hermann) pp 159–67
Heinrich K F J 1967 *Trans. 2nd Nat. Conf. on Electron Probe Microanalysis, Boston, USA* paper no. 7
Henoc J and Maurice F 1975 *J. Phys. D: Appl. Phys.* 8 1542–51
Love, G, Cox M G C and Scott V D 1975 *J. Phys. D: Appl. Phys.* 8 1686–7
—— 1976 *J. Phys. D: Appl. Phys.* 9 7–13
Newbury D E, Yakowitz H and Myklebust R L 1973 *Appl. Phys. Lett.* 23 488–90
Philibert J 1963 *X-ray Optics and X-ray Microanalysis* eds H H Pattee, V E Cosslett and A Enström (New York: Academic Press) pp 379–92
Rao-Sahib T S and Wittry D B 1974 *J. Appl. Phys.* 45 5060–8
Ruste J and Gantois M 1975 *J. Phys. D: Appl. Phys.* 8 872–90
Schmitz U, Ryder P L and Pitsch W 1969 *X-ray Optics and Microanalysis* eds G Mollenstedt and K H Gaukler (Berlin: Springer-Verlag) pp 104–13
Shimizu R, Murata K and Shinoda G 1966 *X-ray Optics and Microanalysis* eds R Castaing, P Deschamps and J Philibert (Paris: Hermann) pp 127–38
Statham P J 1975 *PhD Thesis*, University of Cambridge
Vignes A and Dez G 1968 *J. Phys. D: Appl. Phys.* 1 1309–22
Whiddington R 1914 *Proc. R. Soc.* A 89 554–60
Worthington C R and Tomlin S G 1956 *Proc. Phys. Soc.* A 69 401–12

7.11 Foil Thickness Measurement in Transmission Electron Microscopy.

G. Love, M.G.C. Cox and V.D. Scott, 1977b, Developments in Electron Microscopy and Analysis 1977, ed. D.L. Misell, (Bristol : Inst. of Phys.), Inst. Phys. Conf. Ser. No.36, p.347.

Inst. Phys. Conf. Ser. No. 36 © 1977: Chapter 9

FOIL THICKNESS MEASUREMENT IN TRANSMISSION ELECTRON MICROSCOPY

G Love, M G C Cox and V D Scott

School of Materials Science, University of Bath, Bath, Avon.

1. Introduction

In fine structure studies involving transmission electron microscopy of thin foils it is generally difficult to convert measurements of defect populations or of fine precipitates into quantitative data. The problem in obtaining accurate results is essentially one of measuring the thickness of foil being analysed. Earlier methods, based upon either analysis of extinction contours or of known crystallographic features such as slip traces, cannot be generally applied since:

a. extinction contours are measurable only on those edges of foil which have a sharply tapering section; moreover imaging conditions must be adjusted so that the deviation parameter, s, is zero or large errors may arise (Hirsch, Howie, Nicholson, Pashley and Whelan 1965).

b. known crystallographic features are unlikely to be present in the region of foil requiring analysis.

For quantitative microstructural studies we have been examining several techniques for foil thickness measurements which are feasible when using a transmission electron microscope fitted with scanning transmission (STEM), and/or X-ray analysis (EDS) attachments. The present paper discusses our exploratory work on the assessment and application of quantitative techniques in electron microscopy.

2. Quantitative Techniques

Techniques for determining foil thickness may be divided into 'absolute' methods such as contamination spot (Lorimer and Cliff, 1976) and convergent beam diffraction (Kelly, Jostsons, Blake and Napier, 1975), and those requiring calibration in which X-ray emission from the foil is used (Miller and Scott, 1977).

The contamination spot method requires that the electron beam is focused onto the foil specimen to form a small contamination spot on its upper and lower surfaces. After tilting the foil through a known angle the separation of the spots is measured and the foil thickness calculated using the tilt angle.

The convergent beam technique also requires a focused beam of electrons, convergence of the beam being controlled such that divergent cones of diffracted electrons are imaged; a two beam diffraction condition is required which usually involves tilting the foil through a small angle (1 or 2°). The distance between minima in the intensity profile of the diffraction spot is then measured and the foil thickness determined using $(s^2 + \frac{1}{\varepsilon g^2})\, t^2 = n^2$, where s is the deviation parameter of the minima, εg is the extinction distance for the operating reflection and n is an integer. Since several values of s may be measured corresponding to different values of n it is not essential to know εg in order to establish the foil thickness.

X-ray methods involve measuring the intensity of either characteristic or continuum X-rays generated in specimens by electron bombardment. For electron transparent foils the X-ray intensity is directly proportional to its thickness, (Jacobs and Baborovska 1972), which may then be estimated from a calibration curve determined by similar X-ray intensity measurements on foils of known thickness.

3. Application of the Techniques

Each of the above methods have been applied to thin foils of an Al-Mg-Zn alloy containing a uniform dispersion of fine precipitates. Micrographs are taken of the areas from which the thickness measurement have been made. The accuracy of the various thickness determinations may then be assessed by plotting N, the number of precipitates visible in unit area of foil, versus foil thickness t.

When using the contamination spot method, although linear relationships between N and t were found, extrapolation to N = 0 indicated that on occasions t was being overestimated by several hundred Å. Part of the reason for the discrepancy is due to the presence of an amorphous oxide film together with a layer of contamination on the surface of the foil. The magnitude of this effect is different from one foil to another but, provided the foil is examined in the microscope immediately after being electro-chemically thinned, the intercept value is usually < 150 Å. For improved experimental reproducibility cleaner foils are needed and ion thinning techniques may be advantageous here. The standard deviation of individual points from the straight line of N versus t is better than 10% and for most cases studied nearer to 5%. The absolute accuracy of the technique is however more difficult to establish due to the presence of extraneous surface films.

A plot of N versus characteristic X-ray intensity gave a linear relationship, with the straight line passing close to the origin. The small X-ray count rate still obtained for N = 0 can probably be attributed to the surface oxide film. Relative accuracy of the method was found to be good (∿ 5%) over a foil thickness range ∿ 1,000 Å - 3,000 Å (determined using contamination spot technique) much of the residual error being attributed to the statistics of precipitate counting.

Interpretation of the continuum X-radiation measurements is difficult since contamination build-up at the point of impact of the probe on the specimen produces a time-dependent contribution to the X-ray intensity. Hence meaningful results are possible only if contamination is kept to a minimum, e.g. by scanning the electron beam over a fairly wide area whilst making the X-ray measurements. A further complicating factor is the contribution to the continuum produced by stray scattering of electrons and X-rays within the specimen chamber, although this may be reduced by well collimating the detector and avoiding the use of thin film condenser apertures.

The convergent beam technique is likely to be the most accurate way of measuring foil thickness but to date we have carried out only a limited number of measurements using this method. When plotting N versus foil thickness a straight line is obtained which, within experimental scatter, passed through the origin. This is to be expected

since the technique will measure the metal foil thickness but not any amorphous surface oxide or contamination which may be present. However, the gradient of this line is substantially different from that obtained from the corresponding plot of N versus thickness calculated from contamination spot measurments. Furthermore, values of the extinction distance calculated using the convergent beam diffraction technique are found to be markedly different from those for aluminium quoted in the literature. Both of these points require further investigation.

4. Conclusion

Many of the apparent inconsistencies in foil thickness determinations made by the four techniques studied here may be explained by the fact that each method measures something different. The contamination spot technique determines the total foil thickness including any surface film, the convergent beam diffraction method establishes the metal thickness, while the characteristic X-ray method records the amount of a particular element in an irradiated volume. In the table the various techniques are compared together with their potential areas of application. It should be noted that providing the foil is homogeneous the characteristic X-ray technique offers a reliable and quick method for measuring relative changes in foil thickness. Conversion to absolute thicknesses necessitates, however, calibrating the X-ray intensity measurement as a function of foil thickness using, for example, either the convergent beam diffraction or contamination spot technique. Further studies concerning absolute thickness measurements will involve

a. the influence of strain and defects in the crystal lattice upon the foil thickness determined using the convergent beam diffraction technique and

b. an analysis of the profile of contamination spots in order to determine spot separation more accurately.

5. Acknowledgements

The authors thank JEOL (UK) Ltd for use of their JEM 100C analytical electron microscope and Mr K Ibe for his assistance.

6. References

Hirsch P B, Howie A, Nicholson R B, Pashley D W, and Whelan M J, 1965 Electron Microscopy of Thin Crystals, (London: Butterworths).

Jacobs M H and Baborovska J, 1972, Electron Microscopy 1972 (London: Inst of Phys.) 136.

Kelly P M, Jostons A, Blake R G and Napier J G, 1975 Phys Stat Sol 31, 771.

Lorimer G W, Cliff G, 1976 Development in Electron Microscopy and Analysis ed. J A Venebles (London: Academic Press).

Miller W and Scott V D, 1977, to be published.

TABLE

Method	Contamination Spot	Convergent Beam	Characteristic x-ray	Continuum x-ray
Type of Measurement	Absolute	Absolute	Relative	Relative
Thickness Measured	Total thickness	Crystalline thickness	Total amount of analysed element	Complex
Size of analysed region	~500Å - may be limited by pre-existing films.	>1000Å in practice. No theoretical restriction.	No restriction	Limited by contamination build-up
Accuracy	Systematic errors associated with finite spot size.	Good for pure foils but may be influenced by presence of defects.	Good for relative measurements but absolute accuracy dependent upon calibration.	Good for relative measurement but absolute accuracy dependent upon calibration.
Effect of thickness and atomic number.	Becomes difficult for thick films and for foils of high atomic number.	Little effect	Little effect	May be affected by diffuse scattering within specimen chamber.
Speed of measurement	Fast ~10 sec.	Slow ~ several minutes.	Fast	Fast
Speed of interpretation	Fast but measurement must be made on photographic plates.	Slow, cumbersome graphical techniques required - measurements from photographic plates	Virtually instantaneous once calibration curve has been constructed.	Virtually instantaneous once calibration curve has been constructed.
Comments	Easily applied to all types of specimen	Possibility of measuring thickness in layered structures independently.	Only applicable to chemically homogenous specimens.	

7.12 A Versatile Atomic Number Correction for Electron Probe, Microanalysis.

G. Love, M.G.C. Cox and V.D. Scott,

1978a, J. Phys.D : Appl. Phys., 11, 7.

J. Phys. D: Appl. Phys., Vol. 11, 1978. Printed in Great Britain. © 1978

A versatile atomic number correction for electron-probe microanalysis

G Love, M G Cox† and V D Scott
School of Materials Science, University of Bath, Claverton Down, Bath BA2 7AY, Avon

Received 27 June 1977, in final form 19 September 1977

Abstract. A new atomic number correction is proposed for quantitative electron-probe microanalysis. Analytical expressions for the stopping power S and back-scatter R factors are derived which take into account atomic number of the target, incident electron energy and overvoltage; the latter expression is established using Monte Carlo calculations. The correct procedures for evaluating S and R for multi-element specimens are described. The new method, which overcomes some limitations inherent in either the Duncumb and Reed (1968) or the Philibert and Tixier (1968) atomic number corrections, may readily be used where specimens are inclined to the electron beam.

1. Introduction

In quantitative electron-probe microanalysis the ratio of measured x-ray intensities from specimen and standard has to be multiplied by a correction factor to obtain the true composition of the specimen. The factor is made up of three terms which account for effects of atomic number, x-ray absorption and an x-ray fluorescence, and each of these can be determined independently. In order to calculate the atomic number correction, it is necessary to understand the nature of the electron scattering and ionisation processes which take place in the target. Individual electrons suffer multiple scattering before either coming to equilibrium with the specimen or escaping altogether; some of the scattering events are inelastic, a fraction of which produce x-rays. These energy loss processes are dependent upon the atomic number of the target and, since they will differ in specimen and standard, require quantification in the atomic number correction. Provided the distribution of electrons can be determined as a function of energy and position within the target, the distribution of generated x-rays with depth may be found. Thereafter absorption and fluorescence factors may be established to give the intensity of x-rays finally emitted from the target.

The atomic number correction is of some complexity and has received considerable attention in the literature (see, for example, the reviews by Martin and Poole 1971, Beaman and Isasi 1972, Reed 1975). The method most commonly used is that proposed by Duncumb and Reed (1968) and, while satisfactory for many of the conditions experienced in microanalysis (see above review articles), there is mounting evidence (Love *et al* 1975, Brown and Parobek 1976) that it becomes inaccurate at low electron energies; some possible sources of error in the Duncumb and Reed atomic number correction

† Now with Wilkinson Match Ltd, Research Division, Poyle Road, Colnbrook, Slough, Bucks.

have been pointed out by Heinrich and Yakowitz (1969). A more rigorous correction procedure has been given by Philibert and Tixier (1968) but, since it appears to offer no clear advantage (see above review articles), is little used in practical microanalysis. In the present paper a new atomic number correction is proposed which overcomes some limitations inherent in either of the above treatments. The method can be readily incorporated into existing programmes for quantitative electron-probe microanalysis and has the added advantage that it can be used where specimens are inclined to the electron beam.

2. The atomic number correction

The number of characteristic x-rays generated per incident electron along a small element of path ds in the target is proportional to $(QN\rho/A)\,\mathrm{d}s$, where Q is the ionisation cross-section, N is Avogadro's number, ρ is density and A is atomic weight. Thus the total number of x-rays produced by the electron before coming to rest is proportional to

$$\frac{N}{A}\int_{E_c}^{E_0}\frac{Q}{\mathrm{d}E/\mathrm{d}(\rho s)}.\mathrm{d}E$$

where $-\mathrm{d}E/\mathrm{d}(\rho s)$ is the stopping power, E_0 the energy of the incident electron and E_c the critical ionisation potential for the x-ray line of interest. Since some electrons are back-scattered out of the target with finite energy, there is an effective loss of x-ray production. This may be taken into account by multiplying the above expression by a factor R. The intensity ratio, I_{sp}/I_{st}, of x-rays produced by the ath element of a multi-element specimen to that in a pure element standard is then

$$\left(\frac{I_{sp}}{I_{st}}\right)_a = C_a.\frac{R_{sp}}{R_{st}}.\frac{\int_{E_c}^{E_0}\left(\frac{Q}{\mathrm{d}E/\mathrm{d}(\rho s)}\mathrm{d}E\right)_{sp}}{\int_{E_c}^{E_0}\left(\frac{Q}{\mathrm{d}E/\mathrm{d}(\rho s)}\mathrm{d}E\right)_{st}} \tag{1}$$

where C_a is the weight fraction of the ath element.

This conventionally is written as

$$\left(\frac{I_{sp}}{I_{st}}\right)_a = C_a\frac{R_{sp}}{R_{st}}\frac{S_{st}}{S_{sp}}. \tag{2}$$

Hence the atomic number correction can be treated by considering the factors R and S† independently.

3. The S Factor

The problem in calculating S lies in obtaining an expression for $Q/(\mathrm{d}E/\mathrm{d}(\rho s))$ which is accurate over the range of experimental conditions experienced in microanalysis. Most workers have chosen to adopt the ionisation cross-section proposed by Bethe (1930) and subsequently simplified by Green and Cosslett (1961).

† S is referred to as the stopping power factor and is expressed as

$$\frac{1}{S}=\int_{E_c}^{E_0}\frac{Q}{\mathrm{d}E/\mathrm{d}(\rho s)}.\mathrm{d}E.$$

It should not be confused with the stopping power, $-\mathrm{d}E/\mathrm{d}(\rho s)$.

$Q = \text{const.}/U \ln U$, where U is the overvoltage ($=E/E_c$), together with the continuous energy loss expression of Bethe and Ashkin (1953)

$$\frac{dE}{d(\rho s)} = -78500 \frac{Z}{AE} \ln\left(\frac{1{\cdot}166E}{J}\right)$$

where Z is the atomic number and J is the mean ionisation potential of the target. For a multi-element specimen the additive nature of the energy loss process (Duncumb and Reed 1968) gives

$$\left(\frac{dE}{d(\rho s)}\right)_{sp} = \sum C_i \left(\frac{dE}{d\rho s}\right)_i.$$

Thus

$$\left(\frac{dE}{d(\rho s)}\right)_{sp} = -\frac{78500}{E} \sum \frac{C_i Z_i}{A_i} \ln \frac{1{\cdot}166E}{J_i}$$

$$= -\frac{78500}{E}\left(\sum \frac{C_i Z_i}{A_i} \ln 1{\cdot}166E - \sum \frac{C_i Z_i}{A_i} \ln J_i\right)$$

$$= -\frac{78500}{E}\left[\left(\sum \frac{C_i Z_i}{A_i}\right) \ln 1{\cdot}166E - \left(\sum \frac{C_i Z_i}{A_i}\right) \sum \frac{C_i Z_i}{A_i} \ln J_i \Big/ \left(\sum \frac{C_i Z_i}{A_i}\right)\right]$$

$$= -\frac{78500}{E}\left(\sum \frac{C_i Z_i}{A_i}\right) \ln \frac{1{\cdot}166E}{J'}$$

where

$$\ln J' = \sum \frac{C_i Z_i}{A_i} \ln J_i \Big/ \sum \frac{C_i Z_i}{A_i}.$$

A criticism of the Bethe energy loss equation is that it gives unrealistic results at low electron energies. It predicts that $dE/d(\rho s)$ becomes zero when $E = J'/1{\cdot}166$, whereas $dE/d(\rho s)$ should increase more or less continuously as the electron energy decreases, becoming infinite as $E \to 0$. Rao Sahib and Wittry (1974) have overcome this limitation by using a different energy loss equation for low electron energies, below $E/J' \approx 6$, but we have found that the use of their expression gives a form for S which is unnecessarily complex. An alternative approach for evaluating $dE/d(\rho s)$ is therefore proposed as follows.

We shall begin by writing Bethe's expression in terms of the variable V, where $V = E/J'$:

$$\frac{dE}{d\rho s} = \frac{-1}{J'}\left(\sum \frac{C_i Z_i}{A_i}\right)\left(\frac{78500}{V} \ln 1{\cdot}166V\right) = \frac{-1}{J'}\left(\sum \frac{C_i Z_i}{A_i}\right)\frac{1}{f(V)}. \qquad (3)$$

The function $f(V)$ against V is approximately parabolic at high V values and hence it seems reasonable to express $f(V)$ as a polynomial in $V^{1/2}$, i.e.

$$f(V) = A + BV^{1/2} + CV + DV^{3/2} + \ldots .$$

Now to accord with reality $dE/d(\rho s)$ must tend to infinity as $V \to 0$; consequently $f(V)$ must tend to 0 as $V \to 0$ and thus $A = 0$. Furthermore, a plot of $f(V)/V^{1/2}$ versus $V^{1/2}$ (figure 1*a*) gives a straight line over a wide range of V (E/J' from 9 to 1000), indicating that a second-order polynomial is adequate. With the appropriate constants (figure 1*a*) inserted

$$f(V) = 1{\cdot}18 \times 10^{-5} V^{1/2} + 1{\cdot}47 \times 10^{-6} V$$

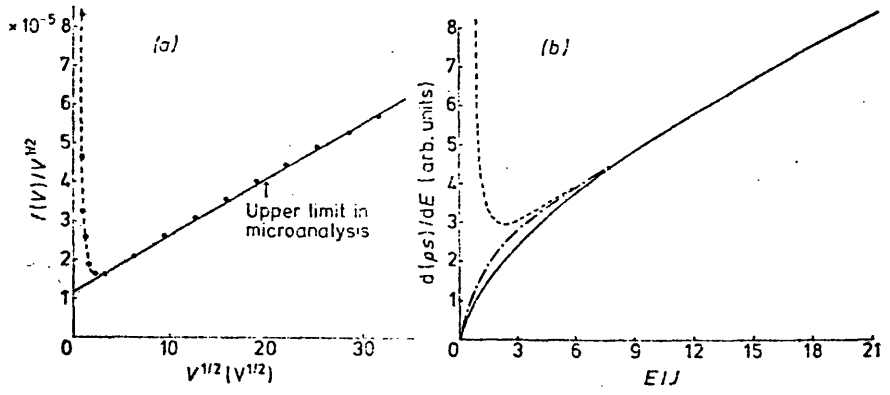

Figure 1. (*a*) Plot of $f(V)/V^{1/2}$ versus $V^{1/2}$. Points have been calculated using the continuous energy loss expression of Bethe and Ashkin (1953). The solid straight line shows the relationship adopted in the present work. (*b*) Plots of d(ρs)/dE versus E/J: - - - Bethe and Ashkin (1953); —— present work; —·— Rao Sahib and Wittry (1974).

which substituted in equation (3) gives

$$\frac{\mathrm{d}E}{\mathrm{d}(\rho s)}=\frac{-1}{J'}\left(\sum\frac{C_iZ_i}{A_i}\right)\frac{1}{1{\cdot}18\times10^{-5}\,(E/J')^{1/2}+1{\cdot}47\times10^{-6}\,(E/J')}. \tag{4}$$

Equation (4) is compared with the Bethe expression in figure 1(*b*); they closely agree for $E/J'>9$ but our expression is more realistic at lower E/J'. This equation will now be used to evaluate the integral in equation (1) as follows (where $U_0=E_0/E_c$):

$$\begin{aligned}
&\int_{E_c}^{E_0}\frac{Q}{\mathrm{d}E/\mathrm{d}(\rho s)}\,\mathrm{d}E\\
&\quad=\int_{U_c}^{1}\frac{Q}{\mathrm{d}U/\mathrm{d}(\rho s)}.\mathrm{d}U\\
&\quad=-\text{const.}\,J'E_c\left[1{\cdot}18\times10^{-5}\left(\frac{E_c}{J'}\right)^{1/2}\int_{U_c}^{1}\frac{\ln U}{U^{1/2}}\,\mathrm{d}U\right.\\
&\qquad\left.+1{\cdot}47\times10^{-6}\left(\frac{E_c}{J'}\right)\int_{U_c}^{1}\ln U\,\mathrm{d}U\right]\Big/\sum\frac{C_iZ_i}{A_i}\\
&\quad=\text{const.}\,J'E_c\left[2{\cdot}36\times10^{-5}\left(\frac{E_c}{J'}\right)^{1/2}[U_0^{1/2}\ln U_0+2\,(1-U_0^{1/2})]\right.\\
&\qquad\left.+1{\cdot}47\times10^{-6}\left(\frac{E_c}{J'}\right)[U_0\ln U_0+(1-U_0)]\right]\Big/\sum\frac{C_iZ_i}{A_i}\\
&\quad=\frac{\text{const.}\,1{\cdot}47\times10^{-6}\,E_c^2}{\sum C_iZ_i/A_i}[U_0\ln U_0+(1-U_0)]\\
&\qquad\times\left[1+16{\cdot}05\left(\frac{J'}{E_c}\right)^{1/2}\frac{U_0^{1/2}\ln U_0+2\,(1-U_0^{1/2})}{U_0\ln U_0+1-U_0}\right].
\end{aligned}$$

When taking a ratio of this expression for specimen and standard (see equation (1))

some of the terms cancel and we may write

$$\frac{1}{S}=\left[1+16{\cdot}05\left(\frac{J'}{E_c}\right)^{1/2}\frac{U_0^{1/2}\ln U_0+2(1-U_0^{1/2})}{U_0\ln U_0+1-U_0}\right]\Big/\sum\frac{C_iZ_i}{A_i}.$$

This may be further simplified since

$$\frac{U_0^{1/2}\ln U_0+2(1-U_0^{1/2})}{U_0\ln U_0+1-U_0}\approx\left(\frac{U_0^{1/2}-1}{U_0-1}\right)^{1{\cdot}07}.$$

The simplification is seen to be justified in figure 2, where the function is plotted logarithmically against $\ln[(U_0^{1/2}-1)/(U_0-1)]$. The points lie on a straight line of slope 1·07

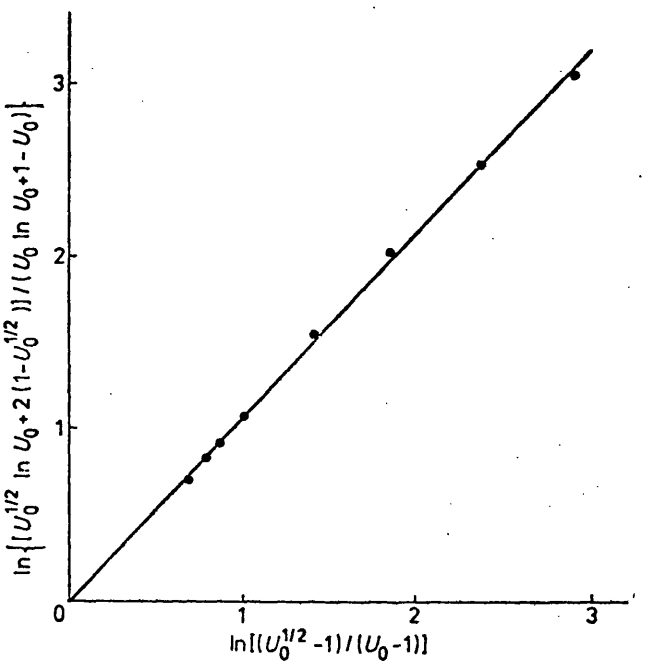

Figure 2. Plot of $\ln\left(\frac{U_0^{1/2}\ln U_0+2(1-U_0^{1/2})}{U_0\ln U_0+1-U_0}\right)$ versus $\ln\left(\frac{U_0^{1/2}-1}{U_0-1}\right)$.

passing through the origin. It should also be noted that the relationship appears satisfactory for a wide range of overvoltages, $1<U_0<300$.

Thus

$$\frac{1}{S}=\left[1+16{\cdot}05\left(\frac{J'}{E_c}\right)^{1/2}\left(\frac{U_0^{1/2}-1}{U_0-1}\right)^{1{\cdot}07}\right]\Big/\sum\frac{C_iZ_i}{A_i}. \tag{5}$$

We would point out that our method of calculating S is more rigorous than that of Duncumb and Reed (1968). These authors use the Bethe expression and assume that because $\ln(1{\cdot}166E/J)$ varies only slowly with E as the electron loses energy, it may be taken outside the integration, i.e.

$$\int_{E_c}^{E_0}\frac{Q}{\mathrm{d}E/\mathrm{d}(\rho s)}\mathrm{d}E\propto\left[\frac{Z}{A}\ln\left(1{\cdot}166\frac{\bar{E}}{J}\right)\right]^{-1}\int_{E_c}^{E_0}\frac{Q(E)}{E}.\mathrm{d}E$$

where $\bar{E}$ is the mean electron energy $\frac{1}{2}(E_0+E_c)$. Since $\int_{E_c}^{E_0}Q(E)/E\,\mathrm{d}E$ is the same for

both specimen and standard, their final expression becomes

$$S=\frac{Z}{A}\ln\left(\frac{1{\cdot}166E}{J}\right).$$

As noted, however, by Heinrich and Yakowitz (1969), Duncumb and Reed's approach is inappropriate for use at very high or very low overvoltages and only at one value of U_0 would it be exact for a particular target material (e.g. at $U_0\approx 3$ for aluminium in gold).

Although mathematical approximations are not used in the method proposed by Philibert and Tixier (1968), their procedure is complex and requires the evaluation of a logarithmic integral by summation of an infinite series. Moreover its validity is affected by the breakdown of the simple Bethe expression as $E \to J$. As may be seen above, our treatment suffers neither disadvantage.

4. The R factor

The aim here is to develop a generalised analytical expression for the electron back-scatter factor R from which values may be calculated for particular experimental conditions. Because of the difficulty in measuring R directly, however, there are few experimental values available in the literature on which to base such an equation and an alternative approach must be adopted. We have chosen for this purpose to use a Monte Carlo method described in a previous paper (Love *et al* 1977) which was developed from the treatment of Curgenven and Duncumb (1971). This approach may be justified since R is dependent upon the back-scattered electron energy distributions and such distributions produced by the Monte Carlo model have been shown to accord with experimental data. R values may be derived using the method as follows. The total number of ionisations produced in the specimen by each electron is summed for a large number of electrons. The ratio of this to the number of ionisations produced by the same number of electrons had no back-scattering occurred, gives R directly. Since R will be dependent upon the back-scatter coefficient η, values of η are also determined concurrently. (η is the probability of an electron incident upon a semi-infinite target leaving it again.)

Values of R and η have been obtained for the elements C, Al, Ti, Cu, Ag, Au at incident electron energies of 5, 10 and 30 keV and at a range of overvoltages (1·1–200). Typical results are illustrated in figure 3, plots of R versus η for different values of U_0, and it may be seen that at a constant overvoltage the curves are independent of E_0, i.e. R is a function of U_0 and η only. We shall now use these data to develop an analytical expression for R.

The number of ionisations produced by an incident electron is given by the expression of Green and Cosslett (1961, 1968) $I=K(U_0-1)^{1\cdot67}$, where K is a constant which depends upon atomic number. The number of ionisations produced by the back-scattered electrons had they remained in the specimen is

$$K\int_1^{U_0}\frac{\mathrm{d}\eta}{\mathrm{d}U}(U-1)^{1\cdot67}\,\mathrm{d}U$$

which at high overvoltages can be approximated to

$$K\eta\,(\bar{U}-1)^{1\cdot67} \tag{6}$$

where $\bar{U}$ is the mean overvoltage of the back-scattered electrons. Thus the number of

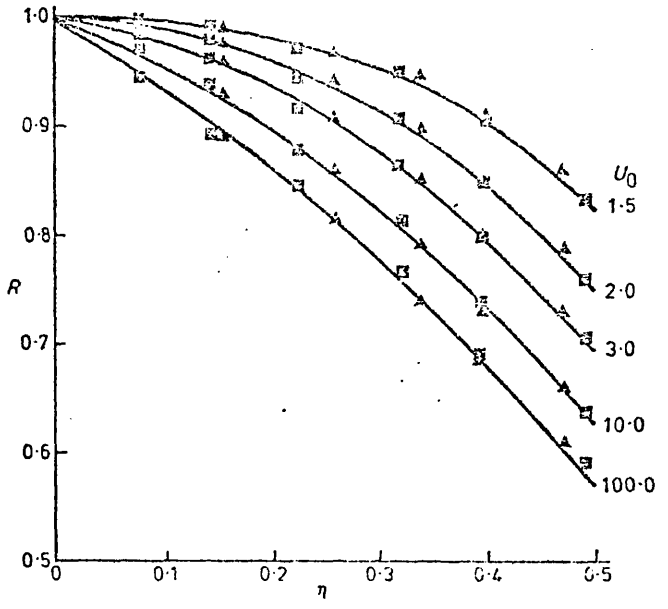

Figure 3. Plots of R versus η for different U_0 values: ▲ 5 keV, ▣ 30 keV.

ionisations produced in the specimen is

$$K\,[(U_0-1)^{1\cdot67}-\eta(\bar{U}-1)^{1\cdot67}]$$

and

$$R\approx 1-\eta\cdot\left(\frac{\bar{U}-1}{U_0-1}\right)^{1\cdot67}. \tag{7}$$

Fitting (1975) has shown from experimental measurements that the mean energy $\bar{E}$ of back-scattered electrons is given by $\bar{E}=0\cdot5E_0\,(1+\eta)$. Hence $\bar{U}=0\cdot5U_0\,(1+\eta)$.

Substituting for $\bar{U}$ in equation (7) gives

$$R\approx 1-\eta\left(\frac{0\cdot5U_0\,(1+\eta)-1}{U_0-1}\right)^{1\cdot67}=1-\eta\,(I(U_0)+\eta G(U_0))^{1\cdot67} \tag{8}$$

which rearranged gives

$$\left(\frac{1-R}{\eta}\right)^{0\cdot6}\approx I(U_0)+\eta G(U_0). \tag{9}$$

This relationship was tested using the R and η data generated by the Monte Carlo program. The results are shown in figure 4, plots of $(1-R/\eta)^{0\cdot6}$ versus η for a number of overvoltages. The points lie close to a series of straight lines, within the statistics of the Monte Carlo treatment, which indicates that the dependence of R upon η is satisfactorily represented by equation (8).

We shall now investigate the overvoltage dependence of the functions $I(U_0)$ and $G(U_0)$. From equation (9) $I(U_0)$ and $G(U_0)$ should be linear functions of $(0\cdot5U_0-1)/(U_0-1)$ and $0\cdot5U_0/(U_0-1)$ respectively. This has been tested by plotting intercepts and gradients of the graphs in figure 4 versus the above functions (see figures *5a* and *5b* respectively). The results show that the relationships are not linear. This is because the approximation used in equation (6) becomes less accurate as $U_0 \to 1$. Consequently,

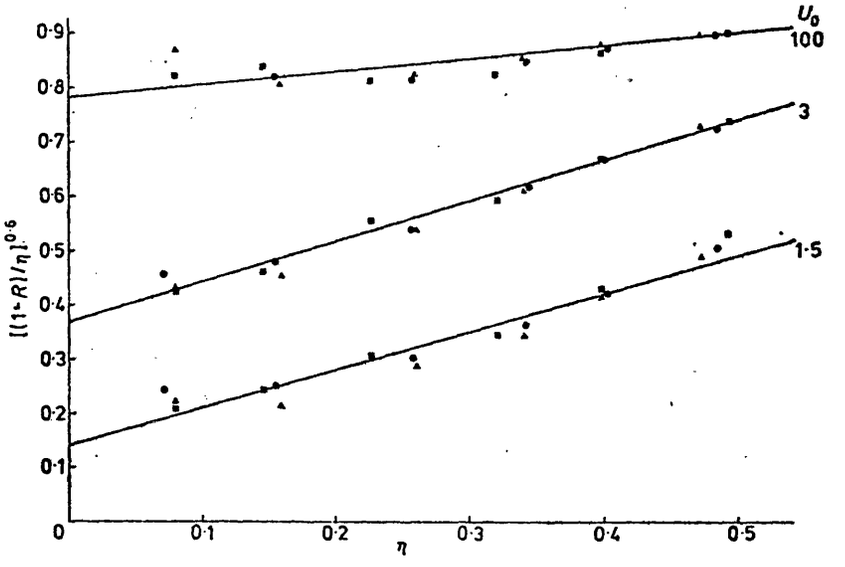

Figure 4. Plots of $[(1-R)/\eta]^{0·6}$ versus η for different U_0 values: ▲ 5 keV, ● 10 keV, ■ 30 keV.

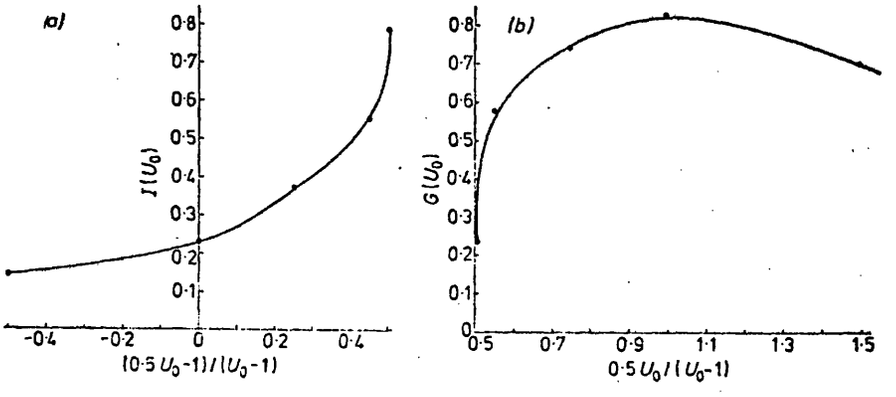

Figure 5. Monte Carlo Results (*a*) plot of $I(U_0)$ versus $(0·5U_0-1)/(U_0-1)$. (*b*) Plot of $G(U_0)$ versus $0·5U_0/(U_0-1)$.

alternative functions of U_0 were investigated and from a least-squares regression analysis of I and G values the following expressions were obtained:

$$I(U_0)=0·33148 \ln U_0+0·05596 (\ln U_0)^2-0·06339 (\ln U_0)^3+0·00947 (\ln U_0)^4 \quad (10)$$

$$G(U_0)=\frac{1}{U_0}[2·87898 \ln U_0-1·51307 (\ln U_0)^2+0·81312 (\ln U_0)^3-0·08241 (\ln U_0)^4]. \quad (11)$$

Both expressions have been constrained to give zero when $U_0=1$ in order to accord with reality. Equations (10) and (11) are then substituted into equation (8) to give R.

In order to devise a method for obtaining R for multi-element specimens we need to know how the back-scattered electron energy distribution is affected by composition of the target. The treatment which follows is based upon the model of an electron trajectory used in our Monte Carlo approach. Consider a large number of electrons incident on a target. If each electron trajectory is divided into a large number of equal steps, then the

fraction of electrons which are back-scattered at the ith step is determined by the deflections of the electrons at each step up to and including the ith. It has been shown previously (Love *et al* 1977) that the deflection angle β at each step is related to $W(=E/E_0)$ by $\cot \beta/2=(\cot \beta_0/2)W(YFL)^{1/2}$ and that $\cot \beta_0/2$ is a function of η only. Hence, $\cot \beta/2=f_1(\eta)W(YFL)^{1/2}$, where YFL is a pseudo random number which takes values between 0 and 1.

The variation of W along a trajectory may be shown to be substantially independent of the nature of the target (see appendix) and is determined by the number of steps the electron has made. Thus $W(YFL)^{1/2}$ is, on average, the same at each step of the trajectory for all targets and hence the fraction back-scattered at the ith step is also a function of η only. Furthermore, since the value of W for these electrons is determined by i, the number of steps taken prior to leaving the target, it follows that $\mathrm{d}\eta/\mathrm{d}W=f_2(\eta)$.

This equation shows that the back-scattered electron energy distribution is dependent more fundamentally upon target composition. Now the value of R (for a given overvoltage) is a function of the back-scattered energy distribution ($\mathrm{d}\eta/\mathrm{d}W$ versus W), which indicates that R for a multi-element specimen may be obtained by substituting the correct value of η_{spec} for the target into equation (8). Two methods have been proposed for deriving η_{spec}:

$$\frac{1}{1-\eta_{\mathrm{spec}}}=\sum\frac{C_i}{1-\eta_i} \qquad \text{(Wittry 1957)}$$

and

$$\eta_{\mathrm{spec}}=\sum C_i\eta_i \qquad \text{(Castaing 1960).}$$

Although the former expression may be more rigorous (Russ 1977), the latter, more commonly used equation, has been found satisfactory by Heinrich (1963), Colby (1966) and Bishop (1966).

There is a dearth of direct experiment determinations of R with which to compare values calculated from equations (8), (10) and (11), apart from data given by Derian and Castaing (1966) on copper and gold at a series of overvoltages which agree, within experimental error, with our calculations. A more extensive range of R values is available from derivations based upon back-scattered energy distributions (Green 1962, Thomas 1963, Springer 1966, Bishop 1966, 1968, Duncumb and Reed 1968). Springer (1966) and Duncumb (cited by Beaman and Isasi 1972) have generalised their results in the form of analytical expressions in Z and U_0; both are complex polynomials of 16 and 36 terms respectively, although Duncumb's equation is regarded as the more satisfactory (for discussion see Martin and Poole 1971). Our calculated values for R agree closely ($\pm 1{\cdot}5\%$) with those of Duncumb and Reed for an incident electron energy of 20 keV on pure elements over a wide range of overvoltages ($1{\cdot}5<U_0<100$). At other incident energies, however, the differences are larger (up to $\sim 5\%$), since our expression for R contains η which has been shown to be energy dependent (Bishop 1966, Heinrich 1966, Drescher *et al* 1970, Darlington and Cosslett 1972) whereas Duncumb and Reed's R values are energy independent and accurate only at 20 keV.

Furthermore, the two approaches give different values of R for a multi-element system since Duncumb and Reed choose a different, and arbitrary, method of averaging, i.e. $R=\sum C_iR_i$. The discrepancies are particularly large for samples containing elements widely different in atomic number and can amount to 6% in unfavourable cases, e.g. gold/carbon.

5. Specimens inclined to the electron beam

5.1. Back-scattering from inclined targets

The Monte Carlo program has been used to examine the back-scatter properties of inclined targets. Typical back-scattered energy distributions for an aluminium specimen at 30°, 45° and 60° inclination are shown in figure 6; also shown is the fraction of elec-

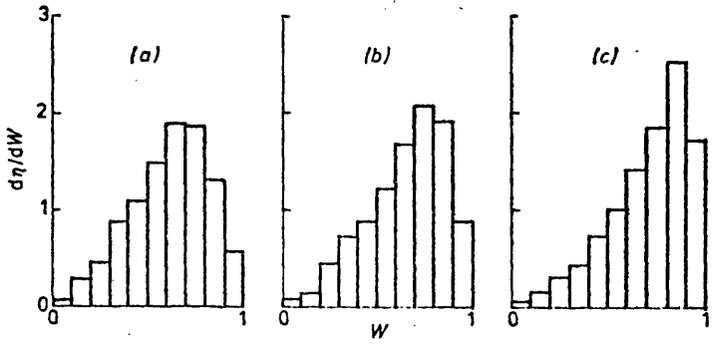

Figure 6. Back-scattered electron energy distributions, $d\eta/dW$ versus W, for Al targets inclined at (*a*) 30°, (*b*) 45° and (*c*) 60°, with η=(*a*) 0·201, (*b*) 0·269, (*c*) 0·376.

trons back-scattered (η). It should be noted that as the inclination increases: (i) the back-scatter coefficient η increases, and (ii) the peak in the energy distribution moves to higher energies. Darlington (1975) has shown that the back-scatter coefficients measured by Drescher *et al* (1970) at various inclinations are well represented by the equation

$$\eta_\alpha = 0{\cdot}891 \left(\frac{\eta}{0{\cdot}891}\right)^{\cos\alpha} \tag{12}$$

where η is the back-scatter coefficient at normal incidence and η_α is the back-scatter coefficient for a specimen inclined at an angle α to the beam normal. The Monte Carlo data and the values calculated from this equation are in excellent agreement (table 1) which validates the Monte Carlo treatment when applied to inclined specimens.

Table 1. Comparison with Monte Carlo data.

Element	U_0	Inclination α (deg)	η		R		
			Monte Carlo	Darlington (1975)	Monte Carlo	Equation (8)	Reed (1971)
Al	3	30	0·201±0·007	0·197	0·937	0·933	
Al	3	45	0·269±0·007	0·259	0·901	0·895	0·892
Al	3	60	0·376±0·008	0·372	0·827	0·818	
Cu	10	30	0·376±0·008	0·366	0·765	0·748	
Cu	10	45	0·431±0·009	0·431	0·715	0·691	0·732
Cu	10	60	0·526±0·01	0·494	0·620	0·575	

The electron energy distributions for Al, Ti and Ag at normal incidence are shown in figure 7, and comparison with figure 6 indicates that the back-scattered energy distribution of an inclined target corresponds closely with that of a target normal to the electron beam having the same back-scatter coefficient. Fitting (1975) has shown that the mean

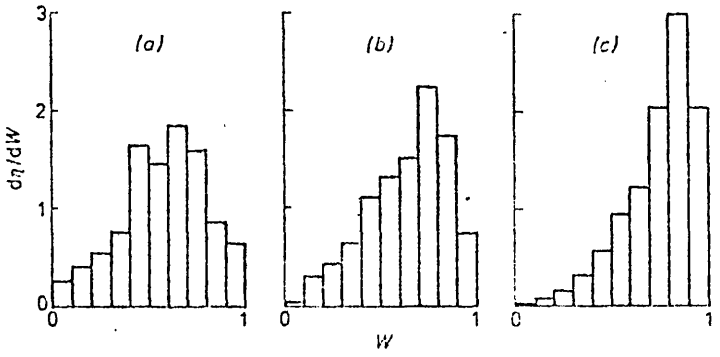

Figure 7. Back-scattered electron energy distributions, $d\eta/dW$ versus W, for (*a*) Al, (*b*) Ti and (*c*) Ag at normal incidence, with $\eta = (a)$ 0·145, (*b*) 0·242, (*c*) 0·425.

fractional energy $\overline{W}$ of the back-scattered electrons where

$$\overline{W} = \frac{\int_0^1 W(dn/dW)\,dW}{\int_0^1 (dn/dW)\,dW}$$

is a linear function of η. A plot of $\overline{W}$ calculated from Monte Carlo data versus η for a range of elements and target inclinations is shown in figure 8. The points all lie close to a single straight line irrespective of target composition or inclination. Hence $\overline{W}$ and therefore the back-scattered energy distributions are functions of η only, irrespective of the target composition and inclination.

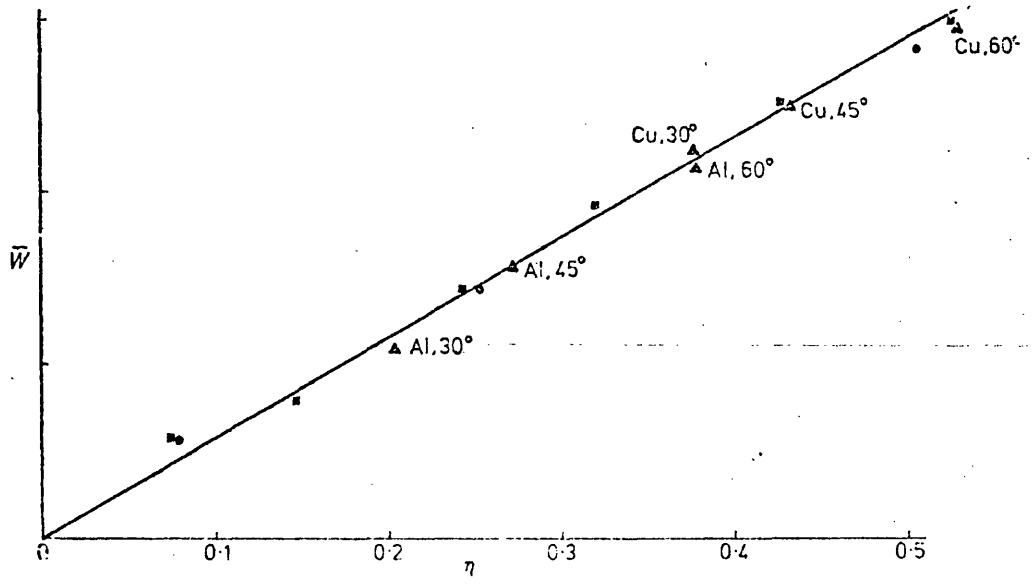

Figure 8. Plot of $\overline{W}$ versus η for a range of elements and target inclinations: ● normal incidence, 10 keV; ■ normal incidence 30 keV; ▲ inclined incidence, 10 and 30 keV.

5.2. Atomic number correction for inclined targets

Since the R factor depends on η and the back-scattered energy distribution, the R factor for an inclined target will be the same as that from a specimen normal to the electron

beam but with the same η value. Hence R for any specimen inclination may be calculated directly from equation (8) provided the correct value of η is inserted. It is considered that equation (12) is sufficiently accurate to use for calculating η values at non-normal incidence, certainly up to α values $\sim 75°$ (Darlington 1975). Typical values for R for inclined targets which have been obtained directly from the Monte Carlo program are given in table 1 together with those obtained using equation (8), and the sets of data show excellent agreement; some 45° electron incidence data of Reed (1971) are also included. Our procedure is preferred to that adopted by most workers, who have used R values for normal incidence due to the lack of data for inclined specimens. Although errors in this approach may be minimised when ratios are taken of specimen to standard, it should be pointed out that discrepancies of up to 10% may occur in some instances. The S factor may be treated as described in §3 since it is not affected by tilting the specimen.

6. Conclusions

A new atomic number correction has been proposed for quantitative electron-probe microanalysis which overcomes limitations inherent in previous models.

An expression for the stopping power, $\mathrm{d}E/\mathrm{d}(\rho s)$, has been deduced which accords with the Bethe equation at high electron energies and is more realistic at low energies where $E \to J$. This permits exact integration of $\int_{E_1}^{E_0} [Q/(\mathrm{d}E/\mathrm{d}(\rho s))]\,\mathrm{d}E$ and yields a simple analytical equation for the stopping power factor S:

$$\frac{1}{S}=\left[1+16{\cdot}05\left(\frac{J'}{E_c}\right)^{1/2}\left(\frac{U_0^{1/2}-1}{U_0-1}\right)^{1{\cdot}07}\right]\Big/\sum_i \frac{C_i Z_i}{A_i}.$$

R factors are derived from Monte Carlo calculations and a generalised analytical expression is developed from which R values may be calculated:

$$R=1-\eta\,[I(U_0)+\eta G(U_0)]^{1{\cdot}67}$$

where

$$I(U_0)=0{\cdot}33148\ln U_0+0{\cdot}05596(\ln U_0)^2-0{\cdot}06339(\ln U_0)^3+0{\cdot}00947(\ln U_0)^4$$

$$G(U_0)=\frac{1}{U_0}[2{\cdot}8789\ln U_0-1{\cdot}51307(\ln U_0)^2+0{\cdot}81312(\ln U_0)^3-0{\cdot}08241(\ln U_0)^4].$$

The importance of selecting the correct method of calculating S and R for multi-element specimens is stressed and the appropriate methods are described.

The proposed atomic number correction may be satisfactorily applied to a wider range of microanalysis conditions than previous expressions. It may be readily used where specimens are inclined to the electron beam and hence should be of special interest to microanalysts who wish to quantify x-ray data obtained using scanning electron microscopes.

In a later paper this atomic number correction will be used for quantitative electron-probe microanalysis. The work will necessarily involve the use of an absorption correction such as the method of Bishop (1974) with an appropriate expression for the mean depth (see Love *et al* 1976), although wherever possible systems will be selected which have relatively large atomic number effects in order to compare the present procedure with the Duncumb and Reed (1968) approach.

Acknowledgments

Thanks are due to Dr P Duncumb for his helpful comments on the paper. The co-operation of the University Computer Unit under the direction of Dr A W Nichol is also acknowledged.

Appendix. The variation of E/E_0 along an electron trajectory

In the present paper an expression has been derived for $dE/d(\rho s)$ which accords with the Bethe treatment at high values of E/J and has realistic limiting behaviour as $E \to 0$

$$\frac{dE}{d(\rho s)} = -\frac{Z}{AJ} \frac{1}{1{\cdot}18 \times 10^{-5} (E/J)^{1/2} + 1{\cdot}47 \times 10^{-6} (E/J)}.$$

This equation may be integrated to give the range (ρs) of an electron as a function of its energy

$$\rho s = -\frac{AJ}{Z} \int_E^0 [1{\cdot}18 \times 10^5 (E/J)^{1/2} + 1{\cdot}47 \times 10^{-6} (E/J)]\, dE$$

and thus

$$\rho s = \frac{A}{Z} (0{\cdot}773 \times 10^{-5} J^{1/2} E^{3/2} + 0{\cdot}735 \times 10^{-6} E^2).$$

For an electron incident on a target with energy E_0 the maximum range is given by

$$\rho s_{max} = \frac{A}{Z} (0{\cdot}773 \times 10^{-5} J^{1/2} E_0^{3/2} + 0{\cdot}735 \times 10^{-6} E_0^2).$$

At some depth ρs the electron will have an energy E. Thus the fraction of the total

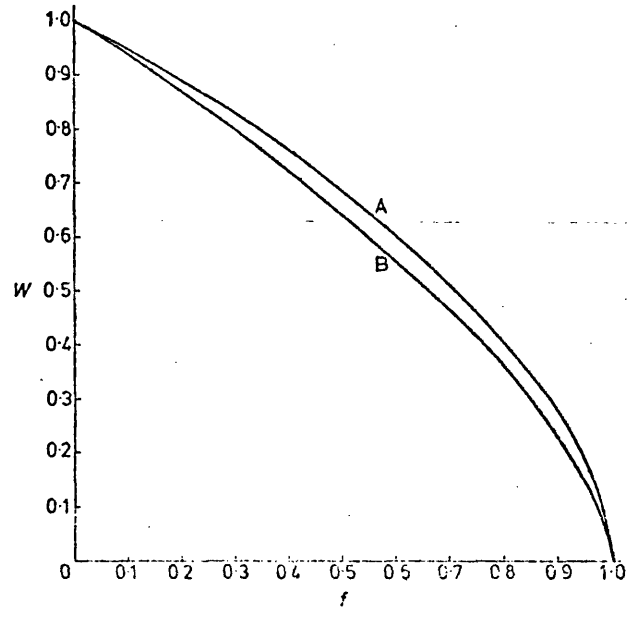

Figure A1. Plots of f versus W for $J/E_0 = 0{\cdot}003$ (curve A) and 0·2 (curve B). These are the extreme conditions likely to be encountered in microanalysis.

trajectory the electron has travelled f is

$$f=1-\frac{\rho s}{(\rho s)_{\max}}=1-\frac{0{\cdot}773\times10^{-5}J^{1/2}E^{3/2}+0{\cdot}735\times10^{-6}E^2}{0{\cdot}773\times10^{-5}J^{1/2}E_0^{3/2}+0{\cdot}735\times10^{-6}E_0^2}$$

$$=1-\left(\frac{E}{E_0}\right)^2\left(\frac{10{\cdot}5\,(J/E)^{1/2}+1}{10{\cdot}5\,(J/E_0)^{1/2}+1}\right).$$

Hence, as $E_0\to\alpha$, $f\to1-(E/E_0)^2$ and, as $E_0\to0$, $f\to1-(E/E_0)^2$. Putting $W=E/E_0$ gives

$$f=1-W^2\left(\frac{10{\cdot}5\,(J/WE_0)^{1/2}+1}{10{\cdot}5\,(J/E_0)^{1/2}+1}\right).$$

A plot of f against W for typical values of J/E_0 is illustrated in figure A1, which indicates that at a given fraction of the trajectory the value of W is almost independent of J/E_0 and hence of the nature of the specimen. The variation is a maximum at an f value $\sim0{\cdot}7$ and for the most extreme conditions encountered in microanalysis this variation is always less than 10%.

References

Beaman D R and Isasi J A 1972 *ASTM Spec. Tech. Publ.* 506

Bethe H A 1930 *Ann. Phys., Lpz.* 5 325–400

Bethe H A and Ashkin J 1953 *Exptl Nucl. Phys.* 1 (New York: Wiley) p 252

Bishop H E 1966 *X-ray Optics and Microanalysis* eds R Castaing, P Deschamps and J Philibert (Paris: Hermann) pp 153–8

—— 1968 *J. Phys. D: Appl. Phys.* 1 673–84

—— 1974 *J. Phys. D: Appl. Phys.* 7 2009–20

Brown J D and Parobek L 1976 *X-ray Spectrometry* 5 36–40

Castaing R 1960 *Adv. Electron. Electron Phys.* 13 eds L L Marton and C Marton (New York: Academic Press) pp 317–86

Colby J W 1966 *The Electron Microprobe* eds T D McKinley, K F J Heinrich and D B Wittry (New York: Wiley) pp 95–188

Curgenven L and Duncumb P 1971 *Tube Investments Res. Rep.* No. 303

Darlington E H 1975 *J. Phys. D: Appl. Phys.* 8 85–93

Darlington E H and Cosslett V E 1972 *J. Phys. D: Appl. Phys.* 5 1967–81

Derian J C and Castaing R 1966 *X-ray Optics and Microanalysis* eds R Castaing, P Deschamps and J Philibert (Paris: Hermann) pp 193–9

Drescher H, Reimer L and Seidel H 1970 *Z. Angew. Phys.* 29 331–6

Duncumb P and Reed S J B 1968 *Quantitative Electron Probe Microanalysis* ed. K F J Heinrich: *NBS Spec. Publ.* 298 pp 133–54

Fitting H J 1975 *J. Phys. D: Appl. Phys.* 8 1481–6

Green M 1962 *PhD Thesis* University of Cambridge

Green M and Cosslett V E 1961 *Proc. Phys. Soc.* 78 1206–14

—— 1968 *J. Phys. D: Appl. Phys.* 1 425–36

Heinrich K F J 1963 *Adv. X-ray Analysis* 7 eds W M Meuller, G Mallett and M Fay (New York: Plenum) pp 325–39

—— 1966 *X-ray Optics and Microanalysis* eds R Castaing, P Deschamps and J Philibert (Paris: Hermann) pp 159–67

Heinrich K F J and Yakowitz H 1969 *X-ray Optics and Microanalysis* eds G Möllenstedt and K H Gaukler (Berlin: Springer-Verlag) pp 151–9

Love G, Cox M G C and Scott V D 1975 *J. Phys. D: Appl. Phys.* 8 1686–701

—— 1976 *J. Phys. D: Appl. Phys.* 9 7–13

—— 1977 *J. Phys. D: Appl. Phys.* 10 7–23

Martin P M and Poole D M 1971 *Metall. Rev.* 5 No. 150 19–46
Philibert J and Tixier R 1968 *Quantitative Electron Probe Microanalysis* ed. K F J Heinrich: *NBS Spec. Publ.* 298 pp 13–33
Rao-Sahib T S and Wittry D B 1974 *J. Appl. Phys.* 45 5060–8
Reed S J B 1971 *J. Phys. D: Appl. Phys.* 4 1910
—— 1975 *Electron Probe Microanalysis* (London: Cambridge UP) pp 198–239
Russ J C 1977 *Edax Editor* 7 13–4
Springer G 1966 *Mikrochim. Acta* 3 587–95
Thomas P M 1963 *Br. J. Appl. Phys.* 14 397–8
Wittry D B 1957 *PhD Thesis* California Institute of Technology

7.13 The Surface Ionisation Function $\Phi(o)$ Derived Using a Monte Carlo Method

G. Love, M.G.C. Cox and V.D. Scott,

1978b, J. Phys. D : Appl. Phys., 11, 23.

J. Phys. D: Appl. Phys., Vol. 11, 1978. Printed in Great Britain. © 1978

The surface ionisation function $\varphi(0)$ derived using a Monte Carlo method

G Love, M G Cox† and V D Scott
School of Materials Science, University of Bath, Claverton Down, Bath BA2 7AY, Avon

Received 29 July 1977

Abstract. Values of the surface ionisation function $\phi(0)$ are calculated for a wide range of elements and overvoltages using a Monte Carlo program which simulates electron interactions in solids. From the data it is shown that $\phi(0)$ is simply a function of electron back-scatter coefficient and overvoltage, and an analytical expression for $\phi(0)$ is derived in terms of these parameters. Values of $\phi(0)$ obtained using the expression are compared with previous results.

1. Introduction

In the development of correction procedures for quantitative electron-probe microanalysis it is necessary to know the distribution with mass depth, ρz, of primary x-rays generated in the target, $\phi(\rho z)$. The fraction of x-rays of a particular wavelength leaving the specimen in the direction of the spectrometer which are not absorbed, $f(\chi)$, is then given by

$$f(\chi)=\frac{\int_0^\infty \phi(\rho z)\exp(-\chi\rho z)\,\mathrm{d}(\rho z)}{\int_0^\infty \phi(\rho z)\,\mathrm{d}(\rho z)}.$$

$\chi=\mu/\rho$ cosec θ, where μ/ρ is the mass absorption coefficient of the specimen for the wavelength of interest, and θ is the x-ray take-off angle. By expanding the exponential as a power series it can be shown (Bishop 1974) that as $\chi\to 0$

$$f(\chi)\underset{\chi\to 0}{=}1-\chi\frac{\int_0^\infty \rho z\phi(\rho z)\,\mathrm{d}(\rho z)}{\int_0^\infty \phi(\rho z)\,\mathrm{d}(\rho z)}=1-\chi\overline{\rho z} \tag{1}$$

and, by expressing $\phi(\rho z)$ as a Maclaurin series, that as $\chi\to\infty$

$$f(\chi)\underset{\chi\to\infty}{=}\frac{\phi(0)}{\chi}\Big/\int_0^\infty (\phi(\rho z)\,\mathrm{d}(\rho z). \tag{2}$$

Hence $f(\chi)$ is dependent primarily upon the mean depth $\rho\bar{z}$ when absorption is small and upon the surface ionisation, $\phi(0)$, when absorption is very large. Consequently, any accurate expression for $f(\chi)$ must incorporate, explicitly or implicitly, both of these parameters. In Philibert's (1963) model, for instance, his full expression contains both $\rho\bar{z}$ and $\phi(0)$, and it thus represents $f(\chi)$ fairly well over a wide range of absorption (Love

† Now with Wilkinson Match Ltd, Research Division, Poyle Road, Colnbrook, Slough, Bucks.

et al 1974b). However, his simplified equation (Philibert 1963) in which $\phi(0)$ is assumed zero is accurate only where absorption is small and its extension to other situations is inadvisable (Bishop 1974, Love *et al* 1975). Likewise, the 'thin-film model' proposed by Duncumb and Melford (1966) which is based upon equation (2) works well for high absorbers but is inappropriate for systems where absorption is low (Duncumb and Melford 1966, Love *et al* 1974a).

The measurement of thin films on substrates using x-ray emission is another area where $\phi(0)$ is important, since the x-ray intensity from the coating is enhanced by electrons which are back-scattered by the substrate into the thin film.

There are, unfortunately, few publications which provide comprehensive $\phi(0)$ data but some experimental values have been determined by Castaing and Descamps (1955), Castaing and Henoc (1966) and Vignes and Dez (1968). Data covering a much wider range of target materials and overvoltages are given by Hutchins and Wantman (1967) and by Reuter (1972) who also produced an analytical expression for $\phi(0)$ based upon his experimental findings. In addition, a set of $\phi(0)$ values has been calculated by Duncumb (ref. 137 in Martin and Poole 1971) using the measured back-scattered electron energy distributions of Bishop (1966).

In an earlier paper (Love *et al* 1977) a Monte Carlo model was used to investigate the dependence of $\overline{\rho z}$ on incident electron energy, overvoltage and back-scatter coefficient and an equation for $\overline{\rho z}$ was developed in terms of these variables. Here, a similar approach is adopted to study the surface ionisation and an analytical expression is established for $\phi(0)$.

2. Data for $\phi(0)$ derived from Monte Carlo program

A Monte Carlo method (Love *et al* 1977) based upon the approach of Curgenven and Duncumb (1971) has been tested previously by comparing calculated back-scattered electron energy distributions and $\phi(\rho z)$ curves with available experimental data. Since the two sets of results gave good agreement, the model was then used to generate more extensive information such as back-scatter factors (Love *et al* 1978). It is employed here to determine $\phi(0)$ values directly.

The contribution to surface ionisation made by an electron as it leaves the specimen at an angle θ to the incident beam direction is proportional to $\psi(U)/\cos\theta$, where U is the overvoltage and $\psi(U)$ is the ionisation cross-section; in the present work the equation of Bethe (1930), $\psi(U)=(\text{const.}/U)\ln U$, has been adopted. The surface ionisation, $\phi(0)$, is then given by

$$\phi(0)=\frac{n_0(\ln U_0)/U_0+\sum_{i=1}^{i=n}\ln U_i/U_i\cos\theta_i}{n_0(\ln U_0/U_0)}$$

where n_0 is the number of electrons incident on the specimen, n is the number back-scattered and U_0 is the 'overvoltage' of the incident electrons. It may be seen from this equation that $\phi(0)$ is always greater than unity because of the contribution from back-scattered electrons and consequently will be dependent upon the fraction back-scattered, $n/n_0=\eta$. Hence η has been evaluated concurrently with $\phi(0)$.

Values for $\phi(0)$ and η have been derived for the elements C, Al, Ti, Cu, Ag and Au at incident electron energies of 5, 10 and 30 keV and at overvoltages of 1·5, 2, 3, 10 and 100; the calculations all refer to electrons at normal incidence. Typical results are illustrated in figure 1, plots of $\phi(0)$ versus η for three different values of U_0. It may be seen

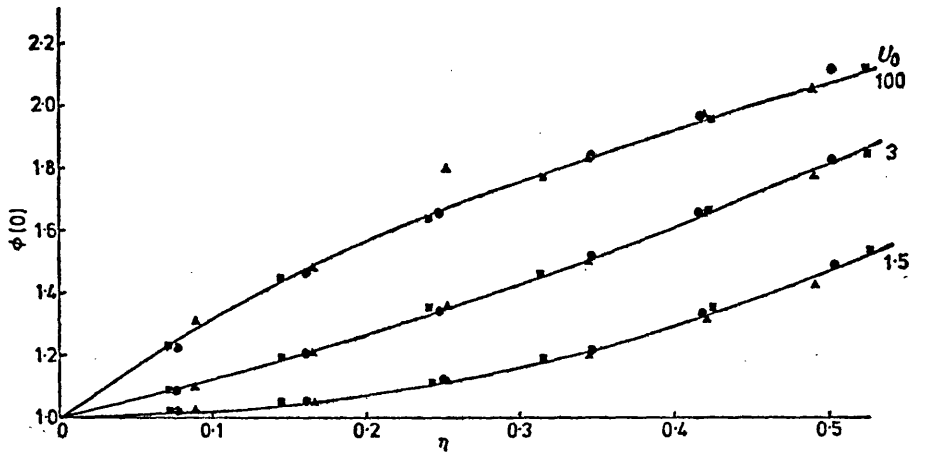

Figure 1. Plots of $\phi(0)$ versus η for overvoltages of 1·5, 3 and 100 V. ▲ 5 keV; ● 10 keV; ■ 30 keV.

that each curve is independent of incident electron energy, i.e. $\phi(0)$ is a function only of η and U_0. We shall now use these findings to develop an analytical expression for $\phi(0)$ which may then be employed to obtain $\phi(0)$ values covering a much wider range of conditions than those illustrated in the figure.

3. Analytical expression for $\phi(0)$

The first stage of the derivation is to develop an expression for $\phi(0)$ in terms of η. Now $\phi(0)$ is defined by $(I_0+I_B)/I_0$, where I_0 is the number of characteristic x-rays produced by the incident electron beam in an infinitesimal layer at the surface of the target and I_B is the number produced by electrons back-scattered through this layer. Thus

$$\phi(0)=1+I_B/I_0$$
$$=1+\eta\,\epsilon_B/\epsilon_0. \qquad (1)$$

ϵ refers to the efficiency of x-ray production and is proportional to $\lambda\,(\ln U)/U$, where λ is the average electron path length through the surface layer. Fitting (1975) has shown from experimental measurements of back-scattered electron energies that their mean energy $\bar{E}$ is given by $\bar{E}=0{\cdot}5\,E_0\,(1+\eta)$, where E_0 is the incident electron energy, and hence $\bar{U}=0{\cdot}5\,U_0\,(1+\eta)$. Consequently, we may make the approximations

$$\epsilon_B\simeq\frac{2\lambda_B}{1+\eta}\,\frac{\ln\,[0{\cdot}5\,U_0(1+\eta)]}{U_0}$$

and

$$\epsilon_0\simeq\lambda_0(\ln U_0)/U_0.$$

Substituting in equation (1) gives

$$\phi(0)=1+\left(\frac{\lambda_B}{\lambda_0}\right)\frac{2\eta}{1+\eta}\,\frac{\ln\,[0{\cdot}5\,U_0\,(1+\eta)]}{\ln U_0}. \qquad (2)$$

Since λ_B/λ_0 is constant

$$\phi(0)=1+\frac{\eta}{1+\eta}\,[I(U_0)+G(U_0)\ln(1+\eta)] \qquad (3)$$

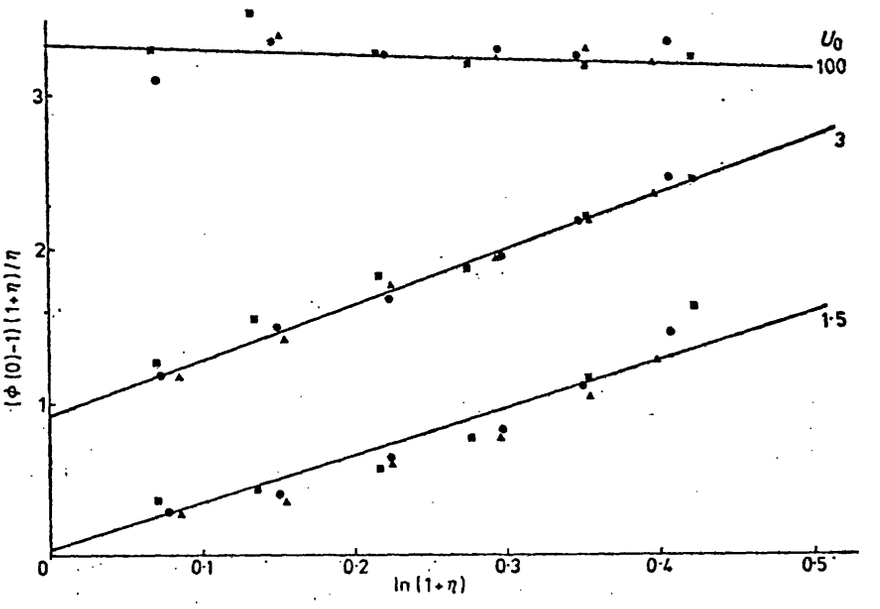

Figure 2. Plots of $(\phi(0)-1)(1+\eta)/\eta$ versus $\ln(1+\eta)$. ▲ 5 keV; ● 10 keV; ■ 30 keV.

and rearranging

$$(\phi(0)-1)\frac{(1+\eta)}{\eta}=I(U_0)+G(U_0)\ln(1+\eta). \tag{4}$$

This relationship was tested using the $\phi(0)$ and η data generated by the Monte Carlo program. Typical results are illustrated in figure 2, plots of $[\phi(0)-1](1+\eta)/\eta$ versus $\ln(1+\eta)$, for three overvoltages. The points lie close to a series of straight lines, within the statistics of the Monte Carlo treatment, which indicates that the dependence of $\phi(0)$ upon η is satisfactorily represented by equation (3).

We shall now proceed to examine the overvoltage dependence of $\phi(0)$, which is included in equation (4) as the terms $I(U_0)$ and $G(U_0)$. From equation (2) it may be deduced that these terms have the form

$$I(U_0)=\frac{2\lambda_B}{\lambda_0}\left(1-\frac{0{\cdot}69}{\ln U_0}\right)$$

and

$$G(U_0)=\frac{2\lambda_B}{\lambda_0}\left(\frac{1}{\ln U_0}\right);$$

i.e., they are both linear functions of $1/\ln U$. However, the values for I and G derived via the intercepts and gradients of the graphs in figure 2 are not linearly dependent upon $1/\ln U_0$ (see figure 3). This failure of equation (2) to predict the correct overvoltage dependence of $\phi(0)$ is because $(1/\bar{U})\ln\bar{U}$ has been assumed equivalent to the mean ionisation cross-section of the back-scattered electrons, an approximation which becomes increasingly worse as $U_0\to 1$. Consequently, alternative functions of U_0 were investigated and from a least-squares regression analysis of I and G values the following empirical expressions were obtained:

$$I(U_0)=3{\cdot}43378-\frac{10{\cdot}78720}{U_0}+\frac{10{\cdot}97628}{U_0^2}-\frac{3{\cdot}62286}{U_0^3} \tag{5}$$

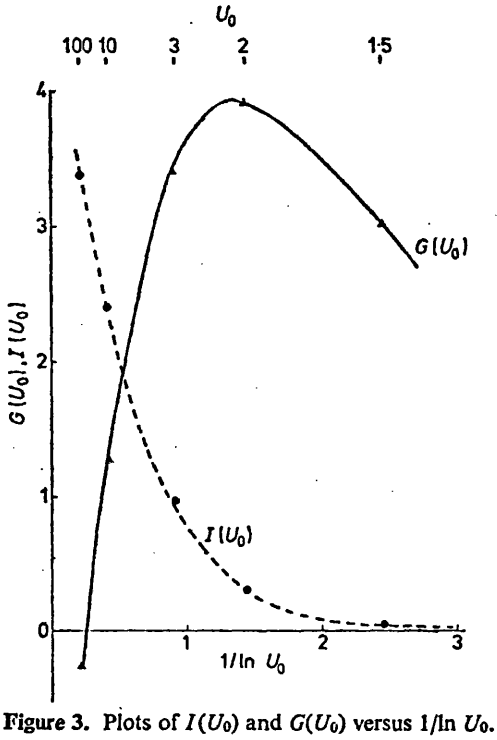

Figure 3. Plots of $I(U_0)$ and $G(U_0)$ versus $1/\ln U_0$.

and

$$G(U_0) = -0{\cdot}59299 + \frac{21{\cdot}55329}{U_0} - \frac{30{\cdot}55248}{U_0^2} + \frac{9{\cdot}59218}{U_0^3}. \tag{6}$$

Both expressions have been constrained to give zero when $U_0 = 1$ in order to accord with physical reality. Hence equations (3), (5) and (6) provide our complete analytical expression for $\phi(0)$. Values for $\phi(0)$ calculated using this agreed closely with data obtained directly from the Monte Carlo model, most of the RMS error of 1·6% being associated with the statistics of the Monte Carlo simulation.

4. Comparison of Monte Carlo results with existing $\phi(0)$ values

There are a number of published values for the surface ionisation but the data in general are not very comprehensive and experimental errors of ~10% or more are sometimes quoted. In assessing the present analytical expression for $\phi(0)$ our calculated values will be compared with published information based upon direct experimental measurement and upon previously calculated data.

Probably the most fundamental method of measuring surface ionisation directly is the tracer method used by Castaing and Descamps (1955), Castaing and Henoc (1966) and Vignez and Dez (1968). They use a self-supporting film and compare the x-ray intensity from this with that measured from the same thickness film deposited on a thick substrate having similar electron scattering characteristics.

Our analytical expression is plotted as a function of ln U_0 for nickel, titanium and aluminium targets in figure 4; (Bishop's (1966) η data at 30 kV has been used in the $\phi(0)$ expression). Direct measurements of $\phi(0)$ by the above method are included in figure 4

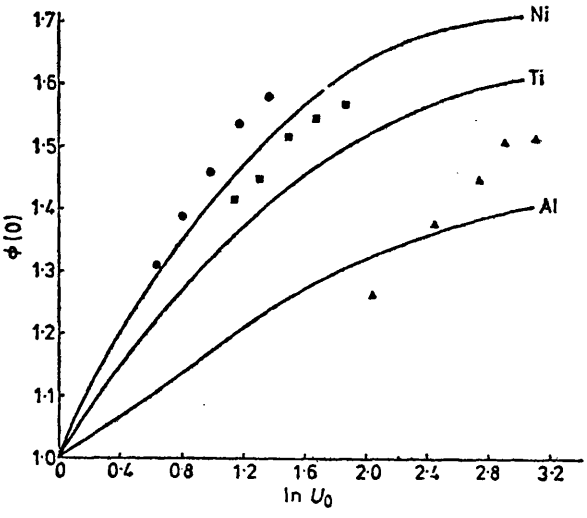

Figure 4. Plots of $\phi(0)$ versus ln U_0 for nickel, titanium and aluminium targets. ——— present analytical expression; ● nickel (Vignes and Dez 1968 1968); ■ titanium (Vignes and Dez 1968); ▲ aluminium (Castaing and Henoc 1966).

for the appropriate target materials. It may be seen that measured values for nickel and titanium are some 5% higher than those given by our analytical expression but since Vignes and Dez (1968) quote an experimental error of 5% it may be concluded that there is good agreement between the two sets of data. Discrepancies appear to be rather greater for aluminium (~7% relative error) but this is still within the error band quoted by Castaing and Henoc (5–10%) and agreement may be considered satisfactory particularly when one considers there may be some uncertainty in the fluorescence correction which these workers applied to this system.

A second method of measuring surface ionisation involves deposition of a thin coating of a selected element upon substrates of different atomic number (Hutchins 1966). The x-ray intensities from the coating are plotted against atomic number of the substrate, and extrapolation to $Z=0$ (i.e. zero back-scattering from the substrate) gives the intensity equivalent to that of an isolated layer of the same thickness. $\phi(0)$ values for different elements are then obtained from this curve by taking the ratio of the x-ray intensity from the film on the substrate element of interest to this extrapolated value. Reuter (1972) has obtained a fairly comprehensive set of $\phi(0)$ values using this method and his results are compared with our calculations in figure 5. Discrepancies appear to be generally 10% or greater and it is possible that Reuter's measurements are in error for the following reasons:

(i) The method used by Reuter assumes that the thin layer of coating does not modify electron scattering by the substrate. This may not be the case since even very thin layers can affect scattering behaviour; for example, ~50% of the electron back-scattering in gold at 10 keV occurs in the outermost 50 Å of the target (derived from results of Cosslett and Thomas 1964, 1965). Although Reuter does not give his coating thicknesses, it must be presumed that they were adequate to give sufficient x-ray intensities for measurement and hence his $\phi(0)$ values may suffer from such an error.

(ii) The extrapolation procedure used by Reuter is subject to considerable error due

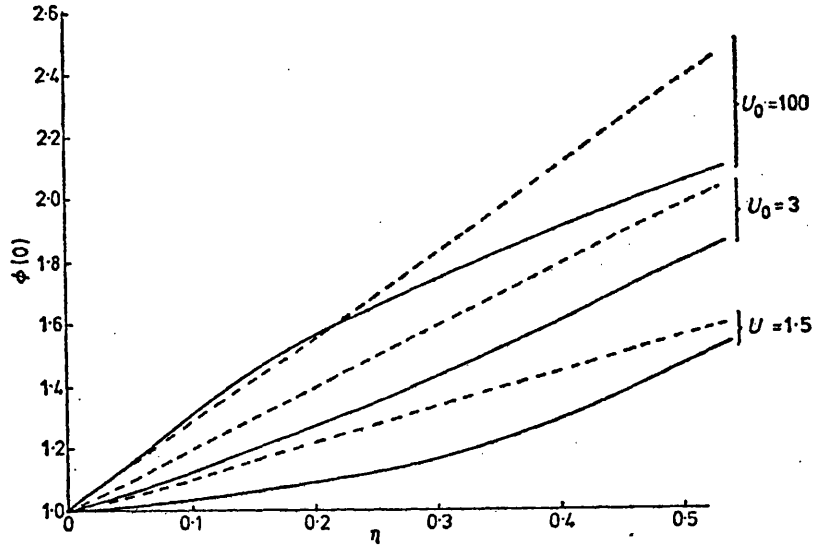

Figure 5. Plots of $\phi(0)$ versus η for overvoltages of 1·5, 3 and 100. ——— present analytical expression; ----- Reuter's (1972) expression.

to the curvature of the plot of x-ray intensity versus Z in the region of low atomic number.

(iii) Continuous and characteristic fluorescence corrections appear to have been ignored; these can lead to errors in excess of 10% of the measured x-ray intensity.

In addition to the above experimental values of $\phi(0)$ some calculated data are available (Duncumb, quoted by Martin and Poole 1971). These results, derived from Bishop's (1966) back-scattered electron energy distributions assuming an ionisation cross-section proportional to $(1/U)\ln U$, are shown in figure 6. The values are generally close to although consistently higher than our own calculated results. Discrepancies are a few percent for lower overvoltages but increase up to ~10% for $U_0=100$. The difference is

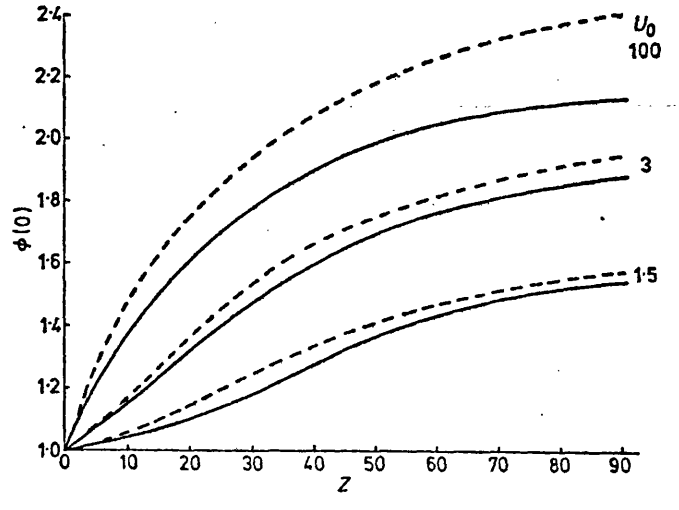

Figure 6. Plots of $\phi(0)$ versus Z for overvoltages of 1·5, 3 and 100. ——— Present analytical expression; ----- Duncumb's results (quoted by Martin and Poole 1971).

not, however, unexpected since P Duncumb (1977 private communication) assumed that the average path length of the back-scattered electrons passing through the surface layer was twice that of the incident electrons (equivalent to assuming that electron escape is equally probable in all directions), whereas the Monte Carlo model predicts a factor of 1·7. Available data agree with our results in giving values of 1·68 for gold and 1·72 for aluminium (Reimer and Drescher 1977, based on the measurements of Reimer and Pfefferkorn 1973).

It should also be noted that, since η is dependent upon electron energy (Bishop 1966, Heinrich 1966, Drescher *et al* 1970, Darlington 1971), so is $\phi(0)$ (see equation 4). This is at variance with the results of workers who have found (or assumed) that $\phi(0)$ is independent of electron energy.

5. Conclusions

Values of the surface ionisation function have been calculated for a wide range of elements and overvoltages using a Monte Carlo method. An analytical expression for $\phi(0)$ is derived in terms of the electron back-scatter coefficient η and overvoltage U; viz.

$$\phi(0)=1+\frac{\eta}{1+\eta}\,(I(U_0)+G(U_0)\ln(1+\eta))$$

where

$$I(U_0)=3{\cdot}43378-\frac{10{\cdot}78720}{U_0}+\frac{10{\cdot}97628}{U_0^2}-\frac{3{\cdot}62286}{U_0^3}$$

and

$$G(U_0)=-0{\cdot}59299+\frac{21{\cdot}55329}{U_0}-\frac{30{\cdot}55248}{U_0^2}+\frac{9{\cdot}59218}{U_0^3}.$$

$\phi(0)$ values obtained using these equations are in close agreement with the limited data obtained by the tracer technique but show discrepancies with results of other methods of measurement; it is considered that the latter values may be in error.

Acknowledgments

Thanks are due to Dr P Duncumb for his helpful comments on the paper. The co-operation of the University Computer Unit under the direction of Dr A W Nichol is also acknowledged.

References

Bethe H A, 1930 *Ann. Phys. Lpz.* 5 325–400
Bishop H E 1966 *PhD Thesis* University of Cambridge
—— 1974 *J. Phys. D: Appl. Phys.* 7 2009–20
Castaing R and Descamps J 1955 *J. Physique* 16 304
Castaing R and Henoc J 1966 *X-ray Optics and Microanalysis* eds R Castaing, P Deschamps and J Philibert (Paris: Hermann) pp 120–6
Cosslett V E and Thomas R N 1964 *Br. J. Appl. Phys.* 15 883–906
—— 1965 *Br. J. Appl. Phys.* 16 779–95
Curgenven L and Duncumb P 1971 *Tube Investments Res. Rep. No.* 303

Darlington E H 1971 *PhD Thesis* University of Cambridge
Drescher H, Reimer L and Seidel H 1970 *Z. Angew. Phys.* 29 331–6
Duncumb P and Melford D A 1966 *X-ray Optics and Microanalysis* eds R Castaing, P Deschamps and J Philibert (Paris: Hermann) pp 240–53
Fitting H J 1975 *J. Phys. D: Appl. Phys.* 8 1481–6
Heinrich K F J 1966 *X-ray Optics and Microanalysis* eds R Castaing, P Deschamps and J Philibert (Paris: Hermann) pp 159–67
Hutchins G A 1966 *The Electron Microprobe* eds T D McKinley, K F J Heinrich and C B Wittry (New York: John Wiley) pp 390–404
Hutchins G A and Wantman R D 1967 *Trans. 2nd Nat. Conf. on Electron Microprobe Analysis, Boston, Mass.* (Boston: MIT Press)
Love G, Cox M G C and Scott V D 1974a *J. Phys. D: Appl. Phys.* 7 2131–41
—— 1974b *J. Phys. D: Appl. Phys.* 7 2142–55
—— 1975 *J. Phys. D: Appl. Phys.* 8 1686–1702
—— 1977 *J. Phys. D: Appl. Phys.* 10 7–23
—— 1978 *J. Phys. D: Appl. Phys.* 11 7–21 (preceding paper)
Martin P M and Poole D M 1971 *Metall. Rev.* 5 no. 150 19–46
Philibert J 1963 *X-ray Optics and Microanalysis* eds H H Pattee, V E Cosslett and E Engström (New York: Academic Press) p 379
Reimer L and Drescher H 1977 *J. Phys. D: Appl. Phys.* 10 805–15
Reimer L and Pfefferkorn G 1973 *Raster-Elektronenmikroskopie* (Springer-Verlag: Berlin) p 39
Reuter W 1972 *X-ray Optics and Microanalysis* eds G Shinoda, K Kohra and T Ichinokawa (Tokyo: Tokyo UP) pp 121–30
Vignes A and Dez G 1968 *J. Phys. D: Appl. Phys.* 1 1309–22

7.14 Evaluation of a New Correction Procedure for Quantitative Electron Probe Microanalysis

G. Love and V.D. Scott,

1978c, J. Phys.D : Appl. Phys.

accepted for publication.

EVALUATION OF A NEW CORRECTION PROCEDURE FOR QUANTITATIVE ELECTRON PROBE MICROANALYSIS

G. Love and V.D. Scott,
School of Materials Science,
University of Bath,
Bath, Avon, BA2 7AY.

ABSTRACT

A new correction procedure for converting electron-probe microanalysis measurements into true weight concentrations is proposed. It incorporates a new atomic number correction and an absorption correction based upon the model of Bishop (Bishop 1974). Unlike earlier treatments the model does not have to rely upon any empirical optimisation of input paremeters. The correction procedure has been tested by applying it to a wide range of microanalysis data including light element results and it is shown to give greater accuracy than the established methods.

1. INTRODUCTION

In the present paper a new correction procedure is proposed for converting microanalysis measurements into elemental weight concentrations. The absorption correction incorporated in this model is based upon the treatment outlined by Bishop (1974) since, as discussed in earlier papers (Bishop 1974, Love et al 1975), the simplified absorption correction of Philibert (Philibert 1963) has limited application. In order to apply the Bishop model a suitable expression for the mean depth of x-ray generation is required and this we obtain by using a Monte Carlo method for simulating electron interactions in solids (Love et al 1977). Atomic number effects in the correction procedure are dealt with using a new approach (Love et al 1978a) rather than the commonly applied Duncumb and Reed method (Duncumb and Reed 1968).

The proposed correction model is evaluated using microanalysis data from a variety of published sources including light element measurements. Results are then compared with those obtained by applying an established correction method which consists of the Duncumb and Reed atomic number correction (Duncumb and Reed 1968), the simplified Philibert absorption correction (Philibert 1963) with Heinrich's constants for σ and h (Heinrich 1967) and Reed's characteristic fluorescence correction (Reed 1965).

2. THE BACKSCATTER COEFFICIENT FOR ELECTRONS

The backscatter coefficient, η, is the ratio of the number, n, of electrons backscattered to the number n_o, of electrons incident on the specimen,

$$\text{i.e.} \quad \eta = \frac{n}{n_o}$$

Since this parameter relates to the number of electrons absorbed by the target and to their spatial distribution and energy, it will be important with respect to both atomic number and absorption effects. Consequently, in our development of the respective correction terms we have chosen to express them explicitly as a function of η. Some experimental values for η are available (Bishop 1966a, Heinrich 1966a, Drescher et al 1970), but instead an analytical expression will be derived here so that our correction method may be made more generally applicable.

Now, as is well known, η is a function of atomic number, Z, and is also dependent upon incident electron energy, E_o. In order to determine the energy dependence of η, values taken from Seidel (cited in Darlington 1975)

are plotted against ln E_o for the elements Al, Cu, Ag and U in figure 1. Seidel's values are used here since they cover a wide range of electron energies, 9-100keV; they were in fact, obtained by a least squares fit to Drescher's experimental data. The points plotted in Figure 1 lie close to a straight line for each particular element and hence we may write

$$\eta = I(Z) + G(Z)\ \ln E_o \qquad (1)$$

where the intercept, I(Z), and the gradient G(Z), are functions of the atomic number of the specimen. Expressions for I(Z) and G(Z) can be obtained by carrying out a regression analysis on data obtained from Figure 1. However, use of equation (1) necessitates extrapolation from $E_o = 0$ to the energies commonly used in microprobe analysis ($E_o \sim 30$keV) and this may give rise to significant errors. The problem may be largely overcome by extrapolating from $E_o = 20$keV which then minimises errors between 10 and 30keV. Thus equation (1) takes the form

$$\eta - \eta_{20} = G(Z)\ln E_o - G(Z)\ln 20$$

i.e.

$$\eta = \eta_{20}\left[1 + \frac{G(Z)}{\eta_{20}}\ln\left(\frac{E_o}{20}\right)\right] \qquad (2)$$

where η_{20} is the backscatter coefficient associated with electrons of energy 20keV and is a function of atomic number of the target. The terms η_{20} and (G/η_{20}) can be represented by the following polynomials in Z

$$\eta_{20} = (-52.3791 + 150.48371Z - 1.07373Z^2 + 0.00716Z^3) \times 10^{-4} \qquad (3)$$

and

$$\frac{G}{\eta_{20}} = (-1112.8 + 30.289Z - 0.15498Z^2) \times 10^{-4} \qquad (4)$$

Hence incorporation of equations (3) and (4) into equation (2) leads to a complete analytical expression for η.

Values of η calculated from this formula gave an RMS error of 2.3% when checked against Seidel's data, a figure which is commensurate with the accuracy of the original experimental results (2-3% Darlington 1975). The formula was next used to calculate η values at 5keV and comparison with Bishop's measurements (Bishop 1966a) on elements ranging from carbon to uranium in the periodic table gave good agreement (RMS error 4.1%). It may be concluded, therefore, that our analytical expression for η works well for all elements and for electron energies in the range 5-100keV, i.e. all conditions likely to be experienced in microanalysis. It should be pointed out, however, that below 5keV errors might arise because η does

Seidel's values of η plotted against $\ln E_o$ for the elements Al, Cu, Ag and U

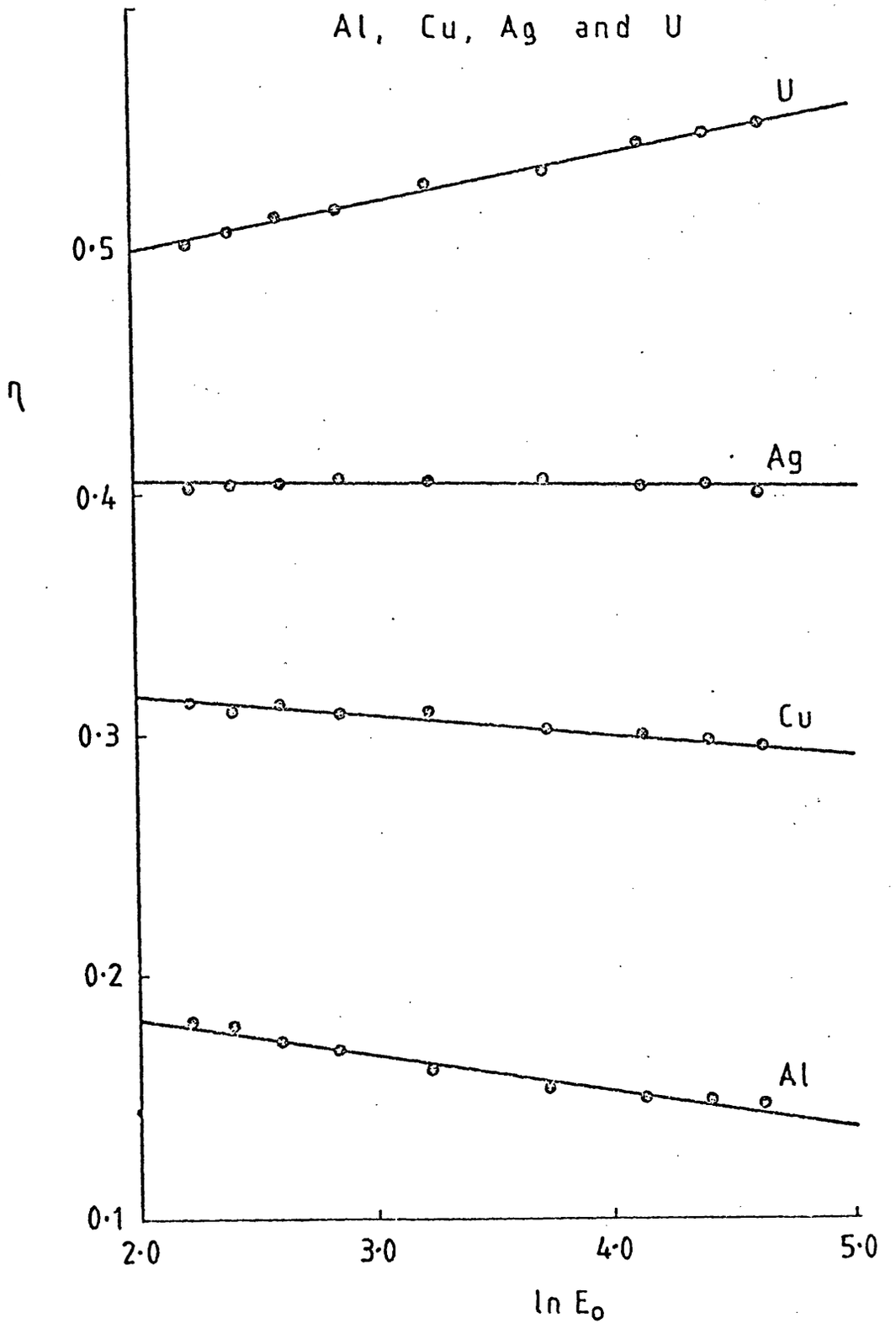

figure 1

not vary smoothly with atomic number (Sternglass 1954, Bishop 1966b and Darlington 1971) and thus cannot be adequately represented by a polynomial in Z.

In order to obtain η values for multi-element specimens we average in the following way

$$\eta_{sp} = \sum C_i \eta_i \qquad \text{Castaing (1960)}$$

where C_i is the weight fraction of the i^{th} element.

3. THE PROPOSED CORRECTION METHOD

3.1 THE ATOMIC NUMBER CORRECTION

The atomic number correction is treated conventionally by considering separately the stopping power factor, S, and the backscatter factor, R, and is written

$$\frac{Isp}{Ist} = C_i \frac{Rsp}{Rst} \cdot \frac{Sst}{Ssp}$$

where the ratio Isp/Ist refers to the intensity of x-rays emitted by the i^{th} element of a multi-element specimen to that in a pure element standard. Analytical expressions for S and R have been derived in a previous paper (Love et al 1978a) and are as follows

$$\frac{1}{S} = \left[1 + 16.05 \left(\frac{J}{Ec}\right)^{0.5} \left(\frac{U_o^{0.5} - 1}{U_o - 1}\right)^{1.07}\right] \Big/ \sum \frac{C_i Z_i}{A_i} \qquad (5)$$

$$R = 1 - \eta \left[I(U_o) + \eta . G(U_o)\right]^{1.67} \qquad (6)$$

where $I(U_o)$ and $G(U_o)$ are functions of overvoltage Uo (= Eo/Ec), and are given by

$$I(U_o) = 0.33148 \ln U_o + 0.05596 (\ln U_o)^2 - 0.06339 (\ln U_o)^3 + 0.00947 (\ln U_o)^4$$

and $$G(U_o) = \frac{1}{U_o} \left[2.87898 \ln U_o - 1.51307 (\ln U_o)^2 + 0.81312 (\ln U_o)^3 - 0.08241 (\ln U_o)^4\right]$$

A is the atomic weight of the specimen and J is the mean ionisation potential of the x-ray line being measured.

Several expressions giving the appropriate value of J for a particular

element have been proposed in the literature. As discussed earlier (Love et al 1977) we shall adopt J/Z = 0.0135keV. For a multi-element specimen the following expression for J is used (Love et al 1978a)

$$\ln(J_{sp}) = \sum \left(\frac{C_i Z_i}{A_i} \ln J_i\right) \Big/ \sum \frac{C_i Z_i}{A_i} \quad \dagger$$

Values of S and R for compound specimens are determined by the incorporation of J_{sp} in equation (5) and η_{sp} in equation (6) respectively (not by weight averaging S and R directly).

3.2 ABSORPTION CORRECTION

The absorption correction is based upon the method proposed by Bishop (1974) which approximates to a rectangle the x-ray distribution with depth. The fractional transmission of the target for x-rays, $f(\chi)$, is then given by

$$f(\chi) = \frac{1 - \exp(-2\chi\overline{\rho z})}{2\chi\overline{\rho z}}$$

where $\chi = (\mu/\rho)\ \mathrm{cosec}\ \theta$, μ/ρ being the mass absorption coefficient of the measured radiation and θ the x-ray take-off angle; $\overline{\rho z}$ is the mean mass depth of x-ray generation.

In an earlier paper (Love et al 1976) a preliminary assessment of the Bishop model was carried out using an expression for $\overline{\rho z}$ derived from the simplified Philibert absorption method (Philibert 1963). However, as a result of the subsequent development of a Monte Carlo method for simulating electron-solid interactions (Love et al 1977), it has been possible to derive a more acceptable and fundamental expression for $\overline{\rho z}$

$$\overline{\rho z} = \rho s_m \frac{(0.49269 - 1.09870\eta + 0.78557\eta^2) \ln U_2}{(0.70256 - 1.09865\eta + 1.00460\eta^2) + \ln U_0}$$

where ρs_m is the average path length of an electron in the target and is given by

$$\rho s_m = \frac{(0.773 \times 10^{-5} J^{0.5} E_0^{1.5} + 0.735 \times 10^{-6} E_0^2)}{\sum C_i Z_i / A_i}$$

† There was an obvious printing error in the expression given on page 9 of the original paper (Love et al 1978a), where the ln term on the left hand side was omitted.

3.3 FLUORESCENCE CORRECTIONS

The characteristic fluorescence correction used here is the one most widely adopted (Reed 1965). A correction for continuum fluorescence was not included in the analysis but it would be sufficiently small to have little effect upon the final conclusions of this work.

4. APPLICATION OF THE PROPOSED CORRECTION

From a survey of published microanalysis data on binary alloy systems, 430 results were selected for assessing correction models; the data have been referred to in earlier papers (Love et al 1975, 1976). Heinrich's mass absorption coefficients (Heinrich 1966b) have been employed throughout. No light element results are included in the above data but light element microanalysis is referred to later in this section. The 430 measurements have been plotted as c/k in a histogram, Figure 2, in order to indicate the order of magnitude of correction required; c is the actual concentration and k the measured value.

Microanalysis data corrected using the new procedure are given in the histogram, Figure 3a. The RMS error was 5.3%, see Table 1 which shows also the percentage of results lying within 2½% and 7½% of the true value. Corrected data using the established procedure are shown in the histogram, Figure 3b. The RMS error was 6.8%, while 49% of the data lay within 2½% of the true value and 84% within 7½% (see Table 1).

It is considered that the improvement achieved by the new correction is associated mainly with a more accurate absorption correction since this factor is usually the largest. In order to assess the respective atomic number corrections, only those data obtained on low absorbing systems ($f(\chi) > 0.8$) will now be considered; this involves 190 microanalysis measurements. The results obtained by applying the new model and the established correction model respectively are summarised in Table 2. The figures show that the new method gives a more accurate correction even for systems where absorption effects are very small, which suggests that our atomic number correction is superior to that of Duncumb and Reed (1968). Support for this view was obtained by investigating the effect of applying together the Duncumb and Reed atomic number correction and the Bishop absorption correction; the corrected results were then found to be worse (RMS error 3%, cf Table 2).

In an earlier paper (Love et al 1977), in which the most appropriate value for J/Z was discussed, it was shown that the mean depth of x-ray generation and hence the absorption correction was insensitive to the precise value adopted. Reasons were given for using J/Z = 0.0135keV,

Histograms of uncorrected microanalysis data [430 systems]; data in block on right of diagram includes results where c/k ranges from 2 to ~15

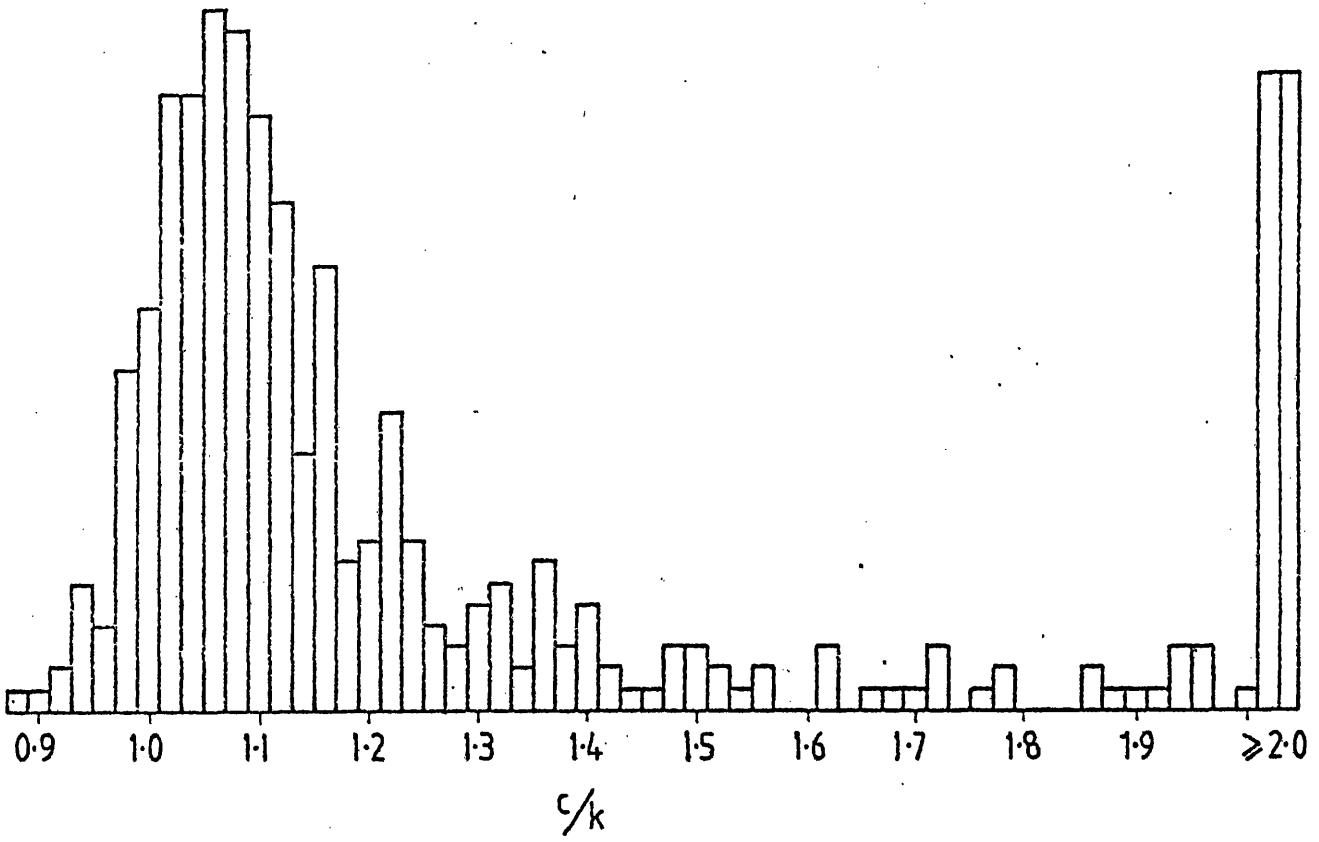

figure 2

Histogram of corrected microanalysis results plotted as k'/k where k' is the intensity ratio predicted by a particular correction method

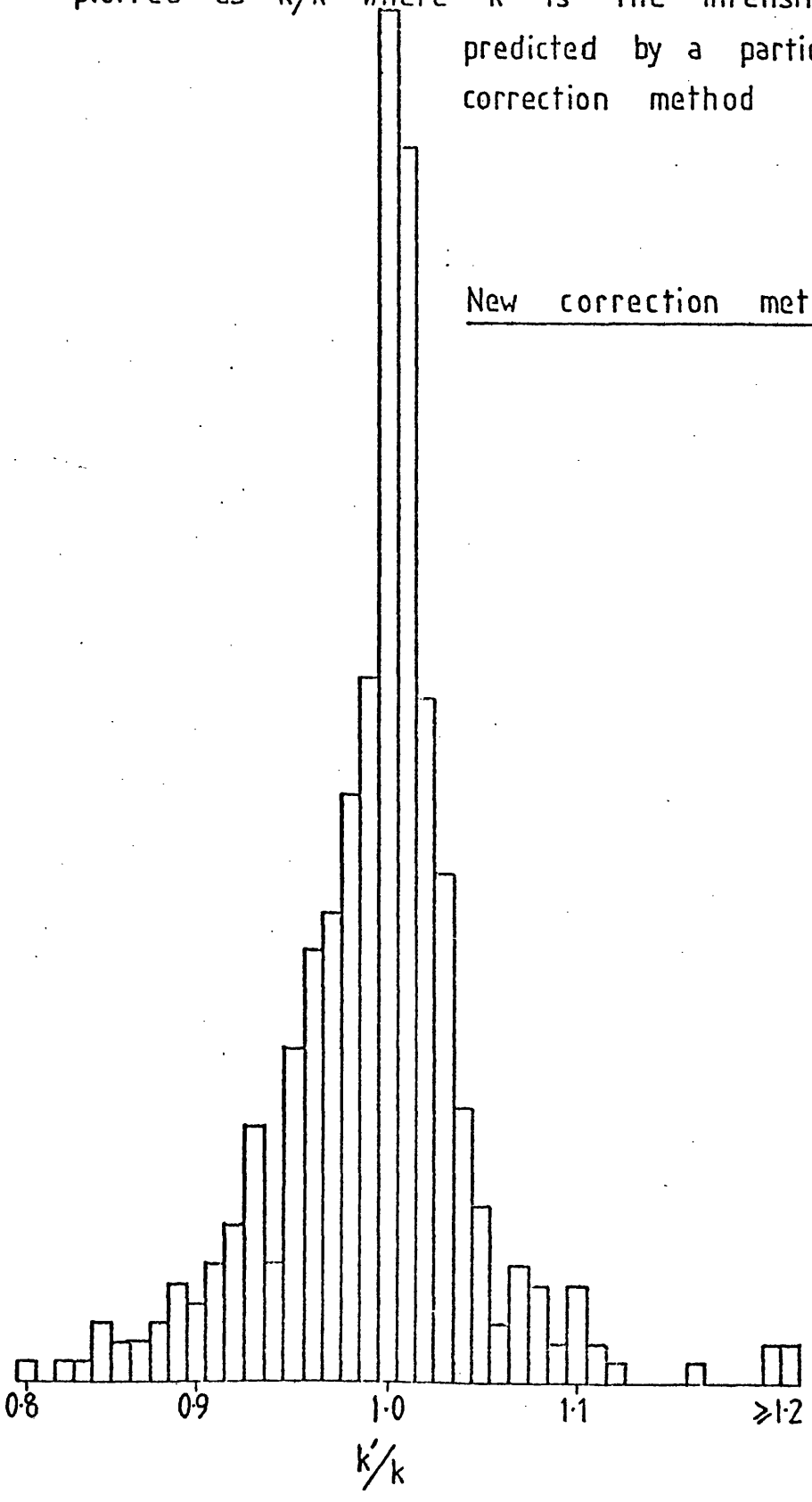

figure 3a

Histogram of corrected microanalysis results plotted as k'/k

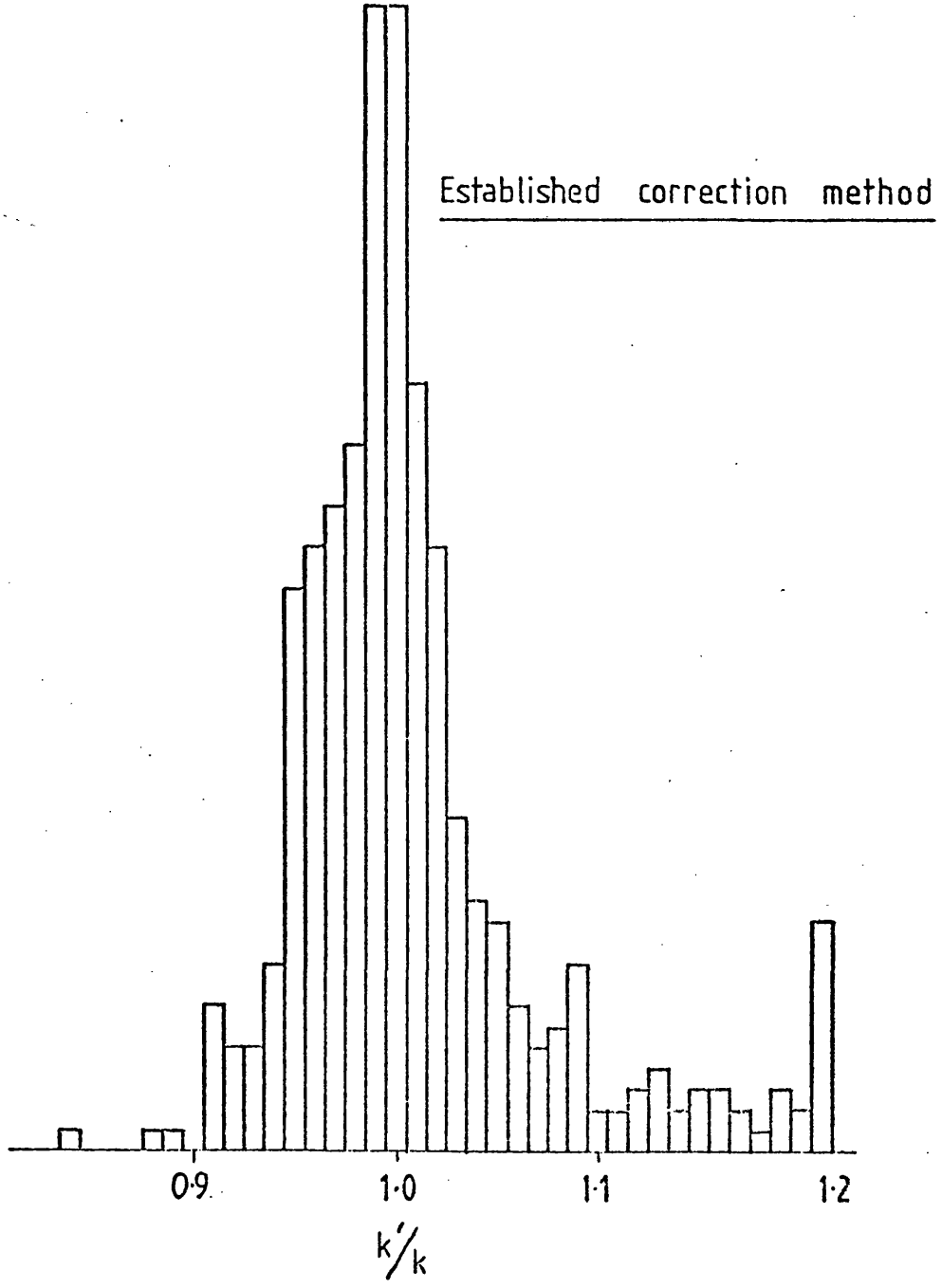

figure 3b

TABLE 1

Model	R.M.S. error %	% of results within 2½% of true conc.	% of results within 7½% of true conc.
New Method	5.3	54	87
Established Method	6.8	49	84

TABLE 2

Model	R.M.S. error %	% of results within 2½% of true conc.	% of results within 7½% of true conc.
New Method	2.4	73	99
Established Method	3.0	70	98

TABLE 3

Model	R.M.S. error %	% of results within 2½% of true conc.	% of results within 7½% of true conc.
New Method	5.6	38	82
Method incorporating full Philibert absorption correction	6.0	46	84

a view which is substantiated by the following. A number of alternative expressions for J/Z were incorporated into our programme: J/Z = 0.0115keV (Wilson 1941), the expressions of Zeller (cited in Ruste 1976) and the equation of Duncumb and Reed (1968). Each was found to give a greater RMS error than that obtained when using J/Z = 0.0135keV; an effect which was more noticeable with the reduced number of systems ($f(\chi)>0.8$) where atomic number corrections are more significant.

Finally, the new correction procedure was applied to some light element data. For this purpose oxygen microanalysis measurements on a range of oxides were used together with mass absorption coefficients calculated previously (Love et al 1974). The results are given in Table 3. Also given in the table are results obtained from applying the full Philibert absorption correction (Philibert 1963) with Duncumb and Melford's constants (Duncumb and Melford 1966) together with the Duncumb and Reed atomic number correction (Duncumb and Reed 1968). As may be seen the new model is at least as good as the older method of correction. It should, of course, be noted that the full Philibert absorption correction is of limited value in quantitative work (see Love et al 1975), since it gives worse results than the simplified Philibert method when applied to heavy element systems.

It could be argued that some of the RMS error in the corrected light element data may be due to inaccuracies in mass absorption coefficients used. These values were calculated by applying the thin film model (Duncumb and Melford 1966) to microanalysis measurements, a method which requires the incorporation of appropriate values for $\phi(o)$, the surface ionisation function. Previously we have used the $\phi(o)$ expression given by Reuter (1972) but recent calculations (Love et al 1978b) would indicate that this may be in error. In future work it is intended to re-evaluate the oxygen analysis data using revised $\phi(o)$ values to see whether improved mass absorption coefficients produce a corresponding improvement in the accuracy of corrected light element data.

5. CONCLUSIONS

A correction procedure for quantitative electron-probe microanalysis is proposed which incorporates a new atomic number correction and an absorption correction based upon Bishop's model containing an appropriate expression for the mean depth of x-ray generation. The method has been applied to a wide range of published microanalysis measurements including light element data and shown to give greater accuracy than previous correction models. It is considered that the accuracy of microanalysis results needs to be improved before the model can be tested more rigorously.

Unlike earlier methods, the new model does not rely upon a 'best fit analysis' approach which adjusts empirically input parameters and it must, therefore, be regarded as a genuine advance towards a universal correction procedure for quantitative electron-probe microanalysis. The next stage is to develop the model so that is may be applied to specimens which are inclined to the electron beam. This geometrical factor is readily included in the atomic number correction (Love et al 1978a) and it now remains to incorporate it in the absorption correction.

6. REFERENCES

Bishop, H.E. 1966a. X-ray Optics and Microanalysis, eds. R. Castaing, P. Deschamps and J. Philibert (Paris : Hermann) pp 153-8.

Bishop, H.E. 1966b, Ph.D. Thesis. University of Cambridge.

Bishop, H.E. 1974. J.Phys.D : Appl. Phys. 7 2009-20.

Castaing, R. 1960 Adv. Electron. Electron Phys., 13 eds. L.L. Marton and C. Marton (New York : Academic Press) pp 317-86.

Darlington, E.H. 1971 Ph.D. Thesis. University of Cambridge.

Darlington, E.H. 1975 J.Phys.D : Appl. Phys. 8 85-93.

Drescher, H., Reimer L. and Seidel, H., 1970 Z. angew. Phys. 29 331-6.

Duncumb, P. and Melford, D.A. 1966. X-ray Optics and Microanalysis ed. R. Castaing, P. Deschamps and J. Philibert, (Paris : Hermann) pp 240-53.

Duncumb, P., and Reed, S.J.B., 1968. Quantitative Electron Probe Microanalysis.

Heinrich, K.F.J., 1966a, X-ray Optics and Microanalysis. ed. R. Castaing, P. Deschamps and J. Philibert (Paris : Hermann) pp 159-67.

Heinrich, K.F.J., 1966b The Electron Microprobe ed. T.D. McKinley, K.F.J. Heinrich and D.B. Wittry (New York : Wiley) pp 296-377.

Heinrich, K.F.J., 1967 Trans. 2nd Natn. Conf. Electron Probe Mircoanalysis, Boston, U.S.A. (Boston : Electron Probe Analysis Society of America) Paper No. 7.

Love, G., Cox, M.G.C. and Scott, V.D. 1974, J.Phys.D : Appl. Phys. 7, 2131.

Love, G., Cox, M.G.C. and Scott, V.D. 1975, J.Phys.D : Appl. Phys. 8 1686-1702.

Love, G., Cox, M.G.C. and Scott, V.D. 1976, J.Phys.D : Appl. Phys, 9 7-13.

Love, G., Cox, M.G.C. and Scott, V.D. 1977, J.Phys.D : Appl. Phys. 10 7-23.

Love, C., Cox, M.G.C. and Scott, V.D., 1978a. J.Phys.D : Appl. Phys. 11 7-21.

Love, G., Cox, M.G.C. and Scott, V.D. 1978b. J.Phys.D : Appl.Phys. 11 23-31.

Philibert, J., 1963 X-ray Optics and X-ray Microanalysis ed. H.H. Pattee, V.E. Cosslett, and A. Engström (New York : Academic Press) pp 379-92.

Reed, S.J.B., 1965 Br. J. Appl. Phys., 16 913.

Reuter, W., 1972 X-ray Optics and Microanalysis eds. G. Shinoda, K. Kohra and T. Ichinokawa (Tokyo : Tokyo UP) pp 121-30.

Ruste, J., 1976, Ph.D. Thesis, University of Nancy.

Sternglass, E.J. 1954, Phys. Rev. 95 345-58.

Wilson, R.R. 1941 Phys. Rev. 60 749.

Acknowledgements

Thanks to Dr. A.W. Nichol for access to computer facilities.